Summer 8-8-2017

Biochemical and Biophysical Studies of Heme Transport Proteins: HtaA, HtaB, and ChtB from the Corynebacterium diphtheriae

Rizvan C. Uluisik
Georgia State University

BIOCHEMICAL AND BIOPHYSICAL STUDIES OF HEME TRANSPORT PROTEINS; HtaA, HtaB, AND ChtB FROM THE *CORYNEBACTERIUM DIPHTHERIAE*

by

RIZVAN C. ULUISIK

Under the Direction of Dabney Dixon, PhD

ABSTRACT

Many pathogenic bacteria require iron for their survival and virulence; in most cases hemin is the main iron source. Pathogens have developed sophisticated heme uptake mechanisms in order to maintain the homeostasis and remain as infectious agents. *Corynebacterium diphtheria* can obtain hemin during human infection through series of conserved domains (CR) of DxtR-regulated and heme-transport-associated (hta) proteins: HtaA, HtaB, ChtA, ChtB and ChtC. HtaA includes two conserved regions (CR1 and CR2) while the other proteins include a single CR domain. These proteins orchestrate the heme transport to the HmuT protein, a lipoprotein which delivers heme to the ABC membrane transporter HmuUV. Homology modeling of HtaA-CR2, HtaB and ChtB based on amino acid sequence indicated that

these proteins have a novel structure. Two tyrosines and one histidine residue are fully conserved in all CR domains. Mutations of these conserved amino acids to alanine significantly lowered the heme binding in comparison to the wild-type proteins. Reconstitution of HtaA-CR2 after removal of the heme with butanone extraction method gave a different form of the protein. UV-visible absorption spectra and resonance Raman spectra data are consistent with heme ligation with an axial tyrosine including a histidine hydrogen-binding partner in HtaA-CR2, HtaB and ChtB. HtaA-CR2 is highly stable to thermal unfolding; the protein was also stable to chemical unfolding using GdnHCl or GdnSCN (up to 4 M at 25^{o}C) . For HtaA-CR2, unfolding could be observed at 37 ^{o}C as a single process at high concentrations of denaturant (6.8 – 7.4 M GdnHCl). In contrast, HtaA-CR2 apoproteins (WT, as well as the Y361A and H412A mutants) unfolded readily with low denaturant concentrations (~ 1.3 M GdnHCl). HtaB shows significantly lower stability; a half-life of 330 min was observed in the presence of 6.6 M GdnHCl at 37 ^{o}C for HtaA-CR2 and a half-life of 39 min was observed in the presence of 4.0 M GdnHCl at 25 ^{o}C for HtaB; ChtB was very similar to HtaB. For HtaB and ChtB, the high amino acid sequence similarity and identity, similar biophysical characteristics and gene deletion studies suggest that these proteins may function interchangeably during the heme uptake process.

INDEX WORDS: Heme, Heme uptake, Heme transfer, Unfolding, Axial ligand, Denaturation, UV-visible absorption spectroscopy, Resonance Raman spectroscopy

BIOCHEMICAL AND BIOPHYSICAL STUDIES OF HEME BINDING PROTEINS; HtaA, HtaB AND ChtB FROM THE *CORYNEBACTERIUM DIPHTHERIAE*

by

RIZVAN C ULUISIK

A Dissertation Submitted in Partial Fulfillment of the Requirements for the Degree of

Doctor of Philosophy

in the College of Arts and Sciences

Georgia State University

2017

BIOCHEMICAL AND BIOPHYSICAL STUDIES OF HEME BINDING PROTEINS; HtaA AND HtaB FROM THE *CORYNEBACTERIUM DIPHTHERIAE*

by

RIZVAN C. ULUISIK

Committee Chair: Dabney Dixon

Committee: Giovanni Gadda

Gangli Wang

Electronic Version Approved:

Office of Graduate Studies

College of Arts and Sciences

Georgia State University

June 2017

DEDICATION

I dedicate this dissertation to my parents Ibrahim and Gonul Uluisik, my sister Ruba Uluisik-Gulsen, my niece Defne Gulsen, and my nephew Umut Gulsen.

ACKNOWLEDGEMENTS

I would like to express my sincere gratitude to my advisor, Dr. Dabney Dixon, for her guidance and support throughout my research.

Thank you my friends those who helped me throughout my research with their expertise and time, especially my colleagues in our research lab, Elizabeth Draganova, Stephanie Thompson, Brandon Ferrell, Cyrianne Keutcha, Carly Wieting, and Robby Kirby.

I also would like to thank my dissertation committee: Dr. Dabney W. Dixon, Dr. Giovanni Gadda, and Dr. Gangli Wang for their advice and expertise throughout the completion of my degree. Additionally, I would like to thank my qualification exam committee members: Dr. Kathryn B. Grant, Dr. Gangli Wang, and Dr. Donald Hamelberg.

The work in our lab would not have been possible without our hard working collaborators. Many thanks go out to Dr. Kenton Rodgers, Dr. Gudrun Lukat-Rodgers, and their research group.

TABLE OF CONTENTS

LIST OF TABLES

LIST OF FIGURES

1 INTRODUCTION

1.1 Iron and heme requirement of pathogenic bacteria

Almost every biological system requires iron as an essential nutrient (Grigg et al., 2010b). Iron can act as reducing and oxidizing center. It plays a number of roles in metabolic pathways such as photosynthesis, respiration, enzyme catalysis, and electron transport (Chipperfield and Ratledge, 2000; Nobles and Maresso, 2011). Iron is commonly found either in the oxidized ferric form [Fe(III)] or the reduced ferrous form [Fe(II)] under physiological conditions. Ferric iron is the most abundant form of iron on earth; however, it is not easily accessible for biological systems due to its low solubility, 1.4×10^{-9} M at pH 7.0 in aerobic environments (Chipperfield and Ratledge, 2000; Nobles and Maresso, 2011). Ferrous ion, under aerobic conditions, can form hydroxyl radicals via Fenton reaction; these radicals damage living organisms by interacting with nucleic acids, lipids and proteins (Krewulak and Vogel, 2008; Braun and Hantke, 2011). In mammals, 99% of the iron is sequestered in proteins, the majority of the iron is found in protoporphyrin IX (heme) (Stojiljkovic and Perkins-Balding, 2002). Heme is bound to a variety of proteins including hemoglobin, hemopexin, albumin, lipoproteins, transferrin and lactoferrin (Grigg et al., 2010a; Grigg et al., 2010b; Braun and Hantke, 2011; Nobles and Maresso, 2011). For pathogenic bacteria, access to heme is restricted in the host environment. Various effective mechanisms evolved in pathogens in order to steal iron from their host (Smith and Wilks, 2012; Benson and Rivera, 2013; Farrand and Skaar, 2014; Rodgers and Lukat-Rodgers, 2014; Wilks and O'Neill, 2014; Sheldon and Heinrichs, 2015; Choby and Skaar, 2016).

1.2 Heme uptake systems in gram-negative bacteria

The majority of our knowledge about heme uptake mechanisms in pathogenic bacteria comes from studies on gram-negative bacteria (Burkhard and Wilks, 2007; Tong and Guo, 2009; Braun and Hantke, 2011; Rodgers and Lukat-Rodgers, 2014; Wilks and O'Neill, 2014). In general, heme uptake starts with a single outer membrane receptor protein which has a high affinity for heme and binds to heme and/or hemoproteins. Some gram-negative species scavenge heme from the extracellular environment through hemophores and transfer the heme to receptor proteins (Jonsson et al., 2003; Mazmanian et al., 2003; Wandersman and Delepelaire, 2004; Wandersman and Delepelaire, 2012). The heme captured by the outer membrane protein is transferred to the inner membrane through periplasmic carrier proteins. These transporters depend on the energy generated by the proton motive force by TonB (a periplasmic complex anchored in the membrane). Heme then shuttles to the cytoplasm through the cell membrane via an ABC transporter, a process that depends on the energy generated by ATPase. Finally, heme oxygenase (HO) degrades heme to biliverdin, carbon monoxide and iron (Nobles and Maresso, 2011).

1.3 Heme uptake systems in gram-positive bacteria

Gram-positive bacteria have a thick peptidoglycan layer rather than an outer membrane. For the acquisition and transportation of heme, these bacteria use both hemophores and cell-wall anchored proteins (Braun and Hantke, 2011; Nobles and Maresso, 2011; Rodgers and Lukat-Rodgers, 2014; Wandersman and Delepelaire, 2014; Wilks and O'Neill, 2014; Sheldon and Heinrichs, 2015). Heme uptake mechanisms of gram-positive pathogens have been primarily investigated in *Staphylococcus aureus*, *Bacillus anthracis*, *Streptococcus pyogenes*, and *Corynebacterium diphtheriae*.

1.3.1 Isd system and NEAT domains in Staphylococcus aureus

S. aureus transports heme using the Isd (iron-regulated surface determinant) system (Gaudin et al., 2011; Grigg et al., 2011). The surface proteins that are covalently attached to the cell wall in the Isd system are IsdA, IsdB, IsdC and IsdH. The covalent attachment of these proteins is catalyzed by sortase enzymes SrtA and SrtB. Most of the Isd proteins are able bind to heme; some of them also bind to hemoproteins such as hemoglobin or the hemoglobin-haptoglobin complex. The binding of heme or hemoproteins by Isd proteins occurs at near-iron transporter domains (NEAT). The domain contains 120 - 125 conserved amino acids, composed of eight β-strands and a 3_{10} α-helix (Honsa et al., 2014; Rodgers and Lukat-Rodgers, 2014; Sheldon and Heinrichs, 2015; Choby and Skaar, 2016). The heme binding NEAT domains have a YXXXY motif in which the first tyrosine coordinates with heme iron and the second tyrosine forms a hydrogen bond with the first tyrosine. Also, a second motif SXXXXY/F has been shown to participate in heme binding. The serine residue hydrogen bonds with one of the heme propionates and the tyrosine or phenylalanine stacks over the heme. Although NEAT domains are the main component of the Isd heme transfer system, not all of the NEAT domains are able to bind heme. Once heme is transported to the plasma membrane, it is then taken up by ABC transporters to the cytosol (Ton-That et al., 2004; Woo et al., 2012).

1.3.2 Heme uptake in Bacillus anthracis

Heme transfer of *B. anthracis* is orchestrated by NEAT proteins IsdX1/2, Hal, BsIK and IsdC (Maresso et al., 2008; Honsa et al., 2014; Sheldon and Heinrichs, 2015; Choby and Skaar, 2016). IsdX1 and IsdX2 are heme and methemoglobin (metHb) binding hemophores that are secreted into the extracellular environment. Hal is a hemoglobin (Hb) binding surface- exposed

protein that includes a cell-wall anchoring sortase signal. BsIK is a heme binding protein that is non-covalently attached to the cell wall.

1.3.3 Heme uptake in Streptococcus pyogenes

S. pyogenes transfers heme using the streptococcal hemoprotein receptor Shr, Shp, HtsA(SiaA) and an ABC transporter. Shr and Shp are surface-exposed and anchored to the cell wall. Shr includes two NEAT domains and can receive heme from metHb (Liu and Lei, 2005; Nygaard et al., 2006; Ouattara et al., 2010; Nobles and Maresso, 2011). In contrast, Shp does not include a NEAT domain and transfers heme to SiaA (Aranda et al., 2007; Ran et al., 2007; Akbas et al., 2016).

1.3.4 Heme uptake in Corynebacterium diphtheriae

C. diphtheriae is a gram-positive aerobic and rod-shaped pathogenic bacterium. It is the causative agent that infects the upper respiratory tracts in humans (Schmitt, 1997b; Hadfield et al., 2000; Collier, 2001; Trost et al., 2012). Although vaccination is available in many countries, diphtheria infections still exist in some developing countries due to low vaccine availability (Mattos-Guaraldi et al., 2003; Wagner et al., 2012). The pathogen requires iron for metabolic reactions and virulence (Schmitt, 1997b; Drazek et al., 2000; Schmitt and Drazek, 2001). The three genes associated with heme uptake in *C. diphtheriae* are *hmuT*, *hmuU* and *hmuV*, which have homology to the genes that are involved in the heme uptake systems of gram-negative bacteria (Drazek et al., 2000). HmuT is a lipoprotein that anchors to the cytoplasmic membrane and serves as a heme receptor. HmuU and HmuV have been suggested to be the transmembrane permease and an ATP-binding protein, respectively (Fig. 1.1). Further studies have shown that *hmuTUV* genes are a part of a large gene group that also contains *htaA*, *htaB* and *htaC* (Kunkle and Schmitt, 2003). The genes are transcribed from diphtheria toxin repressor (DtxR) and iron-

regulated promoters (Schmitt and Holmes, 1991). The genetic map of the *hmu* locus includes two promoter regions; the first one facilitates the transcription of *htaA*, *hmuT*, *hmuU*, *hmuV* and, *htaC* genes; the second one transcribes only the *htaB* gene (Allen and Schmitt, 2009). Deletion of the *htaA* gene, the *hmuTUV* genes, or the complete the *hmu* gene cluster resulted in significantly decreased growth in comparison to wild type when the cells were grown in the presence of hemoglobin as a sole iron source. Removing these genes did not inhibit cell growth completely. The authors concluded that the organism has strategies to transport the heme other than the *hmu* gene cluster system (Allen and Schmitt, 2009). Deletion of the *htaB* gene did not affect the growth of the cells. The study showed that the HtaA and HtaB are mainly associated with the cell membrane and cell wall. Furthermore, surface exposure studies with proteinase K cleavage suggested that HtaA and HtaB are exposed to the cell surface while HmuT is not.

1.4 HtaA in *Corynebacterium diphtheriae*

There are two conserved regions (CR1 and CR2) identified in HtaA with 50% similarity (Allen & Schmitt, 2011). The conserved regions are also approximately 35% identical to a region in HtaB. UV-visible spectroscopy studies showed that GST-HtaA is able to bind heme (no interaction between heme and GST alone was reported) (Allen & Schmitt, 2009). Both CR1 and CR2 in HtaA are able to bind to heme. ELISA experiments showed that HtaA is able bind to Hb strongly. The CR1 and CR2 domains bind Hb with less efficiency than the complete HtaA; however, the CR2 domain binding to Hb was significantly higher than CR1. The authors proposed that the Hb binding to HtaA or the domains occurs at the heme moiety of Hb (Allen and Schmitt, 2011).

Sequence alignment of various CR domains (*C. diphtheriae* HtaA-CR1, HtaA-CR2 and HtaB-CR; *C. ulcerans*-CR1; *C. glutamicum*-CR2; and *C. jeikeium*-CR2) (Fig. 2.8, Chapter 2)

show that two tyrosine residues and once histidine residue are fully conserved (Tyr49, His107 and Tyr197 in CR1; Tyr361, His412 and Tyr490 in CR2) (Allen and Schmitt, 2011). Studies have focused on the first tyrosine (Tyr49Ala in CR1 and Tyr361Ala in CR2) and the histidine (His107 in CR1 and His412 in CR2); replacement of each of these conserved amino acids with alanine resulted in significant decrease in the heme binding. The heme binding results were similar between tyrosine and histidine mutations. Alanine replacement of these conserved residues also decreased the Hb binding, 27%, 88% and 99% decrease in Tyr49Ala, Tyr361Ala, and Tyr49Ala/Tyr361Ala, respectively, in the full length protein. While the Tyr361Ala mutant showed significant decrease in growth in a medium that included Hb as a sole iron source, the Tyr49Ala mutant did not show significant difference in comparison to the wild type (WT) protein.

1.5 HtaB in *Corynebacterium diphtheriae*

HtaB is a membrane-associated protein that is predicted to play a role in the heme uptake mechanism of *C. diphtheriae*. The amino acid sequence of HtaB has 27% identity and 37% similarity to the sequence of HtaA-CR2 (Allen and Schmitt, 2011). The deletion of *htaB* gene did not affect the cell growth in the presence of hemoglobin as a sole iron source (Allen and Schmitt, 2009). Heme titration experiments using UV-visible spectroscopy showed that HtaB binds heme and can acquire heme from holo-HtaA. The sequence alignment of *C. diphtheriae* CR1 and CR2 domains of HtaA, HtaB and HtaA homologs in related *Corynebacterium* species (*C. ulcerenas, C. glutamicum* and *C. jeikeium*) showed that Tyr56, His121 and Tyr221 of HtaB are fully conserved (biophysical characterization of HtaB and its mutants are described in Chapter 4).

1.6 ChtA, ChtB and ChtC in *Corynebacterium diphtheriae*

Allen and Schmitt further identified an additional set of genes (*chta*, *chtb* and *chtc*) that transcribe heme binding proteins in *C. diphtheriae* (Allen et al., 2013). These genes are also regulated by DtxR and iron. The encoded proteins are ChtA, ChtB and ChtC; each contains an N-terminal CR domain (Fig. 1.1). The Cht proteins are cell surface-exposed, include a transmembrane C-terminal region, and can bind either heme or Hb. ChtA shares only 35% sequence similarity with HtaA (only CR domains); however, there are significant similarities between the ChtB and HtaB sequences, 44% identity and 63% similarity (full length proteins). Single deletion of the *htaB* or *chtB* gene slightly decreased cell growth in comparison with WT in the presence of Hb as an iron source. In contrast, a double deletion of *htaB-chtB* showed around a two-fold decrease. Also, a significant similarity is seen between ChtA and ChtC; approximately 44% amino acid sequence identity and 61% similarity (only CR domains).

1.7 Heme protein unfolding

Elucidation of folding and unfolding of wild type and mutant heme proteins provides information about stability of the protein (Bowler, 2007; Lee et al., 2009; Culbertson and Olson, 2010). Guanidinium hydrochloride (GdnHCl) is widely used in unfolding studies (Pace, 1986; Pace and Scholtz, 1997). Fig. 1.2 shows a two-state unfolding curve; the $D_{1/2}$ value can be determined (concentration of the denaturant at 50% unfolded state), by a non-linear least squares fitting to the equation 3 in Chapter 2. UV-visible, fluorescence and circular dichroism spectroscopic techniques are common methods used to study protein unfolding. Using multiple unfolding techniques is beneficial to elucidate the unfolding process. For example, unfolding of whale met-Mb with GdnHCl was performed with UV-visible, fluorescence or circular dichroism spectroscopic techniques (Hargrove et al., 1994; Hargrove and Olson, 1996; Scott et al., 2000;

Culbertson and Olson, 2010). The circular dichroism (CD) data indicated the formation of an intermediate in the unfolding. It was possible to detect the intermediate by fluorescence, which allowed calculation of K_D values for native apo-Mb and the intermediate for heme (10^{-13} M and 10^{-11} M, respectively) (Culbertson and Olson, 2010).

1.8 Tyrosine/histidine ligated heme proteins

Only a handful of His/Tyr ligated heme proteins have been characterized to date. Examples include Has*As* from *Serratia marcescens* (Deniau et al., 2003; Lukat-Rodgers et al., 2008), HmuT from *Yersinia pestis* (Mattle et al., 2010), HmuT from *C. diphtheriae* (Draganova et al., 2015; Draganova et al., 2016), a hemoglobin variant Hb M Saskatoon (Nagai et al., 1991; Jin et al., 2004), the sperm whale myoglobin mutant HisE7Tyr (Egeberg et al., 1990; Pin et al., 1994) and MauG from *Paracoccus dentrificans* (Abu Tarboush et al., 2010; Abu Tarboush et al., 2012).

Has*As* is a hemophore of Gram-negative *Serratia marcescens* that scavenges heme from host heme proteins and bring it to the cell surface receptors (Deniau et al., 2003). The heme binding site is located at the interface of two loops. Tyr75 and His83 coordinate the heme. The tyrosinate group of Tyr75 forms a hydrogen bond with His85 as shown by the crystal structure. His85 plays a significant role in heme ligation and becomes a ligand in the absence of Tyr75. A displacement ITC experiment was used to determine a heme affinity of WT Has*As* with a K_a value of 5.3×10^{-10} M^{-1} (Smith & Wilks, 2012; Deniau et al., 2003). The enthalpy and the entropy of heme binding were -105 kJ mol^{-1} and -44 kJ mol^{-1} K^{-1}, respectively.

The crystal structure of HmuT from *Yersinia pestis* shows two lobes that each consist of a central β sheet surrounded by short α helices (Mattle et al., 2010). A single α-helix connects the two lobes. The structure shows two stacked hemes bound in the cleft between the lobes,

which are ligated with Tyr70 from one lobe and His167 from the other. Tyr70 is fully conserved while His167 exhibits variance shown in the sequence alignment of HmuT from different species. The two hemes were stacked with the propionate groups pointing opposite directions. The authors reported that the binding of two heme are sequential with K_D values of ~0.29 nM and ~29 nM (Mattle et al., 2010). The axial ligand set of HmuT from *C. diphtheriae* was also investigated (Draganova et al., 2015). Resonance Raman (rR) and magnetic circular dichroism (MCD) spectroscopy studies indicated that *C. diphtheriae* HmuT heme is hexacoordinated and H136 and Y235 residues are the axial ligands. The T_m values for the WT, H136A and Y235A mutants are reported as 66.8, 65.1 and 55.5 ^oC, respectively (Draganova et al., 2016).

Hb M Saskatoon has been shown to be a His/Tyr ligated heme protein (Nagai et al., 1989; Jin et al., 2004). The rR and pH profile studies indicated the His/Tyr ligation of high spin hexacoordinate heme structure for Hb M Saskatoon. The rate of enzymatic reduction of Hb M Saskatoon was similar to that of the human adult Hb (Hb A).

The electron paramagnetic resonance (EPR) and the rR spectra of a myoglobin mutant HisE7Tyr (histidine is the seventh residue of the E helix) has been shown to be coordinated with His/Tyr as axial ligands (Egeberg et al., 1990; Pin et al., 1994). The rR and the EPR spectra also closely resembled the spectra of Hb M Saskatoon. These data showed that the replacement of distal histidine with tyrosine in myoglobin resulted in a switch from histidine pentacoordinate to His/Tyr hexacoordinate heme structure.

MauG from *Paracoccus dentrificans* is an enzyme that binds to a diheme with one of the hemes coordinated with histidine and the other with tyrosine (Abu Tarboush et al., 2010; Abu Tarboush et al., 2012; Geng et al., 2013). The enzyme catalyzes the biosynthesis of tryptophan tryptophylquinone (TTQ) cofactor.

The heme in soybean leghemoglobin is coordinated a histidine and water (Sievers et al., 1983; Jones et al., 2002). The protein can be titrated with exogenous phenol to give His/Tyr ligand set (Patel et al., 2003). It should be noted that myoglobin does not bind phenol as an axial ligand because the distal cavity is too small; rather, the phenol binds parallel to the heme (Huang et al., 2012).

1.9 Heme transport proteins with experimental studies on axial ligand hydrogen-bonding

The importance of a hydrogen-bonding partner for heme axial ligands has been investigated for some of the heme transport proteins of pathogenic bacteria. In some instances, mutation of the H-bonding partner has been shown to have a very large effect on heme binding. In other instances, the effect is small. These data are consistent with many factors being important in controlling heme binding, including van der Waals, charge-charge, π-stacking and other H-bonding interactions (Hargrove et al., 1996; Robinson et al., 1997; Deniau et al., 2003; Zheng and Gunner, 2008). Even though a given interaction may not play a decisive role in controlling the heme affinity, it still may be important in the transfer of the heme to the cognate donor/acceptor. The following outlines the current experimental data to our knowledge that investigate the heme transfer proteins with axial ligand hydrogen-bonding partners and the significance of the partnership.

1.9.1 Heme ligand hydrogen-bonding partner of HasA

The crystal structure of *P. aeruginosa* Has*Ap* (Alontaga et al., 2009) and *S. marcescens* Has*As* (Arnoux et al., 1999) show that the heme is hexacoordinated with His32 and Tyr75 as axial ligands. Has*Ap* Tyr75 forms a H-bond with His83 when crystallization is performed at pH 4.6; however, no H-bond interaction was observed when crystals were grown at pH 6.5. Similarly, for Has*As*, no hydrogen bond between Tyr75 and His83 was observed when crystals

were grown at pH 6.0. Alontaga et al. suggested that the H-bond between the Tyr75 and His83 might be an important factor in the heme acquisition or release process (Alontaga et al., 2009). In this hypothesis, heme protein binding is favored when the H-bond is present while the release of heme is favored when the H-bond is absent.

Structural studies of the Has*Ap* Tyr75Ala and His83Ala mutants showed that the Tyr75-heme interaction remained intact in the His83Ala mutant (Kumar et al., 2014). Tyr75 formed a hydrogen bond either with water or ethylene glycol (depending upon the crystallization conditions). These findings suggest that the presence of a H-bonding partner is important for Tyr75 axial ligand. In the Tyr75Ala structure, His83 kept its original position as found in the WT but did not coordinate with the heme iron. The K_a values for heme binding of WT Has*Ap*, Tyr75Ala and His83Ala were determined to be 35, 129 and 30 μM, respectively. These data suggest that Tyr75 is important for heme binding; in contrast, its hydrogen-bonding partner His83 is not playing an important role.

The K_d values for heme with HasA and its mutants by ITC experiments were also reported (Deniau et al., 2003). The Tyr75Ala, His32Ala and His83Ala mutants showed 400-fold, 5-fold and 260-fold decreases in heme binding, respectively, in comparison to the WT Has*As* which has a K_d value of 0.019 nM. For heme binding, the replacement of the H-bonding partner H83 had a significantly higher effect on K_d then replacement of the distal axial ligand itself (His32).

1.9.2 Heme ligand hydrogen-bonding partner of Isd proteins

The crystal structure of *S. aureus* IsdB-NEAT2 revealed that the heme is coordinated with Y440, with Y444 as the H-bonding partner (Gaudin et al., 2011). The UV-visible absorption spectra of Y440A and Y444A variants (reconstituted with equimolar hemin) were more similar

to the spectrum of free heme than to the WT protein. These spectra indicated that the hemin binding of Y440A and Y444A mutants was significantly disrupted. It was suggested that Y444 might be required to stabilize Y440 to bind heme iron and/or stabilize the folding of the NEAT domain.

S. aureus IsdH NEAT3 was crystallized as the apo form of the protein (Watanabe et al., 2008). Using molecular modeling, a heme molecule was docked into the structure. It appears that Y642 is the axial ligand and Y646 is the H-bonding partner. The heme affinity of WT, Y642A, Y646A, and Y642A/Y646A variants was investigated by ITC experiments. Although the affinity of heme was decreased significantly in the mutants, the variants were still able to bind heme with reasonable affinity (K_d values 0.31, 1.20, 0.66, and 1.66 μM for the WT, Y642A, Y646A, and Y642A/Y646A proteins respectively). It was concluded that Y642 and Y646 residues are important, but not essential, for heme binding. However, there are significant differences in the spectra of Y642A and Y646A mutants compared to that of the WT, suggesting that the heme environment is altered in the mutant proteins.

The heme transfer in Isd system between the acceptor-NEAT and donor-NEAT-heme complexes was investigated with molecular dynamic (MD) simulations and quantum mechanics/molecular mechanics (QM/MM) (Moriwaki et al., 2015). It was proposed that during the heme transfer between the NEAT domains, the heme of the donor-acceptor complex could form an intermediate hexacoordinate geometry with two deprotonated tyrosine residues (tyrosines from heme-donor-NEAT and heme-acceptor-NEAT) in such configuration that each tyrosine forms H-bond with a secondary tyrosine residue. The study suggested that protonation of the H-bonding partner tyrosine in the heme-donor-NEAT might initiate the relocation of the hydrogen between two partner tyrosines onto the to the axial ligand tyrosine (the phenolate

converted to phenol) which might result in the dissociation of Fe-O bond. This computational model was demonstrated for IsdH-N3-heme-IsdA-N. The data indicate that a H-bonding partner might play a key role in the transfer of heme between the two NEAT domains.

1.9.3 Dissertation Goals

Iron is an essential micronutrient for many medically important pathogenic bacteria. These pathogens acquire iron mainly in the form of heme using advanced heme uptake and transport protein complexes. A momentum of characterization of the heme uptake systems in pathogenic bacteria has been increasing as these systems are targeted for development of antibacterial drug alternatives. Much of our knowledge about these systems comes from the studies on gram-negative bacteria. In this work, we will undertake the biophysical and biochemical characterization of *C. diphtheriae* heme transport proteins HtaA, HtaB, and ChtB.

The proteins will be purified using affinity column chromatography. Mass spectrometry and SDS-PAGE gel electrophoresis will confirm the purity and the molecular weight of the protein samples. Point amino acid replacements at targeted locations will be performed with site-directed mutagenesis. Heme loading of the proteins will be determined using pyridine hemochrome and Bradford assays.

The nature of the axial ligands will be investigated with UV-visible absorption, fluorescence and CD, and rR spectroscopy. Guanidinium-induced and temperature denaturation techniques will be used to determine the stability of the holoprotein and the apoprotein, as well as the protein unfolding kinetic parameters.

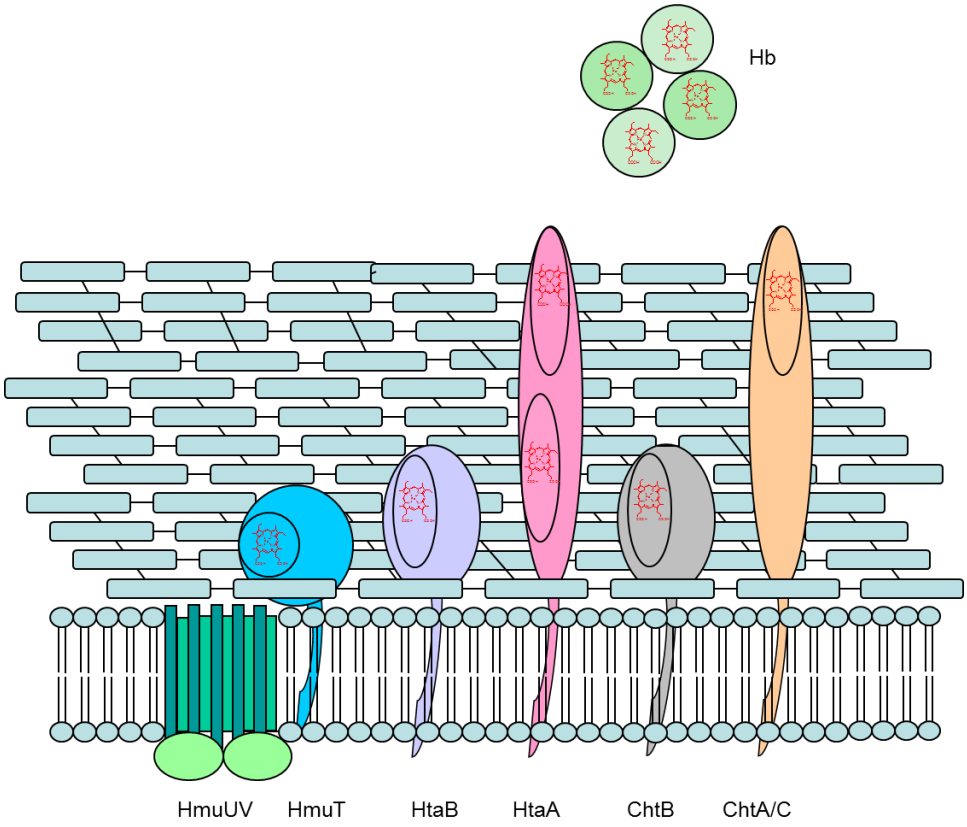

Figure 1.1 Schematic of heme uptake pathway in *C. diphtheriae*.

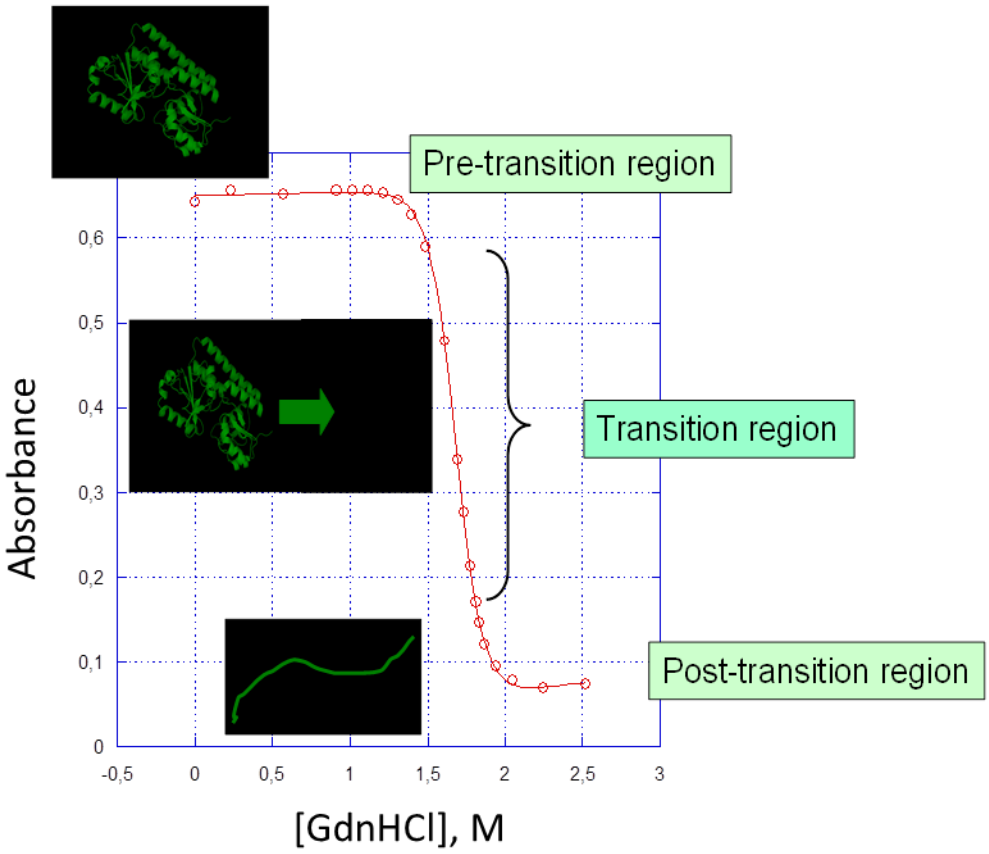

Figure 1.2 A representative two state unfolding curve of a protein. The figure shows the change in the UV-visible absorbance as a function of chemical denaturant concentration.

1.10 References

Abu Tarboush, N., Jensen, L.M., Feng, M., Tachikawa, H., Wilmot, C.M., Davidson, V.L., 2010. Functional importance of tyrosine 294 and the catalytic selectivity for the bis-Fe(IV) state of MauG revealed by replacement of this axial heme ligand with histidine. Biochemistry 49, 9783-9791.

Abu Tarboush, N., Shin, S., Geng, J.F., Liu, A.M., Davidson, V.L., 2012. Effects of the loss of the axial tyrosine ligand of the low-spin heme of MauG on its physical properties and reactivity. FEBS Lett. 586, 4339-4343.

Akbas, N., Draganova, E.B., Block, D.R., Sook, B.R., Chan, Y.F., Zhuo, J., Eichenbaum, Z., Rodgers, K.R., Dixon, D.W., 2016. Heme-bound SiaA from *Streptococcus pyogenes*: Effects of mutations and oxidation state on protein stability. J. Inorg. Biochem. 158, 99-109.

Allen, C.E., Burgos, J.M., Schmitt, M.P., 2013. Analysis of novel iron-regulated, surface-anchored hemin-binding proteins in *Corynebacterium diphtheriae*. J. Bacteriol. 195, 2852-2863.

Allen, C.E., Schmitt, M.P., 2009. HtaA is an iron-regulated hemin binding protein involved in the utilization of heme iron in *Corynebacterium diphtheriae*. J. Bacteriol. 191, 2638-2648.

Allen, C.E., Schmitt, M.P., 2011. Novel hemin binding domains in the *Corynebacterium diphtheriae* HtaA protein interact with hemoglobin and are critical for heme iron utilization by HtaA. J. Bacteriol. 193, 5374-5385.

Alontaga, A.Y., Rodriguez, J.C., Schoenbrunn, E., Becker, A., Funke, T., Yukl, E.T., Hayashi, T., Stobaugh, J., Moenne-Loccoz, P., Rivera, M., 2009. Structural characterization of the hemophore HasAp from *Pseudomonas aeruginosa*: NMR spectroscopy reveals protein-protein interactions between holo-HasAp and hemoglobin. Biochemistry 48, 96-109.

Aranda, R., Worley, C.E., Liu, M., Bitto, E., Cates, M.S., Olson, J.S., Lei, B.F., Phillips, G.N., 2007. Bis-methionyl coordination in the crystal structure of the heme-binding domain of the streptococcal cell surface protein Shp. J. Mol. Biol. 374, 374-383.

Arnoux, P., Haser, R., Izadi, N., Lecroisey, A., Delepierre, M., Wandersman, C., Czjzek, M., 1999. The crystal structure of HasA, a hemophore secreted by *Serratia marcescens*. Nat. Struct. Biol. 6, 516-520.

Benson, D.R., Rivera, M., 2013. Heme uptake and metabolism in bacteria. Met. Ions Life Sci. 12, 279-332.

Bowler, B.E., 2007. Thermodynamics of protein denatured states. Mol. Biosyst. 3, 88-99.

Braun, V., Hantke, K., 2011. Recent insights into iron import by bacteria. Curr. Opin. Chem. Biol. 15, 328-334.

Burkhard, K.A., Wilks, A., 2007. Characterization of the outer membrane receptor ShuA from the heme uptake system of *Shigella dysenteriae* - Substrate specificity and identification of the heme protein ligands. J. Biol. Chem. 282, 15126-15136.

Chipperfield, J.R., Ratledge, C., 2000. Salicylic acid is not a bacterial siderophore: A theoretical study. Biometals 13, 165-168.

Choby, J.E., Skaar, E.P., 2016. Heme synthesis and acquisition in bacterial pathogens. J. Mol. Biol. 428, 3408-3428.

Collier, R.J., 2001. Understanding the mode of action of diphtheria toxin: A perspective on progress during the 20th century. Toxicon 39, 1793-1803.

Culbertson, D.S., Olson, J.S., 2010. Role of heme in the unfolding and assembly of myoglobin. Biochemistry 49, 6052-6063.

Deniau, C., Gilli, R., Izadi-Pruneyre, N., Létoffé, S., Delepierre, M., Wandersman, C., Briand, C., Lecroisey, A., 2003. Thermodynamics of heme binding to the HasA(SM) hemophore: Effect of mutations at three key residues for heme uptake. Biochemistry 42, 10627-10633.

Draganova, E.B., Adrian, S.A., Lukat-Rodgers, G.S., Keutcha, C.S., Schmitt, M.P., Rodgers, K.R., Dixon, D.W., 2016. *Corynebacterium diphtheriae* HmuT: Dissecting the roles of conserved residues in heme pocket stabilization. J. Biol. Inorg. Chem. 21, 875-886.

Draganova, E.B., Akbas, N., Adrian, S.A., Lukat-Rodgers, G.S., Collins, D.P., Dawson, J.H., Schmitt, M.P., Rodgers, K.R., Dixon, D.W., 2015. Heme binding by *Corynebacterium diphtheriae* HmuT: Function and heme environment. Biochemistry 54, 6598-6609.

Drazek, E.S., Hammack, C.A., Schmitt, M.P., 2000. *Corynebacterium diphtheriae* genes required for acquisition of iron from haemin and haemoglobin are homologous to ABC haemin transporters. Mol. Microbiol. 36, 68-84.

Egeberg, K.D., Springer, B.A., Martinis, S.A., Sligar, S.G., Morikis, D., Champion, P.M., 1990. Alteration of sperm whale myoglobin heme axial ligation by site-directed mutagenesis. Biochemistry 29, 9783-9791.

Farrand, A.J., Skaar, E.P., 2014. Heme and infectious diseases, in: Ferreira, G.C., Kadish, K.M., Smith, K.M., Guilard, R. (Eds.), Handbook of Porphyrin Science with Applications to Chemistry, Physics, Materials Science, Engineering, Biology and Medicine, Vol 26: Heme Biochemistry. World Scientific, Hackensack, NJ, pp. 317-377.

Gaudin, C.F.M., Grigg, J.C., Arrieta, A.L., Murphy, M.E.P., 2011. Unique heme-iron coordination by the hemoglobin receptor IsdB of *Staphylococcus aureus*. Biochemistry 50, 5443-5452.

Geng, J.F., Dornevil, K., Davidson, V.L., Liu, A.M., 2013. Tryptophan-mediated charge-resonance stabilization in the bis-Fe(IV) redox state of MauG. Proc. Natl. Acad. Sci. U. S. A. 110, 9639-9644.

Grigg, J.C., Cooper, J.D., Cheung, J., Heinrichs, D.E., Murphy, M.E.P., 2010a. The *Staphylococcus aureus* siderophore receptor HtsA undergoes localized conformational changes to enclose staphyloferrin A in an arginine-rich binding pocket. J. Biol. Chem. 285, 11162-11171.

Grigg, J.C., Mao, C.X., Murphy, M.E., 2011. Iron-coordinating tyrosine is a key determinant of NEAT domain heme transfer. J. Mol. Biol. 413, 684-698.

Grigg, J.C., Ukpabi, G., Gaudin, C.F., Murphy, M.E., 2010b. Structural biology of heme binding in the *Staphylococcus aureus* Isd system. J. Inorg. Biochem. 104, 341-348.

Hadfield, T.L., McEvoy, P., Polotsky, Y., Tzinserling, V.A., Yakovlev, A.A., 2000. The pathology of diphtheria. J. Infect. Dis. 181, S116-S120.

Hargrove, M.S., Krzywda, S., Wilkinson, A.J., Dou, Y., Ikeda-Saito, M., Olson, J.S., 1994. Stability of myoglobin: A model for the folding of heme proteins. Biochemistry 33, 11767-11775.

Hargrove, M.S., Olson, J.S., 1996. The stability of holomyoglobin is determined by heme affinity. Biochemistry 35, 11310-11318.

Hargrove, M.S., Wilkinson, A.J., Olson, J.S., 1996. Structural factors governing hemin dissociation from metmyoglobin. Biochemistry 35, 11300-11309.

Honsa, E.S., Maresso, A.W., Highlander, S.K., 2014. Molecular and evolutionary analysis of NEAr-iron Transporter (NEAT) domains. PLoS One 9.

Huang, X., Wang, C.X., Celeste, L.R., Lovelace, L.L., Sun, S.F., Dawson, J.H., Lebioda, L., 2012. Complex of myoglobin with phenol bound in a proximal cavity. Acta Crystallogr. Sect. F-Struct. Biol. Cryst. Commun. 68, 1465-1471.

Jin, Y.Y., Nagai, M., Nagai, Y., Nagatomo, S., Kitagawa, T., 2004. Heme structures of five variants of hemoglobin M probed by resonance Raman spectroscopy. Biochemistry 43, 8517-8527.

Jones, D.K., Patel, N., Cheesman, M.R., Thomson, A.J., Raven, E.L., 2002. Leghaemoglobin: A model for the investigation of haem protein axial ligation. Inorg. Chim. Acta 331, 303-309.

Jonsson, I.M., Mazmanian, S.K., Schneewind, O., Bremell, T., Tarkowski, A., 2003. The role of *Staphylococcus aureus* sortase A and sortase B in murine arthritis. Microbes Infect. 5, 775-780.

Krewulak, K.D., Vogel, H.J., 2008. Structural biology of bacterial iron uptake. Biochim. Biophys. Acta 1778, 1781-1804.

Kumar, R., Matsumura, H., Lovell, S., Yao, H.L., Rodriguez, J.C., Battaile, K.P., Moenne-Loccoz, P., Rivera, M., 2014. Replacing the axial ligand tyrosine 75 or its hydrogen bond partner histidine 83 minimally affects hemin acquisition by the hemophore HasAp from *Pseudomonas aeruginosa*. Biochemistry 53, 2112-2125.

Kunkle, C.A., Schmitt, M.P., 2003. Analysis of the *Corynebacterium diphtheriae* DtxR regulon: Identification of a putative siderophore synthesis and transport system that is similar to the *Yersinia* high-pathogenicity island-encoded yersiniabactin synthesis and uptake system. J. Bacteriol. 185, 6826-6840.

Lee, A.J., Clark, R.W., Youn, H., Ponter, S., Burstyn, J.N., 2009. Guanidine hydrochloride-induced unfolding of the three heme coordination states of the CO-sensing transcription factor, CooA. Biochemistry 48, 6585-6597.

Liu, M.Y., Lei, B.F., 2005. Heme transfer from streptococcal cell surface protein Shp to HtsA of transporter HtsABC. Infect. Immun. 73, 5086-5092.

Lukat-Rodgers, G.S., Rodgers, K.R., Caillet-Saguy, C., Izadi-Pruneyre, N., Lecroisey, A., 2008. Novel heme ligand displacement by CO in the soluble hemophore HasA and its proximal ligand mutants: Implications for heme uptake and release. Biochemistry 47, 2087-2098.

Maresso, A.W., Garufi, G., Schneewind, O., 2008. *Bacillus anthracis* secretes proteins that mediate heme acquisition from hemoglobin. PLoS Pathog. 4.

Mattle, D., Zeltina, A., Woo, J.S., Goetz, B.A., Locher, K.P., 2010. Two stacked heme molecules in the binding pocket of the periplasmic heme-binding protein HmuT from *Yersinia pestis*. J. Mol. Biol. 404, 220-231.

Mattos-Guaraldi, A., Moreira, L., Damasco, P., Hirata Junior, R., 2003. Diphtheria remains a threat to health in the developing world: An overview. Mem. Inst. Oswaldo Cruz 98, 987-993.

Mazmanian, S.K., Skaar, E.P., Gaspar, A.H., Humayun, M., Gornicki, P., Jelenska, J., Joachmiak, A., Missiakas, D.M., Schneewind, O., 2003. Passage of heme-iron across the envelope of *Staphylococcus aureus*. Science 299, 906-909.

Moriwaki, Y., Terada, T., Tsumoto, K., Shimizu, K., 2015. Rapid heme transfer reactions between NEAr transporter domains of *Staphylococcus aureus*: A theoretical study using QM/MM and MD simulations. PLoS One 10.

Nagai, M., Yoneyama, Y., Kitagawa, T., 1989. Characteristics in tyrosine coordinations of four hemoglobins M probed by resonance Raman spectroscopy. Biochemistry 28, 2418-2422.

Nagai, M., Yoneyama, Y., Kitagawa, T., 1991. Unusual carbon monoxide bonding geometry in abnormal subunits of hemoglobin M Boston and hemoglobin M Saskatoon. Biochemistry 30, 6495-6503.

Nobles, C.L., Maresso, A.W., 2011. The theft of host heme by Gram-positive pathogenic bacteria. Metallomics 3, 788-796.

Nygaard, T.K., Blouin, G.C., Liu, M.Y., Fukumura, M., Olson, J.S., Fabian, M., Dooley, D.M., Lei, B.F., 2006. The mechanism of direct heme transfer from the streptococcal cell surface protein Shp to HtsA of the HtsABC transporter. J. Biol. Chem. 281, 20761-20771.

Ouattara, M., Cunha, E.B., Li, X., Huang, Y.S., Dixon, D.W., Eichenbaum, Z., 2010. Shr of Group A streptococcus is a new type of composite NEAT protein involved in sequestering haem from methaemoglobin. Mol. Microbiol. 78, 739-756.

Pace, C.N., 1986. Determination and analysis of urea and guanidine hydrochloride denaturation curves. Methods Enzymol. 131, 266-280.

Pace, C.N., Scholtz, J.M., 1997. Measuring the conformational stability of a protein, in: Creighton, T. (Ed.), Protein Structure: A Practical Approach, 2nd ed. Oxford University Press, Oxford, pp. 299-321.

Patel, N., Seward, H.E., Svensson, A., Gurman, S.J., Thomson, A.J., Raven, E.L., 2003. Exploiting the conformational flexibility of leghemoglobin: A framework for examination of heme protein axial ligation. Arch. Biochem. Biophys. 418, 197-204.

Pin, S., Alpert, B., Cortès, R., Ascone, I., Chiu, M.L., Sligar, S.G., 1994. The heme iron coordination complex in His64(E7)Tyr recombinant sperm whale myoglobin. Biochemistry 33, 11618-11623.

Ran, Y.C., Zhu, H., Liu, M.Y., Fabian, M., Olson, J.S., Aranda, R.I., Phillips, G.N., Dooley, D.M., Lei, B., 2007. Bis-methionine ligation to heme iron in the streptococcal cell surface protein Shp facilitates rapid hemin transfer to HtsA of the HtsABC transporter. J. Biol. Chem. 282, 31380-31388.

Robinson, C.R., Liu, Y.F., Thomson, J.A., Sturtevant, J.M., Sligar, S.G., 1997. Energetics of heme binding to native and denatured states of cytochrome *b*(562). Biochemistry 36, 16141-16146.

Rodgers, K.R., Lukat-Rodgers, G.S., 2014. Biophysical perspectives on the acquisition, transport, and trafficking of heme in bacteria, in: Ferreira, G.C., Kadish, K.M., Smith, K.M., Guilard, R. (Eds.), Handbook of Porphyrin Science with Applications to Chemistry, Physics, Materials Science, Engineering, Biology and Medicine, Vol. 30: Heme Proteins, Part II. World Scientific, Hackensack, N.J, pp. 251-309.

Schmitt, M.P., 1997. Utilization of host iron sources by *Corynebacterium diphtheriae*: Identification of a gene whose product is homologous for eukaryotic heme oxygenases and is required for acquisition of iron from heme and hemoglobin. J. Bacteriol. 179, 838-845.

Schmitt, M.P., Drazek, E.S., 2001. Construction and consequences of directed mutations affecting the hemin receptor in pathogenic *Corynebacterium species*. J. Bacteriol. 183, 1476-1481.

Schmitt, M.P., Holmes, R.K., 1991. Iron-dependent regulation of diphtheria toxin and siderophore expression by the cloned *Corynebacterium diphtheriae* repressor gene Dtxr in *C. diphtheriae* C7 strains. Infect. Immun. 59, 1899-1904.

Scott, E.E., Paster, E.V., Olson, J.S., 2000. The stabilities of mammalian apomyoglobins vary over a 600-fold range and can be enhanced by comparative mutagenesis. J. Biol. Chem. 275, 27129-27136.

Sheldon, J.R., Heinrichs, D.E., 2015. Recent developments in understanding the iron acquisition strategies of gram positive pathogens. FEMS Microbiol. Rev. 39, 592-630.

Sievers, G., Gadsby, P.M., Peterson, J., Thomson, A.J., 1983. Magnetic circular dichroism spectra of soybean leghaemoglobin *a* at room temperature and 4.2 K. Biochim. Biophys. Acta 742, 637-647.

Smith, A.D., Wilks, A., 2012. Extracellular heme uptake and the challenges of bacterial cell membranes. Curr. Top. Membr. 69, 359-392.

Stojiljkovic, I., Perkins-Balding, D., 2002. Processing of heme and heme-containing proteins by bacteria. DNA Cell Biol. 21, 281-295.

Ton-That, H., Marraffini, L.A., Schneewind, O., 2004. Protein sorting to the cell wall envelope of Gram-positive bacteria. Biochim. Biophys. Acta 1694, 269-278.

Tong, Y., Guo, M., 2009. Bacterial heme-transport proteins and their heme-coordination modes. Arch. Biochem. Biophys. 481, 1-15.

Trost, E., Blom, J., Soares, S.D., Huang, I.H., Al-Dilaimi, A., Schroder, J., Jaenicke, S., Dorella, F.A., Rocha, F.S., Miyoshi, A., Azevedo, V., Schneider, M.P., Silva, A., Camello, T.C., Sabbadini, P.S., Santos, C.S., Santos, L.S., Hirata, R., Mattos-Guaraldi, A.L., Efstratiou, A., Schmitt, M.P., Hung, T.T., Tauch, A., 2012. Pangenomic study of *Corynebacterium diphtheriae* that provides insights into the genomic diversity of pathogenic isolates from cases of classical diphtheria, endocarditis, and pneumonia. J. Bacteriol. 194, 3199-3215.

Uluisik, R.C., Akbas, N., Lukat-Rodgers, G.S., Adrian, S.A., Allen, C.E., Schmitt, M.P., Rodgers, K.R., Dixon, D.W., 2017. Characterization of the second conserved domain in the heme uptake protein HtaA from *Corynebacterium diphtheriae*. J. Inorg. Biochem. 167, 124-133.

Wagner, K.S., White, J.M., Lucenko, I., Mercer, D., Crowcroft, N.S., Neal, S., Efstratiou, A., 2012. Diphtheria in the postepidemic period, Europe, 2000-2009. Emerg. Infect. Dis. 18, 217-225.

Wandersman, C., Delepelaire, P., 2004. Bacterial iron sources: From siderophores to hemophores. Annu. Rev. Microbiol. 58, 611-647.

Wandersman, C., Delepelaire, P., 2012. Haemophore functions revisited. Mol. Microbiol. 85, 618-631.

Wandersman, C., Delepelaire, P., 2014. Heme-delivering proteins in bacteria, in: Ferreira, G.C., Kadish, K.M., Smith, K.M., Guilard, R. (Eds.), Handbook of Porphyrin Science with Applications to Chemistry, Physics, Materials Science, Engineering, Biology and Medicine, Vol 26: Heme Biochemistry, pp. 191-222.

Watanabe, M., Tanaka, Y., Suenaga, A., Kuroda, M., Yao, M., Watanabe, N., Arisaka, F., Ohta, T., Tanaka, I., Tsumoto, K., 2008. Structural basis for multimeric heme complexation through a specific protein-heme interaction - The case of the third NEAT domain of IsdH from *Staphylococcus aureus*. J. Biol. Chem. 283, 28649-28659.

Wilks, A., O'Neill, M.J., 2014. Extracellular heme uptake and metabolism in bacterial pathogenesis, in: Ferreira, G.C., Kadish, K.M., Smith, K.M., Guilard, R. (Eds.), Handbook of Porphyrin Science with Applications to Chemistry, Physics, Materials Science, Engineering, Biology and Medicine, Vol 26: Heme Biochemistry. World Scientific, Hackensack, NJ, pp. 267-315.

Woo, J.S., Zeltina, A., Goetz, B.A., Locher, K.P., 2012. X-ray structure of the *Yersinia pestis* heme transporter HmuUV. Nat. Struct. Mol. Biol. 19, 1310-1315.

Zheng, Z., Gunner, A.R., 2008. Analysis of the electrochemistry of hemes with E(m)s spanning 800 mV. Proteins-Structure Function and Bioinformatics 75, 719-734.

2 CHARACTERIZATION OF THE SECOND CONSERVED DOMAIN IN THE HEME UPTAKE PROTEIN HTAA FROM *CORYNEBACTERIUM DIPHTHERIAE*

This chapter has been published verbatim in Rizvan C. Uluisik, Neval Akbas, Gudrun S. Lukat-Rodgers, Seth A. Adrian, Courtni E. Allen, Michael P. Schmitt, Kenton R. Rodgers, and Dabney W. Dixon. *Journal of Inorganic Biochemistry* 167 (2017) 124-133. The expression, purification, and UV-visible spectroscopy of the WT and mutants were performed at Georgia State University.

2.1 Abstract

HtaA is a heme-binding protein that is part of the heme uptake system in *Corynebacterium diphtheriae*. HtaA contains two conserved regions (CR1 and CR2). It has been previously reported that both domains can bind heme; the CR2 domain binds hemoglobin more strongly than the CR1 domain. In this study, we report the biophysical characteristics of HtaA-CR2. UV-visible spectroscopy and resonance Raman experiments are consistent with this domain containing a single heme that is bound to the protein through an axial tyrosine ligand. Mutants of conserved tyrosine and histidine residues (Y361, H412, and Y490) have been studied. These mutants are isolated with very little heme (≤ 5%) in comparison to the wild-type protein (~20%). Reconstitution after removal of the heme with butanone gave an alternative form of the protein. The HtaA-CR2 fold is very stable; it was necessary to perform thermal denaturation experiments in the presence of guanidinium hydrochloride. HtaA-CR2 unfolds extremely slowly; even in 6.8 M GdnHCl at 37 ºC, the half-life was 5 h. In contrast, the apo forms of WT HtaA-CR2 and the aforementioned mutants unfolded at much lower concentrations of GdnHCl, indicating the role

of heme in stabilizing the structure and implying that heme transfer is effected only to a partner protein in vivo.

Keywords: heme; hemin; hemoglobin; Raman; guanidinium; *Corynebacterium*

2.2 Abbreviations

ABC transporter, ATP-binding cassette transporter; CD, circular dichroism; CO, carbon monoxide; CR, conserved region; CT, charge-transfer; CV, column volume; DMSO, dimethyl sulfoxide; ELISA, enzyme-linked immunosorbent assay; ESI, electrospray ionization; FPLC, fast protein liquid chromatography; GdnHCl, guanidinium hydrochloride; Hb, hemoglobin; Hp, haptoglobin; HS, high spin; HSA, human serum albumin; IPTG, isopropyl β-D-1-thiogalactopyranoside; LS, low-spin; PMSF, phenylmethanesulfonyl fluoride; rR, resonance Raman spectroscopy; SDS-PAGE, sodium dodecyl sulfate polyacrylamide gel electrophoresis; TB, Terrific Broth; WT, wild-type; 5cHS, pentacoordinate, high-spin.

2.3 Introduction

Corynebacterium diphtheriae is an important Gram-positive human pathogen, causing upper respiratory tract infections in humans (Collier, 2001; Trost et al., 2012). Although vaccination is widely available in many countries, diphtheria infections still occur in parts of the world with low vaccine coverage (Wagner et al., 2012). Analysis of the full genome sequence (Trost et al., 2012) is consistent with a number of iron uptake systems in this organism. The iron and heme transporter systems are predicted to be coordinately expressed with the toxin (Schmitt, 1997a; Drazek et al., 2000; Schmitt and Drazek, 2001; Allen and Schmitt, 2015). This, along with the iron requirement for virulence, suggests that iron acquisition is a key component for pathogenicity. Approximately 80% of heme in vivo is found in hemoglobin (Hb) (Farrand and Skaar, 2014), leading to the role of this prosthetic group as a significant source of iron.

Gram-positive pathogens in general use heme as a key source of the iron required for survival and proliferation. Heme uptake pathways have been the subject of recent reviews (Benson and Rivera, 2013; Contreras et al., 2014; Farrand and Skaar, 2014; Rodgers and Lukat-Rodgers, 2014; Wandersman and Delepelaire, 2014; Wilks and O'Neill, 2014; Sheldon and Heinrichs, 2015). The majority of Gram-positive bacteria studied to date employ a series of NEAr-iron Transporter (NEAT) domains in many of the proteins involved in heme transport (Andrade et al., 2002; Honsa et al., 2014; Sheldon and Heinrichs, 2015). These domains are generally located in cell membrane-anchored proteins and serve to extract heme from Hb and haptoglobin-hemoglobin (Hp-Hb) and transfer it to additional heme-binding proteins, with final import through an ABC transporter. Classical NEAT domains comprise about 125 amino acids with a β-strand secondary structure; the canonical examples have a conserved YXXXY heme-binding motif, in which the N-terminal tyrosine of the sequence serves as an axial ligand to the heme and the C-terminal tyrosine is a hydrogen-bonding partner to the first. On the opposite side of the heme ring, a loop starts with a serine which hydrogen bonds to one of the heme propionates. The first system to be studied in detail was the iron-regulated surface-determinant (isd) pathway in *Staphylococcus aureus* (Mazmanian et al., 2003). Of the proteins in this pathway, IsdA, IsdB, IsdC and IsdH bind heme in NEAT domains; leading references can be found in recent work (Tiedemann et al., 2012; Pishchany et al., 2014; Zhu et al., 2014; Moriwaki et al., 2015; Sjodt et al., 2016). The heme uptake system in *Bacillus anthracis* also uses a series of NEAT domains for heme uptake (Honsa et al., 2011; Honsa and Maresso, 2011). In terms of the reliance on the NEAT architecture, uptake pathways studied to date involving Isd proteins in *Streptococcus lugdunenesis* (Zapotoczna et al., 2012) and *Listeria monocytogenes* (Xiao et al., 2011; Malmirchegini et al., 2014), Hal (Balderas et al., 2012) and BslK (Tarlovsky et al., 2010)

in *B. anthracis,* and IlsA in *Bacillus cereus* (Daou et al., 2009; Segond et al., 2014) all use a NEAT-domain strategy (Sheldon and Heinrichs, 2015). Heme uptake in *Streptococcus pyogenes* has also been studied in some detail. Here, the heme is abstracted from Hb via Shr (with two NEAT domains) (Lei et al., 2002; Ouattara et al., 2010; Ouattara et al., 2013) and then passed to Shp, a bis-methionine heme binding protein whose structure resembles the NEAT fold (Aranda et al., 2007).

C. diphtheriae is distinct from the other Gram-positive bacteria cited above in that the major heme acquisition pathway studied to date does not employ NEAT domains. The *hmu* gene cluster comprises two heme-binding surface-anchored proteins, HtaA and HtaB, along with a heme binding lipoprotein (HmuT) and an ABC-type heme transporter (HmuUV) (Allen and Schmitt, 2009; Allen and Schmitt, 2011; Allen et al., 2013; Allen and Schmitt, 2015; Draganova et al., 2015) (Fig. 2.1). HtaA is a 61-kDa, membrane-anchored protein containing two conserved regions, CR1 and CR2, with 50% sequence similarity (Allen and Schmitt, 2011); enzyme-linked immunosorbent assay (ELISA) experiments showed that HtaA binds Hb and is required for heme uptake from Hp-Hb (Allen and Schmitt, 2015). HtaB, a 36 kDa protein, has one CR domain that binds heme, but not Hb (Allen and Schmitt, 2011). HtaA can transfer hemin to HtaB in vitro (Allen and Schmitt, 2011; Allen et al., 2013). HmuT, a lipoprotein anchored to the cytoplasmic membrane, is thought to receive its hemin from either HtaB or HtaA and transfer it to the transmembrane permease HmuU, followed by translocation across the membrane in a process driven energetically by ATP hydrolysis catalyzed by the ATPase, HmuV (Allen and Schmitt, 2009). Deletion of the *htaA* gene, the *hmuTUV* genes or the complete *hmu* gene cluster resulted in significantly decreased growth in comparison to the wild-type (WT) strain when the cells were grown in the presence of Hb as the sole iron source. Recent studies have shown that heme uptake

from Hp-Hb necessitates the presence of one or two additional proteins, ChtA and ChtC, each of which has a single CR domain (Allen and Schmitt, 2015).

HtaA-CR1 and HtaA-CR2 are of interest because they take a position in the overall heme uptake strategy similar to that of the NEAT domains, yet have no significant sequence or structural homology to these more well-studied structures. Both HtaA-CR1 and HtaA-CR2 bind hemin; they bind Hb with less affinity than the complete HtaA, with the CR2 domain binding Hb more strongly than CR1 (Allen and Schmitt, 2011). The domains bind hemin-albumin (HSA), Hp-Hb, and myoglobin, with the binding to HtaA-CR2 being stronger than that to HtaA-CR1 in each case (Allen and Schmitt, 2015).

Sequence alignment of selected *Corynebacterium* CR domains shows that one histidine and two tyrosine residues are fully conserved (Y361, H412 and Y490 in HtaA-CR2) (Fig. 2.8) (Allen and Schmitt, 2011). Mutation of these conserved residues in HtaA-CR2 showed that all three are important for heme binding and uptake. For heme binding, the order was WT > Y490A > H412A ≈ Y361A. HtaA-CR2 Y361A was isolated with the lowest heme loading of the three mutants. Y361A also bound less Hb than either H412A or Y490A; the single amino acid substitutions Y361A and H412A in the full-length HtaA reduced Hb binding by almost 90%. In line with the hypothesis that Y361 is an axial ligand, mutation of this residue to alanine completely abolished the ability of the cells to use heme or Hb as iron sources. In addition, the GST-tagged CR2 Y361A mutant did not bind Hp-Hb, in contrast to the WT domain, which had an EC_{50} of 200 nM, nor did it bind heme-HSA, while the WT domain had an EC_{50} of 350 nM (Allen and Schmitt, 2015).

Given the crucial role of HtaA in heme acquisition by this important pathogen and, specifically, the second conserved domain with its presumably novel structural features, we have

undertaken a study of the biophysical characteristics of HtaA-CR2. Resonance Raman (rR) spectroscopy was used to probe structural and electronic features of the bound heme along with binding aspects of the heme pocket. The stability of the protein fold was investigated via chemical and thermal denaturation techniques.

2.4 Experimental

2.4.1 Site-directed mutagenesis

The HtaA-CR2 was previously constructed in pET24a(+) (Allen and Schmitt, 2009). Recombinant HtaA-CR2 mutants were made by site-directed mutagenesis by using a QIAprep Spin Miniprep Kit according to the manufacturer's instructions. The primers were from Sigma Aldrich for Y361A, H412A and Y490A substitutions (Table 2.1). Primers (500 ng) were mixed with 100 ng of pET24a(+) template plasmid in the reaction mixture. DpnI restriction endonuclease was used to remove the methylated template. The mutated plasmids were isolated from the reaction mixture and transformed into the competent *E. coli* strain BL21(DE3). Sequence analysis was used to confirm the mutations.

2.4.2 Expression and purification

Wild type and the mutant proteins were expressed and purified using the same protocol. Terrific Broth (TB) with the inclusion of 50 μg/ml kanamycin was used as the media. A small-scale culture was incubated at 37 ^{o}C/220 rpm for 16 h. This culture (10 ml) was inoculated into a large-scale culture (500 ml) and incubated at 37 ^{o}C/220 rpm until the OD_{600} reached 0.8. The cultures were induced by adding 50 μM isopropyl-β-D-thiogalactopyranoside (IPTG) and allowed to grow for 16 h. The cells were harvested by centrifugation at 3100 rpm/4 ^{o}C for 30 min. The pellets were collected and stored in a -80 ^{o}C freezer overnight.

The cell pellet was re-suspended in buffer A (100 mM Tris-HCl, 150 mM NaCl, pH 8.0). The cells were lysed on ice for 30 min in a buffer A solution containing 10 mM $MgCl_2$, 0.1 mM phenylmethanesulfonyl fluoride (PMSF), 0.2 mg/mL lysozyme, 5 µg/mL DNase I (from bovine pancreas, Roche) and 5 µg/mL RNase A (from bovine pancreas, Roche). The cells were treated with a cell disrupter, and cell debris was removed by centrifugation at 6500 rpm/4 ^{o}C for 30 min.

A GE Healthcare ÄKTA fast protein liquid chromatography instrument (FPLC) was used for purification at 4˚C. The HtaA-CR2 solution was loaded onto a Strep-Tactin Superflow column (5 mL, IBA BioTAGnology) which had been equilibrated with buffer A. Buffer A [5 column volumes (CV)] was used to wash the unbound material. The Strep-Tactin bound HtaA-CR2 protein was eluted with a linear gradient of 10 CV of buffer B (100 mM Tris-HCl, 150 mM NaCl, 2.5 mM *d*-desthiobiotin, pH 8.0). The purity of the fractions was tested by sodium dodecyl sulfate polyacrylamide gel electrophoresis (SDS-PAGE). Heme loading was approximately WT (20%), Y361A (1%), H412A (2%), and Y490A (5%).

2.4.3 Addition of hemin to apoHtaA-CR2

Four methods were used to add hemin to apoHtaA-CR2 in an effort to increase the heme loading. The first set of experiments involved preparation of fully apoHtaA-CR2 via the butanone extraction method (Teale, 1959). An HtaA-CR2 solution at a pH value of 2.0 was prepared by adding 1 M HCl dropwise. Equal amounts of the acidic HtaA-CR2 solution and ice-cold 2-butanone were mixed. The mixture was vortexed for approximately 30 s and set on ice. After a 30 min incubation, layers of aqueous apoprotein at the bottom and organic heme-butanone at the top were formed. The bottom solution was removed by a pipette and dialyzed against 20 mM Tris-HCl pH 7.0 at 4 °C overnight. A stock hemin solution was prepared by dissolving hemin in DMSO using the literature extinction coefficient (Collier et al., 1979). The concentration of

apoprotein was determined by using an ExPASy extinction coefficient (Gasteiger et al., 2005) of 24,075 $M^{-1}cm^{-1}$ at 280 nm. The apoHtaA-CR2 solution was titrated with the hemin solution by adding 1 μl aliquots; the solution was stirred for 30 min after each addition. At the end of the titration, the stoichiometric ratio of hemin and apoprotein was 1:1. Reconstituted HtaA-CR2 was dialyzed against 50 mM Tris-HCl pH 7.0 overnight. Reconstitution of the WT protein by this method gave a hemin-bound form that was spectrally distinct from the as-isolated protein.

The second set of experiments involved addition of hemin to the as-isolated protein (approximately 20% heme loaded). The protein was prepared in 50 mM Tris-HCl pH 7.0. A solution of hemin in DMSO was added in increments to a final ratio of hemin to apoHtaA-CR2 of ~ 1.5. The protein solution was equilibrated 30 min after each addition of hemin.

The third set of experiments involved hemin transfer from metHb on a column. Strep-tag purified HtaA-CR2 (a sample of 1 ml of about 70% apoprotein, 0.01 μmol apoHtaA-CR2, A_{Soret}:A_{280} ~ 0.6) in buffer A was loaded onto a 5 mL Strep-Tactin column. A metHb solution (equine, Sigma-Aldrich, 200 μM hemin) was prepared in buffer A (2 ml, approximately 0.4 μmol metHb subunits, 40-fold excess hemin) and loaded onto the column. The column was allowed to stand for 19 h at 4 ^{o}C. Excess Hb was removed by washing the column with 40 CV of buffer A. Fractions were checked by UV-visible spectroscopy to make sure the eluent was free of hemin and protein. Bound HtaA-CR2 was eluted with 100% buffer B. Approximately 0.0082 μmol holoHtaA-CR2 (A_{Soret}:A_{280} ~ 2.0) was obtained.

The fourth set of experiments involved attempted transfer from Hb in solution. Partially heme-loaded HtaA-CR2 (11.5 μM protein, 5.6 μM hemin) was titrated with human metHb. Additions of metHb to the initial solution (5.6 μM hemin, 0 μM from Hb), brought the total concentration of hemin to 9.6 μM (4 μM from Hb) and 12.1 μM (6.5 μM from Hb). Because the

major bands of the optical absorbance spectra overlap, Soret-excited (406.7 nm excitation) rR spectra were also recorded in order to track whether rR features of metHb disappeared in favor of those for holoHtaA-CR2.

2.4.4 Purification of apo- and holoHtaA-CR2

In another approach to isolating the holoprotein, a solution of Strep-tag purified HtaA-CR2 (A_{Soret}:A_{280} ~ 0.7) was initially passed through a 5-mL HiTrap Butyl FF hydrophobic interaction column (Fischer Scientific). The Butyl FF column was equilibrated with 5 CV of 20 mM NaH_2PO_4 at pH 7.0 followed by 5 CV of the binding buffer [20 mM NaH_2PO_4 and 1.5 M $(NH_4)_2SO_4$ at pH 7.0]. The sample was loaded and the column was washed with 5 CV of binding buffer. The elution was carried out with a decreasing linear gradient of ammonium phosphate (1.5 - 0 M). A single chromatographic peak was observed. Fractions showing heme absorbance were pooled to give a sample with a A_{Soret}:A_{280} ~ 0.9 (holoprotein recovery of 85%). After concentration and buffer exchange using an Amicon filter, the sample was passed through a Phenyl FF column using the same elution conditions. The chromatogram showed two overlapping peaks. The majority of the holoprotein was found at the start of the second peak (A_{Soret}:A_{280} ~ 2.0). The latter fractions from this peak were mainly apoprotein. This elution order is consistent with the apoprotein being more hydrophobic than the holoprotein. The fractions that contained significant holoprotein were pooled and concentrated. After passing through both hydrophobic columns, the A_{Soret}:A_{280} ratio increased from the as-isolated value of ~ 0.7 to ~ 2.0. Approximately 40% of the holoprotein was recovered from the initial sample after the two columns. Variations on this separation showed that although the Butyl FF column did not give a significant separation, protocols in which this step was omitted resulted in a lower final A_{Soret}:A_{280} ratio.

2.4.5 UV-visible and circular dichroism absorbance spectroscopy

UV-visible absorbance spectra were recorded either with a single beam (Varian Cary 50 Bio) or a dual beam scanning spectrophotometer (OLIS-14). The measurements were made using a quartz cuvette having a 1.0 cm path length. Circular dichroism (CD) spectra were recorded using a Jasco J-810 spectropolarimeter using quartz Suprasil cuvettes with a 1 mm path length. Protein samples were recorded in 10 mM KH_2PO_4 buffer at pH 7.0; concentrations were adjusted to 10 μM. The final spectra represent an average of 5 scans.

2.4.6 Time scale of unfolding

The UV-visible spectrum of HtaA-CR2 was monitored over time at 37 °C as a function of the GdnHCl concentration from 6.6 to 7.4 M. The protein and the GdnHCl solutions were prepared in 50 mM Tris-HCl, pH 7.0. The GdnHCl concentration was determined by the refractive index method (Pace and Scholtz, 1997). Absorbance measurements were recorded every 10 min for 24 h. The absorbance at 405 nm (A_{405}) vs. time was fit to a single-term exponential function: equation (1)

$$A_t = (A_0 - A_\infty)exp(-k_U t) + A_\infty \quad (1)$$

where A_t is the absorbance at any time during the unfolding reaction, A_0 is the initial absorbance, A_∞ is the absorbance of the completely unfolded protein, $(A_0 - A_\infty)$ is the total ΔA for complete unfolding, and k_U is the unfolding rate constant. These experiments were run on as-isolated holo/apo mixtures. A sample with 7.0 M GdnHCl (35% holo/65% apo) was dialyzed after unfolding to evaluate the reversibility of the process. Approximately 40% of the protein was recovered, perhaps because the apoprotein precipitated (apoprotein precipitation was also observed in other experiments). The recovered protein was about 25% heme loaded. The

spectrum of this holoprotein was similar, but not identical, to that of the original as-isolated holoprotein.

2.4.7 Thermal unfolding of HtaA-CR2 in presence of GdnHCl

Thermal unfolding of HtaA-CR2 was carried out with the UV-visible spectrophotometer equipped with a TC125 Quantum Northwest temperature controller. A screw-top quartz cuvette with 1-cm path length was used. Holo HtaA-CR2 in 50 mM Tris-HCl pH 7.0 was prepared in GdnHCl concentrations of 1.5, 1.75, 2.0, 2.5 and 3.0 M. The thermal unfolding was carried out from approximately 45 to 90 ^{o}C. The spectrum was recorded every 1 ^{o}C after a 1 min incubation at each temperature.

Kaleidagraph (version 4.01, Synergy Software) was used to fit the data using a two-state protein unfolding model equation (2) (Swint and Robertson, 1993):

$$A = \frac{(A_F + m_F T) + (A_U + m_U T) exp\left[\frac{\Delta H_m}{R(T_m^{-1} - T^{-1})}\right]}{1 + exp\left[\frac{\Delta H_m}{R(T_m^{-1} - T^{-1})}\right]} \quad (2)$$

where A is the absorbance at any temperature along the unfolding curve, A_F is the absorbance of the folded state, A_U is the absorbance of the unfolded state, m_F is the slope of A vs. T for the folded state, m_U is the analogous slope for the unfolded state, T_m is the temperature at which the protein is half unfolded, ΔH_m is the enthalpy of unfolding, R is the ideal gas constant, and T is the temperature (Kelvin).

2.4.8 Guanidinium-induced unfolding of HtaA-CR2 mutants

The guanidinium denaturation of HtaA-CR2 mutants (Y361A, H412A, and Y490A, all almost entirely in their apo forms) were investigated by following emission spectra on a Perkin Elmer

LS fluorescence spectrophotometer. Apo WT protein was isolated by chromatographic separation on a hydrophobic column. Its chemically-induced unfolding was followed using the single-cuvette titration technique (Arnesano et al., 1998; Wittung-Stafshede, 1999; Andersen et al., 2002; Roncone et al., 2005). The protein in 50 mM Tris-HCl pH 7.0 was excited at 285 nm and the emission spectrum was monitored between 300 and 500 nm. The emission intensity decreased as a function of GdnHCl concentration.

The unfolding curves were analyzed using equation (3) (Pace and Scholtz, 1997):

$$A = \frac{(A_F + m_F[D]) + (A_U + m_U[D]) exp\left[\frac{m([D]-[D]_{1/2})}{RT}\right]}{1 + exp\left[\frac{m([D]-[D]_{1/2})}{RT}\right]} \quad (3)$$

where A is the absorbance at any denaturant concentration along the fitted denaturation curve, A_F is the absorbance of the folded state, A_U is the absorbance of the unfolded state, m is the slope at the midpoint, m_F is the slope of the folded state, m_U is the slope of the unfolded state, [D] is the concentration of GdnHCl, $[D]_{½}$ is the concentration of GdnHCl at the midpoint of the unfolding curve, R is the ideal gas constant, and T is the temperature (Kelvin).

2.4.9 Resonance Raman spectroscopy

Resonance Raman scattering was excited with either 406.7- or 413.1-nm emission from a Kr^+ laser, or 441.6 nm from a HeCd laser. The laser beam was focused to a line parallel to the spectrograph entrance slit. Scattered light collected in the 135° backscattering geometry (f/1) was passed through a polarization filter, holographic notch filter, and polarization scrambler. The laser image was then focused on the entrance slit of a 0.67-m, f/4.7 Czerny-Turner spectrograph fitted with 1200 and 2400 g/mm gratings and a LN_2-cooled CCD detector (1340×400 array of

20×20 μm pixels, 26.8×8.0 mm^2 image area). The spectrometer was calibrated against the Raman shifts of toluene, dimethylformamide, acetone, and methylene bromide. Spectra were recorded at ambient temperature from samples contained in spinning 5-mm NMR tubes. UV-visible absorbance spectra were recorded from the rR samples before and after spectral acquisition to assess whether sample integrity had been compromised by exposure to the laser beam. Laser power at the samples ranged from 5 to 10 mW.

2.4.10 Electrospray ionization (ESI) mass spectrometry

ESI spectra were obtained using a Waters Micromass Q-TOF spectrometer in the positive mode. The fully holoprotein was prepared by adding of hemin to the as-isolated protein (approximately 20% heme loaded) as previously described. The protein solution (10 μM) was then dialyzed against 20 mM ammonium acetate, pH 6.8. Spectra were recorded (flow rate 10 μl/min) at the following collision energy voltages: 5, 10, 15, 20, 25, 30, and 40 V. All other parameters were held constant (capillary voltage 3000 V, cone voltage 18 V, extraction voltage 1.5 V, desolvation gas temperature 100 ^oC and source temperature 80 ^oC). Deconvolution of the charged state was performed using the MaxEnt program with the MassLynx™ software. Peaks were rounded to the nearest Dalton; peak heights were used to calculate holoprotein percentages.

2.5 Results

2.5.1 HtaA-CR2 spectroscopy

The UV-visible absorbance spectrum of as-isolated ferric HtaA-CR2 is shown in Fig. 2.2A. The Soret maximum is at 405 nm, and bands are seen in the visible region at 502, 537, and 624 nm. The charge-transfer (CT) band at 624 nm is characteristic of high-spin heme, common for axial tyrosine ligation (Du et al., 2011; Tiedemann and Stillman, 2011). The ferric protein was reduced smoothly, albeit slowly, with dithionite ion ($S_2O_4^{2-}$) to give the ferrous species with a Soret at

424 nm and α/β bands at 544 and 569 nm. The reduction took ca. 30 min at pH 7.0 and ambient temperature without significant side products, as evinced by the isosbestic behavior of the visible absorbance spectra in Fig. 2.9 The addition of CO gave the ferrous carbonyl species with a Soret band at 415 nm (Fig. 2.2A).

Soret-excited rR spectra were recorded from the ferric, ferrous and ferrous carbonyl heme complexes of HtaA-CR2. Fig. 2.2B shows spectra in the frequency region of the porphine in-plane skeletal modes. The largest band in this region arises from the totally symmetric core breathing mode, ν_4, which occurs near 1370 cm^{-1} for the ferric oxidation state and ferrous π-acid complexes, such as heme carbonyls (Sharma et al., 1989; Jin et al., 2004; Eakanunkul et al., 2005). The ν_4 band in ferrous hemes falls near 1360 cm^{-1} (Lukat-Rodgers et al., 2008). The ν_4 frequencies are consistent with ferric (a), ferrous (b) and ferrous carbonyl (c) hemes, respectively. The ν_3 bands fall in Raman shift regions characteristic of both oxidation and spin states of the iron center, with those of ferric (1490 cm^{-1}) and ferrous (1473 cm^{-1}) HtaA-CR2 falling at frequencies consistent with pentacoordinate, high-spin (5cHS) iron centers (Sharma et al., 1989; Jin et al., 2004; Eakanunkul et al., 2005). The 1501-cm^{-1} ν_3 band in the HtaA-CR2-CO spectrum is typical of the low-spin (LS) heme carbonyl complexes (Lukat-Rodgers et al., 2008).

The spectral features of ferric HtaA-CR2 are essentially independent of pH between 5.8 and 9.5, as seen in the similarity among the rR spectra in Fig. 2.10. Furthermore, there were no ^{18}O- or ^{2}H-sensitive bands in the low-frequency spectrum at pH 9.8 (data not shown), as would be expected if a hemin hydroxide were forming in alkaline solution (Eakanunkul et al., 2005). The ν_{Fe-CO} and ν_{C-O} regions of the heme carbonyl spectrum are shown in Fig. 2.3. Isotope sensitivity of the 535-, 572- and 1949-cm^{-1} Raman shifts in the ^{13}CO isotopolog allow their assignments to the ν_{Fe-CO}, δ_{FeCO} and ν_{C-O} modes, respectively. The backbonding correlation plot

in Fig. 3C shows that the as-isolated HtaA-CR2-CO is homogeneous and falls on the line correlating heme carbonyls having a charge neutral *trans* O-bound ligand (Linder et al., 2014).

2.5.2 Approaches to holoprotein

As-isolated, HtaA-CR2 was only ~20% heme loaded. As more fully heme-loaded protein was desirable for the biophysical studies, various approaches were used to increase the amount of holoprotein in the sample. Passing the protein through two hydrophobic columns resulted in protein that was about 95% heme loaded. However, loss of protein in this lengthy procedure led to additional efforts to prepare samples with high heme loading. Full-length HtaA can take up hemin from Hb (metHbA) as previously demonstrated by UV-visible spectroscopy (Allen and Schmitt, 2011). Those experiments involved binding of 100 µl of 30 µM as-isolated Strep-tag-labeled HtaA to a column, incubation with an equivalent volume of 30 µM Hb for 30 min, and isolation of the resulting HtaA. The heme loading had increased. An ELISA assay showed that both HtaA and the CR2 domain were able to bind Hb.

Transfer of hemin from metHb to HtaA-CR2 on a preparative scale was examined in this study as a means of generating more completely heme-loaded HtaA-CR2. As-isolated protein was loaded on a Strep-Tactin column. A metHb solution containing 40× excess of hemin was loaded into the column void volume and remained in contact with the HtaA-CR2-loaded resin for 19 h. After isolation, the amount of holoHtaACR-2 had increased approximately two-fold. It is clear from this significant increase in cofactor loading that hemin is passed from metHb to HtaA-CR2 when the HtaA-CR2 is bound to the affinity column.

The hemin transfer reaction was also examined in solution with 5.9 µM apoHtaA-CR2 (in a mixture with 5.6 µM holoprotein) and human metHbA (concentrations of 0, 4.0 and, 6.5 µM heme). Fig. 2.11 shows the UV-visible absorbance (A) and Soret-excited rR spectra (B) of those

reaction mixtures. Examination of the starting HtaA-CR2 Raman spectrum reveals ν_3 at 1490 cm^{-1} and a relatively large ν_3:ν_4 intensity ratio, consistent with the hemin being 5cHS with an O-bound axial ligand. If titration with metHbA were to transfer hemin efficiently to HtaA-CR2, a simultaneous and proportionate increase in all its band intensities would be expected. However, the ν_3:ν_4 intensity ratio decreased with each addition of metHbA while the porphine core marker bands reporting oxidation and spin states shifted monotonically toward their metHbA frequencies. Additionally, the UV-visible absorbance spectra contained bands attributable to a mixture of metHbA and hemin-loaded HtaA-CR2. Thus, significant transfer of hemin from metHbA to HtaA-CR2 was not observed in solution under dilute and near-stoichiometric conditions.

Finally, hemin loading could also be effected by titrating the as-isolated protein with hemin itself in DMSO to give a sample that was ~50% heme loaded. The spectra of holoHtaA-CR2 obtained via all of these procedures are shown in Fig. 2.12. The spectra are similar, but not identical. This observation may reflect mixtures of more than one conformation of the protein. Some of the HtaA-CR2 may also contain protoporphyrin rather than hemin. This has been observed in previous studies involving isolation of recombinant heme proteins (Pluym et al., 2007; Sudhamsu et al., 2010). Consistent with this idea, an electrospray mass spectrum of HtaA-CR2 showed peaks for both protoporphyrin and hemin in the low molecular weight region and an HtaA-CR2 solution extracted with butanone showed a fluorescence peak appropriate for protoporphyrin (Ricchelli et al., 1991) (data not shown).

2.5.3 Reconstitution after full unfolding: A second form of HtaA-CR2

The classic approach to reconstitution of a heme protein is to remove all tetrapyrroles using the butanone extraction method (Teale, 1959) and then reconstitute the apoprotein with hemin

dissolved in DMSO. The UV-visible absorbance spectrum of HtaA-CR2 reconstituted in this manner was distinct from that of the as-isolated protein, with its Soret band being shifted to higher energy, the appearance of a shoulder at 370 nm, and broadening and shifting of the α/β bands (Fig. 2.12). Additionally, whereas the as-isolated protein could be reduced with dithionite at pH 7, the reconstituted protein could only be reduced under an atmosphere of CO. This method has been used to prepare ferrous heme carbonyls of proteins having highly negative reduction potentials; e.g., WT *Serratia marcescens* HasA-CO (heme reduction potential of −550 mV) and HasA mutants with reduction potentials of approximately −350 mV and lower (Lukat-Rodgers et al., 2008). The fact that this technique was necessary to reduce reconstituted HtaA-CR2 is consistent with it having a significantly negative reduction potential, which is in turn consistent with an axial tyrosinate ligand in the ferric state. CD spectra of the apoHtaA isolated via hydrophobic interaction chromatography and via butanone treatment were also different (Fig. 2.13), in line with the observations on the holoprotein.

Although the UV-visible spectra of the as-isolated and protein reconstituted after full unfolding were different, the Soret-excited rR spectrum of reconstituted ferric HtaA-CR2 (data not shown) was similar to that of the as-isolated protein, exhibiting features characteristic of a 5cHS form. Moreover, the large I(ν_3):I(ν_4) ratio of 0.70 (Eakanunkul et al., 2005) and its lack of spectral sensitivity to changes in pH argue for the hemin being bound to the protein through an O-bound axial ligand, such as the phenol side chain of Tyr (Draganova et al., 2015). By contrast, the rR spectrum of the ferrous carbonyl form of reconstituted HtaA-CR2 was distinct from that of its as-isolated counterpart. The correlation plot (Fig. 2.3C) reveals two forms of the reconstituted HtaA-CR2-CO complex; one very close to the as-isolated point with $\nu_{Fe–CO}$ and $\nu_{C–O}$ frequencies of 536 and 1947 cm^{-1}, respectively, and the second with frequencies of 497 and

1947 cm^{-1}, putting it on the plot near the correlation line for a *trans* histidine ligand. This indicates that there are two forms of ferrous-CO species, one with *trans* histidine and the other with a *trans* O-bound ligand such as tyrosine or water. These spectral and chemical differences indicate that addition of hemin to apoHtaA-CR2 created via butanone extraction yields a different form of the holoprotein than that isolated after purification. For consistency, the biophysical studies reported herein were all performed on samples of the as-isolated HtaA-CR2, without unfolding of the protein or addition of hemin in the laboratory.

2.5.4 Time scale of protein unfolding in chemical denaturation

HtaA-CR2 is quite stable to treatment with denaturing agents and heat. GdnHCl-induced unfolding of HtaA-CR2 was not observed at room temperature over many hours for denaturant concentrations up to 4 M. Even at 7.0 M GdnHCl, the protein was not completely unfolded after 24 h at ambient temperature. The unfolding was then evaluated as a function of GdnHCl at 37 ^{o}C. At each concentration, the unfolding curve was well modeled by a single-term exponential decay function, suggesting a single first-order unfolding process (Fig. 2.4). At the indicated GdnHCl concentrations, the unfolding half-lives were: 6.6 M (330 min), 6.8 M (300 min), 7.0 M (260 min), 7.2 M (250 min), and 7.4 M (215 min) GdnHCl. Fig. 2.14 shows the dependence of the unfolding rate constant, k_u, on the concentration of GdnHCl. A rate constant at 37 °C in the absence of denaturant of $1.3 \pm 0.1 \times 10^{-6}$ s^{-1} ($t_{1/2}$ = 144 h) was calculated by extrapolation to the *y*-intercept.

2.5.5 Thermal unfolding of HtaA-CR2 in the presence of GdnHCl

Thermal denaturation was monitored in the presence of increasing amounts of GdnHCl. As the temperature was increased, the Soret absorbance gradually decreased and shifted about 12 nm to higher energy (data not shown). The protein solutions were cooled to room temperature at the

end of each experiment. Around 30% of the original Soret absorbance was recovered in solutions of 1.5 and 1.75 M GdnHCl. No recovery was observed in solutions in which the concentration of GdnHCl was greater than 1.75 M. Because the protein was so stable (i.e., not fully reaching equilibrium at each temperature), only apparent T_m values could be calculated. For example, at 1.5 M denaturant, the apparent T_m was 77 ^oC (Fig. 2.5). Extrapolation of a plot of T_m vs. the concentration of GdnHCl to zero denaturant concentration suggests an apparent intrinsic T_m of 84 ^oC for HtaA-CR2 (Fig. 2.15).

2.5.6 Guanidinium-induced unfolding of apoHtaA-CR2 and its mutants

Fluorescence spectroscopy was used to gain insight into the stability of the apoprotein forms of WT HtaA-CR2 and its mutants. Tryptophan emission was monitored as a function of the concentration of GdnHCl. Fig. 2.6 shows a representative example of the unfolding curve of apo Y490A. The midpoint denaturation concentrations were 1.34 ± 0.02 M for apo WT HtaA-CR2 and 1.25 ± 0.02, 1.28 ± 0.01, 1.41 ± 0.01 M for Y361A, H412A and Y490A, mutants, respectively.

2.5.7 ESI Mass spectrometry

The stability of the holoprotein was also evaluated using mass spectrometry. The mass spectrum of a fully holo WT sample was recorded as a function of collision voltage from 5 - 40 V. The observed percentage of holoprotein decreased from approximately 70% to approximately 20% (Fig. 2.7). The as-isolated mutants had less than 5% heme, and so were not studied with this method.

2.6 Discussion

2.6.1 HtaA-CR2 axial ligands

Sequence alignment indicates three probable axial ligands that are completely conserved in HtaA *Corynebacterium* sequences: Tyr361, His412, and Tyr490. Previous experimental data indicate that Y361 is more likely than Y490 to be the axial ligand (Allen and Schmitt, 2011). Sequence alignment of a variety of homologous proteins is in line with this expectation, as the region around Y361 shows greater conservation than the region around Y490. Optical spectroscopy of WT HtaA-CR2 shows three bands in the α/β region. This three-banded pattern, with a band near 630 nm, is characteristic of a tyrosine axial ligand as found in various heme uptake proteins in a variety of species (Table 2.2).

Consistent with the UV-visible spectral pattern, several aspects of the rR spectrum support a 5cHS hemin with an axial Tyr ligand. First, the ν_3 and ν_4 frequencies of 1490 and 1372 cm^{-1} are indicative of ferric 5cHS hemin (Sharma et al., 1989; Jin et al., 2004; Eakanunkul et al., 2005). Second, the high I(ν_3):I(ν_4) ratio is characteristic of an O-bound axial ligand. Although this spectral fingerprint is well established in a number of 5cHS Tyr-bound hemins (Ho et al., 2007; Jepkorir et al., 2010; Draganova et al., 2015), the possibility of a 5cHS aqua or hydroxo complex could not be excluded based solely on the spectrum of the WT protein. Therefore, rR spectra of HtaA-CR2 were recorded at high pH and pD in $^{18}OH_2$ and OD_2 to determine whether there were any isotope-sensitive bands in the $\nu_{Fe–OH}$ region of the spectrum. The lack of ^{18}O- or ^{2}H-sensitive bands further supports the conclusion that the O-bound axial ligand is endogenous. Third, the insensitivity of the HtaA-CR2 spectrum to pH is consistent with an axial Tyr ligand (Eakanunkul et al., 2005). Finally, ferric hemin protein complexes having axial Tyr ligands are well known for their negative reduction potentials. Those complexes are generally either slow to

reduce in the presence of $S_2O_4^{2-}$ or simply do not reduce unless a strongly-coordinating ligand that favors Fe(II) over Fe(III), such as CO, is present to drive the reduction (Lukat-Rodgers et al., 2008). HtaA-CR2 exhibits this behavior, being only slowly reduced in the presence of excess $S_2O_4^{2-}$ at pH 7 (Fig. S2.2).

The observation of Allen and Schmitt that mutation of H412 makes as much of a difference in heme binding as mutation of Y361 (Allen and Schmitt, 2011) is consistent with H412 playing a role in the heme pocket. In the current study, run on a larger scale with FPLC purification of the proteins, the Y361A and H412A mutants bound only 1-2% heme; Y490A was somewhat more heme loaded (consistent with this residue not being involved directly with heme binding). Many proteins in heme-uptake pathways with tyrosine as an axial ligand have a hydrogen-bonding partner in the binding pocket (Draganova et al., 2015). In some instances mutation of the hydrogen-bonding partner has been shown to have a very large effect on heme binding, e.g., removal of the H-bonding partner H83 in the *S. marcescens* hemophore HasA resulted in a loss in heme affinity of more than 2500-fold (Deniau et al., 2003). In other instances, the effect is small, e.g., mutation of the H81 hydrogen-bonding partner in *Pseudomonas aeruginosa* HasA did not change the heme association constant (Kumar et al., 2014). These data are consistent with many factors being important in controlling heme binding, including van der Waals, salt bridging, π-stacking and other hydrogen-bonding interactions. Even though a given interaction may not play a decisive role in controlling the heme affinity, it may be mechanistically important in the transfer of the heme to the cognate acceptor.

2.6.2 Reconstituted HtaA-CR2

The significant 370-nm absorbance in the UV-visible spectrum of HtaA-CR2 reconstituted with hemin itself is consistent with binding of a π-stacked heme dimer. Although we have not pursued

structural characterization of this complex, the suggestion of complex with dimeric heme has considerable precedence. Hemin readily forms π-stacked as well as μ-oxo dimers in solution (Asher et al., 2009; Kuter et al., 2012). X-ray data have shown that *Yersinia pestis* HmuT can bind heme as a π-stacked dimer; this form of the holoprotein had an absorbance band at 373 nm in solution (Mattle et al., 2010). X-ray data has also shown that *Mycobacterium tuberculosis* MhuD has the ability to bind π-stacked heme, although this complex is enzymatically inactive (Graves et al., 2014). Finally, π-stacked dimers have been found at the interface between two heme trafficking proteins in the crystal structures of ChaN from *Campylobacter* (Chan et al., 2006), IsdH from *S. aureus* (Watanabe et al., 2008), and Shp from *S. pyogenes* (Aranda et al., 2007).

2.6.3 Heme transfer from Hb to HtaA-CR2

Hemoglobin serves as a source of heme for *C. diphtheriae*; mutations in the *htaA* gene reduce the ability of the organism to employ Hb as an iron source (Allen and Schmitt, 2009). Hemin can be transferred from Hb to HtaA as shown previously on a small scale (Allen and Schmitt, 2011) and in this work as a possible preparative procedure for holoHtaA-CR2.

In contrast, significant hemin transfer from Hb to HtaA-CR2 was not observed at lower concentrations of the proteins in solution. These experiments were run over ~ 2 h with an initial ratio [metHb]/[apoHtaA-CR2] of 0.7 and a final ratio of 1.1 (6.5 μM hemin in Hb). In comparison, the affinity column experiments were run for 19 h with a [metHb]/[apoHtaA-CR2] ratio of approximately 40. As the value of K_d for tetrameric metHbA is 1.5×10^{-6} M (Edelstein et al., 1970; Hargrove et al., 1997) both experimental conditions (6.5 μM and 200 μM hemin in metHb) give rise to mixtures of dimer of αβ (1.2 and 8.3 μM αβ dimer, respectively) and $(\alpha\beta)_2$ tetramer [1.0 and 46 μM $(\alpha\beta)_2$ tetramer, respectively]. The role of the dimer is significant

because the hemin dissociation rate constants for the α chain are 0.6 and 0.3 h^{-1} in the dimer and tetramer, respectively; the corresponding rate constants for the β chain are 15 and 1.5 h^{-1} (Hargrove et al., 1997). The tetramer to dimer conversion is rapid (1 – 10 sec^{-1}) and autoxidation of Hb is facile outside erythrocytes (Hargrove et al., 1997). Although hemin transfer may occur within the complex (the K_d value of HbA:HtaA-CR2 is approximately 300 nM (Allen et al., 2013)), these rate constants for loss of hemin from Hb are fast enough to be consistent with passive loss of the prosthetic group from either the tetramer or the dimer followed by HtaA-CR2 uptake from solution on the time scales of these experiments. It is possible that the heme transfer observed in the affinity column experiments can be largely explained by longer contact times with the Hb and differences in the [αβ]/[apoHtaA] ratios. The microenvironment on the column may also be conducive to heme transfer. By contrast, the spectroscopically (UV-vis and rR) tracked reactions carried out at lower metHb concentration in solution were too slow to affect a similar passive transfer during the window of observation.

2.6.4 Comparison of the holo and apo forms of HtaA-CR2

As noted above, holoHtaA-CR2 is exceptionally stable, with unfolding incomplete even after 24 h in 7 M GdnHCl at 37 ^{o}C. In stark contrast, apoHtaA-CR2 unfolded readily, with a midpoint for unfolding of 1.34 ± 0.02 M at room temperature. The mutants behaved similarly, with $D_{1/2}$ values ranging only from 1.25 to 1.41 M for the Y361A, H412A and Y490A mutants. Thus, heme plays a deterministic role in the stability of the protein fold.

The importance of the full HtaA-CR2 structure for binding the heme tightly is also seen in the fact that all three mutants were isolated with at most 5% bound heme, in comparison with the WT protein, which had about 20% heme loading. Mutation of axial ligands need not lead to such a dramatic loss in heme binding for *b*-type heme uptake proteins. For example, as-isolated

holoprotein with mutated axial ligands can be purified for *C. diphtheriae* HmuT (Draganova et al., 2015), *P. aeruginosa* HasA (Jepkorir et al., 2010), *S. pyogenes* SiaA/HtsA (Sook et al., 2008) and *S. pyogenes* Shp (Ran et al., 2013).

2.6.5 Thermal and chemical denaturation

HtaA-CR2 exhibits very high stability. Even in 6.8 M GdnHCl at 37 ^{o}C, the half-life for protein denaturation was 5 h. The only other non-hyperthermophilic heme proteins of which we are aware that are approximately as stable as HtaA-CR2 are the Class III plant peroxidases (Amisha Kamal and Behere, 2008; Bernardes et al., 2015). For example, soybean peroxidase has a half-life for denaturation of 3.3 h at 25 ^{o}C in 6.8 M GdnHCl (Amisha Kamal and Behere, 2008). Horseradish peroxidase unfolds approximately 300 times more quickly under these conditions.

The origin of hyperstability is multifaceted and includes hydrogen-bonding, internal packing of hydrophobic residues, optimization of salt bridges, and factors that restrict flexibility (including dimerization) (Vieille and Zeikus, 2001; Sanchez-Ruiz, 2010; Wijma et al., 2013). Significant stability in heme transfer proteins presumably protects the organism from the deleterious effects of reactive oxygen species produced in the presence of free hemin and also allows the hemin to be transferred to a specific partner protein. Proteins in heme uptake pathways may have evolved very stable heme-bound folds so that heme cannot be released spontaneously or during non-specific encounters with other bio-macromolecules. This stability may reflect a mechanistic requirement for heme transfer to be "triggered" by the formation of a highly specific protein-protein complex with the appropriate heme-accepting partner wherein the heme would be available for transfer. A number of studies have led to the conclusion that transient protein-protein complexes are involved in heme transfer including investigations of the pathways from Shp to HtsA in *S. pyogenes* (Liu and Lei, 2005; Nygaard et al., 2006); in the Isd

proteins of *S. aureus* (Muryoi et al., 2008; Villareal et al., 2011; Abe et al., 2012); from IsdX1 to IsdC and IsdX2 (Fabian et al., 2009) and BslKN to IsdC (Tarlovsky et al., 2010) in *B. anthracis*; and from Hbp1 to Hbp2 in *L. monocytogenes* (Malmirchegini et al., 2014).

2.6.6 Mass spectrometry

When the collision voltage was increased from 5 - 40 V, holo HtaA-CR2 lost about 70% of its heme. By comparison, previous studies on HmuT, another protein in the pathway, showed only 10% heme loss over this collision voltage range (Draganova et al., 2015). HmuT had a T_m of 67 ^oC in buffer without denaturant while HtaA had essentially the same T_m (specifically, 69 ^oC) only in buffer with 3.0 M GdnHCl. The gas phase and solution phase data do not show a direct correlation, but give complementary information on protein stability, as also observed in previous studies on myoglobin and cytochrome b_5 (Hunter et al., 1997).

2.7 Conclusions

The UV-visible absorbance spectra of as-isolated ferric HtaA-CR2 as well as the Raman spectra, including placement on the ferrous-CO back bonding plots, are consistent with a tyrosine axial ligand. In that the H412A mutant also has very low heme loading, and shows significant reduction of Hb binding compared to WT, this residue may play a role in the heme pocket, perhaps as the hydrogen-bonding partner to Y361 or elsewhere near the heme. Reconstitution of WT HtaA-CR2 with hemin gave a different form of the protein. Transfer of hemin from Hb depended on the conditions of the experiment, being favored in on-column protocols at hundreds of micromolar metHb subunit concentrations. HtaA-CR2 is highly stable. In chemical denaturation experiments, no unfolding was observed even up to 4 M GdnHCl over 24 h at room temperature. At higher concentrations of GdnHCl (6.6 – 7.4 M), a single unfolding process was observed at 37 ^oC. The protein was also stable to heat; it was necessary to perform thermal

denaturation experiments in the presence of GdnHCl (1.5 – 3.0 M). In contrast, the apo forms of the WT protein and the mutants unfolded readily, suggesting that the bound heme is playing a significant role in the stability of the protein. The very high stability of the holoprotein may protect the bacteria against adventitious loss of heme during the uptake process. HtaA-CR2 joins other heme uptake proteins, such as many of those with NEAT domains, in using a tyrosine as the axial ligand. Changes in the hydrogen-bonding of an axial tyrosine may be employed to promote heme transfer to the next protein in the pathway.

2.8 Corresponding Authors

*Department of Chemistry, Georgia State University, Atlanta, Georgia 30302-3965. Phone: 404-413-5508. Fax: 404-413-5505. E-mail: ddixon@gsu.edu.

*Department of Chemistry and Biochemistry, North Dakota State University, Fargo, North Dakota 58108-6050. Phone: 701-231-8746. Fax: 701-231-8831. E-mail: Kent.Rodgers@ndsu.edu.

2.9 Funding Sources

This work was supported by the National Institutes of Health Grants AI072719 (to K.R.R.), GM094039 (to G.L.R.) the Research Corporation (to D.W.D.) and the Molecular Basis of Disease Program at Georgia State University (R.C.U.)

2.10 Acknowledgments

We thank John H. Dawson and Daniel P. Collins for contributions to the preliminary data. We also thank Siming Wang for technical assistance with the mass spectrometry experiments and insightful discussions.

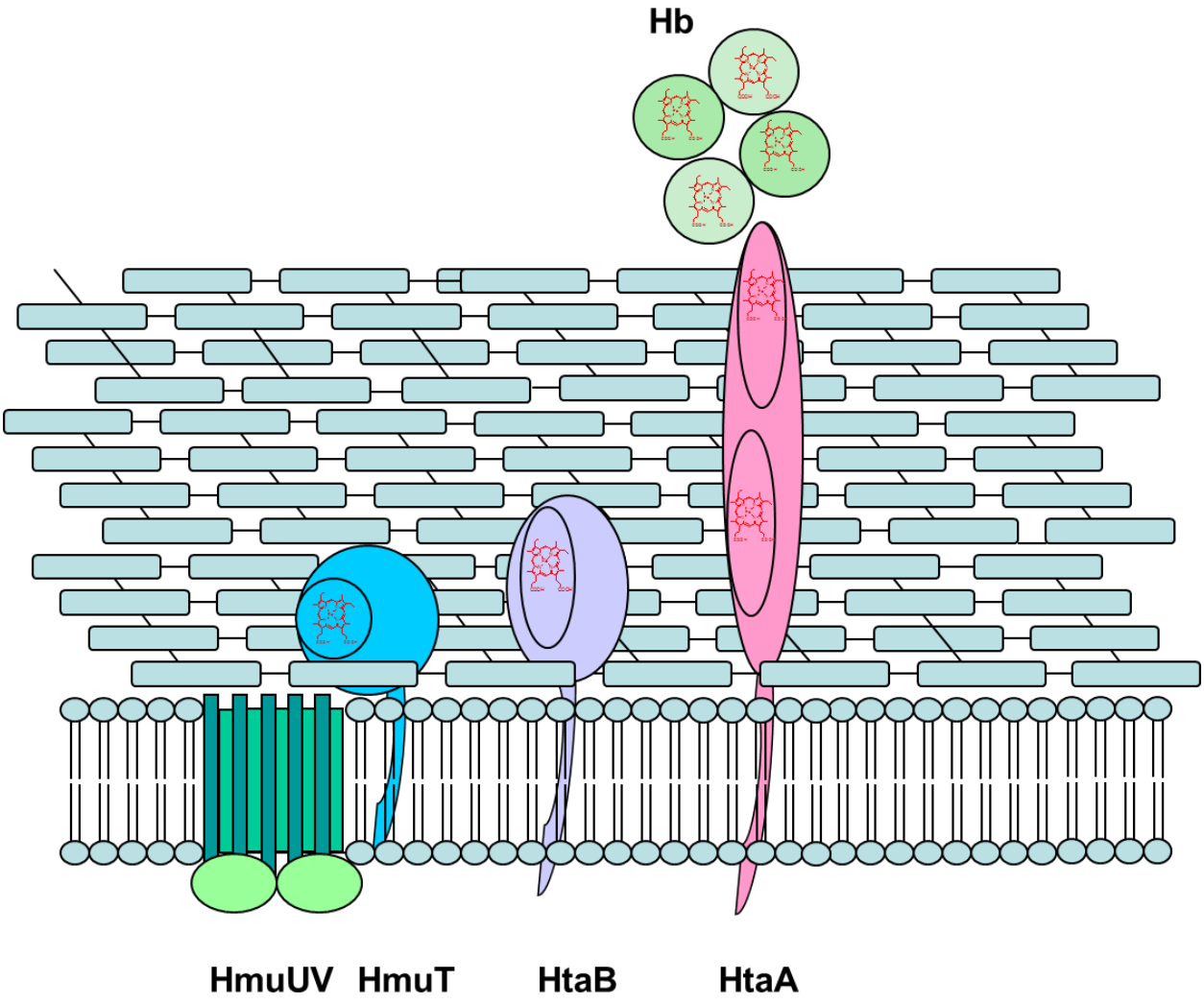

Figure 2.1 Schematic of heme uptake proteins in the *hmu* pathway of *C. diphtheriae*.

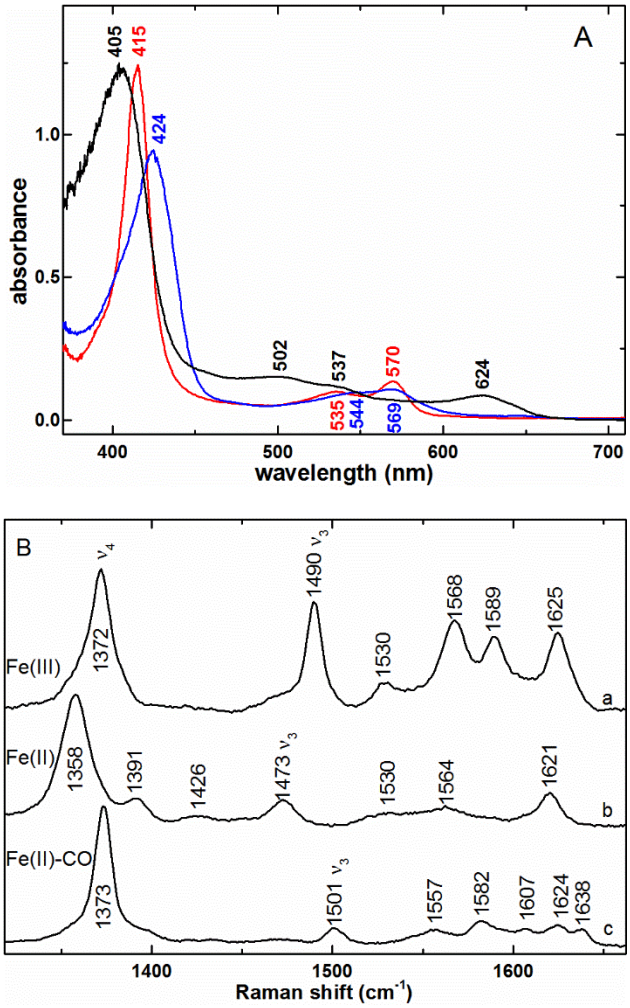

Figure 2.2 A) UV-visible spectra of ferric (black ─), ferrous (blue ─), and ferrous carbonyl (red ─) complexes of HtaA-CR2.

The ferric and ferrous carbonyl samples were in 50 mM Tris-HCl pH 7.0; the ferrous HtaA-CR2 was in 50 mM Tris-HCl pH 7.0. B) High-frequency rR spectra of a) ferric HtaA-CR2, 406.7 nm excitation, b) ferrous HtaA-CR2, 413.1 nm excitation, and c) ferrous-CO HtaA-CR2 complex, 413.1 nm excitation, under the same buffer conditions listed in A. Laser powers incident on the sample for a and b were 5 - 8 mW while c was acquired with 2.5 mW.

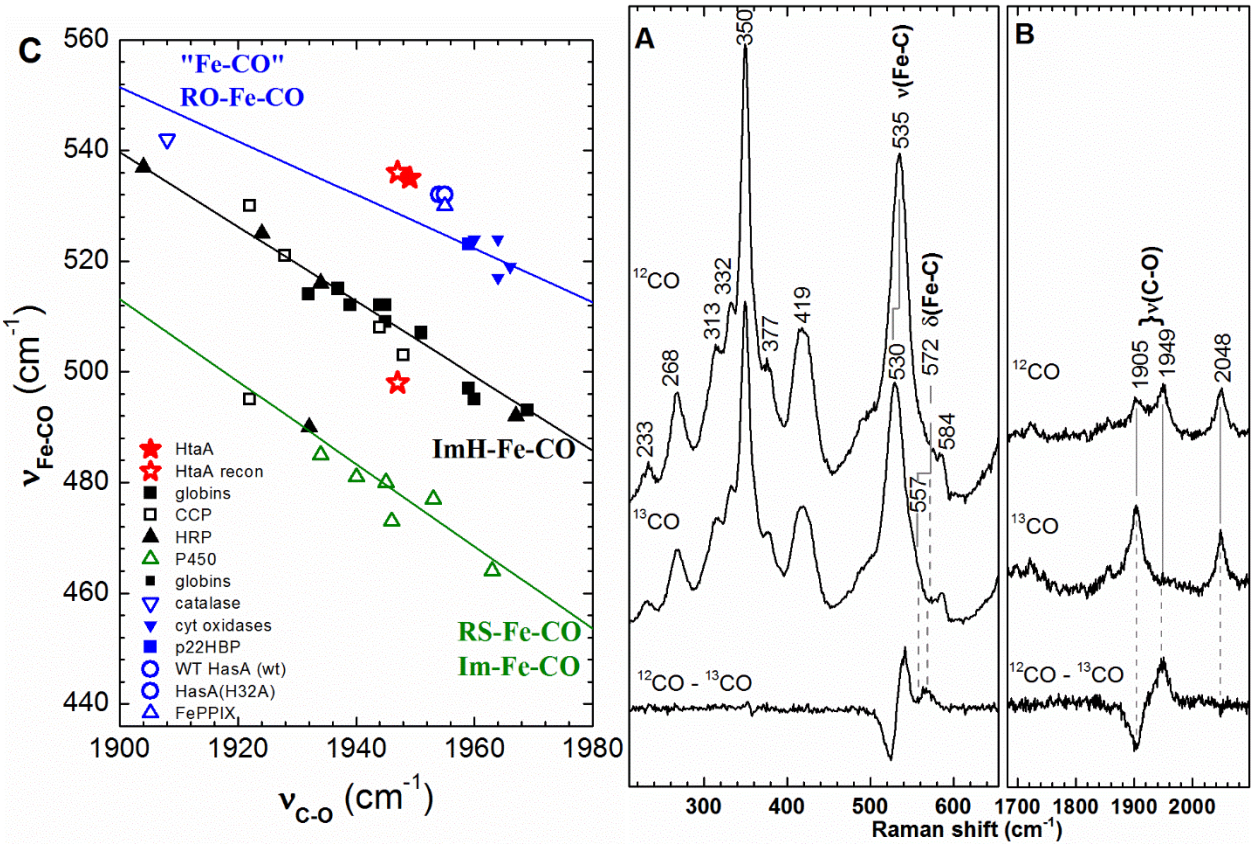

Figure 2.3 Resonance Raman characterization of the ferrous HtaA-CR2 carbonyl complex.

A) Low frequency region and B) C-O stretching region of the rR spectra of the isotopomers of HtaA-CR2-CO recorded using 413.1 nm: HtaA-CR2-^{12}CO (top), HtaA-CR2-^{13}CO (middle) and difference [HtaA-CR2-^{12}CO - HtaA-CR2-^{13}CO] (bottom) spectra. The ferrous carbonyl complex was prepared in 50 mM Tris-HCl pH 7.8. C) The ν_{Fe-CO}/ν_{C-O} correlation plot of ferrous carbonyl proteins with the as-isolated HtaA-CR2-CO indicated by a solid red star. Reconstituted HtaA-CR2-CO is a mixture of two heme carbonyl species, indicated by open red stars. One is near the point for the as-isolated protein, and the other is near the black line for heme carbonyls having *trans* imidazole ligands. The green line is the least squares line for six-coordinate Fe−CO adducts in which the proximal ligand is thiolate or imidazolate and the blue line represents a compilation of model complexes and heme proteins, wherein the ligand *trans* to CO is likely to charge neutral and coordinated through an oxygen atom (Linder et al., 2014).

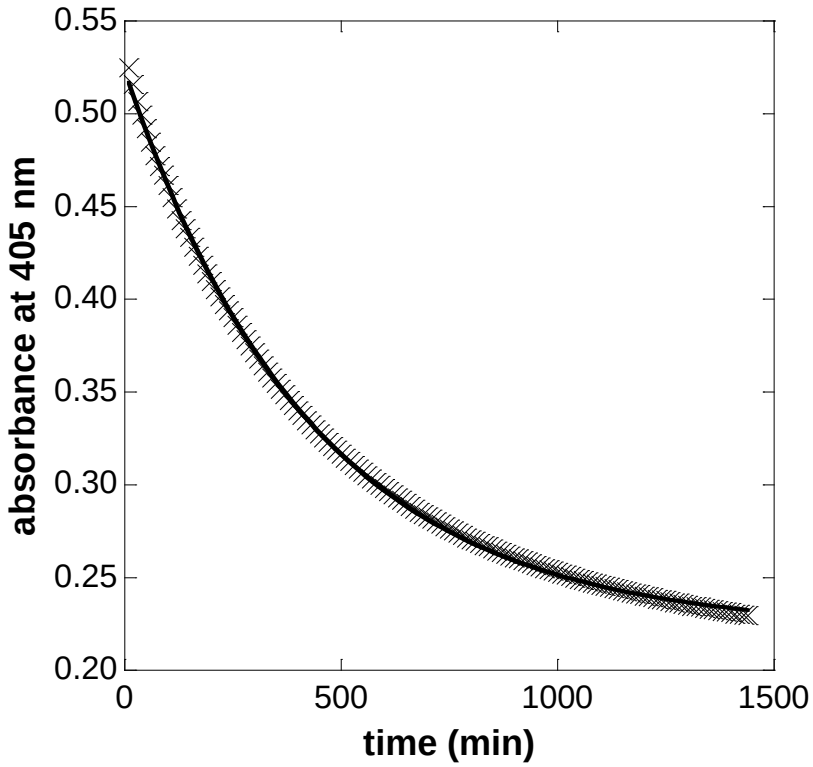

Figure 2.4 Time scale of WT HtaA-CR2 unfolding in the presence of 6.8 M GdnHCl.

The unfolding reaction was carried out in 50 mM Tris-HCl pH 7.0. The data were fit using the single-term exponential decay function shown in Eq. 1.

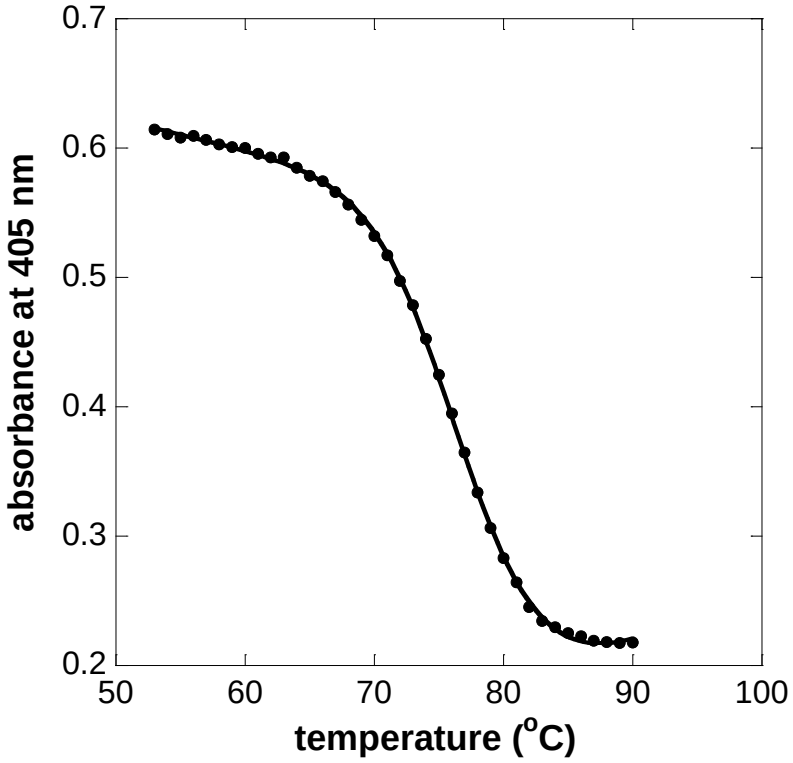

Figure 2.5 Soret absorbance of HtaA-CR2 at 405 nm in 1.5 M GdnHCl as a function of temperature.

Points are experimental values of A_{405}; the solid line shows the nonlinear least squares fit of the Soret absorbance to the function in Eq. 2. The fit yielded a value of 77 ºC for T_m.

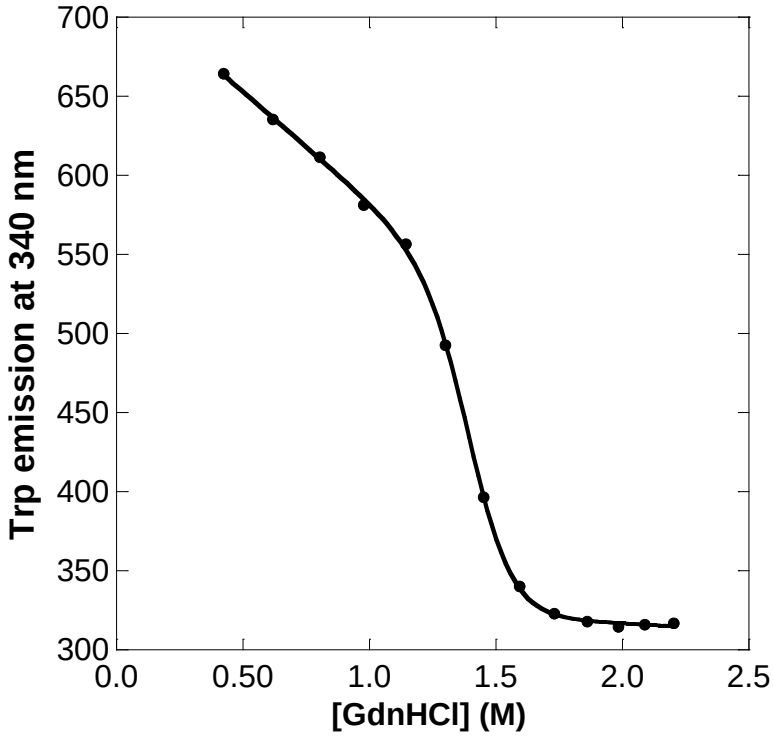

Figure 2.6 Tryptophan emission of Y490A apoHtaA-CR2 as a function of GdnHCl concentration.

The reaction was in 50 mM Tris-HCl pH 7.0. Data points were recorded after chemical equilibration (5 - 20 min). Solid points are photon counts per second at 340 nm, and the solid line is the fit using the function in Eq. 3.

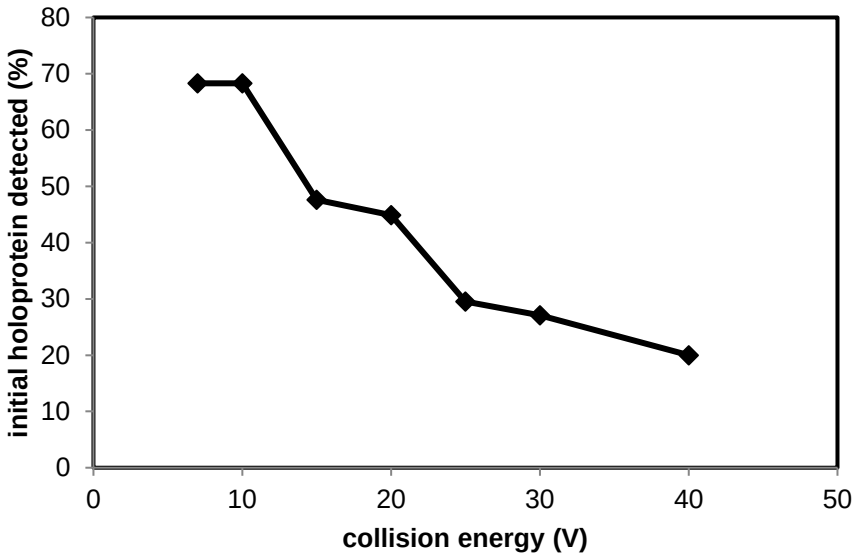

Figure 2.7 Electrospray ionization mass spectrometry detection of heme-bound holohtaa-cr2 as a function of collision energy voltage. the protein solution was prepared in 20 mm ammonium acetate, pH 6.8.

2.11 References

Abe, R., Caaveiro, J.M.M., Kozuka-Hata, H., Oyama, M., Tsumoto, K., 2012. Mapping ultra-weak protein-protein interactions between heme transporters of *Staphylococcus aureus*. J. Biol. Chem. 287, 16477-16487.

Allen, C.E., Burgos, J.M., Schmitt, M.P., 2013. Analysis of novel iron-regulated, surface-anchored hemin-binding proteins in *Corynebacterium diphtheriae*. J. Bacteriol. 195, 2852-2863.

Allen, C.E., Schmitt, M.P., 2009. HtaA is an iron-regulated hemin binding protein involved in the utilization of heme iron in *Corynebacterium diphtheriae*. J. Bacteriol. 191, 2638-2648.

Allen, C.E., Schmitt, M.P., 2011. Novel hemin binding domains in the *Corynebacterium diphtheriae* HtaA protein interact with hemoglobin and are critical for heme iron utilization by HtaA. J. Bacteriol. 193, 5374-5385.

Allen, C.E., Schmitt, M.P., 2015. Utilization of host iron sources by *Corynebacterium diphtheriae*: Multiple hemoglobin-binding proteins are essential for the use of iron from the hemoglobin-haptoglobin complex. J. Bacteriol. 197, 553-562.

Alontaga, A.Y., Rodriguez, J.C., Schoenbrunn, E., Becker, A., Funke, T., Yukl, E.T., Hayashi, T., Stobaugh, J., Moenne-Loccoz, P., Rivera, M., 2009. Structural characterization of the hemophore HasAp from *Pseudomonas aeruginosa*: NMR spectroscopy reveals protein-protein interactions between holo-HasAp and hemoglobin. Biochemistry 48, 96-109.

Amisha Kamal, J.K.A., Behere, D.V., 2008. Kinetic stabilities of soybean and horseradish peroxidases. Biochem. Eng. J. 38, 110-114.

Andersen, N.H., Nørgaard, A., Jensen, T.J., Ulstrup, J., 2002. Sequential unfolding of the two-domain protein *Pseudomonas stutzeri* cytochrome *c*(4). J. Inorg. Biochem. 88, 316-327.

Andrade, M.A., Ciccarelli, F.D., Perez-Iratxeta, C., Bork, P., 2002. NEAT: A domain duplicated in genes near the components of a putative Fe(3+) siderophore transporter from Gram-positive pathogenic bacteria. Genome Biol. 3, RESEARCH0047.

Aranda, R., Worley, C.E., Liu, M., Bitto, E., Cates, M.S., Olson, J.S., Lei, B.F., Phillips, G.N., 2007. Bis-methionyl coordination in the crystal structure of the heme-binding domain of the streptococcal cell surface protein Shp. J. Mol. Biol. 374, 374-383.

Arnesano, F., Banci, L., Bertini, I., Koulougliotis, D., 1998. Solution structure of oxidized rat microsomal cytochrome *b*(5) in the presence of 2 M guanidinium chloride: Monitoring the early steps in protein unfolding. Biochemistry 37, 17082-17092.

Asher, C., de Villiers, K.A., Egan, T.J., 2009. Speciation of ferriprotoporphyrin IX in aqueous and mixed aqueous solution is controlled by solvent identity, pH, and salt concentration. Inorg. Chem. 48, 7994-8003.

Balderas, M.A., Nobles, C.L., Honsa, E.S., Alicki, E.R., Maresso, A.W., 2012. Hal is a *Bacillus anthracis* heme acquisition protein. J. Bacteriol. 194, 5513-5521.

Benson, D.R., Rivera, M., 2013. Heme uptake and metabolism in bacteria. Met. Ions Life Sci. 12, 279-332.

Bernardes, A., Textor, L.C., Santos, J.C., Cuadrado, N.H., Kostetsky, E.Y., Roig, M.G., Bavro, V.N., Muniz, J.R.C., Shnyrov, V.L., Polikarpov, I., 2015. Crystal structure analysis of peroxidase from the palm tree *Chamaerops excelsa*. Biochimie 111C, 58-69.

Caillet-Saguy, C., Turano, P., Piccioli, M., Lukat-Rodgers, G.S., Czjzek, M., Guigliarelli, B., Izadi-Pruneyre, N., Rodgers, K.R., Delepierre, M., Lecroisey, A., 2008. Deciphering the structural role of histidine 83 for heme binding in hemophore HasA. J. Biol. Chem. 283, 5960-5970.

Chan, A.C.K., Lelj-Garolla, B., Rosell, F.I., Pedersen, K.A., Mauk, A.G., Murphy, M.E.P., 2006. Cofacial heme binding is linked to dimerization by a bacterial heme transport protein. J. Mol. Biol. 362, 1108-1119.

Collier, G.S., Pratt, J.M., De Wet, C.R., Tshabalala, C.F., 1979. Studies on haemin in dimethyl sulphoxide/water mixtures. Biochem. J. 179, 281-289.

Collier, R.J., 2001. Understanding the mode of action of diphtheria toxin: A perspective on progress during the 20th century. Toxicon 39, 1793-1803.

Contreras, H., Chim, N., Credali, A., Goulding, C.W., 2014. Heme uptake in bacterial pathogens. Curr. Opin. Chem. Biol. 19, 34-41.

Daou, N., Buisson, C., Gohar, M., Vidic, J., Bierne, H., Kallassy, M., Lereclus, D., Nielsen-LeRoux, C., 2009. IlsA, a unique surface protein of *Bacillus cereus* required for iron acquisition from heme, hemoglobin and ferritin. PLoS Pathog. 5.

Deniau, C., Gilli, R., Izadi-Pruneyre, N., Létoffé, S., Delepierre, M., Wandersman, C., Briand, C., Lecroisey, A., 2003. Thermodynamics of heme binding to the HasA(SM) hemophore: Effect of mutations at three key residues for heme uptake. Biochemistry 42, 10627-10633.

Draganova, E.B., Akbas, N., Adrian, S.A., Lukat-Rodgers, G.S., Collins, D.P., Dawson, J.H., Schmitt, M.P., Rodgers, K.R., Dixon, D.W., 2015. Heme binding by *Corynebacterium diphtheriae* HmuT: Function and heme environment. Biochemistry 54, 6598-6609.

Drazek, E.S., Hammack, C.A., Schmitt, M.P., 2000. *Corynebacterium diphtheriae* genes required for acquisition of iron from haemin and haemoglobin are homologous to ABC haemin transporters. Mol. Microbiol. 36, 68-84.

Du, J., Sono, M., Dawson, J.H., 2011. The H93G myoglobin cavity mutant as a versatile scaffold for modeling heme iron coordination structures in protein active sites and their characterization with magnetic circular dichroism spectroscopy. Coord. Chem. Rev. 255, 700-716.

Eakanunkul, S., Lukat-Rodgers, G.S., Sumithran, S., Ghosh, A., Rodgers, K.R., Dawson, J.H., Wilks, A., 2005. Characterization of the periplasmic heme-binding protein ShuT from the heme uptake system of *Shigella dysenteriae*. Biochemistry 44, 13179-13191.

Edelstein, S.J., Rehmar, M.J., Olson, J.S., Gibson, Q.H., 1970. Functional aspects of the subunit association-dissociation equilibria of hemoglobin. J. Biol. Chem. 245, 4372-4381.

Ekworomadu, M.T., Poor, C.B., Owens, C.P., Balderas, M.A., Fabian, M., Olson, J.S., Murphy, F., Balkabasi, E., Honsa, E.S., He, C., Goulding, C.W., Maresso, A.W., 2012. Differential function of Lip residues in the mechanism and biology of an anthrax hemophore. PLoS Pathog. 8.

Fabian, M., Solomaha, E., Olson, J.S., Maresso, A.W., 2009. Heme transfer to the bacterial cell envelope occurs via a secreted hemophore in the Gram-positive pathogen *Bacillus anthracis*. J. Biol. Chem. 284, 32138-32146.

Farrand, A.J., Skaar, E.P., 2014. Heme and infectious diseases, in: Ferreira, G.C., Kadish, K.M., Smith, K.M., Guilard, R. (Eds.), Handbook of Porphyrin Science with Applications to Chemistry, Physics, Materials Science, Engineering, Biology and Medicine, Vol 26: Heme Biochemistry, 26 ed. World Scientific, Hackensack, NJ, pp. 317-377.

Gasteiger, E., Hoogland, C., Gattiker, A., Duvaud, S., Wilkins, M.R., Appel, R.D., Bairoch, A., 2005. Protein identification and analysis tools on the ExPASy server, in: Walker, J.M. (Ed.), The Proteomics Protocols Handbook. Humana Press, Totowa, N.J, pp. 571-607.

Graves, A.B., Morse, R.P., Chao, A., Iniguez, A., Goulding, C.W., Liptak, M.D., 2014. Crystallographic and Spectroscopic Insights into Heme Degradation by *Mycobacterium tuberculosis* MhuD. Inorg. Chem. 53, 5931-5940.

Hargrove, M.S., Whitaker, T., Olson, J.S., Vali, R.J., Mathews, A.J., 1997. Quaternary structure regulates hemin dissociation from human hemoglobin. J. Biol. Chem. 272, 17385-17389.

Ho, W.W., Li, H.Y., Eakanunkul, S., Tong, Y., Wilks, A., Guo, M.L., Poulos, T.L., 2007. Holo- and apo-bound structures of bacterial periplasmic heme-binding proteins. J. Biol. Chem. 282, 35796-35802.

Honsa, E.S., Fabian, M., Cardenas, A.M., Olson, J.S., Maresso, A.W., 2011. The five near-iron transporter (NEAT) domain anthrax hemophore, IsdX2, scavenges heme from hemoglobin and transfers heme to the surface protein IsdC. J. Biol. Chem. 286, 33652-33660.

Honsa, E.S., Maresso, A.W., 2011. Mechanisms of iron import in anthrax. Biometals 24, 533-545.

Honsa, E.S., Maresso, A.W., Highlander, S.K., 2014. Molecular and evolutionary analysis of NEAr-iron Transporter (NEAT) domains. PLoS One 9.

Honsa, E.S., Owens, C.P., Goulding, C.W., Maresso, A.W., 2013. The near-iron transporter (NEAT) domains of the anthrax hemophore IsdX2 require a critical glutamine to extract heme from methemoglobin. J. Biol. Chem. 288, 8479-8490.

Hunter, C.L., Mauk, A.G., Douglas, D.J., 1997. Dissociation of heme from myoglobin and cytochrome *b*(5): Comparison of behavior in solution and the gas phase. Biochemistry 36, 1018-1025.

Jepkorir, G., Rodriguez, J.C., Rui, H., Im, W., Lovell, S., Battaile, K.P., Alontaga, A.Y., Yukl, E.T., Moenne-Loccoz, P., Rivera, M., 2010. Structural, NMR spectroscopic, and computational investigation of hemin loading in the hemophore HasAp from *Pseudomonas aeruginosa*. J. Am. Chem. Soc. 132, 9857-9872.

Jin, Y.Y., Nagai, M., Nagai, Y., Nagatomo, S., Kitagawa, T., 2004. Heme structures of five variants of hemoglobin M probed by resonance Raman spectroscopy. Biochemistry 43, 8517-8527.

Kumar, R., Lovell, S., Matsumura, H., Battaile, K.P., Moenne-Loccoz, P., Rivera, M., 2013. The hemophore HasA from *Yersinia pestis* ($HasA_{yp}$) coordinates hemin with a single residue, Tyr75, and with minimal conformational change. Biochemistry 52, 2705-2707.

Kumar, R., Matsumura, H., Lovell, S., Yao, H.L., Rodriguez, J.C., Battaile, K.P., Moenne-Loccoz, P., Rivera, M., 2014. Replacing the axial ligand tyrosine 75 or its hydrogen bond partner histidine 83 minimally affects hemin acquisition by the hemophore HasAp from *Pseudomonas aeruginosa*. Biochemistry 53, 2112-2125.

Kuter, D., Venter, G.A., Naidoo, K.J., Egan, T.J., 2012. Experimental and time-dependent density functional theory characterization of the UV-visible spectra of monomeric and μ-oxo dimeric ferriprotoporphyrin IX. Inorg. Chem. 51, 10233-10250.

Lei, B.F., Smoot, L.M., Menning, H.M., Voyich, J.M., Kala, S.V., Deleo, F.R., Reid, S.D., Musser, J.M., 2002. Identification and characterization of a novel heme-associated cell surface protein made by *Streptococcus pyogenes*. Infect. Immun. 70, 4494-4500.

Linder, D.P., Silvernail, N.J., Barabanschikov, A., Zhao, J.Y., Alp, E.E., Sturhahn, W., Sage, J.T., Scheidt, W.R., Rodgers, K.R., 2014. The diagnostic vibrational signature of pentacoordination in heme carbonyls. J. Am. Chem. Soc. 136, 9818-9821.

Liu, M.Y., Lei, B.F., 2005. Heme transfer from streptococcal cell surface protein Shp to HtsA of transporter HtsABC. Infect. Immun. 73, 5086-5092.

Lukat-Rodgers, G.S., Rodgers, K.R., Caillet-Saguy, C., Izadi-Pruneyre, N., Lecroisey, A., 2008. Novel heme ligand displacement by CO in the soluble hemophore HasA and its proximal ligand mutants: Implications for heme uptake and release. Biochemistry 47, 2087-2098.

Malmirchegini, G.R., Sjodt, M., Shnitkind, S., Sawaya, M.R., Rosinski, J., Newton, S.M., Klebba, P.E., Clubb, R.T., 2014. Novel mechanism of hemin capture by Hbp2, the hemoglobin-binding hemophore from *Listeria monocytogenes*. J. Biol. Chem. 289, 34886-34899.

Mattle, D., Zeltina, A., Woo, J.S., Goetz, B.A., Locher, K.P., 2010. Two stacked heme molecules in the binding pocket of the periplasmic heme-binding protein HmuT from *Yersinia pestis*. J. Mol. Biol. 404, 220-231.

Mazmanian, S.K., Skaar, E.P., Gaspar, A.H., Humayun, M., Gornicki, P., Jelenska, J., Joachmiak, A., Missiakas, D.M., Schneewind, O., 2003. Passage of heme-iron across the envelope of *Staphylococcus aureus*. Science 299, 906-909.

Mokry, D.Z., Nadia-Albete, A., Johnson, M.K., Lukat-Rodgers, G.S., Rodgers, K.R., Lanzilotta, W.N., 2014. Spectroscopic evidence for a 5-coordinate oxygenic ligated high spin ferric heme moiety in the *Neisseria meningitidis* hemoglobin binding receptor. Biochim. Biophys. Acta 1840, 3058-3066.

Moriwaki, Y., Terada, T., Tsumoto, K., Shimizu, K., 2015. Rapid heme transfer reactions between NEAr transporter domains of *Staphylococcus aureus*: A theoretical study using QM/MM and MD simulations. PLoS One 10.

Muryoi, N., Tiedemann, M.T., Pluym, M., Cheung, J., Heinrichs, D.E., Stillman, M.J., 2008. Demonstration of the iron-regulated surface determinant (Isd) heme transfer pathway in *Staphylococcus aureus*. J. Biol. Chem. 283, 28125-28136.

Nygaard, T.K., Blouin, G.C., Liu, M.Y., Fukumura, M., Olson, J.S., Fabian, M., Dooley, D.M., Lei, B.F., 2006. The mechanism of direct heme transfer from the streptococcal cell surface protein Shp to HtsA of the HtsABC transporter. J. Biol. Chem. 281, 20761-20771.

Ouattara, M., Cunha, E.B., Li, X., Huang, Y.S., Dixon, D.W., Eichenbaum, Z., 2010. Shr of Group A streptococcus is a new type of composite NEAT protein involved in sequestering haem from methaemoglobin. Mol. Microbiol. 78, 739-756.

Ouattara, M., Pennati, A., Devlin, D.J., Huang, Y.S., Gadda, G., Eichenbaum, Z., 2013. Kinetics of heme transfer by the Shr NEAT domains of Group A Streptococcus. Arch. Biochem. Biophys. 538, 71-79.

Pace, C.N., Scholtz, J.M., 1997. Measuring the conformational stability of a protein, in: Creighton, T. (Ed.), Protein Structure: A Practical Approach, 2nd ed. Oxford University Press, Oxford, pp. 299-321.

Pishchany, G., Sheldon, J.R., Dickson, C.F., Alam, M.T., Read, T.D., Gell, D.A., Heinrichs, D.E., Skaar, E.P., 2014. IsdB-dependent hemoglobin binding is required for acquisition of heme by *Staphylococcus aureus*. J. Infect. Dis. 209, 1764-1772.

Pluym, M., Muryoi, N., Heinrichs, D.E., Stillman, M.J., 2008. Heme binding in the NEAT domains of IsdA and IsdC of *Staphylococcus aureus*. J. Inorg. Biochem. 102, 480-488.

Pluym, M., Vermeiren, C.L., Mack, J., Heinrichs, D.E., Stillman, M.J., 2007. Protoporphyrin IX and heme binding properties of *Staphylococcus aureus* IsdC. J. Porph. Phthalo. 11, 165-171.

Ran, Y.C., Malmirchegini, G.R., Clubb, R.T., Lei, B.F., 2013. Axial ligand replacement mechanism in heme transfer from streptococcal heme-binding protein Shp to HtsA of the HtsABC transporter. Biochemistry 52, 6537-6547.

Ricchelli, F., Jori, G., Gobbo, S., Tronchin, M., 1991. Liposomes as models to study the distribution of porphyrins in cell membranes. Biochim. Biophys. Acta 1065, 42-48.

Rodgers, K.R., Lukat-Rodgers, G.S., 2014. Biophysical perspectives on the acquisition, transport, and trafficking of heme in bacteria, in: Ferreira, G.C., Kadish, K.M., Smith, K.M., Guilard, R. (Eds.), Handbook of Porphyrin Science with Applications to Chemistry, Physics, Materials Science, Engineering, Biology and Medicine, Vol. 30: Heme Proteins, Part II. World Scientific, Hackensack, N.J, pp. 251-309.

Roncone, R., Monzani, E., Labo, S., Sanangelantoni, A.M., Casella, L., 2005. Catalytic activity, stability, unfolding, and degradation pathways of engineered and reconstituted myoglobins. J. Biol. Inorg. Chem. 10, 11-24.

Sanchez-Ruiz, J.M., 2010. Protein kinetic stability. Biophys. Chem. 148, 1-15.

Schmitt, M.P., 1997. Transcription of the *Corynebacterium diphtheriae hmuO* gene is regulated by iron and heme. Infect. Immun. 65, 4634-4641.

Schmitt, M.P., Drazek, E.S., 2001. Construction and consequences of directed mutations affecting the hemin receptor in pathogenic *Corynebacterium species*. J. Bacteriol. 183, 1476-1481.

Segond, D., Khalil, E.A., Buisson, C., Daou, N., Kallassy, M., Lereclus, D., Arosio, P., Bou-Abdallah, F., Le Roux, C.N., 2014. Iron Acquisition in Bacillus cereus: The Roles of IlsA and Bacillibactin in Exogenous Ferritin Iron Mobilization. PLoS Pathog. 10.

Sharma, K.D., Andersson, L.A., Loehr, T.M., Terner, J., Goff, H.M., 1989. Comparative spectral analysis of mammalian, fungal, and bacterial catalases. Resonance Raman evidence for iron-tyrosinate coordination. J. Biol. Chem. 264, 12772-12779.

Sharp, K.H., Schneider, S., Cockayne, A., Paoli, M., 2007. Crystal structure of the heme-IsdC complex, the central conduit of the Isd iron/heme uptake system in *Staphylococcus aureus*. J. Biol. Chem. 282, 10625-10631.

Sheldon, J.R., Heinrichs, D.E., 2015. Recent developments in understanding the iron acquisition strategies of gram positive pathogens. FEMS Microbiol. Rev. 39, 592-630.

Sjodt, M., Macdonald, R., Spirig, T., Chan, A.H., Dickson, C.F., Fabian, M., Olson, J.S., Gell, D.A., Clubb, R.T., 2016. The PRE-derived NMR model of the 38.8-kDa tri-domain IsdH protein from Staphylococcus aureus suggests that it adaptively recognizes human hemoglobin. J. Mol. Biol. 428, 1107-1129.

Sook, B.R., Block, D.R., Sumithran, S., Montañez, G.E., Rodgers, K.R., Dawson, J.H., Eichenbaum, Z., Dixon, D.W., 2008. Characterization of SiaA, a streptococcal heme-binding protein associated with a heme ABC transport system. Biochemistry 47, 2678-2688.

Sudhamsu, J., Kabir, M., Airola, M.V., Patel, B.A., Yeh, S.R., Rousseau, D.L., Crane, B.R., 2010. Co-expression of ferrochelatase allows for complete heme incorporation into recombinant proteins produced in *E. coli*. Protein Expr. Purif. 73, 78-82.

Swint, L., Robertson, A.D., 1993. Thermodynamics of unfolding for turkey ovomucoid third domain: Thermal and chemical denaturation. Protein Sci. 2, 2037-2049.

Tarlovsky, Y., Fabian, M., Solomaha, E., Honsa, E., Olson, J.S., Maresso, A.W., 2010. A *Bacillus anthracis* S-Layer homology protein that binds heme and mediates heme delivery to IsdC. J. Bacteriol. 192, 3503-3511.

Teale, F.W., 1959. Cleavage of the heme protein by acid methyl ethyl ketone. Biochim. Biophys. Acta 35, 543.

Tiedemann, M.T., Heinrichs, D.E., Stillman, M.J., 2012. Multiprotein heme shuttle pathway in *Staphylococcus aureus*: Iron-regulated surface determinant cog-wheel kinetics. J. Am. Chem. Soc. 134, 16578-16585.

Tiedemann, M.T., Muryoi, N., Heinrichs, D.E., Stillman, M.J., 2009. Characterization of IsdH (NEAT domain 3) and IsdB (NEAT domain 2) in *Staphylococcus aureus* by magnetic circular dichroism spectroscopy and electrospray ionization mass spectrometry. J. Porph. Phthalo. 13, 1006-1016.

Tiedemann, M.T., Stillman, M.J., 2011. Application of magnetic circular dichroism spectroscopy to porphyrins, phthalocyanines and hemes. J. Porph. Phthalo. 15, 1134-1149.

Tong, Y., Guo, M., 2007. Cloning and characterization of a novel periplasmic heme-transport protein from the human pathogen *Pseudomonas aeruginosa*. J. Biol. Inorg. Chem. 12, 735-750.

Trost, E., Blom, J., Soares, S.D., Huang, I.H., Al-Dilaimi, A., Schroder, J., Jaenicke, S., Dorella, F.A., Rocha, F.S., Miyoshi, A., Azevedo, V., Schneider, M.P., Silva, A., Camello, T.C., Sabbadini, P.S., Santos, C.S., Santos, L.S., Hirata, R., Mattos-Guaraldi, A.L., Efstratiou, A., Schmitt, M.P., Hung, T.T., Tauch, A., 2012. Pangenomic study of *Corynebacterium diphtheriae* that provides insights into the genomic diversity of pathogenic isolates from cases of classical diphtheria, endocarditis, and pneumonia. J. Bacteriol. 194, 3199-3215.

Vieille, C., Zeikus, G.J., 2001. Hyperthermophilic enzymes: Sources, uses, and molecular mechanisms for thermostability. Microbiol. Mol. Biol. Rev. 65, 1-43.

Villareal, V.A., Spirig, T., Robson, S.A., Liu, M., Lei, B., Clubb, R.T., 2011. Transient Weak Protein-Protein Complexes Transfer Heme Across the Cell Wall of *Staphylococcus aureus*. J. Am. Chem. Soc. 133, 14176-14179.

Wagner, K.S., White, J.M., Lucenko, I., Mercer, D., Crowcroft, N.S., Neal, S., Efstratiou, A., 2012. Diphtheria in the postepidemic period, Europe, 2000-2009. Emerg. Infect. Dis. 18, 217-225.

Wandersman, C., Delepelaire, P., 2014. Heme-delivering proteins in bacteria, in: Ferreira, G.C., Kadish, K.M., Smith, K.M., Guilard, R. (Eds.), Handbook of Porphyrin Science with Applications to Chemistry, Physics, Materials Science, Engineering, Biology and Medicine, Vol 26: Heme Biochemistry, pp. 191-222.

Watanabe, M., Tanaka, Y., Suenaga, A., Kuroda, M., Yao, M., Watanabe, N., Arisaka, F., Ohta, T., Tanaka, I., Tsumoto, K., 2008. Structural basis for multimeric heme complexation through a specific protein-heme interaction - The case of the third NEAT domain of IsdH from *Staphylococcus aureus*. J. Biol. Chem. 283, 28649-28659.

Wijma, H.J., Floor, R.J., Janssen, D.B., 2013. Structure- and sequence-analysis inspired engineering of proteins for enhanced thermostability. Curr. Opin. Struct. Biol. 23, 588-594.

Wilks, A., O'Neill, M.J., 2014. Extracellular heme uptake and metabolism in bacterial pathogenesis, in: Ferreira, G.C., Kadish, K.M., Smith, K.M., Guilard, R. (Eds.), Handbook of Porphyrin Science with Applications to Chemistry, Physics, Materials Science, Engineering, Biology and Medicine, Vol 26: Heme Biochemistry. World Scientific, Hackensack, NJ, pp. 267-315.

Wittung-Stafshede, P., 1999. Effect of redox state on unfolding energetics of heme proteins. Biochim. Biophys. Acta 1432, 401-405.

Xiao, Q., Jiang, X., Moore, K.J., Shao, Y., Pi, H., Dubail, I., Charbit, A., Newton, S.M., Klebba, P.E., 2011. Sortase independent and dependent systems for acquisition of haem and haemoglobin in *Listeria monocytogenes*. Mol. Microbiol. 80, 1581-1597.

Zapotoczna, M., Heilbronner, S., Speziale, P., Foster, T.J., 2012. Iron-Regulated Surface Determinant (Isd) Proteins of *Staphylococcus lugdunensis*. J. Bacteriol. 194, 6453-6467.

Zhu, H., Li, D.F., Liu, M.Y., Copie, V., Lei, B.F., 2014. Non-heme-binding domains and segments of the *Staphylococcus aureus* IsdB protein critically contribute to the kinetics and equilibrium of heme acquisition from methemoglobin. PLoS One 9.

2.12 Supplementary Information

Table 2.1 HtaA-CR2 site-directed mutagenesis primers. The mutation sites are shown bold

Primer Name	Primer sequence (5'-3')
Y361A-Forward	GTCGTTCCAGTCT**GCG**ATCACTGGTTC
Y361A-Reverse	GAACCAGTGAT**CGC**AGACTGGAACGAC
H412A-Forward	CGTTTTAGTGGTG**CGC**ACGGCATCTTG
H412A-Reverse	CAAGATGCCGTG**CGC**ACCACTAAAACG
Y490A-Forward	CGCTGGCTTC**GCG**GAAGCTGGCTCTG
Y490A-Reverse	CAGAGCCAGCTTCC**GCG**AAGCCAGCG

Table 2.2 The Soret maximum and α/β bands of Tyr-ligated ferric heme transfer proteins.

Protein	Ligand(s)	Soret band (nm)	Q bands (nm)				Reference
S. aureus IsdA	Tyr	406	503	535		628	(Pluym et al., 2008)
S. aureus IsdBN2	Tyr	405	504	538		630	(Tiedemann et al., 2009)
S. aureus IsdC	Tyr	400	500	535		630	(Sharp et al., 2007)
P. aeruginosa HasA	Tyr/His	407	495	540	577	616	(Alontaga et al., 2009)
Y. pestis HasA	Tyr	403	498	535		620	(Kumar et al., 2013)
S. marcesans HasA	Tyr/His	406	494	537	568	618	(Caillet-Saguy et al., 2008)
P. aeruginosa PhuT	Tyr	400	500	534		624	(Tong and Guo, 2007)
S. dysenteriae ShuT	Tyr	400	500	521		617	(Eakanunkul et al., 2005)
N. *meningitidis* HmbR	Tyr	400	490	533	566	616	(Mokry et al., 2014)
B. anthracis IsdX1	Tyr	400	505	540		630	(Ekworomadu et al., 2012)
B. anthracis IsdX2-N3	Tyr	403	500		nr[a]	630	(Honsa et al., 2013)
B. anthracis IsdX2-N5	Tyr	404	500		nr[a]	630	(Honsa et al., 2013)
C. diphtheriae HmuT	Tyr/His	407	492	546	569	616	(Draganova et al., 2015)

[a]Not reported.

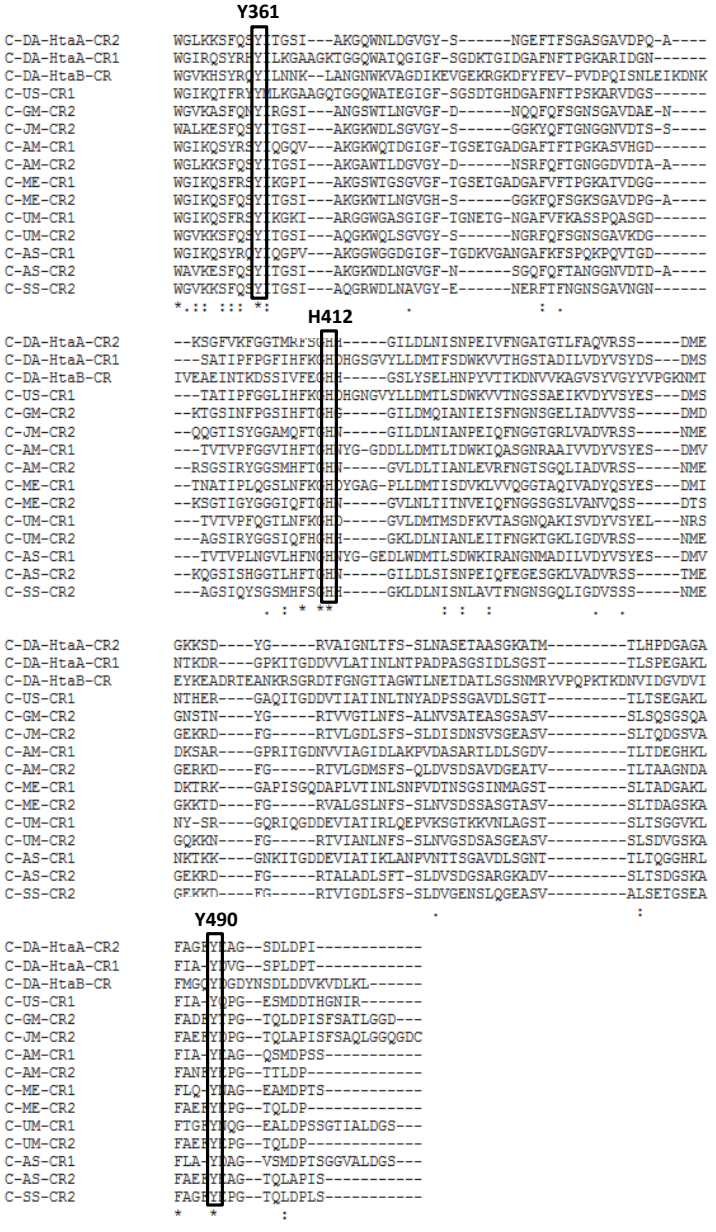

Figure 2.8 Clustal omega alignment of CR domains for C-DA (*C. diphtheriae*) HtaA CR1 and CR2 domains, HtaB and HtaA homologs from various *corynebacterium* species. C-US, *C. ulcerans*. C-GM, *C. glutamicum*. C-JM, *C. jeikeium*. C-AM, *C. aurimucosum*. C-ME, *C. mustelae*. C-UM, *C. urealyticum*. C-AS, *C. auriscanis*. C-SS, *C. simulans*. three conserved residues are shown (HtaA-CR2 numbering): Tyr361, His412 and Tyr490.

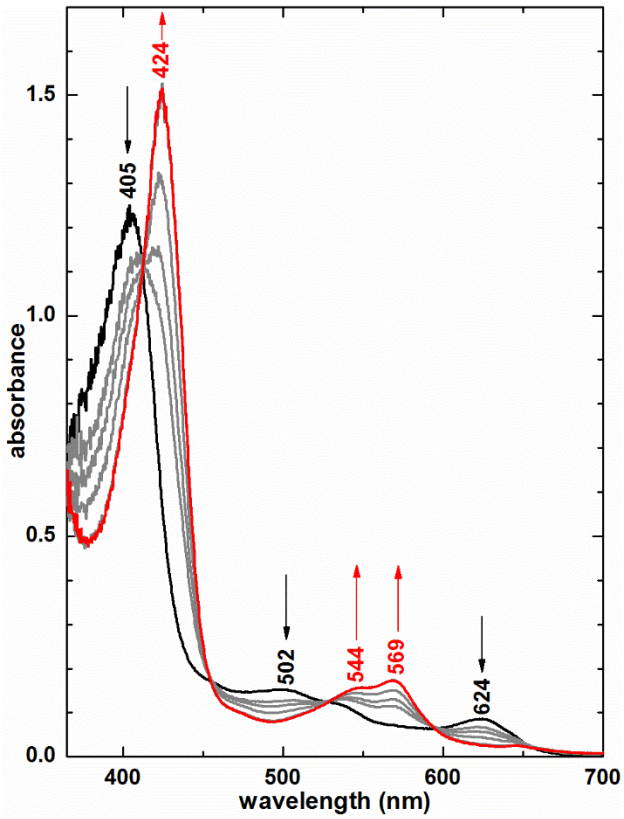

Figure 2.9 UV-visible absorbance spectra recorded at 3 min intervals during the reduction of ferric HtaA-CR2 with dithionite at pH 7.0 and ambient temperature.

Arrows indicate the direction of the absorbance change upon reduction of Fe(III) (black trace) to Fe(II) (red trace). Isosbestic points are observed at 413, 455, 528, and 595 nm.

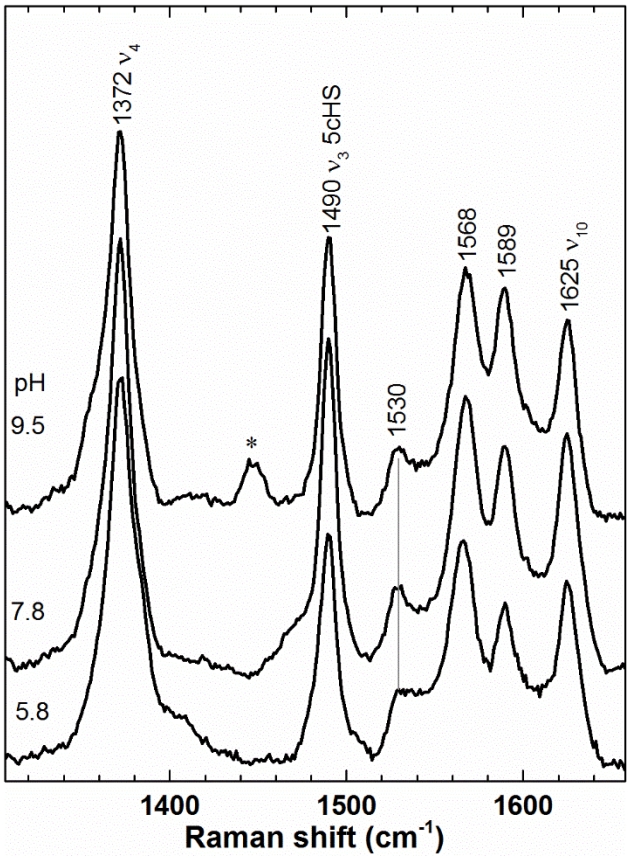

Figure 2.10 Soret (413.1 nm)-excited rR spectra at the indicated pH values.

Note the insensitivity of core marker frequencies and relative intensities to differences in pH. This is typical of hemin that is bound to the protein through the phenol side chain of a proximal Tyr residue (Eakanunkul et al., 2005). * marks a buffer band.

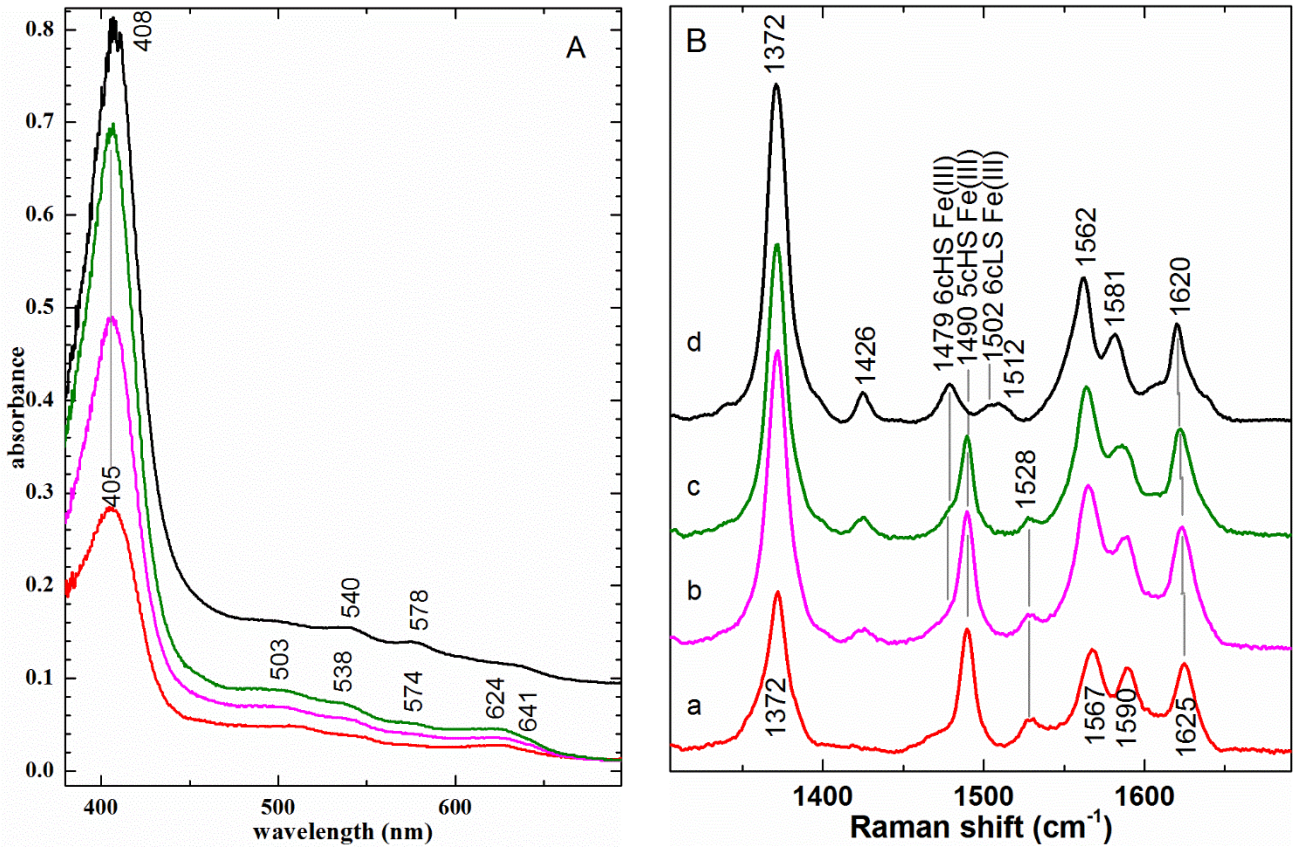

Figure 2.11 Partially heme loaded HtaA-CR2 titrated with metHbA.

Total ferric HtaA-CR2 concentration was 11.5 µM with 5.6 µM heme (uncertainty in concentrations estimated to be ±10%). MetHbA was added to HtaA-CR2 titrimetrically to the following concentrations: 0 µM (a, — red), 4 µM (b, — magenta), and 6.5 µM (c, — green). A) UV-visible spectra. B) Resonance Raman spectra recorded with 406.7-nm excitation. MetHbA spectrum is shown in black (d, —). The UV-visible and resonance Raman spectra were recorded from the same samples, which were 100 mM in Tris-HCl at pH 7.8.

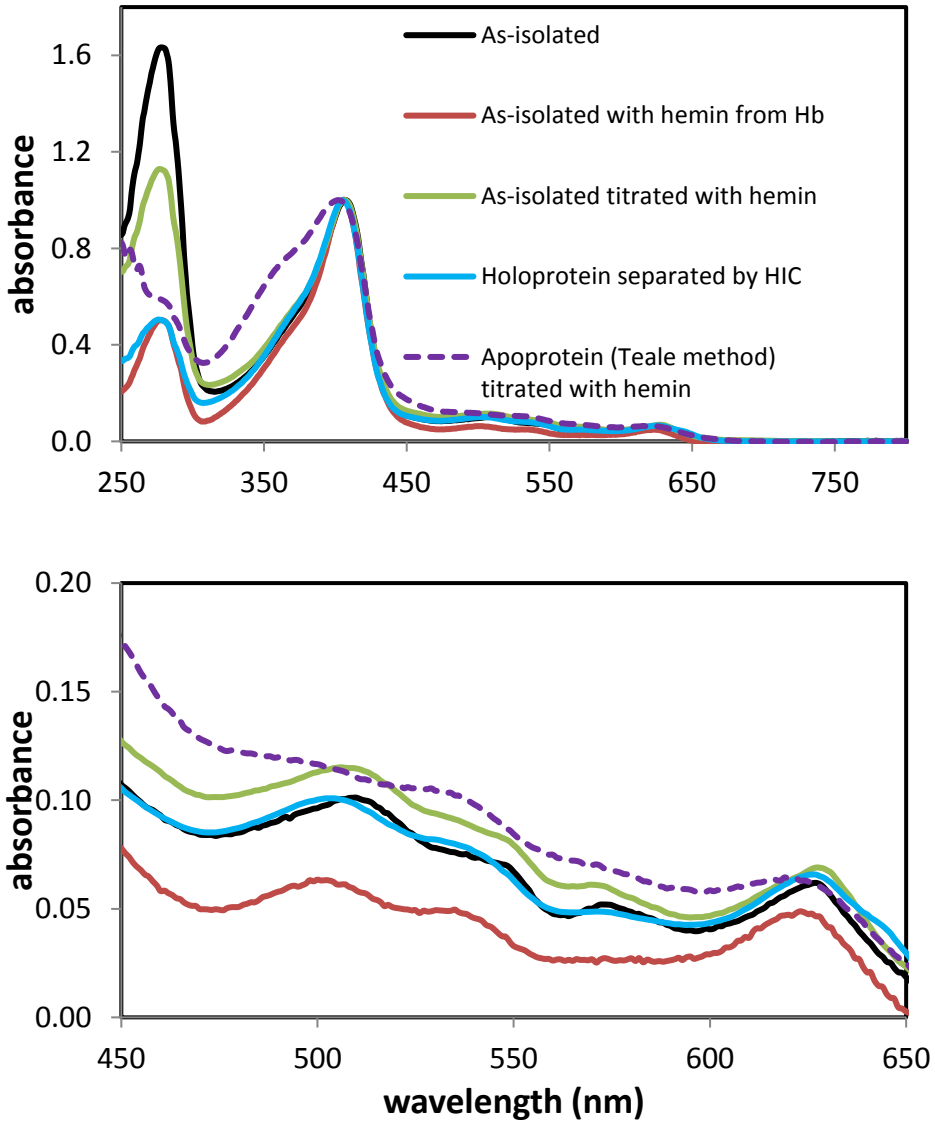

Figure 2.12 UV-visible spectra of HtaA-CR2 as-isolated (around 20% heme loaded protein, black), reconstituted on a Strep-tag column with hemin from Hb (red), titrated with hemin (green), after hydrophobic column separation of the holo portion of the as-isolated protein (blue) and reconstituted after unfolding using the Teale method (purple). The proteins were prepared in 50 mM Tris-Cl pH 7.0. Spectra are normalized to 1.0 at the Soret.

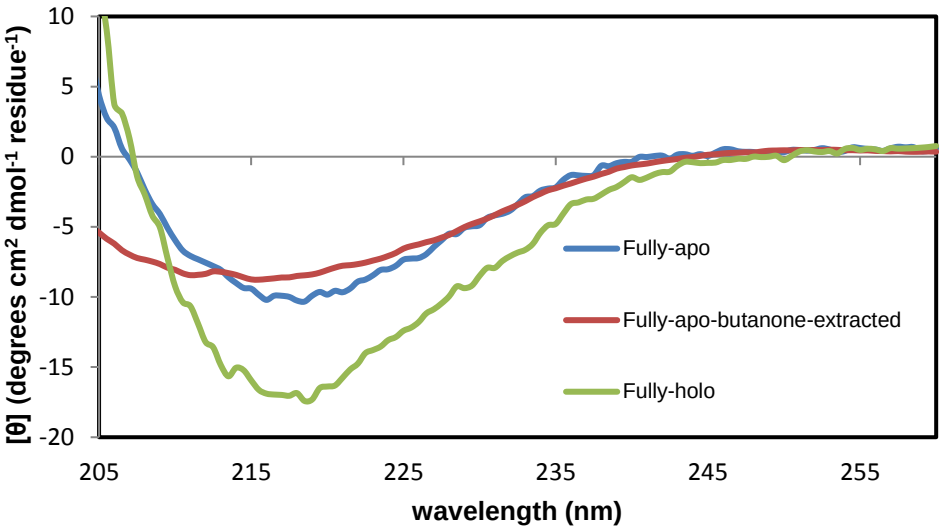

Figure 2.13 CD spectra of holo and apo HtaA-CR2. The spectra were recorded in 10 mM potassium phosphate, pH 7.0.

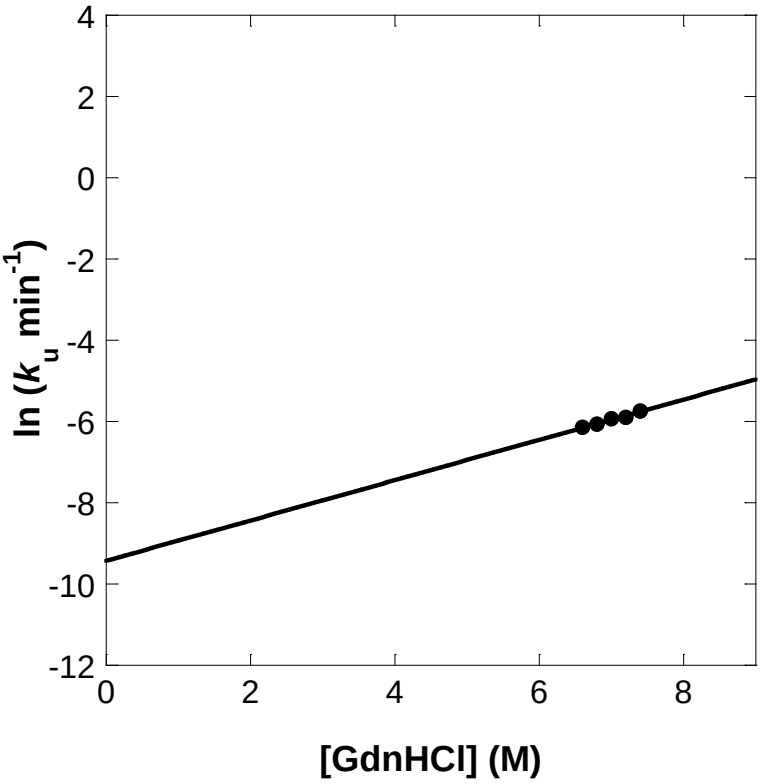

Figure 2.14 Dependence of unfolding kinetic rate constants of HtaA-CR2 on GdnHCl concentration at 37 ºC.

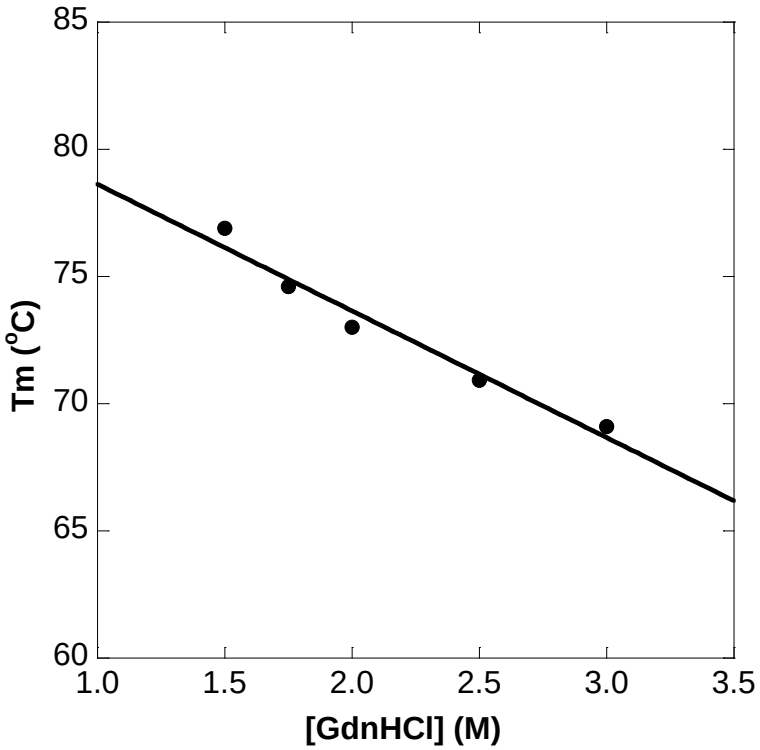

Figure 2.15 T_m of HtaA-CR2 as a function of the concentration of GdnHCl. The data were fit with a linear function, which yielded a T_m value of 84 °C in the absence of the denaturant.

2.13 Supplemental References

Alontaga, A.Y., Rodriguez, J.C., Schoenbrunn, E., Becker, A., Funke, T., Yukl, E.T., Hayashi, T., Stobaugh, J., Moenne-Loccoz, P., Rivera, M., 2009. Structural characterization of the hemophore HasAp from *Pseudomonas aeruginosa*: NMR spectroscopy reveals protein-protein interactions between holo-HasAp and hemoglobin. Biochemistry 48, 96-109.

Caillet-Saguy, C., Turano, P., Piccioli, M., Lukat-Rodgers, G.S., Czjzek, M., Guigliarelli, B., Izadi-Pruneyre, N., Rodgers, K.R., Delepierre, M., Lecroisey, A., 2008. Deciphering the structural role of histidine 83 for heme binding in hemophore HasA. J. Biol. Chem. 283, 5960-5970.

Draganova, E.B., Akbas, N., Adrian, S.A., Lukat-Rodgers, G.S., Collins, D.P., Dawson, J.H., Schmitt, M.P., Rodgers, K.R., Dixon, D.W., 2015. Heme binding by *Corynebacterium diphtheriae* HmuT: Function and heme environment. Biochemistry 54, 6598-6609.

Eakanunkul, S., Lukat-Rodgers, G.S., Sumithran, S., Ghosh, A., Rodgers, K.R., Dawson, J.H., Wilks, A., 2005. Characterization of the periplasmic heme-binding protein ShuT from the heme uptake system of *Shigella dysenteriae*. Biochemistry 44, 13179-13191.

Ekworomadu, M.T., Poor, C.B., Owens, C.P., Balderas, M.A., Fabian, M., Olson, J.S., Murphy, F., Balkabasi, E., Honsa, E.S., He, C., Goulding, C.W., Maresso, A.W., 2012. Differential function of Lip residues in the mechanism and biology of an anthrax hemophore. PLoS Pathog. 8.

Honsa, E.S., Owens, C.P., Goulding, C.W., Maresso, A.W., 2013. The near-iron transporter (NEAT) domains of the anthrax hemophore IsdX2 require a critical glutamine to extract heme from methemoglobin. J. Biol. Chem. 288, 8479-8490.

Kumar, R., Lovell, S., Matsumura, H., Battaile, K.P., Moenne-Loccoz, P., Rivera, M., 2013. The hemophore HasA from *Yersinia pestis* ($HasA_{yp}$) coordinates hemin with a single residue, Tyr75, and with minimal conformational change. Biochemistry 52, 2705-2707.

Mokry, D.Z., Nadia-Albete, A., Johnson, M.K., Lukat-Rodgers, G.S., Rodgers, K.R., Lanzilotta, W.N., 2014. Spectroscopic evidence for a 5-coordinate oxygenic ligated high spin ferric heme moiety in the *Neisseria meningitidis* hemoglobin binding receptor. Biochim. Biophys. Acta 1840, 3058-3066.

Pluym, M., Muryoi, N., Heinrichs, D.E., Stillman, M.J., 2008. Heme binding in the NEAT domains of IsdA and IsdC of *Staphylococcus aureus*. J. Inorg. Biochem. 102, 480-488.

Sharp, K.H., Schneider, S., Cockayne, A., Paoli, M., 2007. Crystal structure of the heme-IsdC complex, the central conduit of the Isd iron/heme uptake system in *Staphylococcus aureus*. J. Biol. Chem. 282, 10625-10631.

Sievers, F., Higgins, D.G., 2014. Clustal Omega, accurate alignment of very large numbers of sequences. Methods Mol. Biol. 1079, 105-116.

Tiedemann, M.T., Muryoi, N., Heinrichs, D.E., Stillman, M.J., 2009. Characterization of IsdH (NEAT domain 3) and IsdB (NEAT domain 2) in *Staphylococcus aureus* by magnetic circular dichroism spectroscopy and electrospray ionization mass spectrometry. J. Porph. Phthalo. 13, 1006-1016.

Tong, Y., Guo, M., 2007. Cloning and characterization of a novel periplasmic heme-transport protein from the human pathogen *Pseudomonas aeruginosa*. J. Biol. Inorg. Chem. 12, 735-750.

3 CHARACTERIZATION OF HTAA-CR2 FROM *CORYNEBACTERIUM DIPHTHERIAE*

This chapter describes additional work on *C. diphtheriae* HtaA-CR2, in addition to the work in Chapter 2. Site-directed mutagenesis of the mutants, expression, purification, UV-visible absorption spectroscopy, thermal unfolding, chemical unfolding, and mass spectrometry were performed at Georgia State University.

3.1 Materials and Methods

3.1.1 Site Directed Mutagenesis

Recombinant HtaA-CR2 mutants were constructed by site directed mutagenesis for the Y361A, H412A and Y490A substitutions. Wild type pET24a (+) plasmids, which include the HtaA-CR2 sequence in BL21(DE3) cells, were a gift from Dr. Michael Schmitt. These cells were inoculated into 5 ml Luria-Bertani (LB) medium in the presence of 50 μg/ml kanamycin. The culture was incubated overnight at 37 ^{o}C then centrifuged at 8000 rpm for 30 min. The wild type plasmids were extracted from the cell pellet using a Qiagen plasmid extraction kit according to the manufacturer's instructions. The concentration of wild type plasmids were determined as 106 ng/μl using a NanoDrop UV-visible spectrophotometer (one absorbance unit of plasmid at 260 nm corresponds to ~50 ng/μl).

PCR Reaction: Five different PCR reaction mixtures were prepared by varying the concertation of plasmid, primers (Sigma Aldrich, Chapter 2) and dimethyl sulfoxide (DMSO). A control reaction was prepared excluding only Pfu DNA polymerase (Table 3.1). The instrument settings were 95 ^{o}C for melting (30 sec), 57 ^{o}C for annealing (1.0 min), and 68 ^{o}C for extending (10.0

min) for each cycle. The number of cycles was 20 and the reaction mixtures were held 4 ^{o}C at the end. PCR reaction mixtures were visualized by gel electrophoresis.

Gel Electrophoresis: The 1% (w/v) agarose gel was prepared in water and heated in a water bath. The DNA gel plate was sealed with duct tape, filled with the gel solution and allowed to solidify. The PCR products (10 μl) were added to 2 μl of 6X DNA loading dye (Thermo Scientific) and the mixture was loaded into the gel. The running buffer was 1X TAE (0.04 M Tris-Acetate, 0.001 M EDTA). The separation was performed at 70 V/20 mA for 70 min. The gel was treated with 1X SYBR Safe (Invitrogen) DNA gel stain solution in the absence of light for 30 min. The DNA bands were visualized using a UVP BioDoc-IT imaging system.

DpnI Digestion: To remove the methylated wild-type plasmids from the PCR product mixtures the endonuclease DpnI (from *Diplococcus pneumoniae*) was used. The enzyme and the restriction enzyme buffer were from Sigma Aldrich. DpnI (2 μl of 10U/μl), the buffer (5 μl), the PCR product mixture (38 μl) and, water (6 μl) mixture was incubated at 37 ^{o}C for 2 h (1 μl DpnI was added at the beginning and 1 μl more at the end of the first hour). After digestion, the reaction mixtures were stored at -20 ^{o}C.

Transformation of the Mutated Plasmids into Competent Cells: The competent cells BL21 (DE3) were from Dr. Zehava Eichenbaum's lab. The plasmids (1 μl) were mixed with 50 μl competent cells and incubated on ice for 20 min. Heat shock was applied immediately by incubating in a water bath (42 ^{o}C) for 45 sec followed by incubation on ice for 2 min. A warm solution of 250 μl of LB media without any antibiotic was added to the mixture and incubated at 37 ^{o}C for 1 h. The mixture was inoculated onto agar plates prepared with 50 μg/ml kanamycin. The plates were incubated overnight at 37 ^{o}C.

DNA Sequencing to Confirm the Mutation: A single colony was selected from the transformation plate. Part of the colony was inoculated on an agar-kanamycin stock-plate to preserve the same cell line, the plated incubated overnight at 37 ^{o}C, airtight sealed and stored in 4 ^{o}C; the remaining part of the colony was inoculated into 5 ml LB-kanamycin medium for overnight growth at 37 ^{o}C. The plasmids were extracted from the LB culture and submitted to the Georgia State University DNA sequencing facility for forward and reverse sequencing (pET plasmid system sequencing primers were used). The Clustal Omega sequence alignment program was used to align the wild-type and mutated gene sequence for HtaA-CR2.

Upon confirming the mutation, cells from the stock plate were grown in 10 ml LB-kanamycin media. The stock clones were prepared by adding 20% glycerol to the LB culture (total 1 ml). The stocks transferred to cryogenic tubes, flash frozen in liquid nitrogen for at least 2 min and stored at -80 ^{o}C.

3.1.2 Maximizing Holo HtaA-CR2 Expression

The Strep-HtaA-CR2 protein was expressed in *E. coli* strain BL21(DE3). LB or Terrific Broth (TB) was used as the media. LB broth was prepared by adding 10 g of tryptone/peptone, 10 g of NaCl, and 5 g of yeast extract to 1000 ml of water. TB was prepared by adding 12 g of tryptone, 24 g of yeast extract, 4 ml glycerol and 100 ml of phosphate buffer (0.17 M KH_2PO_4, 0.72 M K_2HPO_4) in 1000 ml water. The media was autoclaved on liquid cycle, allowed to cool to room temperature, and 50 μg/ml kanamycin added. A small scale reaction, 60 ml of LB media, was inoculated with BL21(DE3)/pET24a(+) strains including the expression vector of HtaA-CR2 protein. The small scale media was incubated in the shaker at 37^{o}C/220 rpm for 16 h. An aliquot of this culture (10 ml) was inoculated in a larger scale media (200 or 400 ml) and incubated at 37^{o}C/220 rpm till the OD_{600} a value of 0.8. The cultures were induced by adding 50, 200 or 1000

μM isopropyl-β-D-thiogalactopyranoside (IPTG). Then the cultures were allowed to grow for 3, 6, 8 or 18 h before harvesting. The cells were harvested by centrifuging at 3100rpm/4 ^{o}C for 30 min. The pellets were collected and stored in a -80 ^{o}C freezer overnight. The cell pellets were re-suspended with buffer A (100 mM Tric-Cl, 150 mM NaCl pH 8.0). Cells were lysed with mini EDTA-free protease inhibitor cocktail tablet and incubated on ice for 30 min. The cells were treated with a Microfluidics M-110P cell disrupter and cell debris was removed by centrifugation at 6500rpm/4 ^{o}C for 30 min.

A GE Healthcare ÄKTA fast protein liquid chromatography instrument (FPLC) was used for purification at 4˚C. The HtaA-CR2 solution was loaded onto a Strep-Tactin Superflow column (5 mL, IBA BioTAGnology) which had been equilibrated with Buffer A. Buffer A [5 column volumes (CV)] was also used to wash the unbound material. The streptactin-bound HtaA-CR2 protein was eluted with 10 CV of Buffer B (100 mM Tris-Cl, 150 mM NaCl, 2.5 mM *d*-desthiobiotin, pH 8.0). A linear gradient of buffer A and B was used going from 100% A to 100% B over 5 CV. The purity of the fractions was tested with sodium dodecyl sulfate polyacrylamide gel electrophoresis (SDS-PAGE).

3.1.3 Expression and Purification of HtaA-CR2

An expression and purification protocol for HtaA-CR2 was established using following conditions. TB was used as a media including 50 μg/ml. A small amount of media (60 ml of LB) was inoculated with BL21(DE3)/pET24a(+) strains which included the expression vector for the HtaA-CR2 protein. The small-scale media was incubated in the shaker at 37 ^{o}C/220 rpm for 16 h. An aliquot (10 ml) was inoculated in large-scale media (200 or 400 ml) and the reaction incubated at 37 ^{o}C/220 rpm until the OD_{600} reached 0.8. The cultures were induced by adding 50 μM IPTG. The cultures were allowed to grow 16 h before harvesting. The cells were harvested

by centrifuging at 3100 rpm/4 ºC for 30 min. The pellets were collected and stored in a -80 ºC freezer overnight.

The cell pellets were re-suspended with buffer A (100 mM Tris-Cl, 150 mM NaCl pH 8.0). The cells were lysed in a solution containing 100 mM Tris-Cl, 150 mM NaCl, pH 8.0, 10 mM $MgCl_2$, 0.1 mM phenylmethanesulfonyl fluoride (PMSF), 0.2 mg/mL lysozyme, 5 μg/mL DNase I (from bovine pancreas, Roche) and 5 μg/mL RNase A (from bovine pancreas, Roche) and incubated on ice for 30 min. The cells were treated with cell disrupter and cell debris was removed by centrifugation at 6500 rpm/4 ºC for 30 min.

FPLC purification was performed using a Strep-Tactin Superflow column (5 mL, IBA BioTAGnology) as previously described.

3.1.4 Holoprotein and Apoprotein Separation of HtaA-CR2

HiTrap 5 ml Butyl FF and HiTrap 5 ml Phenyl FF hydrophobic interaction columns (HIC) were from GE Healthcare. NaH_2PO_4, $(NH_4)_2SO_4$ and NaCl were from Fisher Scientific. The as-isolated protein solution from the Strep-tag purification was first separated on the Butyl FF column and further separated on the Phenyl FF column using the FPLC system at 4 ºC. The columns were equilibrated with 5 CV of 20 mM NaH_2PO_4 pH 7.0 followed by 5 CV of the binding buffer 20 mM NaH_2PO_4, 1.5 M $(NH_4)_2SO_4$ at pH 7.0 or 20 mM NaH_2PO_4, 4 M NaCl at pH 7.0. Each column was washed with 5 CV of binding buffer upon sample loading onto the column. The elution was carried out with a linear gradient of sodium phosphate (1.5 - 0 M) or sodium chloride buffer (4 – 0 M). The column pressure and flow rate were at the limits as suggested by the manufacturer. The Soret/280 nm absorbance ratio of the fractions was measured by using a Cary 50 Bio UV-visible spectrophotometer. The fractions were concentrated by using Amicon Ultra 10K centrifugal filter and stored -80 ºC freezer in 50 mM Tris-Cl pH 7.0 buffer.

3.1.5 Extinction Coefficient Measurement

The extinction coefficient of HtaA-CR2 at the Soret was determined by using the pyridine hemochrome assay (Berry and Trumpower, 1987). Equal amounts of a HtaA-CR2 solution and a pyridine hemochrome solution (2.0 ml pyridine, 150 μl 2 M KOH and 1850 μl water) were mixed and vortexed for 30 s. The total heme concentration was determined by spectroscopic measurement of heme-pyridine complex with an extinction coefficient of 34530 M^{-1} cm^{-1} at 557 nm (Berry and Trumpower, 1987). The extinction coefficient of 1.2 x 10^5 M^{-1} cm^{-1} for HtaA-CR2 at Soret was calculated by using Beer's law from the absorbance value at Soret and molar concentration of heme; an average of five experiments is reported (Table 3.2). The holoprotein concentrations were determined using the extinction coefficient. The heme loading was estimated by comparing the holoprotein with the total (holoprotein and apoprotein) protein concentration that was determined using Bradford assay (described below).

3.1.6 Bradford Assay for HtaA-CR2

Bovine serum albumin (BSA) was from Thermo Scientific. The Coomassie Blue protein assay reagent was from Sigma Aldrich. BSA and HtaA-CR2 solutions were prepared in 25 mM Tris-Cl pH 7.0. Table 3.3 gives the amounts of protein and Coomassie Blue solution in each sample. Each sample was prepared in duplicate. The absorbance of each solution at 595 nm was recorded after 10 min incubation at room temperature and the duplicate values averaged. To construct a standard curve, the 595 nm absorbance was plotted as a function of the amount of BSA in each solution. The 595 nm absorbance of HtaA-CR2 solution was 0.123 (4 μl protein solution + 796 μl buffer + 200 μl Coomassie Blue) and the concentration calculated as 14.3 μM.

3.1.7 Size Exclusion Chromatography of HtaA-CR2

The Sephacryl column (16/60 S-200 HR) was from GE Healthcare. The markers were from Sigma-Aldrich: blue dextran (2000 kDa), horse heart cytochrome *c* (12.4 kDa), bovine erythrocyte carbonic anhydrase (29 kDa), bovine serum albumin (66 kDa), yeast alcohol dehydrogenase (150 kDa) and sweet potato β-amylase (200 kDa).

The marker proteins and HtaA-CR2 were prepared in 50 mM Tris-Cl and 100 or 400 mM NaCl pH 7.0. The concentrations were between 2 to 10 mg/ml for the markers and 0.5 mg/ml for HtaA-CR2. The column was equilibrated and the proteins were eluted using the same buffer. The void volume of the column (V_0) was 39 ml as determined by the elution time of the blue dextran.

3.1.8 HtaA-CR2 Heme Extraction and Reconstitution

Apo-HtaA-CR2 was produced via the butanone extraction method (Teale, 1959) . An HtaA-CR2 solution at a pH value of ~2.0 was prepared by adding 1 M HCl dropwise. Equal amounts of the acidic HtaA-CR2 solution and ice cold 2-butanone were mixed. The mixture was vortexed approximately 30 s and set on ice. After 30 min, layers of aqueous apoprotein on the bottom and organic heme-butanone at the top were formed. The bottom solution was removed by pipette and dialyzed against 20 mM Tris-Cl pH 7.0 at 4 °C overnight. The organic heme-butanone layer was discarded.

A stock hemin solution was prepared by dissolving 2 mg of hemin in 1 ml of DMSO. The concentration was determined spectroscopically by using extinction coefficient of 179000 $M^{-1}cm^{-1}$ at 404 nm (Collier et al., 1979). The concentration of apoprotein was determined by using ExPASy extinction coefficient of 24075 $M^{-1}cm^{-1}$ at 280 nm. The apo HtaA-CR2 solution was titrated with the hemin solution by adding 1 μl aliquots; the solution was stirred 30 min after

each addition. At the end of the titration, the stoichiometric ratio of hemin and apoprotein was 1:1. Reconstituted HtaA-CR2 was dialyzed against 50 mM Tris-Cl pH 7.0 overnight.

3.1.9 Apoprotein and Holoprotein Separation

A mixture of apoprotein (80%) and holoprotein (20%) Strep-tag purified HtaA-CR2 protein solution was passed through HiTrap 5 ml Butyl FF and Phenyl FF hydrophobic interaction (HIC) columns in sequence to separate the apoprotein and holoprotein as previously described in chapter 2 (Uluisik et al., 2017).

3.1.10 Homology Modeling

HtaA-CR2 was visualized with 3D I-TASSER homology modelling method (Roy et al., 2010) (http://zhanglab.ccmb.med.umich.edu/I-TASSER/). PyMol was used for molecular visualization (DeLano, 2015).

3.1.11 Electronic Absorption of Chemical Denaturation

Guanidinium hydrochloride (GdnHCl) or guanidinium thiocyanate (GdnSCN) was used to observe the chemical unfolding behavior of HtaA-CR2. The absorbance change in the Soret peak of HtaA-CR2 was followed as a function of guanidinium hydrochloride concentration by UV-visible spectroscopy. The GdnHCl and GdnSCN concentrations were determined via the refractive index method (Pace and Scholtz, 1997). This was a single cuvette experiment in which HtaA-CR2 was titrated with the denaturant and the solution was allowed to reach the equilibrium (defined as a change of less than 0.002 absorbance of two consecutive measurements) before recording the absorbance and adding the next aliquot of titrant. The average time between the measurements was five minutes.

3.1.12 Thermal Unfolding of HtaA-CR2 Using Fluorescence Spectroscopy

The tryptophan emission of HtaA-CR2 as a function of temperature was followed using a ISS PC1 photon counting spectrofluorometer. These experiments were performed at Dr. Roger Wartell's laboratory at the Georgia Institute of Technology. The electrical current was 13 amp; the excitation and emission slit widths were 1 mm and 2 mm, respectively. A screw top cuvette with 1 cm path length was used. The HtaA-CR2 solution was prepared in 50 mM Tris-Cl pH 7.0 containing 3.0 M GdnHCl. The excitation wavelength was 285 nm. The emission intensity at 350 nm was recorded as a function of temperature between 40 and 90 ^{o}C (ramped at 0.5 ^{o}C per min). Data were also recorded for a solution of buffer and GdnHCl without protein. Data reported are the spectrum with protein minus that without the protein.

3.1.13 Thermal Unfolding of HtaA-CR2 in Presence of GdnHCl

Thermal unfolding of HtaA-CR2 was carried out with a UV-visible spectrophotometer equipped with temperature control (TC 125, Quantum Northwest). A screw top cuvette with 1 cm path length was used. GdnHCl was dissolved in 50 mM Tris-Cl pH 7.0 and the concentration (6.4 M) was determined by the refractive index method (Pace and Scholtz, 1997). Holo HtaA-CR2 in 50 mM Tris-Cl pH 7.0 was mixed with various concentrations of GdnHCl from 1.5 M to 3.0 M. The thermal unfolding was carried out from 45 to 85 ^{o}C (3.0 M) or 50 to 90 ^{o}C (1.5 M). The spectrum was recorded every 1 ^{o}C after 1 min incubation.

A two-state protein unfolding model was used to fit the data (Swint and Robertson, 1993):

$$A = \frac{(A_F + m_F T) + (A_U + m_U T) exp\left[\frac{\Delta H_m}{R(T_m^{-1} - T^{-1})}\right]}{1 + exp\left[\frac{\Delta H_m}{R(T_m^{-1} - T^{-1})}\right]} \quad (1)$$

where Y_{abs} is the absorbance at any point along the fitted unfolding curve, Y_F is the absorbance of the folded state, Y_U is the absorbance of the unfolded state, m_F is the slope of the folded state, m_U is the slope of the unfolded state, T_m is the temperature at which the protein is half unfolded, ΔH_m is the enthalpy of unfolding, R is the gas constant, and T is the temperature (Kelvin). Kaleidagraph (version 4.01, Synergy Software) was used to fit the data.

T_m and ΔH_m values in the absence of the denaturant were estimated from the linear extrapolation of T_m vs [GdnHCl] or ΔH_m vs [GdnHCl] plots respectively.

ΔS_m values were calculated for each at the T_m temperature [where the Gibbs' free energy change (ΔG_o) equals to zero] using the following equation (Wen et al., 2007):

$$\Delta H_m = (T_m) \times (\Delta S_m) \quad (2)$$

The unfolding ΔC_p value was calculated using the linear least-squares fit of the following equation (Kumar and Bhuyan, 2009):

$$\Delta H_m = \Delta C_p (T_m) + b \quad (3)$$

where b is the y intercept.

The Gibbs' free energy change (ΔG_o) of the thermal unfolding process was calculated using the following equation (Kumar and Bhuyan, 2009):

$$\Delta G_o = \Delta H_m (1 - T/T_m) + \Delta C_p [T - T_m - T \ln (T/T_m) \quad (4)$$

3.1.14 Electrospray Ionization MS of HtaA-CR2

Electrospray ionization mass spectrometry (ESI) was performed using an Orbitrap mass analyzer in positive mode to determine the molecular weight of the protein. Samples were prepared in water. The capillary voltage was 3500 V and the flow rate was 5 μL/min. Deconvolution of the charge state distribution was performed with the MaxEnt program included with the MassLynx™ software. The peaks are rounded to the nearest Dalton.

The heme dissociation of HtaA-CR2 in gas phase was investigated with Waters Micromass Q-TOF instrument by changing the collision energy using the mildest conditions for the other parameters: capillary voltage 3000 V, cone voltage 18 V, extraction voltage 1.5 V, desolvation gas temperature 100 ^{o}C and source temperature 80 ^{o}C (Chapter 2) (Uluisik et al., 2017).

3.2 Results and Discussion

3.2.1 Site Directed Mutagenesis

Work in the Schmitt laboratory has shown that three possible heme-binding residues are fully conserved in the CR domains of various *Corynebacterium* species: two tyrosines and one histidine, numbered Y361, H412 and Y490 in conserved domain 2 (CR2) (Fig. 3.1), these residues are also conserved between CR1 and C2 domains (Allen & Schmitt, 2011).

To look in more detail at the spectroscopic signatures of each of these putative ligands, all three were mutated to alanine using site-directed mutagenesis. The gel electrophoresis of the PCR reactions under different conditions are shown in Fig. 3.2. The top bands correspond to the PCR product which includes hybrid (mutated and non-mutated) wild-type amplified plasmids. In each reaction, an amplification band appeared; all of these bands have a similar intensity. These

results indicate that varying the ratio of plasmid and primer concentrations (1:6 or 1:12) or DMSO concentrations (2 or 5%) did not affect the PCR reactions. The bottom bands are the excess primer fragments. The control reaction confirms that the amplification did not take place in the absence of pfu-DNA polymerase. One of the five reactions was selected randomly for DpnI digestion to remove wildtype strand from the hybrid plasmids and transform of the mutated plasmids into the competent cells. Figs. 3.3 and 3.4 show the nucleic acid sequence alignment of wild type and Y361A mutant for HtaA-CR2. In the forward and reverse alignment only TAC nucleotides (triplet codon for tyrosine) are replaced with GCG (triplet codons for alanine) which confirms the target mutation; the alignment also confirms that the rest of the sequences are identical. Similar results were observed for the H412A and Y490A mutants.

3.2.2 Maximizing WT Holo HtaA-CR2 Expression

In an effort to maximize the amount of holoprotein, a literature search was performed to look at growth conditions used for other heme binding proteins in the last 20 years. Table 3.4 shows examples of the growth conditions. A number of the protocols used TB. IPTG varied widely from 10 µM to 1 mM. Most protocols added 5-aminolevulinic acid (δ-ALA), which varied from 0.1 to 2.5 mM; δ-ALA is the product of the first step in heme biosynthesis (Warren and Smith, 2009). Some protocols added iron in form of the sulfate or chloride salt. In general, high incubation temperatures (27 – 37 ^{o}C) and long incubation times (as long as 48 h) were used. The final amount of protein varied widely from approximately 5 to 120 mg/L.

Recombinant HtaA-CR2 gene expression was optimized by varying the growth medium LB or TB, oxygen availability, IPTG concentration, incubation time, and addition of δ-ALA, $FeSO_4$ and/or hemin. The concentration of holoprotein was estimated from the Soret absorbance of the solution after cell disruption and centrifugation. For samples purified by

FPLC, the concentrations of holoprotein and apoprotein were determined from the Soret (408 nm) and the 280 nm bands, respectively, using a ratio of 2.0 for the fully holoprotein (determined using Bradford and pyridine hemochrome assays)

Preliminary experiments indicated that TB was better for holoprotein growth than LB (data not shown). δ-ALA is the precursor in the heme biosynthesis pathway and is used to increase the amount of heme in expression heme binding proteins (Sudhamsu et al., 2010). Addition of 0.1 mM δ-ALA and 0.7 mM $FeSO_4$ into the growth culture did not increase protein yield (Table 3.5, 1-A and 1-B). δ-ALA concentrations of 0.5 and 1.0 mM gave similar amounts of holoprotein (Table 3.5, 2-A and 2-B); increasing the concentration of δ-ALA to 2 mM reduced the amount of holoprotein (Table 3.5, 3-A vs. 3-B). The difference in incubation time between these two experiments precludes more detailed conclusions. It might be possible that the integration of heme into apoprotein step might slow; however, we did not see evidence for a lag in heme incorporation upon addition of exogenous heme in reconstitution experiments. Use of low amounts of IPTG can allow cells to grow slowly, with the possibility that prosthetic group biosynthesis could keep up with the production of apoprotein under slow growth conditions. A four-fold difference of IPTG (50 vs. 200 μM) showed no appreciable difference in holoprotein yield (Table 3.5, 2-B and 2-C). IPTG was therefore maintained at 50 μM. Oxygen availability to the growth culture can have a limiting effect on gene expression. At least a two-fold increase in the holo HtaA-CR2 concentration was observed when a larger flask was used for the same amount of growth culture (Table 3.5, 2-C and 2-D), consistent with the role of increased oxygen concentration in promoting HtaA production. Expression overnight rather than for 8 h also resulted in slightly higher amounts of holoprotein (Table 3.5, 3-A and 3-D). Therefore overnight expression was maintained.

Although the strain of *E. coli* used does not have a heme uptake pathway, addition of heme may result in increased amounts of holoprotein due to reconstitution during the workup. Two expressions performed, one with added hemin and one without, which were taken all the way through FPLC purification. Although the conditions were different, the Soret/280 nm ratios were similar, indicating that added hemin does not significantly increase the amount of holoprotein (Table 3.5, 1-C, with hemin had a ratio of 0.2 and 3-A, without hemin, had a ratio of 0.5). In the end, growth conditions were chosen as 50 μM IPTG, 0.5 mM δ-ALA, and an overnight expression at 28 ^{o}C in TB media with high oxygen availability.

3.2.3 Expression and Purification of HtaA-CR2

The wild type (WT) protein and all three mutants were purified by FPLC. The FPLC chromatograms of WT (Fig. 3.5) and the mutants (not shown) were similar. The chromatogram, following the absorbance at 280 nm, shows excellent separation for the protein peak. The purity of the pooled protein fractions was evaluated with SDS-PAGE (Fig. 3.6). The HtaA-CR2 bands are in line with the theoretical molecular weight (27.3 kDa) and show minimal contamination.

3.2.4 UV-Visible Absorption Spectroscopy

Fig. 3.7 shows the characteristic peaks for HtaA-CR2 between 250 and 800 nm. The maximum for the Soret band is at 407 nm and four α/β bands are at 509, 547, 573 and 626 nm. The spectrum is similar to that of the phenol complex of leghemoglobin *a* (Jones et al., 2002). The band at 626 is indicative of a high-spin iron, common for tyrosine ligation (Tiedemann and Stillman, 2011; Rodgers and Lukat-Rodgers, 2014).

An overlay of the fully heme-loaded protein, a sample that was largely apoprotein, and a sample that was a mixture of holoprotein and apoprotein showed identical spectra, as seen in Fig. 3.8. Thus, the UV-visible spectroscopy of the holoprotein is not affected by the presence of

apoprotein. The UV-visible spectra were consistent across purifications; comparisons of the α/β bands of various purified samples of the protein are shown in Fig. 3.9.

The UV-visible spectra of Y361A, H412A and Y490A show that these proteins purified mainly in apoprotein form (Fig. 3.10). The Soret/280 ratio was 0.02 for Y361A, 0.04 for H412A and 0.08 for Y490A. Considering that the Soret/280 ratio is 0.6 for as-isolated WT HtaA-CR2 and 2.0 when the protein is fully heme loaded, the heme content of the mutants are low (less than 5%). These data indicate the importance of these conserved residues in the heme binding of HtaA-CR2. These data are in line with previous studies by Schmitt et al. (Allen and Schmitt, 2011). TheY361 residue has been proposed as the axial ligand with H412 as the possible hydrogen bonding partner (Uluisik et al., 2017). The role of Y490 in heme binding is not yet well understood.

3.2.5 Separation of holo and apo WT HtaA-CR2

Heme association with the protein is driven by amino acid axial ligand interactions with the heme iron, electrostatic interactions between the protein and the heme propionate groups, and various hydrophobic interactions between the heme and the protein (Hargrove et al., 1996; Robinson et al., 1997; Deniau et al., 2003; Zheng and Gunner, 2008). One can presume that the apoprotein form of a heme protein might be more hydrophobic then the holoprotein form of the protein both due to increased hydrophobic surface area in the heme binding pocket and to the absence of the charged Fe(III) center and the propionate groups of the bound heme. Hydrophobic interaction columns (HIC) have been used to separate apoprotein and holoprotein heme binding by exploiting this hydrophobicity difference (Jepkorir et al., 2010).

To separate the holoprotein and apoprotein, the Strep-tag purified HtaA-CR2 solution was passed through Butyl FF and Phenyl FF hydrophobic interaction columns in sequence. The

first experiment involved a binding buffer containing 1.5 M $(NH_4)_2SO_4$. An HtaA-CR2 holoprotein and apoprotein mixture (Soret/280 ratio of 0.7) was passed through a Butyl FF column. A single peak was observed (Fig. 3.11). Fractions 5-7 were pooled to give a sample with a Soret/280 ratio of 0.94; the holoprotein recovery was 85% based on the Soret absorbance.

The sample was then passed through a Phenyl FF column. The FPLC chromatogram showed two overlapping peaks (Fig. 3.12). Fraction 7 had only a small amount of holoprotein (data not shown). The initial fraction of the second peak (9) contained a high holoprotein concentration (Soret/280 nm ratio of 2.2). The majority of the apoprotein eluded in the latter fractions as shown in the Fig. 3.12. The fractions that contained holoprotein (8 – 10) were pooled and concentrated. The Soret/280 ratio increased from ~0.7 (as-isolated) to ~2 after passing through both columns (Fig. 3.13). This was in agreement with the increase in the heme loading from 20% to 100% as determined from the Bradford and pyridine hemochrome assays. Approximately 40% of the holoprotein was recovered from the initial sample after the two columns. Evaluation of heme loading via the pyridine hemochrome and Bradford assays showed that the fully holoprotein had one heme per molecule of HtaA-CR2.

In refining apoprotein and holoprotein separation, the salt type might be a major factor to consider. The second experiment involved a binding buffer containing 4 M NaCl in place of 1.5 M $(NH_4)_2SO_4$. Although the Soret/280 ratio nm was similar to the previous experiment after the second column (1.91), the final holoprotein overall recovery was significantly lower (21%) (data not shown).

3.2.6 Size Exclusion Chromatography of WT HtaA-CR2

Some heme transfer proteins form dimers or higher oligomers in solution (Watanabe et al., 2008). To investigate possible oligomer formation of HtaA-CR2, size exclusion

chromatography was performed. Five protein markers were used to create the calibration curve within 12.4 to 200 kDa range. The retention volumes (V_e) for cytochrome *c*, carbonic anhydrase, bovine serum albumin, alcohol dehydrogenase and β-amylase were 78, 66, 54, 48 and 45 ml, respectively. The retention volume for HtaA-CR2 was around 60 ml (Fig. 3.14). The molecular weight for HtaA-CR2 was calculated to be 50.1 ± 6.6 kDa (Fig. 3.15). These data are consistent with theoretical value of 54.6 kDa for a dimer of HtaA-CR2. Because dimerization can be a function of the ionic strength of the solution, the experiment was run again at 400 mM NaCl; the results were the same as at 100 mM NaCl (data not shown). The experiment was also run varying the heme concentration of the protein (20% or 80% heme loaded) at 100 mM NaCl and the results were again similar (data not shown). This indicates that the dimerization in solution is not a strong function of the ionic strength of the solution or the holoprotein/apoprotein ratio.

Watanabe has shown that the extent of heme binding depends on the oligomeric state of the protein for IsdH NEAT3 (Watanabe et al., 2008). We have observed a similar phenomenon for Shr-N1 from *S. pyogenes* (unpublished data from the Dixon laboratory). In the case of HtaA-CR2, we only observe the dimer and can isolate, via hydrophobic interaction chromatography, a fully heme-loaded dimer (e.g., one heme per monomer in the dimer).

3.2.7 HtaA-CR2 Heme Extraction and Reconstitution

Heme extraction and reconstitution of HtaA-CR2 was used to increase the heme loading of the protein. The reconstituted HtaA-CR2 spectrum is different than the as-isolated spectra (Fig. 3.16). The Soret band is blue shifted around 10 nm and there is shoulder appearing at 370 nm which might be the free heme in solution or a non-specific binding of heme to the protein. The α/β bands are broader. All of these observations indicate that attempts to add heme to the

protein do not give the same form of the protein that is isolated after purification (Chapter 2) (Uluisik et al., 2017).

3.2.8 Homology Modeling

The homology modeling of HtaA-CR2 was performed by I-TASSER program (Roy et al., 2010). The server predicts the 3D structure through amino acid sequence alignment of a protein and multiple structurally known proteins from protein data bank (PDB).The five closest model proteins chosen by the I-TASSER program were outer membrane protease (OMPT) from *E. coli*, plasminogen activator (Pla) from *Y. pestis*, D-aminoacylase from *Alcaligenes faecalis*, allene oxide cyclase from *Arabidopsis thaliana* and dihydroorotase from the hyperthermophile *Aquifex aeolicus*. The closest sequence of OMPT had only 8.4% identity. It can be seen that most of the protein in the homology model is unstructured (Fig. 3.17). This indicates that HtaA-CR2 is indeed a novel protein, with limited sequence and structural homology to known proteins.

3.2.9 Chemical unfolding of HtaA-CR2

Unfolding of proteins in heme transfer pathways can be used to understand the ease with which these proteins may transfer heme. The degree of protein stability might be also useful to predict the functional characteristics. An initial attempt was made to perform a GdnHCl titration of HtaA-CR2. Fig. 3.18 shows the absorbance of HtaA-CR2 as a function of GdnHCl concentration up to 4.5 M. Almost no spectral change was seen. A second experiment with the much stronger denaturing agent guanidinium thiocyanate (GdnSCN) also showed no significant spectra change up to 4 M denaturant (Fig. 3.19). These data indicate that HtaA-CR2 is significantly stable protein. This high structural stability may avoid heme loss and allow multiple cycles of a single protein for heme uptake and release. Studies of the unfolding kinetics at high

concentrations of GdnHCl were completed and have been published (Chapter 2) (Uluisik et al., 2017).

3.2.10 Thermal Unfolding of HtaA-CR2

Thermal unfolding of HtaA-CR2 in the presence of 1.5, 1.75, 2, 2.5 and 3 M GdnHCl was shown in Chapter 2. Additional data and analysis are below.

Spectra in 1.5 M GdnHCl as a function of temperature showed that the Soret band gradually decreased as the temperature increased and blue shifted about 12 nm (Fig. 3.20). Similar results were observed at all GdnHCl concentrations tested. The protein solutions were cooled to room temperature at the end of each experiment. Approximately 30% Soret recovery was observed with the solutions of 1.5 and 1.75 M GdnHCl present (Fig. 3.20 inset). No recovery was observed when the GdnHCl concentration was higher than 1.75 M (data not shown). These data indicate that majority of the thermal unfolding in the presence of chemical denaturant is irreversible.

If the unfolding is in thermodynamic equilibrium at each point along the titration, thermodynamic parameters for the unfolding process can be calculated via non-linear least squares fitting of the data to equation 1. Fig. 3.21 – 3.25 show the fittings for each GdnHCl concentration. ΔS_m values were calculated for each at the T_m temperature [where the Gibbs' free energy change (ΔG_o) equals to zero] using the equation 2. The thermodynamic parameters are given in Table 3.6.

When higher concentrations of the denaturant were present, the T_m values decreased. ΔH_m and ΔS_m values also decreased as the concentration of GdnHCl increased. To obtain values for the thermodynamic parameters in the absence of denaturant, these data sets were each extrapolated to zero with a linear function to give a T_m value of 84 ^oC, ΔH_m value of 364

$kJmol^{-1}$, and ΔS_m value of 1033 $Jmol^{-1}K^{-1}$ (Fig. 3.26, 3.27, and 3.28, respectively). Assuming the enthalpy of unfolding is independent of the concentration of GdnHCl (Pfeil, 1993), the theoretical heat capacity change (ΔC_p) value of 6.9 $kJmol^{-1}K^{-1}$ was determined for using the slope of the plot of ΔH_m vs T_m (eq. 3) (Fig. 3.29). Finally, the standard Gibbs' free energy change, ΔG_o (H_2O, 25 °C) of 25.7 kJ mol^{-1} computed using the modified Gibbs-Helmholtz equation (eq. 4) (Wen et al., 2007; Kumar and Bhuyan, 2009). The theoretical dependence of the free energy of unfolding on the temperature is expected to be parabolic in shape. Fig. 3.30 shows a plot of the free energy of unfolding vs. temperature for HtaA-CR2 and selected proteins from the literature (Table 3.7). The curves tend to be similar despite significant differences in the thermodynamic parameters. Most studies perform thermal unfolding experiments by waiting approximately two minutes at each temperature. Concerned, in view of the apparent stability of this protein, that perhaps a two minute wait time was not enough, we performed kinetic studies described in Chapter 2 and in more detail below. In fact, HtaA-CR2 unfolds very slowly. Therefore, although our data formed smooth patterns and were similar to examples in the literature, we were concerned that these observations maybe fortuitous, and the parameters calculated may not reflect the true thermodynamic nature of this protein. These data were not published.

3.2.11 Unfolding Kinetics

The unfolding kinetic rate constant value of 1.3 x 10^{-6} s^{-1} at 37 ^oC for HtaA-CR2 was previously reported (Uluisik et al., 2017). The apparent value was calculated using extrapolation method from the plot of unfolding rate constants vs. denaturant concentration (Fig. S2.7 Chapter 2, Table 3.8). These data indicate that the protein unfolds very slowly, which is consistent with our previous stability results. A literature search was made to compare the unfolding kinetics of

HtaA-CR2 with other heme proteins (Table 3.9). The data are limited, but HtaA-CR2 unfolds more slowly than the cytochromes from the mesophilic bacteria, though more quickly than soybean and horseradish peroxidases.

3.2.12 Tryptophan Emission Spectrum of HtaA-CR2 as a Function of Temperature

The tryptophan emission as a function of temperature in the presence of 3 M GdnHCl was investigated as another method of evaluating the unfolding behavior of HtaA-CR2. First, temperature dependence of the emission of a solution of 3 M GdnHCl was determined at 350 nm (Fig. 3.31); these data points were subtracted from the data collected from HtaA-CR2 in the presence of 3 M GdnHCl. Second, the emission spectra were measured at 40 and 90 ^{o}C to determine the degree of the spectral change between low and high temperatures. The λ_{max} remained the same between 40 and 90 ^{o}C (Fig. 3.32) but the intensity decreased by approximately 50% with increasing temperature. Finally, the emission intensity of HtaA-CR2 was monitored as a function of temperature in the presence of 3 M GdnHCl at 350 nm. The emission spectra showed three distinct behaviors. The emission intensity decreased from 40 to 58 ^{o}C, increased from 58 to 73 ^{o}C, and decreased from 73 - 90 ^{o}C (Fig. 3.33). The protein sample was around 20% heme loaded. The unconventional unfolding pattern might be due to the collection of data from both apoprotein and holoprotein unfolding. Previously, an apparent T_m of ~70 ^{o}C was determined for HtaA-CR2 in presence of 3 M GdnHCl using UV-visible spectroscopy (Uluisik et al., 2017). It is tempting to hypothesize that the decrease in emission spectra can be assigned to the unfolding of the apoprotein; the emission increase in 58 - 73 ^{o}C might be the unfolding of the holoprotein in conjunction with release of the heme and the fluorescence emission quenching. This hypothesis is also consistent with T_m of ~70 ^{o}C as being approximately a midpoint of 58 - 73 ^{o}C.

3.2.13 Apoprotein/Holoprotein Characterization of HtaA-CR2 as a Function of ESI Collision Energy

The ESI-MS spectrum of HtaA-CR2 showed peaks in the charge distribution between +10 and +15 (Fig. 3.34). The spectra also showed singly charged peaks at in the 560 - 700 ppm region which corresponded to free heme and PPIX. The deconvoluted mass spectrum showed multiple peaks (data not shown). The 27315 peak was the molecular ion which is consistent with the theoretical molecular weight of 27319 (from ExPASy) for apo-HtaA-CR2. Higher molecular weight peaks of significant intensity and increasing by 21-25 ppm increments suggest that majority of apo HtaA-CR2 formed Na^+ adduct(s).

In Chapter 2, the ease of heme dissociation of HtaA-CR2 in the gas phase was investigated via ESI mass spectrometry using a Waters Micromass Q-TOF instrument (Uluisik et al., 2017). Initially, preliminary data were collected by studying the model system myoglobin which binds heme tightly. The effects of different parameters such as capillary voltage, extraction voltage, cone voltage, desolvation gas flow rate, desolvation gas temperature, source temperature and collision energy of ESI MS instrument on heme binding of myoglobin were investigated. In general, variation of the parameters did not change the holoprotein/apoprotein ratio significantly (Table 3.10). However, varying the collision energy between 5 and 40 V showed heme loading from 95% holoprotein at low collision energy to 0% at high collision energy (Fig. 3.35). Fig. 3.36 shows the charge state distributions and the deconvoluted spectrum for each parameter that was tested. The charge states were mainly +8, +9 and +10 for the holoprotein and +7, +8 and +9 for the apoprotein form of the protein. The linear dependence of the percent of holoprotein on the collision energy was also found in a study of sperm whale myoglobin by Mauk and colleagues (Hunter et al., 1997).

Heme binding of HtaA-CR2 was carried out by changing the collision energy using the mildest conditions for the other parameters (capillary voltage 3000 V, cone voltage 18 V, extraction voltage 1.5 V, desolvation gas temperature 100 ^{o}C and source temperature 80 ^{o}C). Experiments were conducted on two preparations of HtaA-CR2, varying the collision energy between 5 and 60V. The first was with the as-isolated protein which was approximately 20% heme loaded. Due to the high concentration of apoprotein, the initial protein signals were mainly from the apo form; the sample showed approximately 10% holoprotein peaks up to 20V and fully apoprotein above that (Fig. 3.37). The charge envelope was between +14 and +20 when collision energy was 5 V. The envelope was shifted to the right (+10 to +15) when collision energy was 60 V, perhaps indicating at the high collision energy the protein goes through a conformational change that exhibits a different set of solvent exposed ionizable groups.

Second, the experiments were performed with a sample that was approximately 90% heme loaded. The holoprotein signal was 70% at the lowest collision energy and 20% at the highest voltage; these data has been published (Uluisik et al., 2017).

3.3 Abbreviations

δ-ALA, 5-aminolevulinic acid; BSA, bovine serum albumin; CV, column volume; DMSO, dimethyl sulfoxide; ESI, electrospray ionization; FPLC, fast protein liquid chromatography; GdnHCl, guanidinium hydrochloride; GdnSCN, guanidinium thiocyanate; HIC, hydrophobic interaction column; IPTG, isopropyl β-D-1-thiogalactopyranoside; LB, Luria-Bertani; Mb, myoglobin; PDB, protein data bank PMSF, phenylmethanesulfonyl fluoride; SDS-PAGE, sodium dodecyl sulfate polyacrylamide gel electrophoresis; TB, Terrific Broth; WT, wild-type.

Table 3.1 PCR reaction mixtures of HtaA-CR2 for Y361A, H412A and Y490A mutations

Reaction	**1**	**2**	**3**	**4**	**5**	**C**
Wild type plasmid (μl)	1 (106 ng)	0.5 (53 ng)	1	0.5	0.5	0.5
Forward primer (μl)	6 (500 ng)	3 (250 ng)	6	3	6	3
Reverse primer (μl)	6 (500 ng)	3 (250 ng)	6	3	6	3
dNTP mix (μl)	1 (0.2 mM)	1	1	1	1	1
DMSO (μl)	2.5 (5%)	2.5	1 (2%)	1	2.5	1
Pfu polymerase (μl)	1	1	1	1	1	none
10 x Pfu Buffer (μl)	5	5	5	5	5	5
Nanopure water (μl)	27.5	34	29	35.5	28	35.5
Total volume (μl)	50	50	50	50	50	50

Table 3.2 HtaA-CR2 extinction coefficients

Trial	ϵ_{407} (M^{-1} cm^{-1})	Notes
1	1.13×10^5	New Batch RU_II_001
2	1.23×10^5	HtaA-CR2 Purified RU_I_040
3	1.19×10^5	HtaA-CR2 Purified RU_I_040
4	1.25×10^5	HtaA-CR2 Purified RU_I_040
5	1.10×10^5	HtaA-CR2 Purified RU_I_035
Average	1.18×10^5	

Table 3.3 Bradford Assay Standard Curve

BSA (μl)	Buffer (μl)	Commassie Blue (μl)	Abs at 595 nm
2	798	200	0.075
4	796	200	0.130
6	794	200	0.169
8	792	200	0.195
10	790	200	0.235

Bovine serum albumin (BSA) concentration was 0.39 μg/μl (determined based on 280 nm absorbance). Buffer was 25 mM Tris-Cl pH 7.0. Reported absorbances are the average of two measurements.

Table 3.4 Expression and growth conditions of various heme proteins

Protein	Organism	Broth	IPTG (mM)	δ-ALA (mM)	Growth temp and time	Amount	Reference
Multiheme cytochrome	*Geobacter sulfurreducens* in *E. coli*	nr	nr	nr	30 °C, 16 h	nr	(Londer et al., 2006)
Hemoglobin I	*Lucina pectinata* in *E. coli*	TB	1	nr	30 °C, 3 h	32 mg/L	(León et al., 2004)
Cytochrome b_5	Rabbit in *E. coli*	TB	0.01	0.5	37 °C, 16 h	121 mg/L	(Mulrooney and Waskell, 2000)
Indoleamine 2,3-dioxygenase	Human in *E. coli*	LB	0.1	0.5	30 °C	3 – 5 mg/L	(Austin et al., 2004)
CYP1B1	Human in *E. coli*	Small scale LB. Large scale TB.	1	2.5	30 °C, 24 h	920 nmol/L	(Jansson et al., 2000)
Cytochrome P450	*Musca domestica* in *E. coli*	Small scale LB. Large scale TB.	1	0.5	28 °C, 48 h	15 mg/L	(Zhang et al., 2010)
Catalase	*Psychrobacter* in *E. coli*	LB	0.01	4	27 °C	nr	(Kimoto et al., 2008)
Cytochrome P450-2C9	Human in *E. coli*	Small scale LB. Large scale TB.	0.5 or 0.1	0.5 or 0.1	30 °C, 48 h	nr	(Hao et al., 2007)
Cytochrome b_5	OM gene in *E. coli*	Minimal media	1	0.1	nr	15 – 25 mg/L	(Rivera and Walker, 1995)
Cytochrome P450	*Streptomyces griseolus* in *E. coli*	TB	1	1	25 °C, 24 - 48 h	nr	(Hussain and Ward, 2003)
Cystathionine β-synthase	Human in *E. coli*	NZCYMT media	0.5	0.3	37 °C, 21 h	nr	(Kery et al., 1995)

Table 3.5 Expression of HtaA-CR2 gene from *Corynebacterium diphtheriae* in *E. coli* [BL21(DE3)/pET24a(+)]

Exp Number	Flask Size (ml)	Medium (ml)	IPTG (μM)	δ-ALA (mM)	Incubation Time[c] (h)	Temp (^{o}C)	Cell Paste (gr)	Soret Abs[d]	Soret/Abs280	holo HtaA (mg)
1-A	2000	200 LB	1000	-	3	28	0.6	0.1	-	1.2
1-B	2000	200 LB	1000	0.1[b]	3	28	0.6	0.1	-	1.2
1-C	2000	200 LB	1000[a]	-	3	28	1.0	0.3	0.2	2.5
2-A	250	200 TB	200	1.0	6	26	0.6	0.3	-	3.4
2-B	250	200 TB	200	0.5	6	26	0.6	0.3	-	3.9
2-C	250	200 TB	50	0.5	6	26	0.6	0.3	-	3.6
2-D	2000	200 TB	50	0.5	6	26	2.4	0.6	-	8.7
3-A	2000	400 TB	50	0.5	18	28	8.9	1.3	0.5	17.4
3-B	2000	400 TB	50	2.0	8	28	5.0	0.6	-	7.50
3-C	2000	200 TB	50	0.5	8	28	3.1	0.6	-	8.0
3-D	2000	400 TB	50	0.5	8	28	7.4	1.2	-	12.8

[a]Hemin (1.0 μM) was added after 10 min after adding IPTG. [b]$FeSO_4$ (0.7 mM) was included in the growth media as an additive along with δ-ALA. [c]Incubation time after adding IPTG. [d]From the first cell lysate fraction if there are two. The Soret absorbance was used to calculate the mg of the protein by using extinction coefficient of 1.2×10^{-5} M^{-1} cm^{-1}. TB is Terrific broth. LB is Luria Bertani broth.

Table 3.6 Thermodynamic parameters of thermal unfolding of HtaA-CR2

[GdnHCl] M	[a]T_m (^oC)	[b]ΔH_m (kJ mol^{-1})	[c]ΔS_m (J $mol^{-1}K^{-1}$)
1.50	77.0 ± 0.5	311.7 ± 6.2	890.1 ± 17.6
1.75	75.1 ± 0.5	305.0 ± 14.7	875.8 ± 42.2
2.00	73.3 ± 0.5	292.3 ± 8.6	843.7 ± 24.8
2.50	71.1 ± 0.5	280.5 ± 7.1	814.8 ± 20.5
3.00	69.7 ± 0.5	259.5 ± 7.9	749.0 ± 22.8

[ab]The values were calculated from nonlinear least squares fitting of the Soret absorbance vs. temperature (Fig. 21 - 25) by using equation 1. [c]Since ΔG equals to zero at T_m, $\Delta H_m = (T_m)(\Delta S_m)$ equation was used to calculate the ΔS_m values.

Table 3.7 Thermodynamic parameters of various heme binding proteins

Protein	T_m (K)	T_m (°C)	ΔC_p (kJ/mol.K)	ΔH_m (kJ/mol)	ΔS_m (J/mol.K)	Reference
Hydrogenobacter thermophilus cyt c_{552}	412 ± 3	139 ± 1	3.4 ± 0.5	393 ± 33	954 ± 80	(Wen et al., 2007)
Pseudomonas aeruginosa cyt c_{551}	351 ± 1	80 ± 1	4.8 ± 0.5	301 ± 16	853 ± 45	(Wen et al., 2007)
[a]Soybean peroxidase	359	85	3.9	192	520	(Amisha Kamal and Behere, 2002)
[a]Rabbit holo-cyt b_5	344	70	6.0	329	nr	(Pfeil, 1993)
Corynebacterium diphtheriae HtaA-CR2	358 ± 4	84 ± 1	6.9 ± 0.9	364 ± 5	1033 ± 17	This work
[a]Horse heart Myoglobin	355	81	9.7	510	nr	(Kumar and Bhuyan, 2009)
Horse cyt *c*	361 ± 1	87 ± 1	6.6 ± 0.6	314 ± 19	nr	(Saini et al., 2010)
Escherichia coli cyt b_{562}	340 ± 3	67 ± 1	9.9 ± 1.6	393 ± 21	nr	(Feng and Sligar, 1991)

[a]The standard deviation values are not reported. The values are not reported (nr).

Table 3.8 Unfolding rate constants of HtaA-CR2 in the presence of GdnHCl

[GdnHCl], M	k, min^{-1}	[a]$t_{1/2}$, h
6.6	0.00214 ± 0.00001	5.49
6.8	0.00232 ± 0.00001	4.97
7.0	0.00265 ± 0.00002	4.36
7.2	0.00276 ± 0.00002	4.19
7.4	0.00322 ± 0.00003	3.59
0 (Calculated)	0.00008 ± 0.00001	144

[a]Half-life values were calculated for the first order protein unfolding processes using the equation of $t_{1/2} = 0.693 / k$.

Table 3.9 Unfolding rate constants of various heme binding proteins

Protein	Temp (°C)	pH	Rate constant (s^{-1}) at [GdnHCl] = 0	Reference
[a]Cytochrome c_{552} from *Thermus thermophilus*	10	7.0	6.7×10^{-10}	(Travaglini-Allocatelli et al., 2003)
[a]Cytochrome c_{552} from *Thermus thermophilus*	10	2.1	3.7×10^{-6}	(Travaglini-Allocatelli et al., 2003)
[a]Cytochrome c_{552} from *Hydrogenobacter thermophilus*	10	4.7	4.0×10^{-4}	(Travaglini-Allocatelli et al., 2005)
[b]Soybean peroxidase	25	7.0	1.5×10^{-11}	(Amisha Kamal and Behere, 2008)
[b]Horseradish peroxidase	25	7.0	1.7×10^{-8}	(Amisha Kamal and Behere, 2008)
[a]Cytochrome c_{6A} from *Arabidopsis thaliana*	20	7.0	3.5×10^{-6}	(Mason et al., 2012)
[a]Cytochrome c_{6A} C67/73S from *Arabidopsis thaliana*	20	7.0	5.2×10^{-4}	(Mason et al., 2012)
[a]Cytochrome c_6 from *Phormidium laminosum*	20	7.0	1.4×10^{-1}	(Mason et al., 2012)
[a]Cytochrome c_{551} from *Pseudomonas aeruginosa*	10	4.7	6.0×10^{-2}	(Travaglini-Allocatelli et al., 1999)
[a]Cytochrome c_{551} from *Pseudomonas aeruginosa*	10	3.0	3.3×10^{-1}	(Travaglini-Allocatelli et al., 1999)
HtaA-CR2 from *Corynebacterium diphtheriae*	37	7.0	$1.3 \pm 0.1 \times 10^{-6}$	(Uluisik et al., 2017)

[a]The rate constants were calculated using the chevron plots. [b]Standard deviation values are not reported.

Table 3.10 The percentage of holomyoglobin in the gas phase as a function of various ESI Q-TOF parameters

Parameter	Parameter Range	% Holo Range[a]
Capillary Voltage	2500 – 4500 V	100 – 100
Extraction Voltage	1.5 – 3.5 V	100 – 92
Cone Voltage	12 – 50 V	100 – 67
Desolvation Gas Flow Rate	350 – 600 L/h	100 – 100
Desolvation Gas Temperature	130 – 200 ^{o}C	100 – 95
Source Temperature	80 – 150 ^{o}C	100 – 94
Collision Energy	5 – 40 V	95 – 0

[a]The percentage of holomyoglobin at lowest and highest value of the parameter that was tested. The values were determined based on the peak heights of the deconvoluted data.

Figure 3.1 ClustalW alignment of HtaACR2 domains of *C. diphtheria*, *C. aurimucosum*, *C. jeikeium* and *C. ulcerans* identified three conserved residues for ligand binding: Tyr361, His412 and Tyr490.

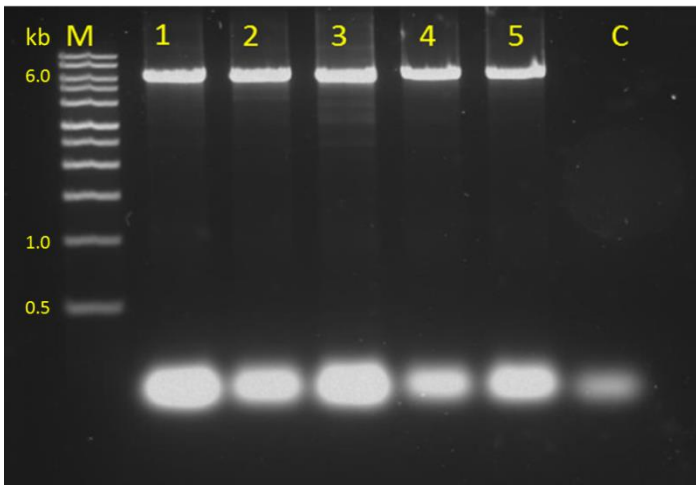

Figure 3.2 The gel electrophoresis of HtaA-CR2 Y361A site-directed mutagenesis PCR products under five different conditions (described in table RUII055A). C is the control. M is the DNA ladder (New England BioLabs).

```
HtaA-CR2        -----------------------------------GATGCGACTCGAACATCCCCTCA 23
Y361A-F         GGCAAGCTGGAGCCACCCGCAGTTCGAAAAGGGTGCAGATGCGACTCGAACATCCCCTCA 120
                                                   ***********************

HtaA-CR2        AACGCAACGAAGCGCTGGAACGACACGAGGATCTTCGGAAAGAATCGCCAATTCTTCCCC 83
Y361A-F         AACGCAACGAAGCGCTGGAACGACACGAGGATCTTCGGAAAGAATCGCCAATTCTTCCCC 180
                ************************************************************

HtaA-CR2        TCAATGCGATGCATCCTCTCGGGGTGTTACTCAGGCTCACGCAGCGTGGGGCTTGAAAAA 143
Y361A-F         TCAATGCGATGCATCCTCTCGGGGTGTTACTCAGGCTCACGCAGCGTGGGGCTTGAAAAA 240
                ************************************************************

HtaA-CR2        GTCGTTCCAGTCTTACATCACTGGTTCTATAGCAAAGGGGCAATGGAACCTTGATGGCGT 203
Y361A-F         GTCGTTCCAGTCTGCGATCACTGGTTCTATAGCAAAGGGGCAATGGAACCTTGATGGCGT 300
                ************   ********************************************

HtaA-CR2        TGGTTATTCCAACGGAGAGTTCACCTTCTCTGGCGCGTCGGGAGCAGTAGATCCACAAGC 263
Y361A-F         TGGTTATTCCAACGGAGAGTTCACCTTCTCTGGCGCGTCGGGAGCAGTAGATCCACAAGC 360
                ************************************************************

HtaA-CR2        AAAATCTGGATTCGTAAAATTCGGCGGAACGATGCGTTTTAGTGGTCATCACGGCATCTT 323
Y361A-F         AAAATCTGGATTCGTAAAATTCGGCGGAACGATGCGTTTTAGTGGTCATCACGGCATCTT 420
                ************************************************************

HtaA-CR2        GGATCTCAATATTTCCAATCCAGAAATTGTTTTCAACGGTGCTACCGGAACTTTGTTCGC 383
Y361A-F         GGATCTCAATATTTCCAATCCAGAAATTGTTTTCAACGGTGCTACCGGAACTTTGTTCGC 480
                ************************************************************

HtaA-CR2        CCAAGTTCGCTCGTCTGACATGGAAGGCAAGAAGTCAGATTATGGTCGAGTAGCTATCGG 443
Y361A-F         CCAAGTTCGCTCGTCTGACATGGAAGGCAAGAAGTCAGATTATGGTCGAGTAGCTATCGG 540
                ************************************************************

HtaA-CR2        CAATCTTACTTTTAGCTCTTTGAATGCTTCTGAAACCGCGGCTAGTGGCAAAGCCACAAT 503
Y361A-F         CAATCTTACTTTTAGCTCTTTGAATGCTTCTGAAACCGCGGCTAGTGGCAAAGCCACAAT 600
                ************************************************************

HtaA-CR2        GACATTGCATCCAGATGGTGCTGGCGCATTCGCTGGCTTCTATGAAGCTGGCTCTGACCT 563
Y361A-F         GACATTGCATCCAGATGGTGCTGGCGCATTCGCTGGCTTCTATGAAGCTGGCTCTGACCT 660
                ************************************************************

HtaA-CR2        TGATCCGATCACTTTCGATGCCCAACTCGGCGGAGCAGCCGATTGTTCTACTGGAACAAA 623
Y361A-F         TGATCCGATCACTTTCGATGCCCAACTCGGCGGAGCAGCCGATTGTTCTACTGGAACAAA 720
                ************************************************************

HtaA-CR2        TGCAGCTGCTGTTCCTGTTTCAGGTGGGAAGGAATCGTCGATTCCTTCCGGAAAATCTGA 683
Y361A-F         TGCAGCTGCTGTTCCTGTTTCAGGTGGGAAGGAATCGTCGATTCCTTCCGGAAAATCTGA 780
                ************************************************************

HtaA-CR2        AGGGGGCACCTCTGCAGGCTATGAAAGTGGCGCTAAAAACTTCAAGATTCGTTCTGCGGC 743
Y361A-F         AGGGGGCACCTCTGCAGGCTATGAAAGTGGCGCTAAAAACTTCAAGATTCGTTCTGCGGC 840
                ************************************************************
```

Figure 3.3 DNA sequence alignment of wild type HtaA-CR2 and the HtaA-CR2 Y361A mutant in forward direction. The missing stars represent the mutation codon in fourth row (TAC = Tyr, GCG= Ala). Clustal Omega was used for the alignment (Sievers and Higgins, 2014).

```
HtaA-CR2        --------------GATGCGACTCGAACATCCCCTCAAACGCAACGAAGCGCTGGAACGA 46
Y361A-R         TCGAAAAGGGTGCAGATGCGACTCGAACATCCCCTCAAACGCAACGAAGCGCTGGAACGA 420
                             *********************************************

HtaA-CR2        CACGAGGATCTTCGGAAAGAATCGCCAATTCTTCCCCTCAATGCGATGCATCCTCTCGGG 106
Y361A-R         CACGAGGATCTTCGGAAAGAATCGCCAATTCTTCCCCTCAATGCGATGCATCCTCTCGGG 480
                ************************************************************

HtaA-CR2        GTGTTACTCAGGCTCACGCAGCGTGGGGCTTGAAAAAGTCGTTCCAGTCTTACATCACTG 166
Y361A-R         GTGTTACTCAGGCTCACGCAGCGTGGGGCTTGAAAAAGTCGTTCCAGTCTGCGATCACTG 540
                ************************************************   *******

HtaA-CR2        GTTCTATAGCAAAGGGGCAATGGAACCTTGATGGCGTTGGTTATTCCAACGGAGAGTTCA 226
Y361A-R         GTTCTATAGCAAAGGGGCAATGGAACCTTGATGGCGTTGGTTATTCCAACGGAGAGTTCA 600
                ************************************************************

HtaA-CR2        CCTTCTCTGGCGCGTCGGGAGCAGTAGATCCACAAGCAAAATCTGGATTCGTAAAATTCG 286
Y361A-R         CCTTCTCTGGCGCGTCGGGAGCAGTAGATCCACAAGCAAAATCTGGATTCGTAAAATTCG 660
                ************************************************************

HtaA-CR2        GCGGAACGATGCGTTTTAGTGGTCATCACGGCATCTTGGATCTCAATATTTCCAATCCAG 346
Y361A-R         GCGGAACGATGCGTTTTAGTGGTCATCACGGCATCTTGGATCTCAATATTTCCAATCCAG 720
                ************************************************************

HtaA-CR2        AAATTGTTTTCAACGGTGCTACCGGAACTTTGTTCGCCCAAGTTCGCTCGTCTGACATGG 406
Y361A-R         AAATTGTTTTCAACGGTGCTACCGGAACTTTGTTCGCCCAAGTTCGCTCGTCTGACATGG 780
                ************************************************************

HtaA-CR2        AAGGCAAGAAGTCAGATTATGGTCGAGTAGCTATCGGCAATCTTACTTTTAGCTCTTTGA 466
Y361A-R         AAGGCAAGAAGTCAGATTATGGTCGAGTAGCTATCGGCAATCTTACTTTTAGCTCTTTGA 840
                ************************************************************

HtaA-CR2        ATGCTTCTGAAACCGCGGCTAGTGGCAAAGCCACAATGACATTGCATCCAGATGGTGCTG 526
Y361A-R         ATGCTTCTGAAACCGCGGCTAGTGGCAAAGCCACAATGACATTGCATCCAGATGGTGCTG 900
                ************************************************************

HtaA-CR2        GCGCATTCGCTGGCTTCTATGAAGCTGGCTCTGACCTTGATCCGATCACTTTCGATGCCC 586
Y361A-R         GCGCATTCGCTGGCTTCTATGAAGCTGGCTCTGACCTTGATCCGATCACTTTCGATGCCC 960
                ************************************************************

HtaA-CR2        AACTCGGCGGAGCAGCCGATTGTTCTACTGGAACAAATGCAGCTGCTGTTCCTGTTTCAG 646
Y361A-R         AACTCGGCGGAGCAGCCGATTGTTCTACTGGAACAAATGCAGCTGCTGTTCCTGTTTCAG 1020
                ************************************************************

HtaA-CR2        GTGGGAAGGAATCGTCGATTCCTTCCGGAAAATCTGAAGGGGGCACCTCTGCAGGCTATG 706
Y361A-R         GTGGGAAGGAATCGTCGATTCCTTCCGGAAAATCTGAAGGGGGCACCTCTGCAGGCTATG 1080
                ************************************************************

HtaA-CR2        AAAGTGGCGCTAAAAACTTCAAGATTCGTTCTGCGGCAACGGACGATTCCGGTATTGATC 766
Y361A-R         AAAGTGGCGCTAAAAACTTCAAGATTCGTTCTGCGGCAACGGACGATTCCGGTATTGATC 1140
                ************************************************************
```

Figure 3.4 DNA sequence alignment of wild type HtaA-CR2 and the HtaA-CR2 Y361A mutant in the reverse direction. The missing stars represent the mutation codon in third row (TAC = Tyr, GCG= Ala). Clustal Omega was used for the alignment (Sievers and Higgins, 2014).

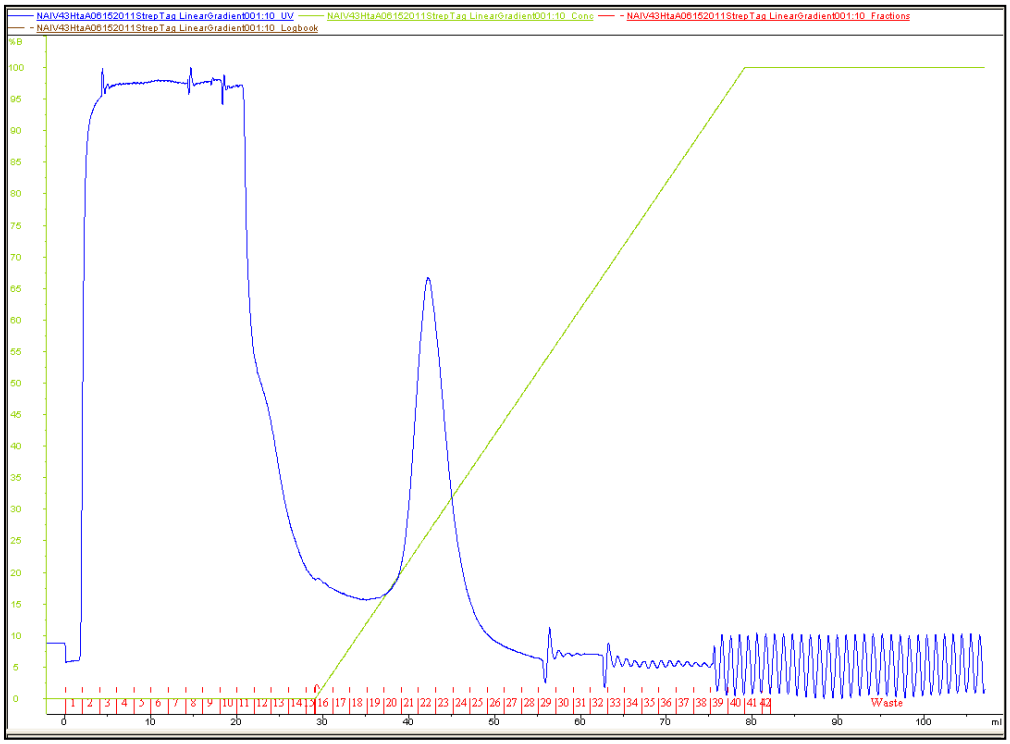

Figure 3.5 Chromatogram of the purification of HtaA-CR2. The separation was conducted at 4 °C using a GE Healthcare ÄKTA fast protein liquid chromatography instrument (Amersham BioSciences). The sample was loaded onto a Strep-Tactin Superflow column (5 ml) equilibrated with buffer A (100 mM Tris-HCl, 150 mM NaCl, pH 8.0). Unbound material was washed out with 5 CV of buffer A. HtaA-CR2 was eluted with 10 CV of buffer B containing 100 mM Tris-HCl, 150 mM NaCl, 2.5 mM desthiobiotin, pH 8.0 applied via a linear gradient. The flow rate was 2 ml/min.

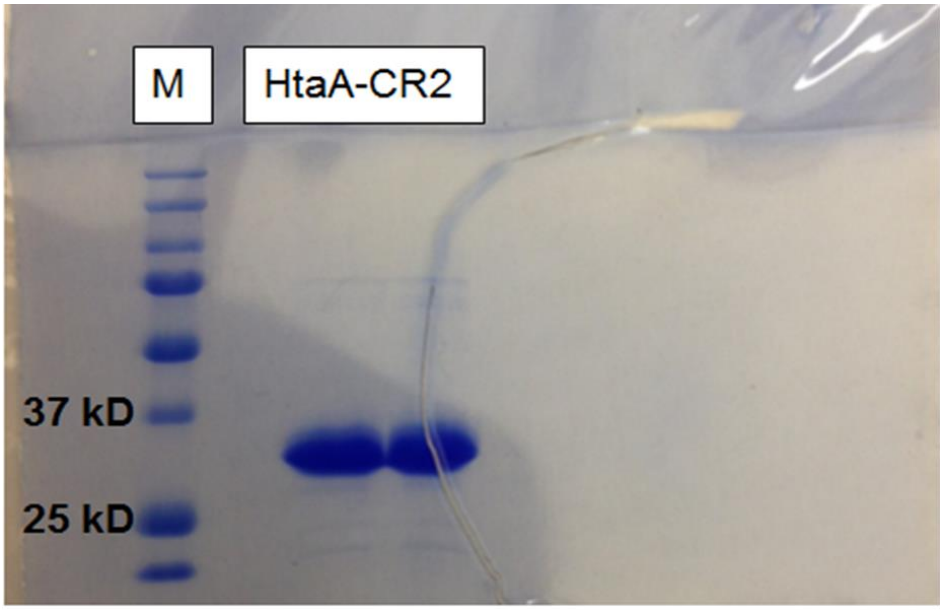

Figure 3.6 SDS-PAGE gel of pooled FPLC fractions of HtaA-CR2 using 5 to 15% acrylamide gel. M is the protein ladder.

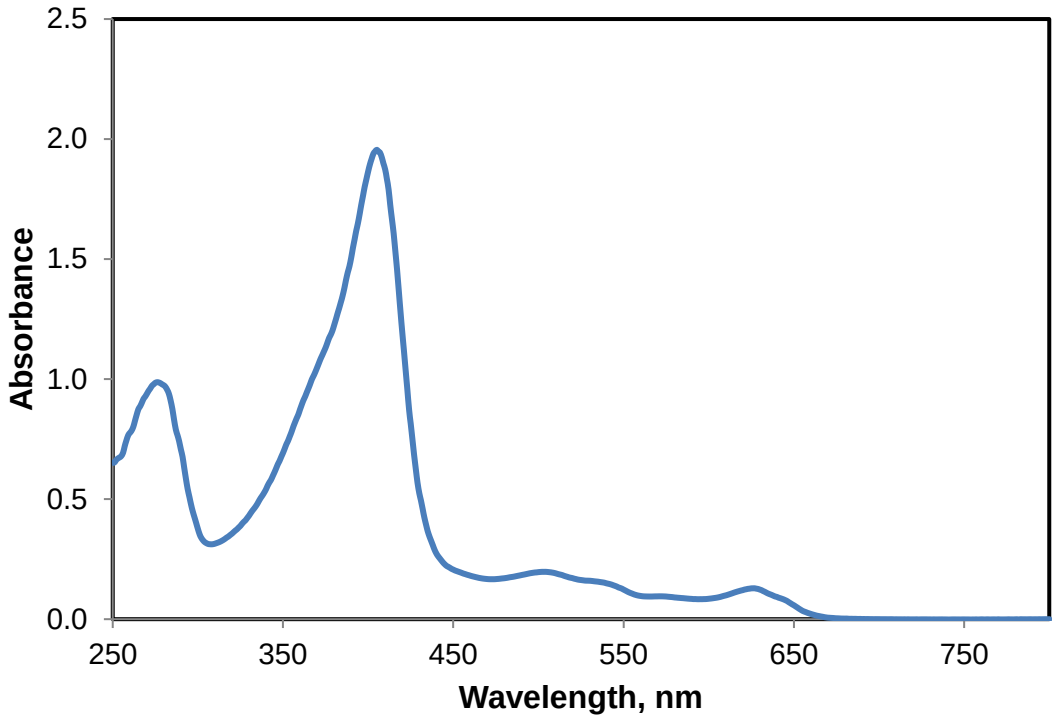

Figure 3.7 UV-visible absorption spectra of HtaA-CR2 in 50 mM Tris-Cl pH 7.0. The Soret peak is at 407 nm and four α/β bands are at 509, 547, 573 and 626 nm.

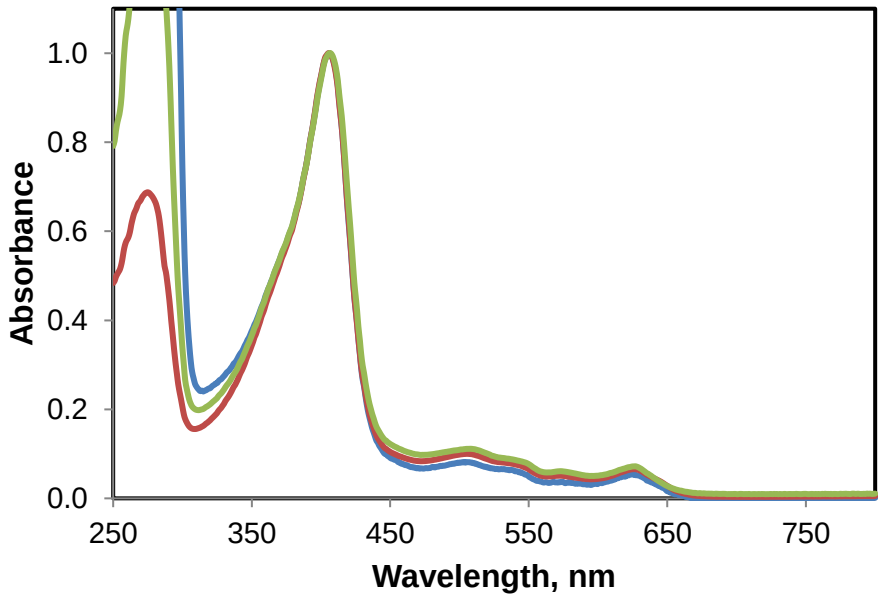

Figure 3.8 HtaA-CR2 overlay of the fully heme-loaded protein (red), mixture of holoprotein and apoprotein (green), and a sample that was largely apoprotein (blue). The data were normalized to 1 at Soret. The protein samples were prepared in 50 mM Tris-Cl pH 7.0.

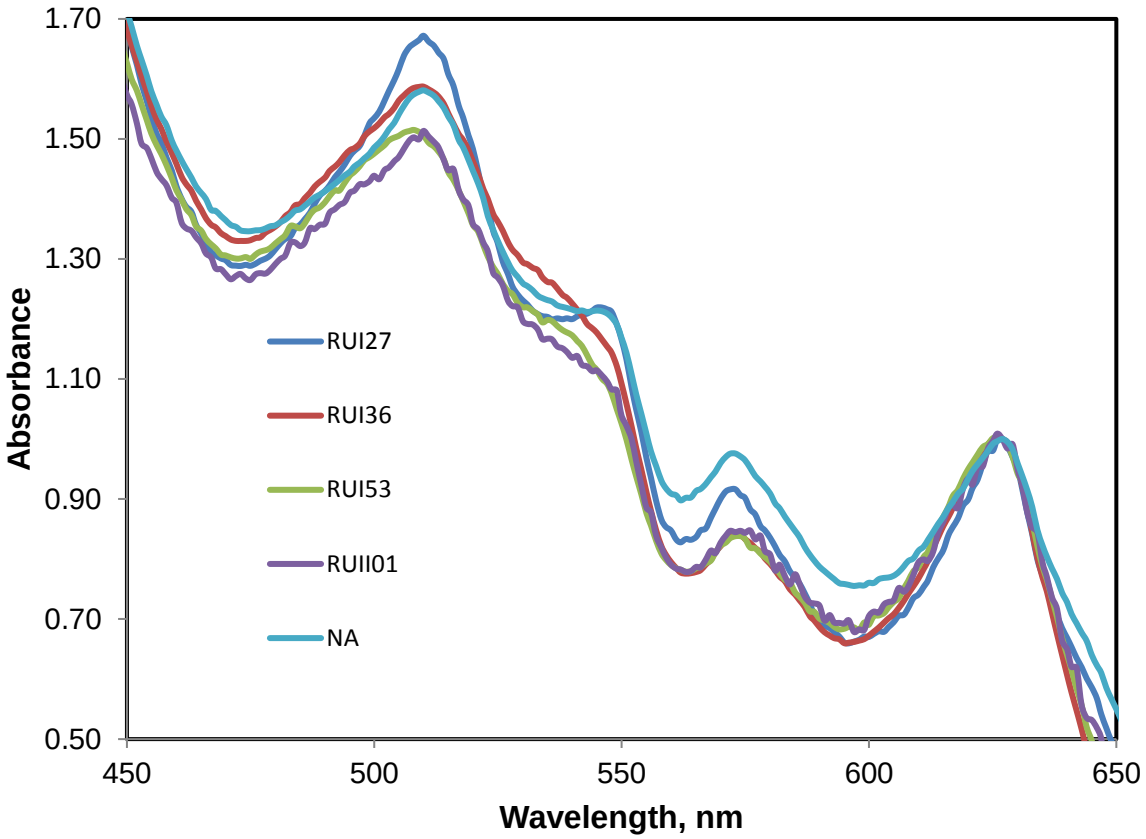

Figure 3.9 Variations in the α/β bands of HtaA-CR2 from various batch purifications. The spectra were normalized at 627 nm. RUI27, RUI36, RUI53, and RUII01 represent the laboratory notebook numbers. NA is the HtaA-CR2 spectrum was taken from Dr. Neval Akbas's work.

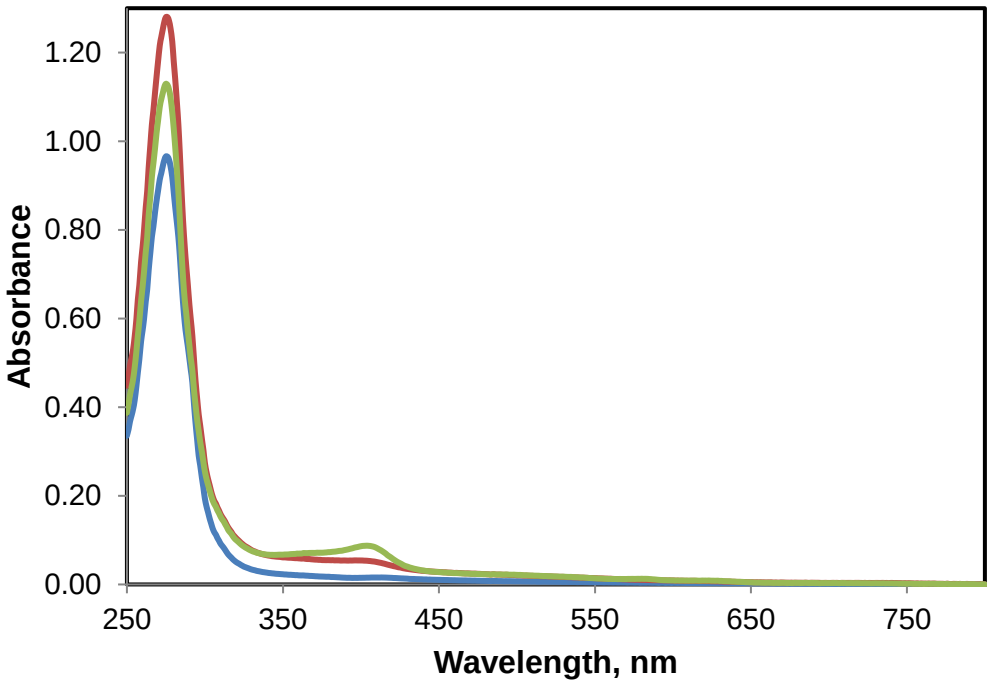

Figure 3.10 UV-visible absorbance spectra of the HtaA-CR2 mutants. The proteins were prepared in 50 mM Tris-Cl pH 7.0. The Y490A mutant (green line), H412A mutant (red line), and Y361A mutant (blue line). All have very low heme loading, as indicated by the ratio of the absorbances at the Soret and 280 nm band.

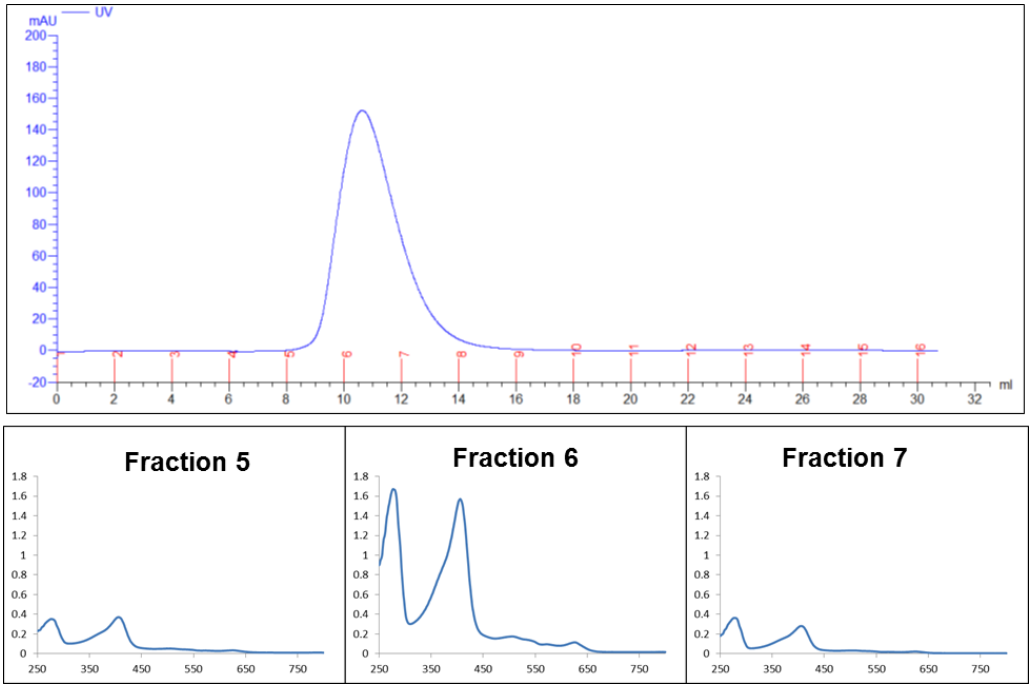

Figure 3.11 Top panel: The FPLC chromatogram of HtaA-CR2 elution from a Butyl FF hydrophobic interaction column. A linear gradient of ammonium phosphate buffer (1.5 – 0 M) 20 mM NaH_2PO_4 and 1.5 M $(NH_4)_2SO_4$ pH 7.0 was used. Bottom panel: UV-visible spectra of three fractions collected. The Soret/280 nm ratios were 0.95, 0.94, and 0.78 for Frac5, Frac6 and Frac7, respectively.

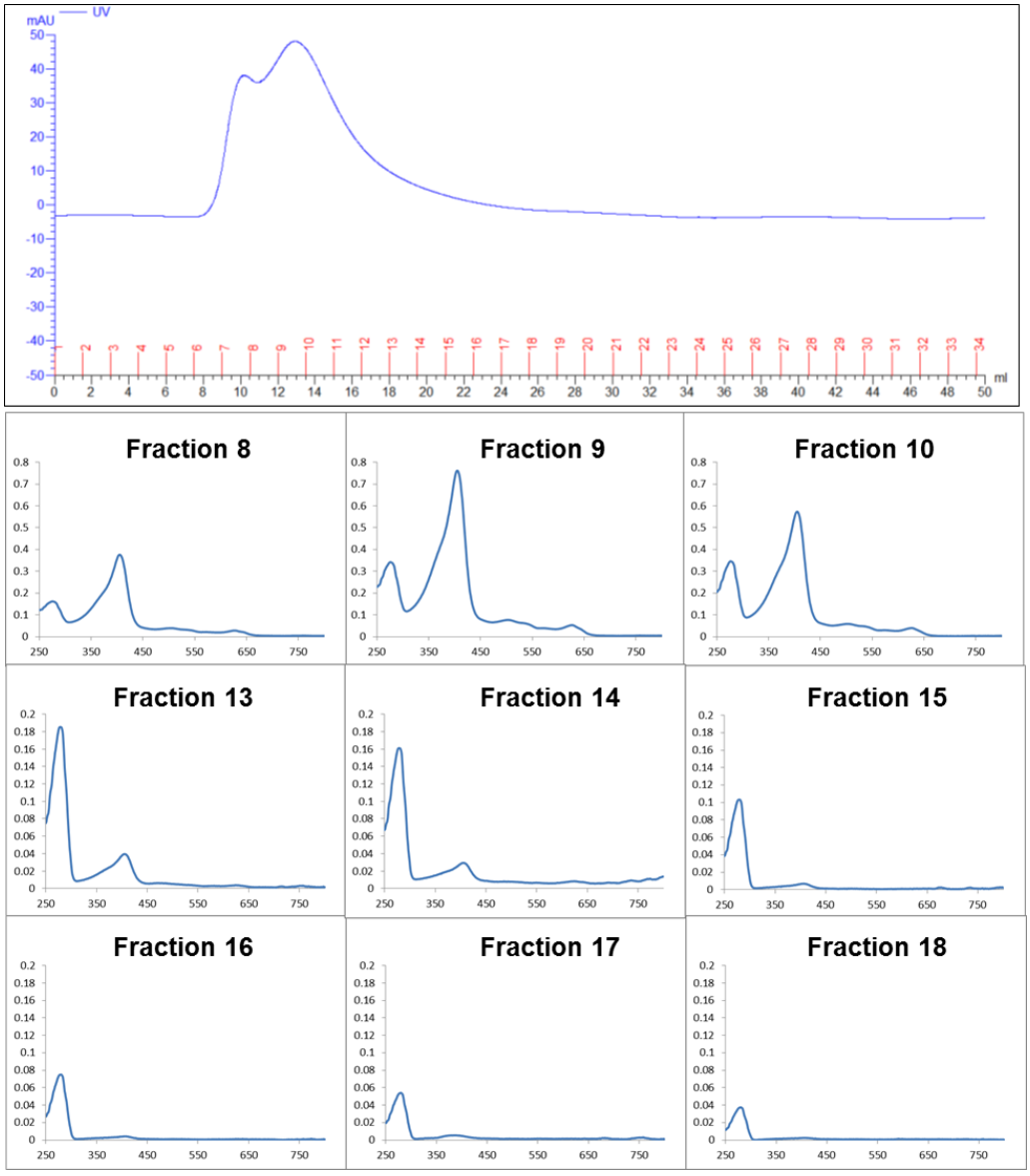

Figure 3.12 Top panel: The FPLC chromatogram of HtaA-CR2 elution from a Phenyl FF hydrophobic interaction column. A linear gradient of ammonium phosphate buffer (1.5 – 0 M) 20 mM NaH_2PO_4 and 1.5 M $(NH_4)_2SO_4$ pH 7.0 was used. Bottom panel: UV-visible spectra of the fractions that were collected. The Soret/280 nm ratios were 2.2, 2.2 and 1.7 for Frac8, FracB9 and Frac10 respectively. The ratios were 0.2, 0.2, 0.07, 0.06, 0.08 and 0.05 for Frac13, Frac14, Frac15, Frac16, Frac17 and Frac18, respectively.

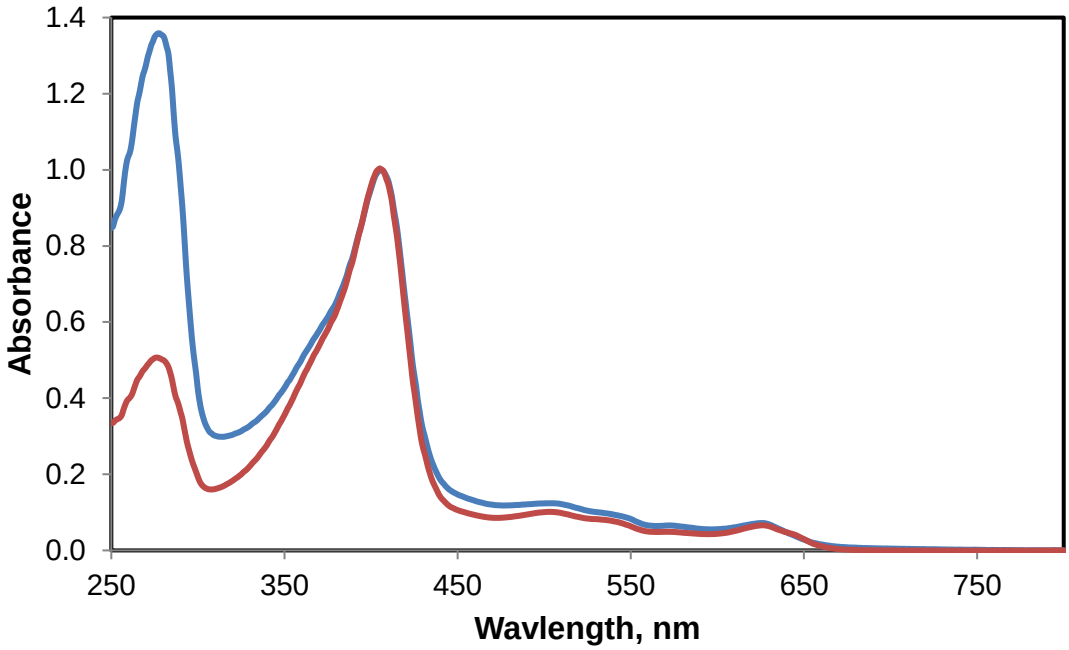

Figure 3.13 HtaA-CR2 as isolated after Strep-tag purification (about 20% heme loaded, blue line). Approximately, fully heme loaded protein sample after Butyl FF and Phenyl FF HIC columns (red line). The data were normalized to 1 at Soret.

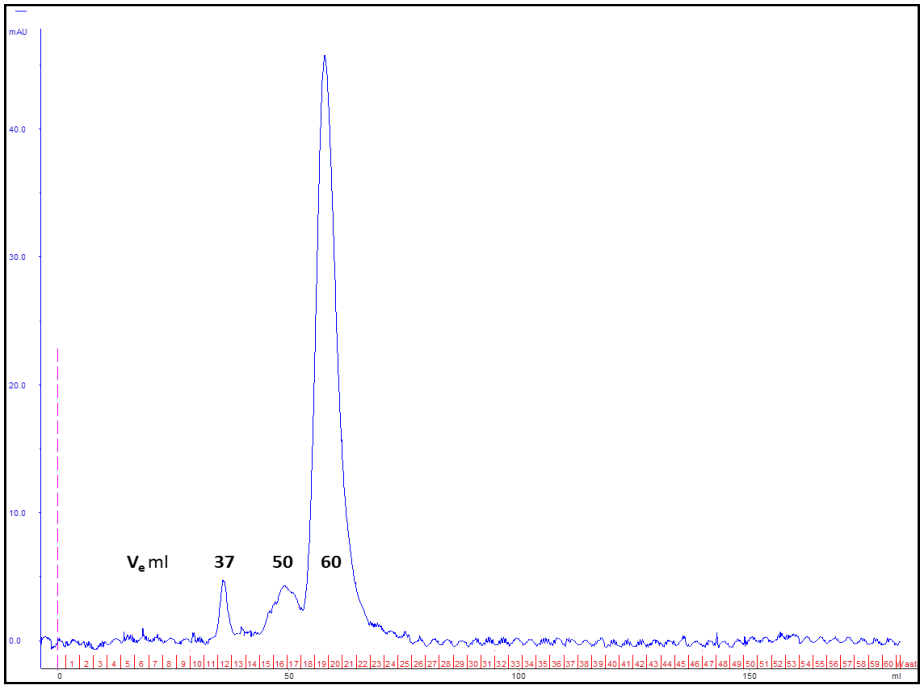

Figure 3.14 Size exlution chromatography of as-solated HtaA-CR2 in 50 mM Tris-Cl 100 mM NaCl pH 7.0. The protein sample passed through the Sephacryl column (16/60 S-200 HR). Peaks represent the retention volumes.

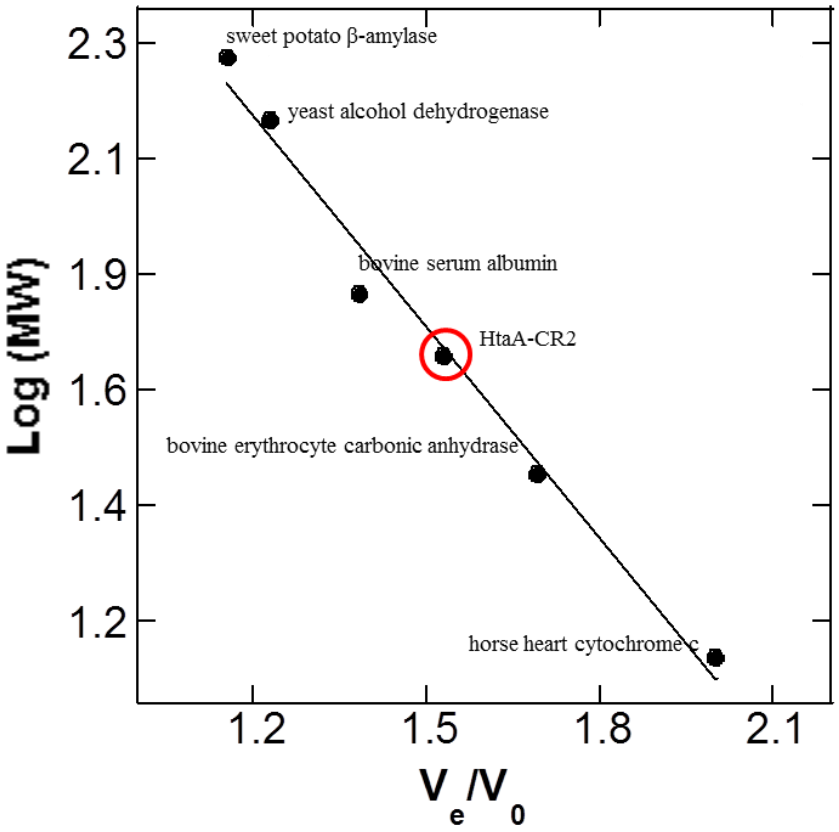

Figure 3.15 Size exclusion chromatography (SEC) calibration curve for as-isolated HtaA-CR2. All of the samples were prepared in 50 mM Tris-Cl 100 mM NaCl pH 7.0 and passed through the Sephacryl column (16/60 S-200 HR). The retention volume (V_e) and the void volume (V_0) ratios as a function of the molecular weights are plotted for the five protein markers: horse heart cytochrome *c* (12.4 kDa), bovine erythrocyte carbonic anhydrase (29 kDa), bovine serum albumin (66 kDa), yeast alcohol dehydrogenase (150 kDa) and sweet potato β-amylase (200 kDa). A molecular weight of 50.1 ± 6.6 kDa was calculated for HtaA-CR2.

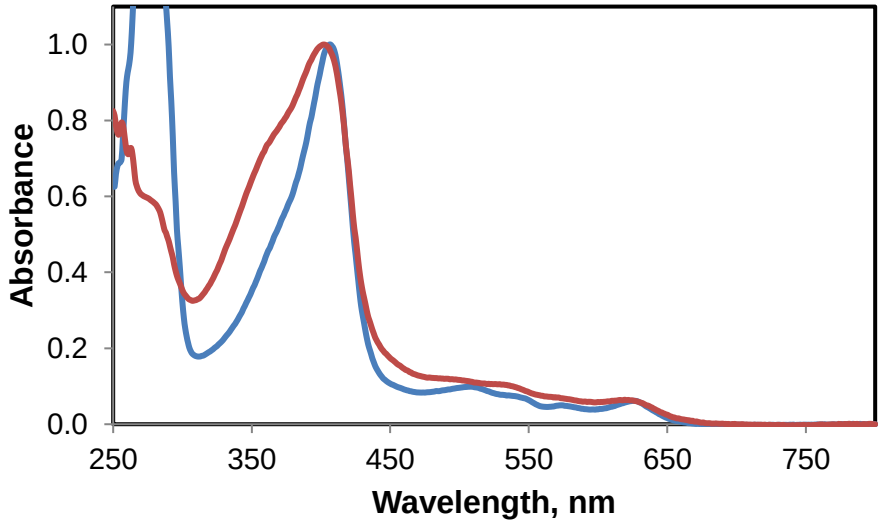

Figure 3.16 HtaA-CR2 as isolated after Strep-tag purification (about 20% heme loaded, blue line). Reconstituted HtaA-CR2 using butanone extraction method (red line). The data were normalized to 1 at Soret.

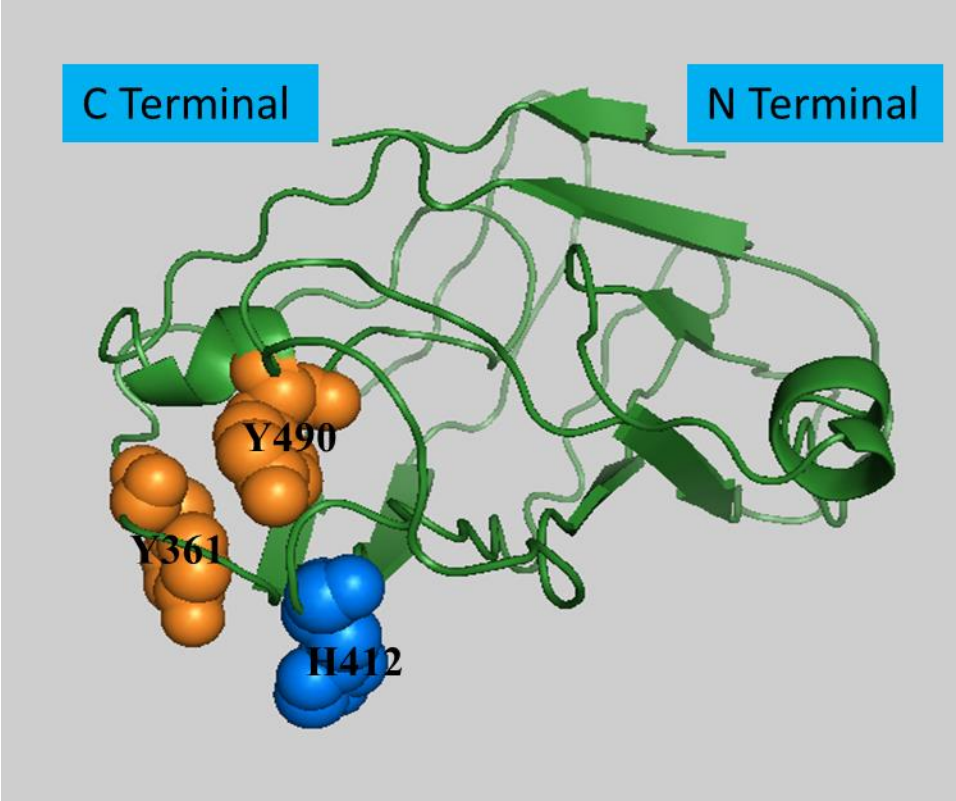

Figure 3.17 I-TASSER homology model of HtaA-CR2. PyMol was used for molecular visualization.

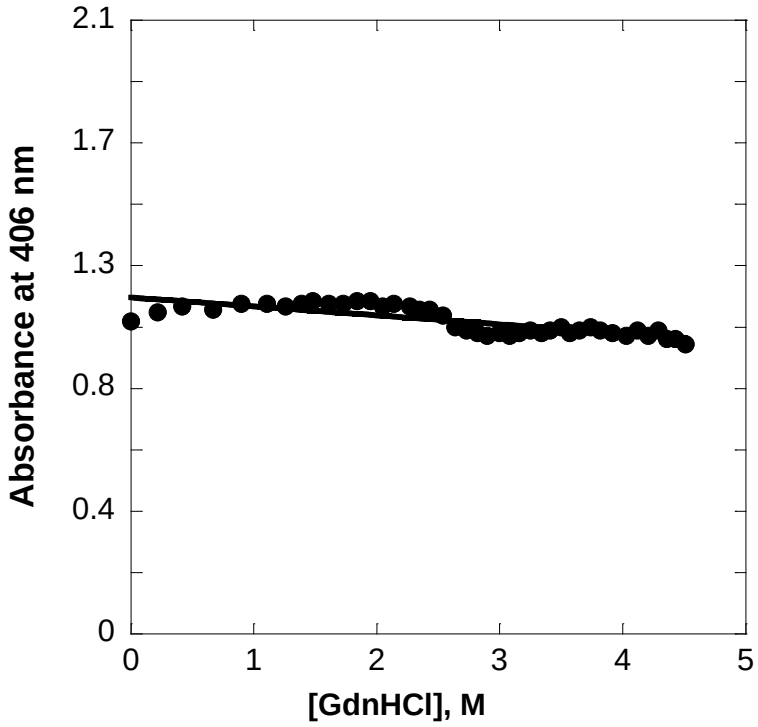

Figure 3.18 The Soret absorption of HtaA-CR2 in 50 mM Tris-Cl pH 7.0 buffer as a function of GdnHCl concentration.

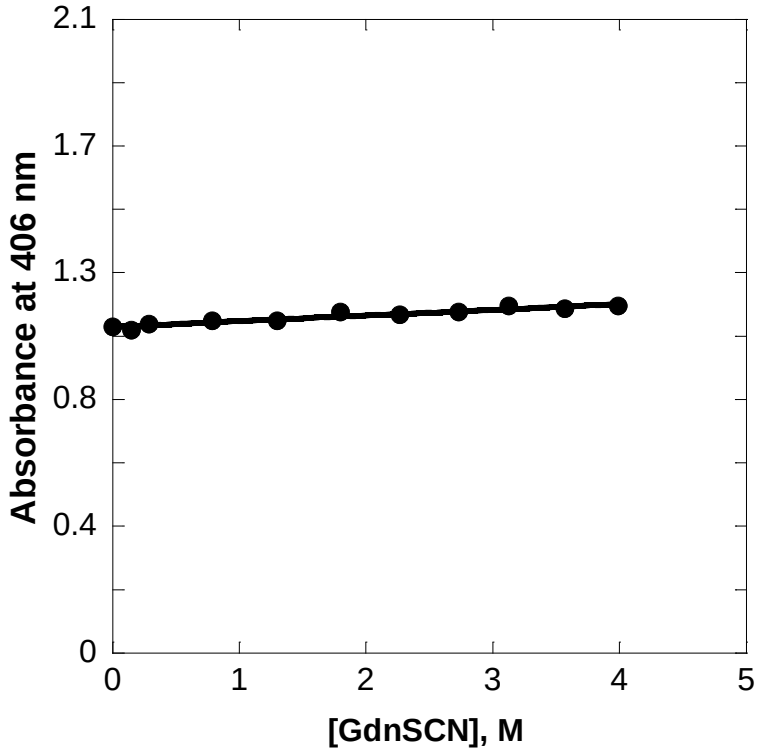

Figure 3.19 The Soret absorption of HtaA-CR2 in 50 mM Tris-Cl pH 7.0 buffer as a function of GdnSCN concentration.

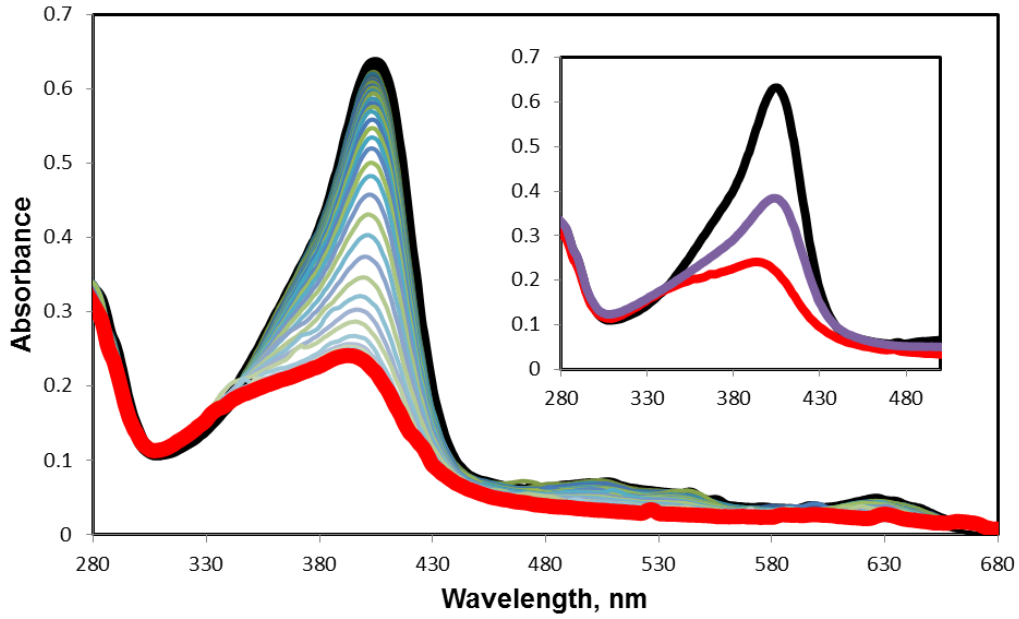

Figure 3.20 The absorbance spectra of thermal denaturation of HtaA-CR2 in the presence of 1.5 M GdnHCl. The buffer was 50 mM Tris-Cl pH 7.0. The black line is the folded spectrum and the red line is the unfolded spectrum. The inset shows the spectra at 50 ºC (black), 90 ºC (red), and after the sample cooled down to room temperature (purple).

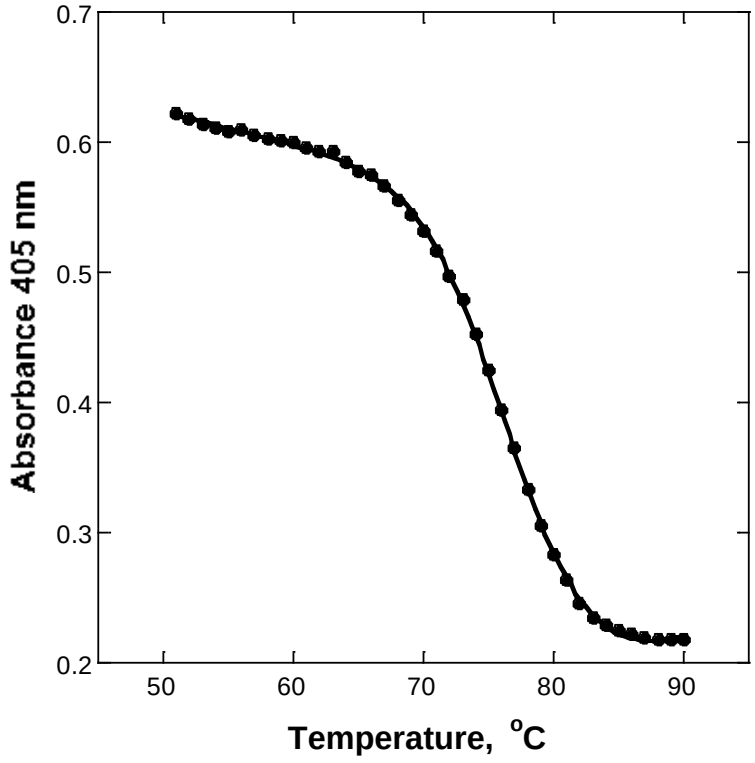

Figure 3.21 Nonlinear least squares fitting of the Soret absorbance of HtaA-CR2 in 1.5 M GdnHCl as a function of temperature. A T_m value of 77 ºC and ΔH_m was calculated.

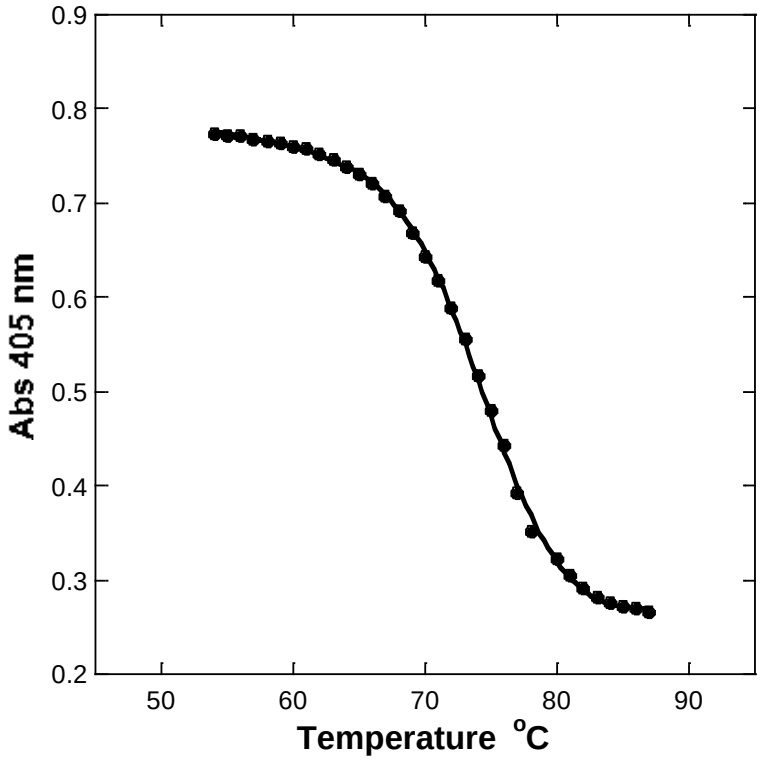

Figure 3.22 Nonlinear least squares fitting of the Soret absorbance of HtaA-CR2 in 1.75 M GdnHCl as a function of temperature. A T_m value of 75 ºC was calculated.

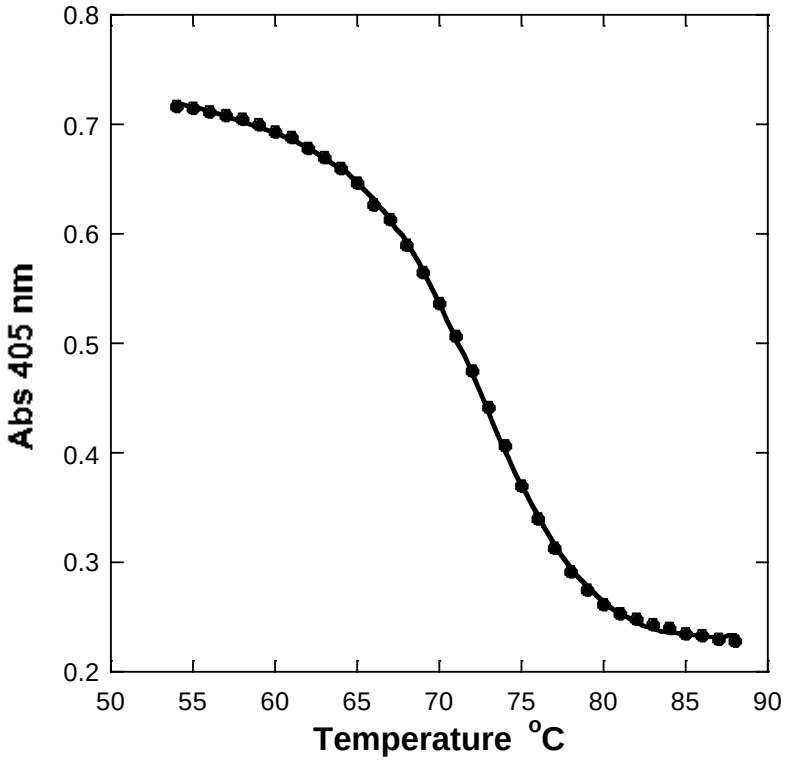

Figure 3.23 Nonlinear least squares fitting of the Soret absorbance of HtaA-CR2 in 2.0 M GdnHCl as a function of temperature. A T_m value of 73 °C was calculated.

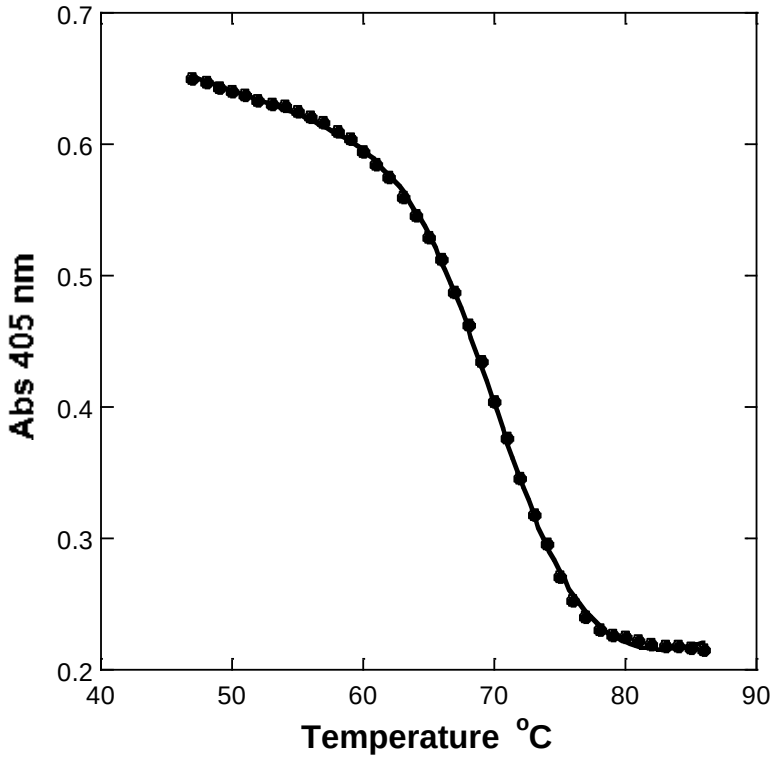

Figure 3.24 Nonlinear least squares fitting of the Soret absorbance of HtaA-CR2 in 2.5 M GdnHCl as a function of temperature. A T_m value of 71 °C was calculated.

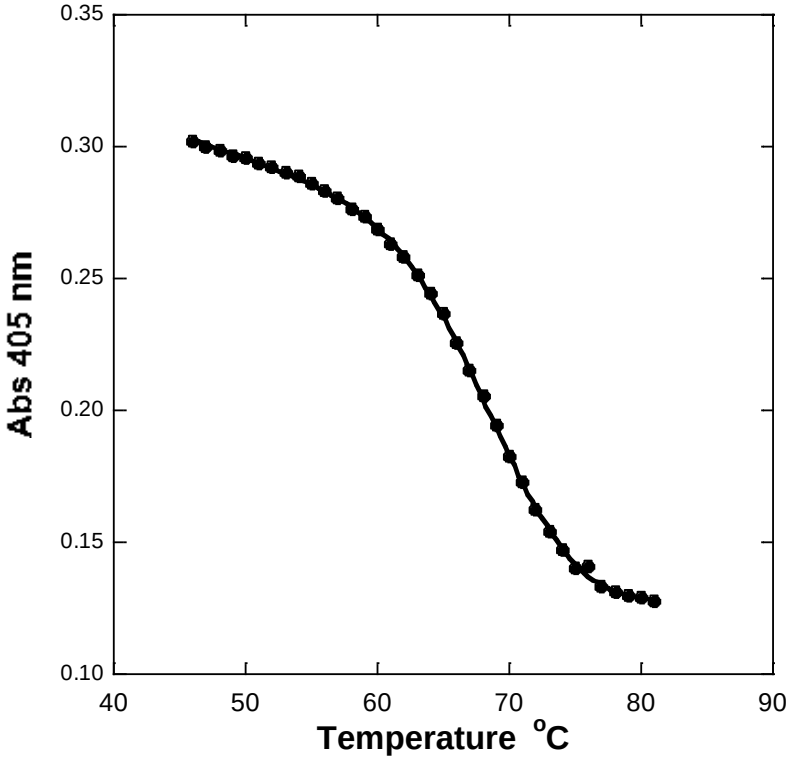

Figure 3.25 Nonlinear least squares fitting of the Soret absorbance of HtaA-CR2 in 3.0 M GdnHCl as a function of temperature. A T_m value of 70 °C was calculated.

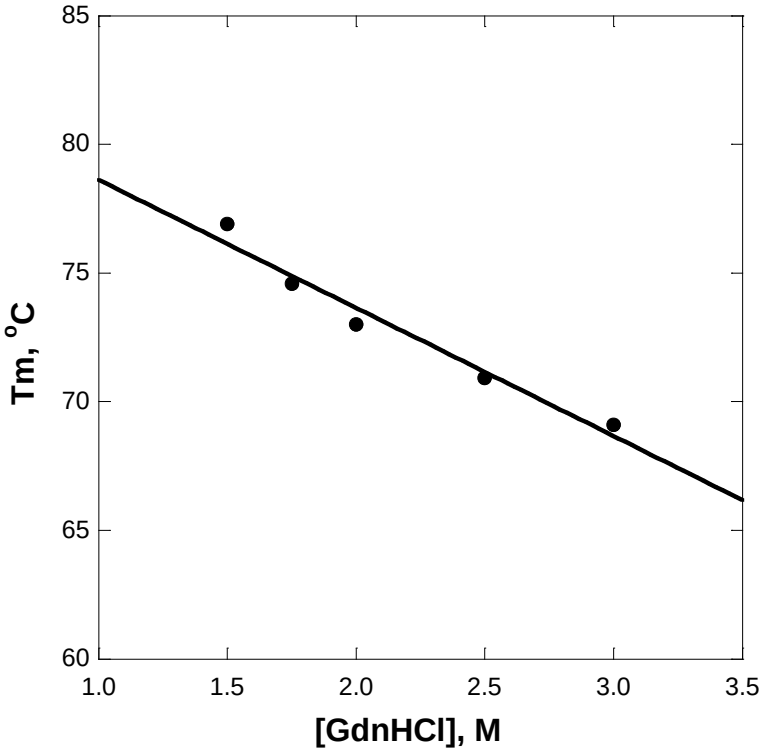

Figure 3.26 T_m values of HtaA-CR2 as a function of GdnHCl concentration. The data were fit with a linear equation to give an apparent T_m value of 84 ºC in the absence of denaturant.

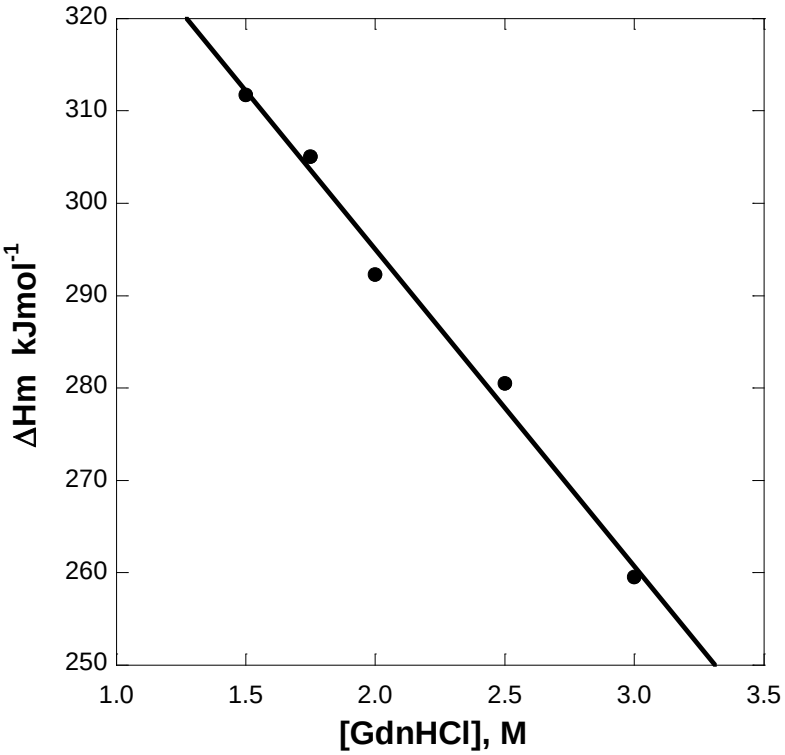

Figure 3.27 ΔH_m values of HtaA-CR2 as a function of GdnHCl concentration. The data were fit with a linear equation to give a theoretical ΔH_m value of 364 kJmol^{-1} in the absence of denaturant.

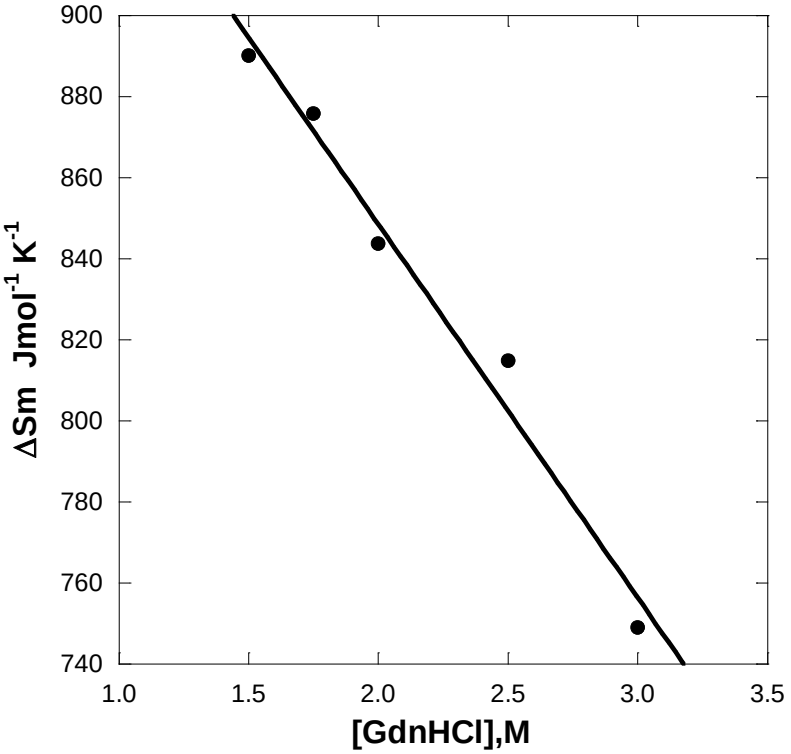

Figure 3.28 ΔS_m values of HtaA-CR2 as a function of GdnHCl concentration. The data were fit with a linear equation to give a theoretical ΔS_m value of 1033 $Jmol^{-1}$ K^{-1} in the absence of denaturant.

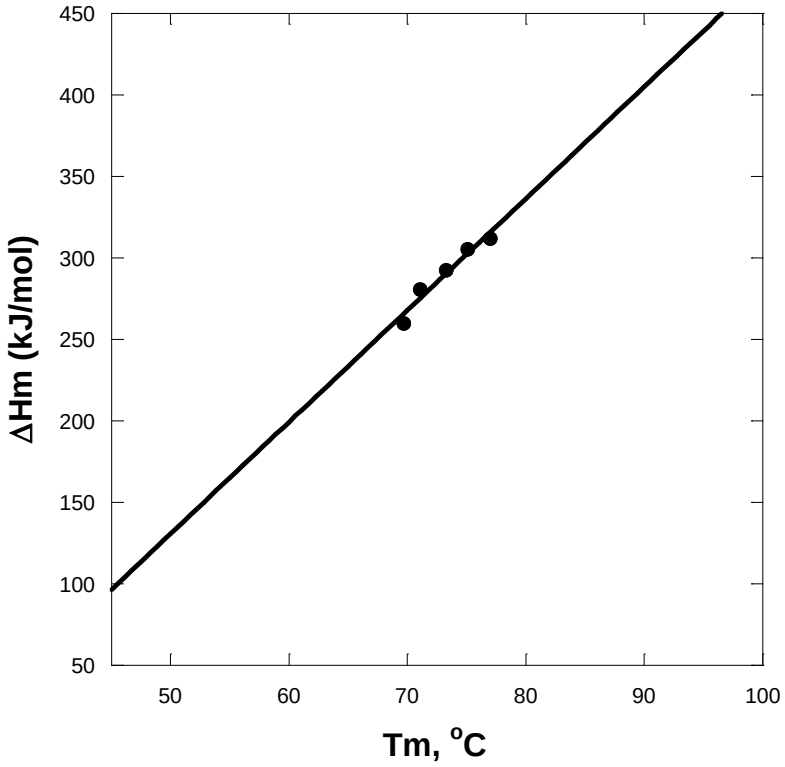

Figure 3.29 ΔH_m values of HtaA-CR2 (at various concentrations of GdnHCl) vs. T_m of each reaction. ΔC_p was calculated from the slope of the line.

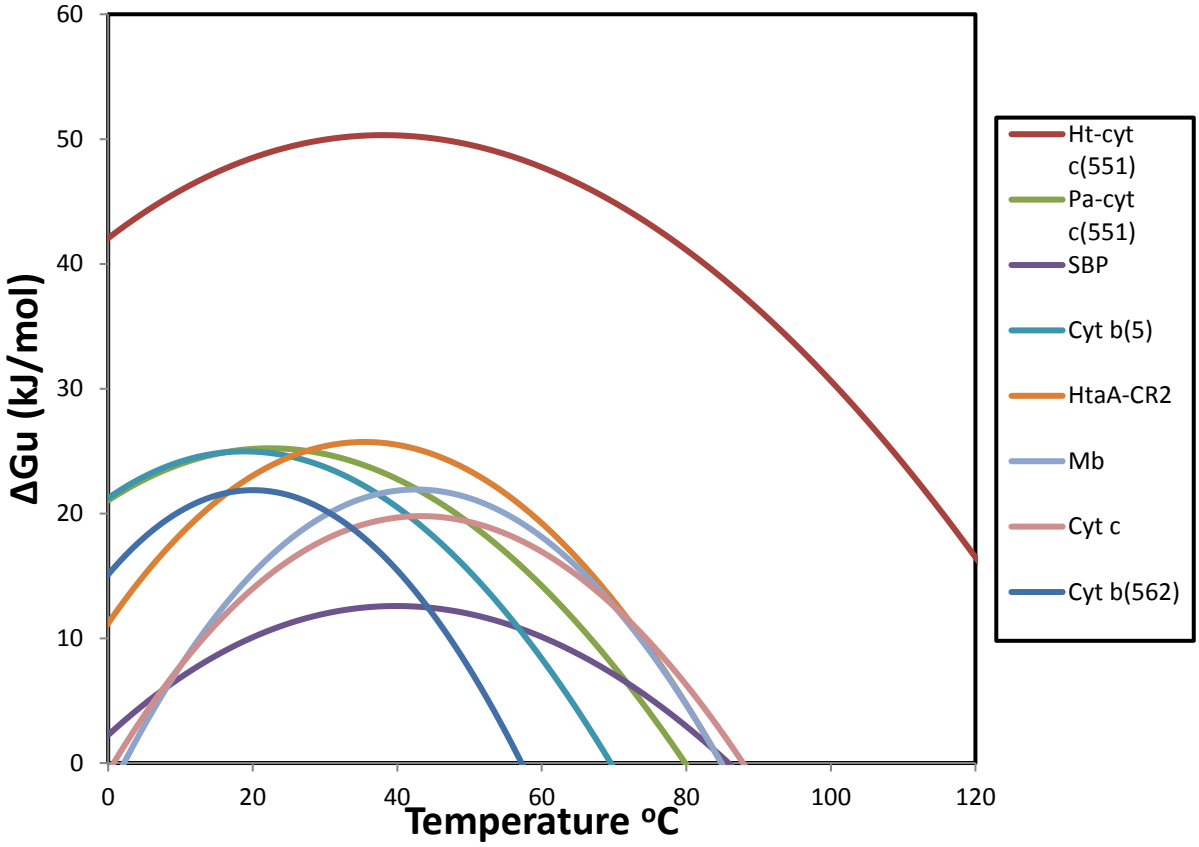

Figure 3.30 ΔG_0 as a function of temperature of various heme binding proteins. The coloring is shown in the right panel. The references are given in Table 7.

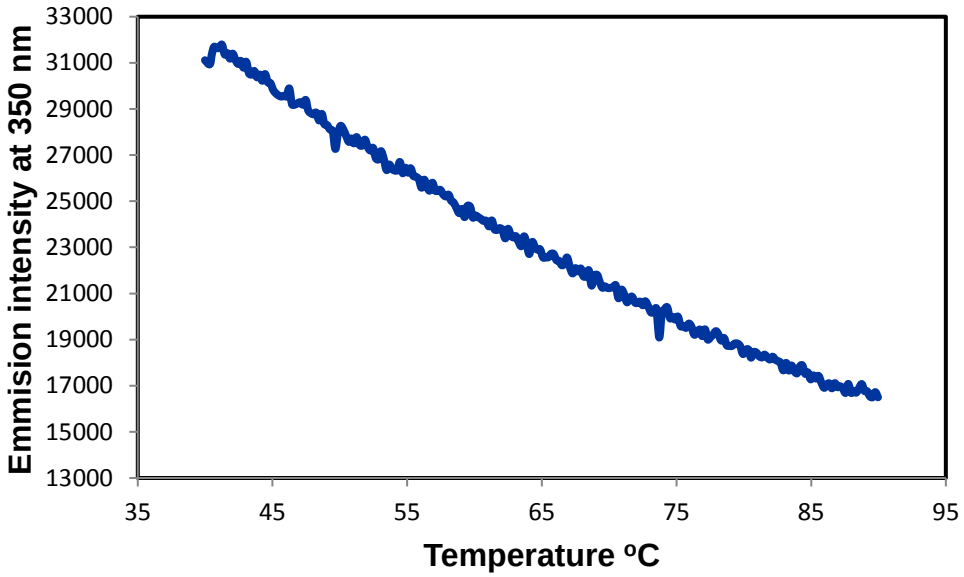

Figure 3.31 The emission intensity of 3 M GdnHCl at 350 nm as a function of temperature. The denaturant was prepared in 50 mM Tris-Cl pH 7.0.

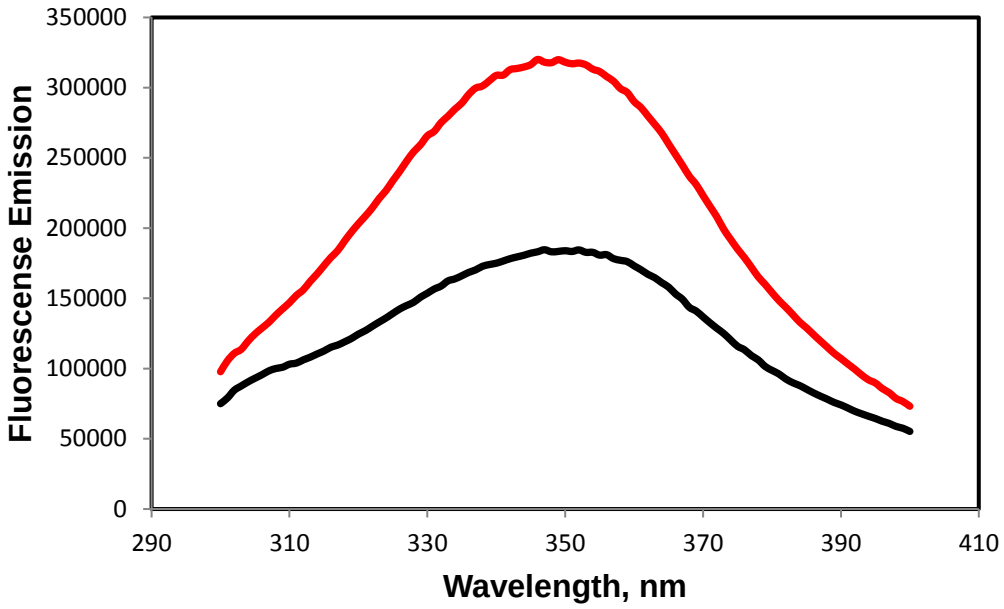

Figure 3.32 Fluorescence emission spectrum of HtaA-CR2 in the presence of 3 M GdnHCl at 40 ºC (red) and 90 ºC (black). The protein solution was prepared in 50 mM Tris-Cl pH 7.0.

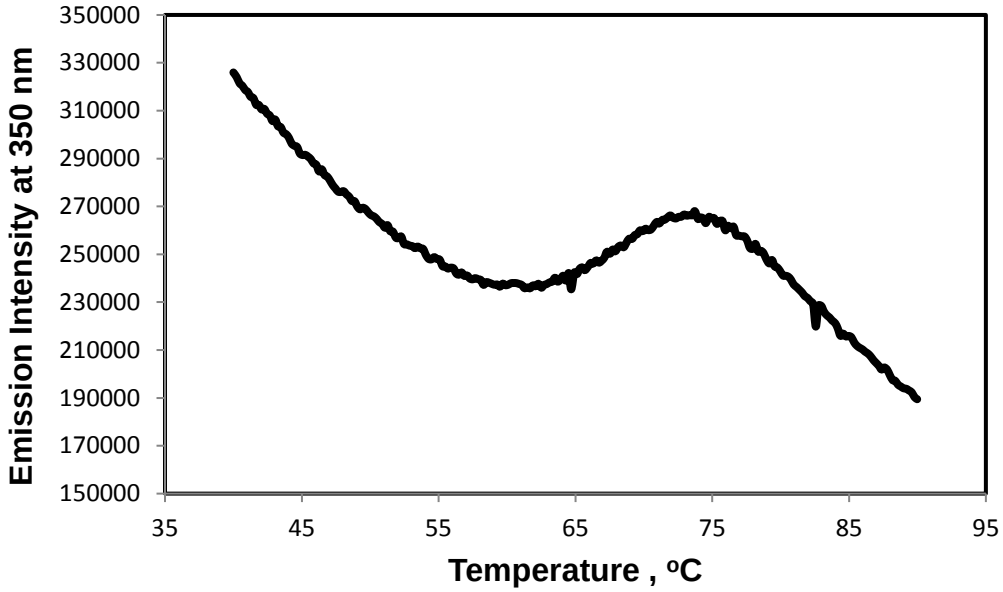

Figure 3.33 The emission intensity of HtaA-CR2 in the presence of 3 M GdnHCl as a function of temperature. The protein solution was prepared in 50 mM Tris-Cl pH 7.0.

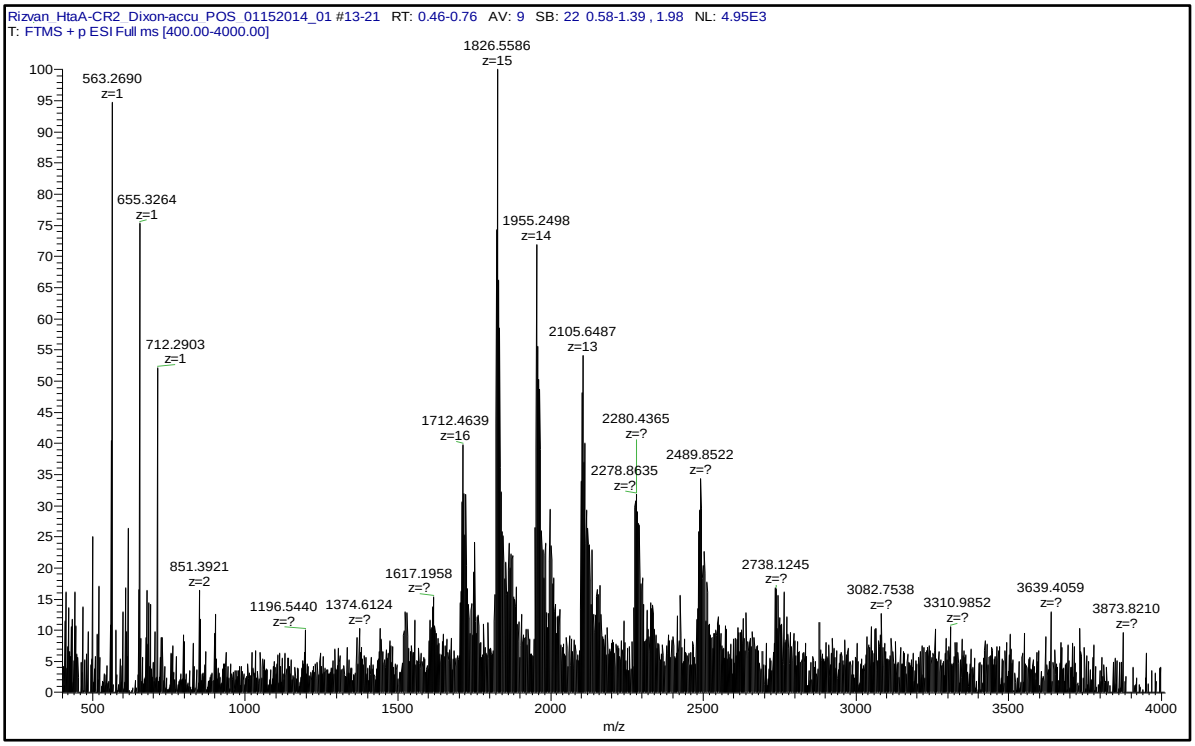

Figure 3.34 Electrospray mass spectrum of HtaA-CR2. The charge distribution bands are shown. The sample was prepared in water.

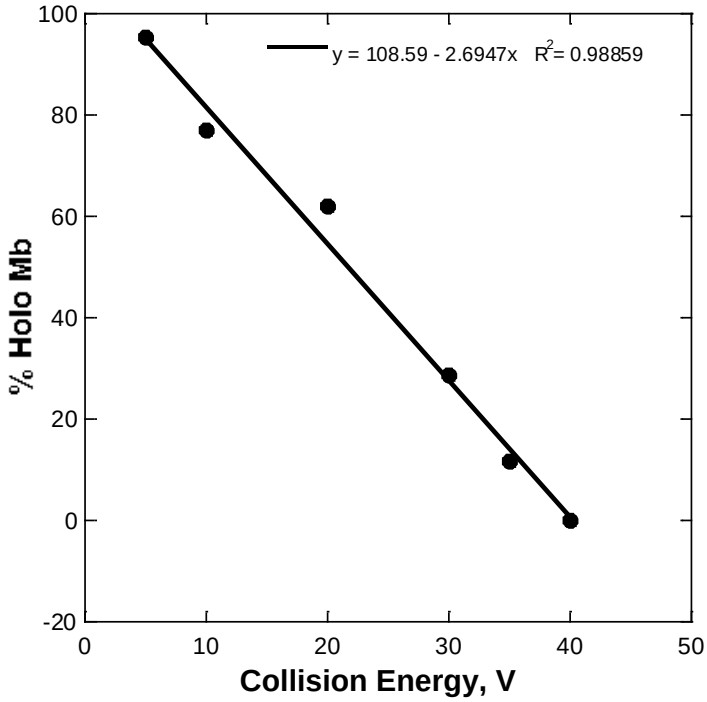

Figure 3.35Mb holoprotein/apoprotein ratio as a function of collision energy. A Waters Micromass ESI Q-TOF was used in the positive ion mode.

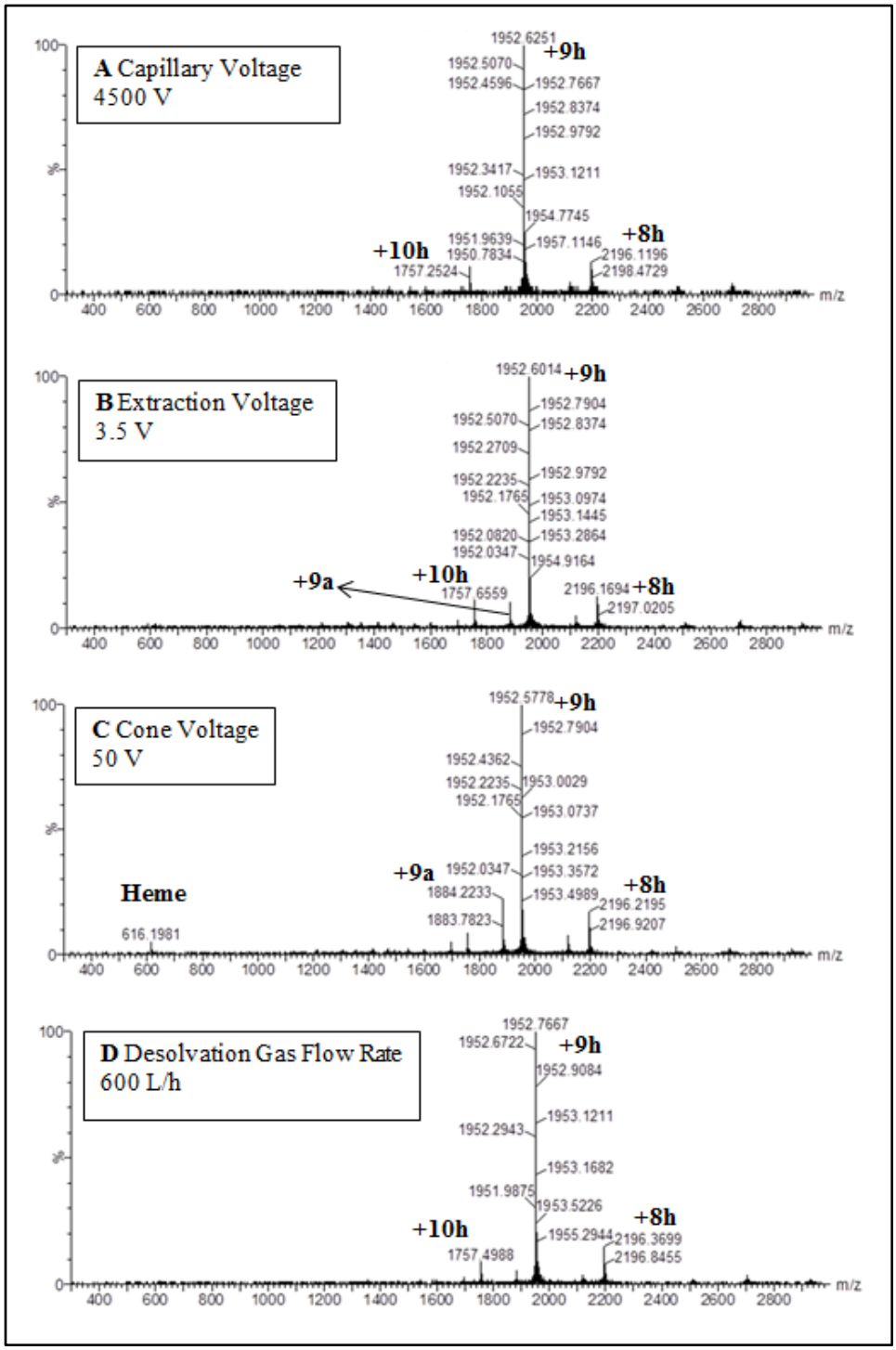
A Capillary Voltage
4500 V
1952.6251
+9h
1952.5070
1952.4596
1952.7667
1952.8374
1952.9792
1952.3417
1953.1211
1952.1055
1954.7745
1951.9639
1957.1146
+8h
+10h
1950.7834
2196.1196
1757.2524
2198.4729
B Extraction Voltage
3.5 V
1952.6014
+9h
1952.7904
1952.5070
1952.8374
1952.2709
1952.2235
1952.9792
1952.1765
1953.0974
1953.1445
1952.0820
1953.2864
1952.0347
1954.9164
+9a
+10h
1757.6559
2196.1694
+8h
2197.0205
C Cone Voltage
50 V
1952.5778
+9h
1952.7904
1952.4362
1952.2235
1953.0029
1952.1765
1953.0737
1953.2156
+9a
1952.0347
1953.3572
+8h
Heme
1884.2233
1953.4989
2196.2195
1883.7823
2196.9207
616.1981
D Desolvation Gas Flow Rate
600 L/h
1952.7667
1952.6722
+9h
1952.9084
1953.1211
1952.2943
1953.1682
1951.9875
1953.5226
+8h
+10h
1955.2944
2196.3699
1757.4988
2196.8455
%
m/z
400
600
800
1000
1200
1400
1600
1800
2000
2200
2400
2600
2800

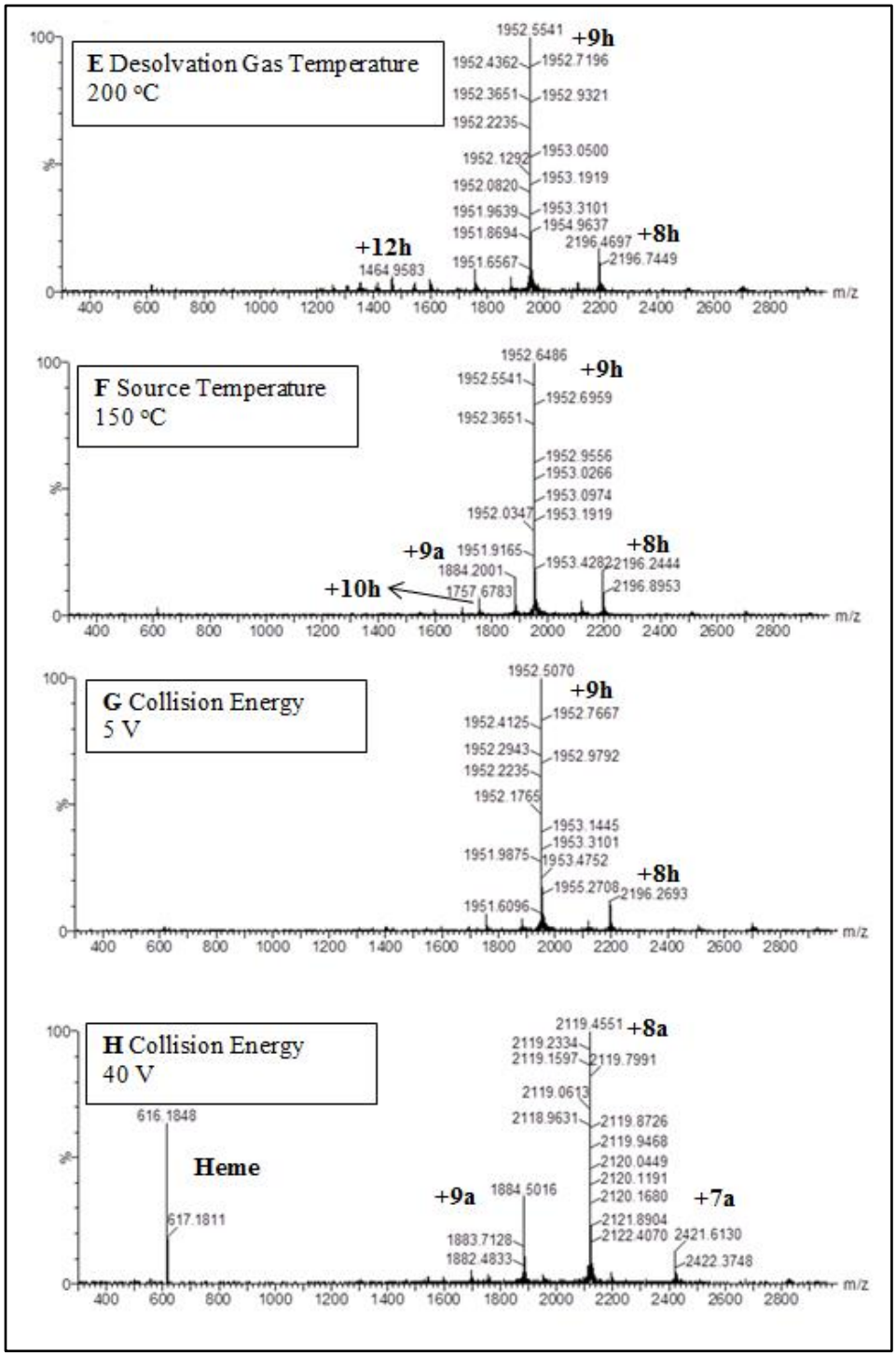

Figure 3.36 Positive ESI of Mb using a Waters Micromass Q-TOF.

Charge distribution peaks shown, "a" represents apoprotein, "h" represents holoprotein. Various parameters (capillary voltage, extraction voltage, cone voltage, desolvation gas flow rate, desolvation gas temperature, source temperature and, collision energy) were tested as shown in Table 10. Panel A - F show examples of the mass spectrum of Mb at the

highest value of each parameter. Panel G and panel H show the mass spectrum of Mb at lowest value and the highest value of collision energy respectively.

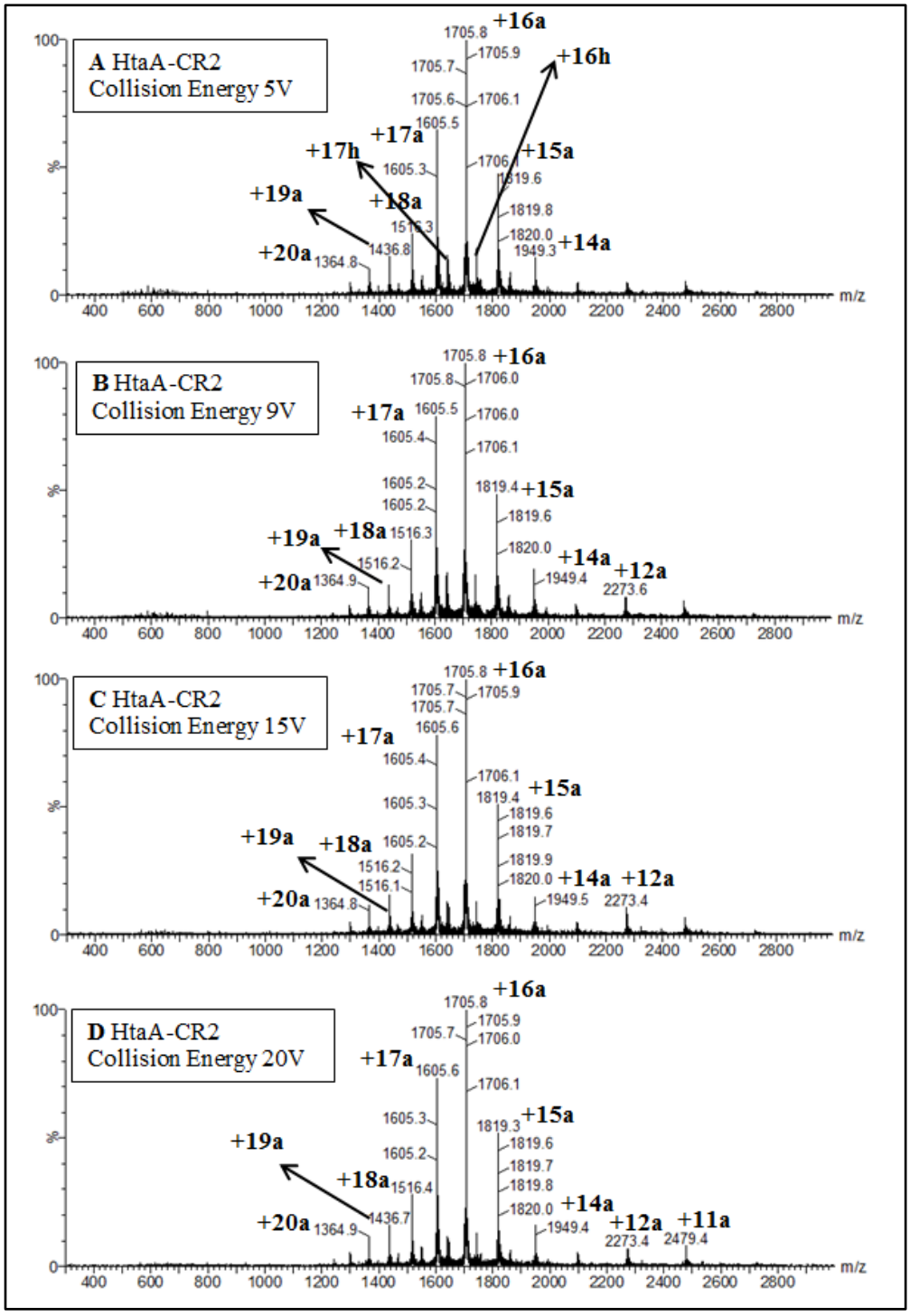

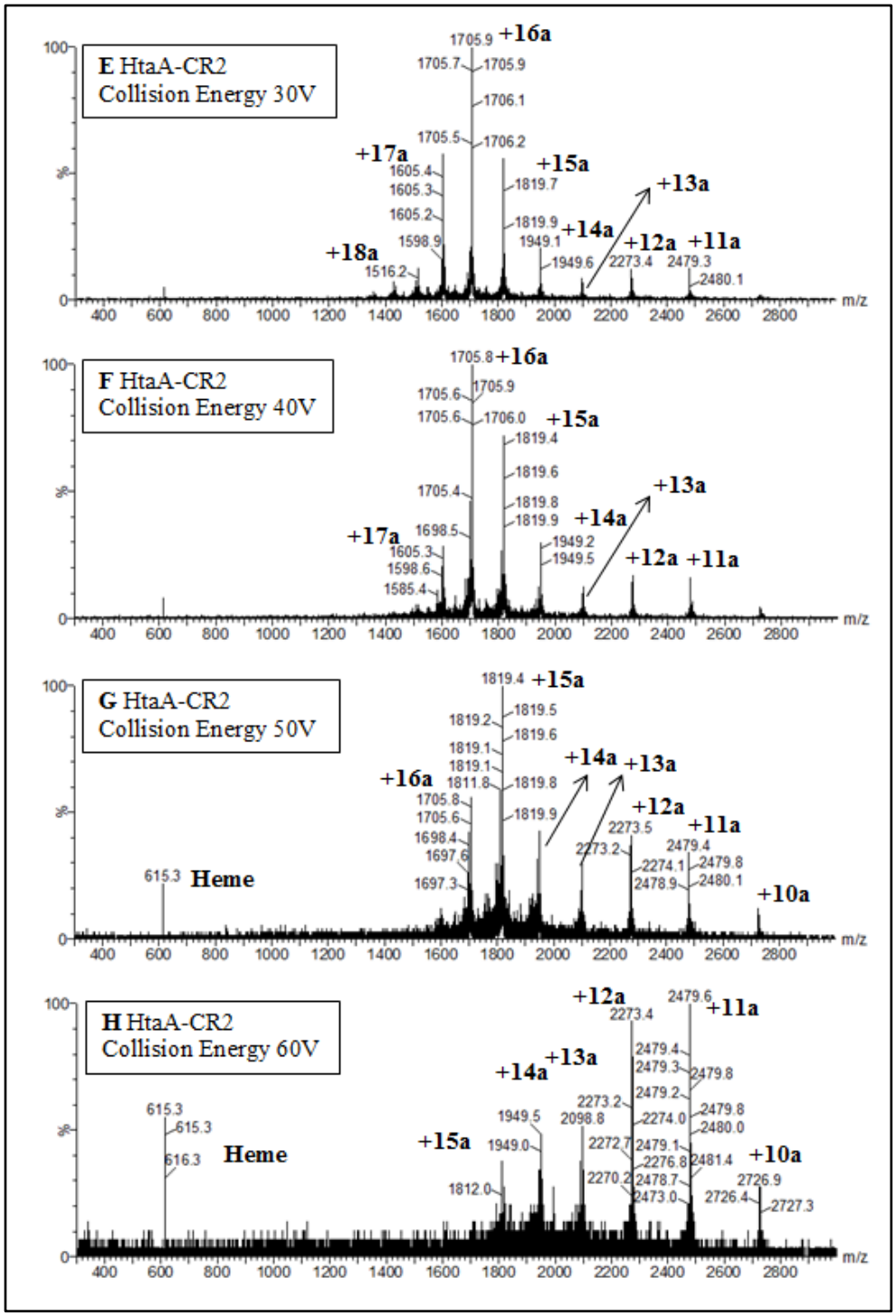
E HtaA-CR2
Collision Energy 30V
+16a
+17a
+15a
+13a
+14a
+12a
+11a
+18a
F HtaA-CR2
Collision Energy 40V
+16a
+15a
+13a
+14a
+17a
+12a
+11a
G HtaA-CR2
Collision Energy 50V
+15a
+16a
+14a
+13a
+12a
+11a
+10a
615.3 Heme
H HtaA-CR2
Collision Energy 60V
+12a
+11a
+14a
+13a
+15a
+10a
615.3 Heme
m/z
%

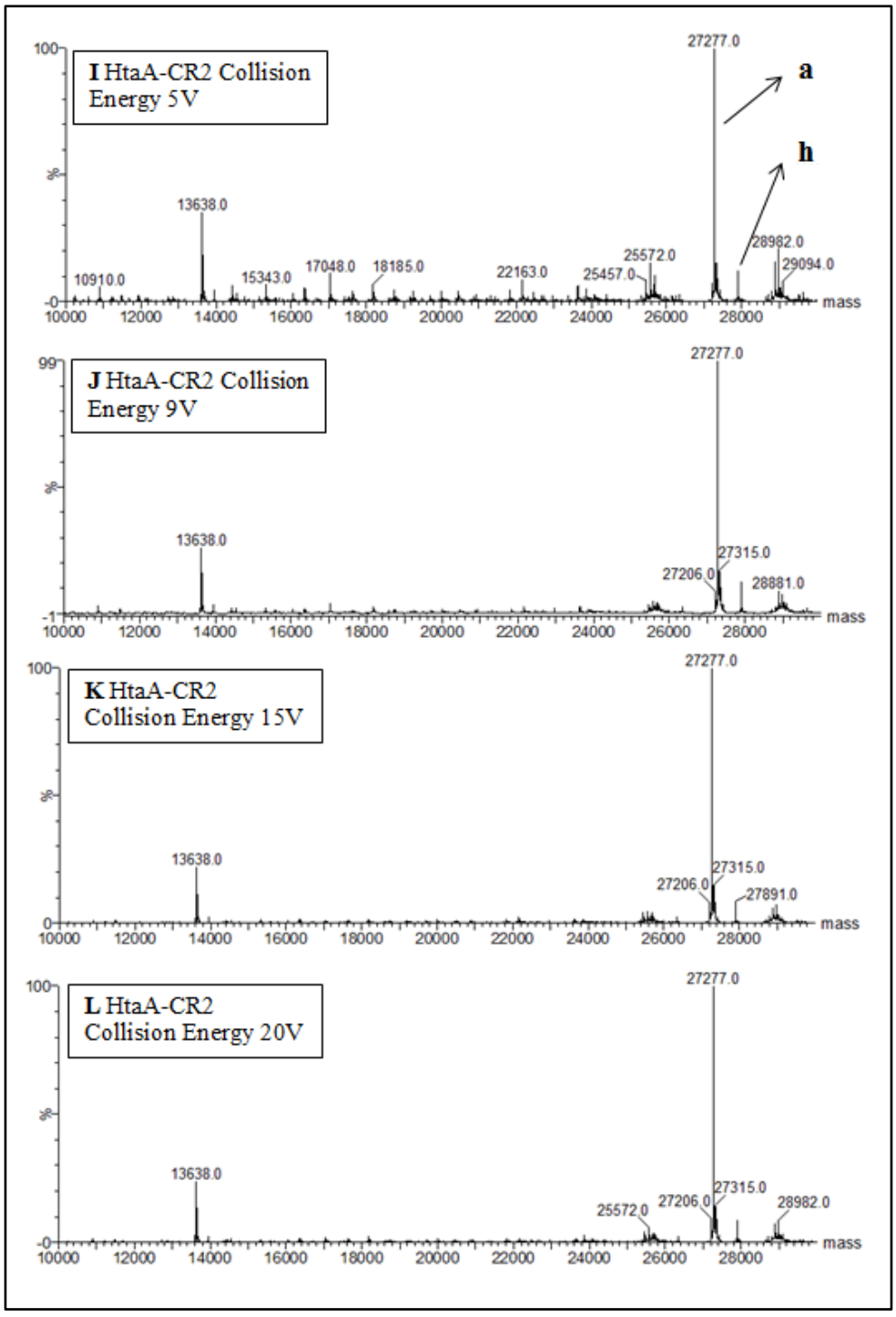
I HtaA-CR2 Collision Energy 5V
27277.0
a
h
13638.0
10910.0
15343.0
17048.0
18185.0
22163.0
25457.0
25572.0
28982.0
29094.0
mass
J HtaA-CR2 Collision Energy 9V
27277.0
13638.0
27315.0
27206.0
28881.0
mass
K HtaA-CR2 Collision Energy 15V
27277.0
13638.0
27315.0
27206.0
27891.0
mass
L HtaA-CR2 Collision Energy 20V
27277.0
13638.0
27315.0
27206.0
25572.0
28982.0
mass

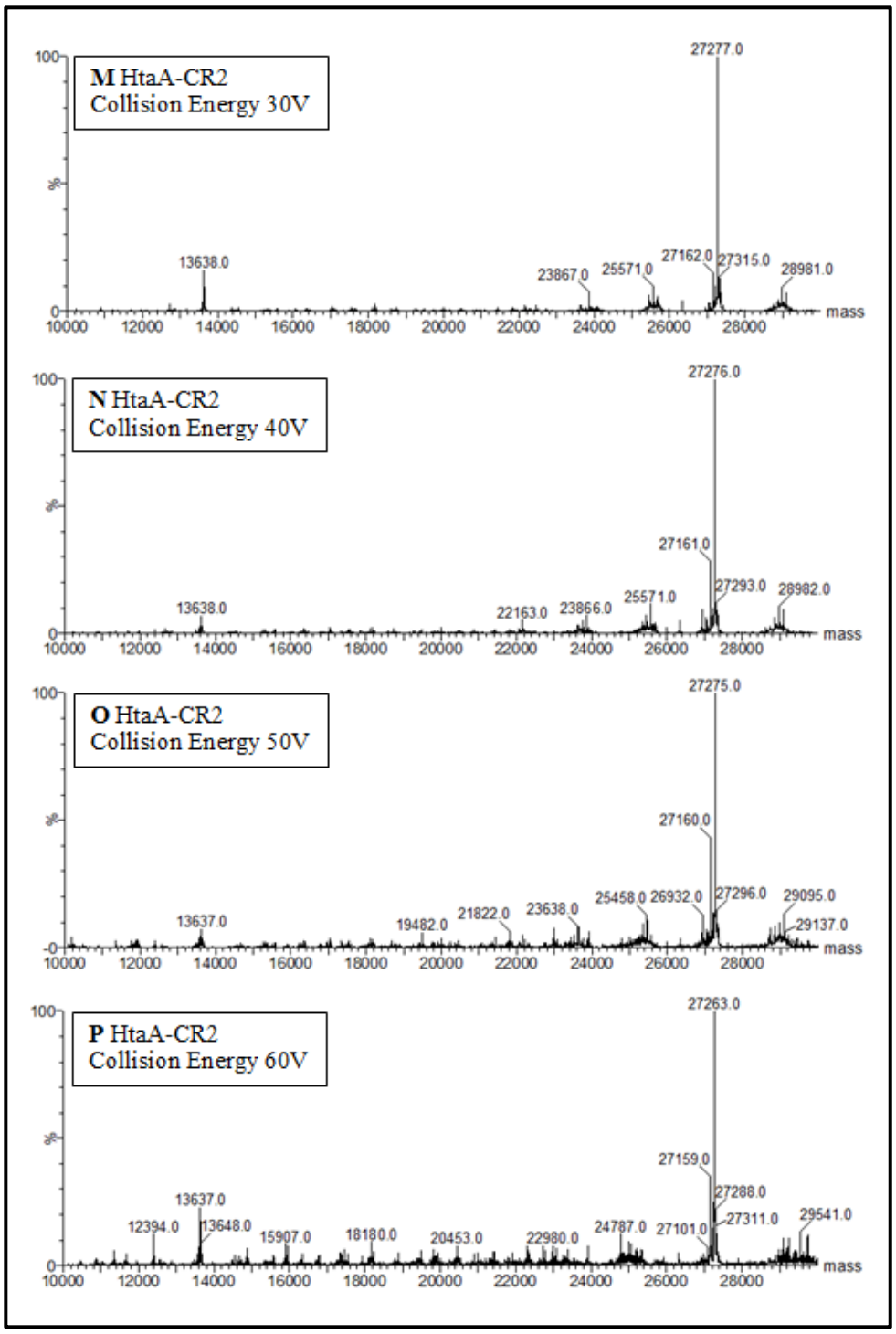

Figure 3.37 Positive ESI of HtaA-CR2 using a Waters Micromass Q-TOF.

The capillary, cone and extraction voltages were 3000, 18 and 1.5 V, respectively. Desolvation gas and source temperatures were 100 and 80 °C, respectively. HtaA-CR2 was prepared in 50 mM ammonium acetate, pH 7.0. The collision energy was varied from 5 to 60 V. The charge distribution peaks are shown in panel A - H. Corresponding

deconvoluted spectrum are shown in panel I - P. The +16a peak (1705.8 m/z) corresponds to the apo form of myoglobin (A - G). +16h peak (1744.3 m/z, not labeled in the spectrum) corresponds to the holo form of myoglobin which is present only when 5 to 20 V collision energies applied (A - D). The peaks labeled as "a" and "h" corresponds to apoprotein and holoprotein respectively, in the deconvoluted spectrum (I-P).

3.4 References

Allen, C.E., Schmitt, M.P., 2011. Novel hemin binding domains in the *Corynebacterium diphtheriae* HtaA protein interact with hemoglobin and are critical for heme iron utilization by HtaA. J. Bacteriol. 193, 5374-5385.

Amisha Kamal, J.K., Behere, D.V., 2002. Thermal and conformational stability of seed coat soybean peroxidase. Biochemistry 41, 9034-9042.

Amisha Kamal, J.K.A., Behere, D.V., 2008. Kinetic stabilities of soybean and horseradish peroxidases. Biochem. Eng. J. 38, 110-114.

Austin, C.J.D., Mizdrak, J., Matin, A., Sirijovski, N., Kosim-Satyaputra, P., Willows, R.D., Roberts, T.H., Truscott, R.J.W., Polekhina, G., Parker, M.W., Jamie, J.F., 2004. Optimised expression and purification of recombinant human indoleamine 2,3-dioxygenase. Protein Expression and Purification. 37, 392-398.

Berry, E.A., Trumpower, B.L., 1987. Simultaneous determination of hemes *a*, *b*, and *c* from pyridine hemochrome spectra. Anal. Biochem. 161, 1-15.

Collier, G.S., Pratt, J.M., De Wet, C.R., Tshabalala, C.F., 1979. Studies on haemin in dimethyl sulphoxide/water mixtures. Biochem. J. 179, 281-289.

DeLano, W., L., 2015. The PyMOL Molecular Graphics System, Version 1.7.4 Schrödinger, LLC. http://www. pymol. org.

Deniau, C., Gilli, R., Izadi-Pruneyre, N., Létoffé, S., Delepierre, M., Wandersman, C., Briand, C., Lecroisey, A., 2003. Thermodynamics of heme binding to the HasA(SM) hemophore: Effect of mutations at three key residues for heme uptake. Biochemistry 42, 10627-10633.

Feng, Y.Q., Sligar, S.G., 1991. Effect of heme binding on the structure and stability of *Escherichia coli* apocytochrome b_{562}. Biochemistry 30, 10150-10155.

Hao, D.C., Zhu, P.H., Yang, S.L., Yang, L., 2007. Enhanced production of human cytochrome P4502C9 by *Escherichia coli* BL21(DE3)pLysS through the novel use of grey relational analysis and Plackett-Burman design. World J. Microbiol. Biotechnol. 23, 71-78.

Hargrove, M.S., Wilkinson, A.J., Olson, J.S., 1996. Structural factors governing hemin dissociation from metmyoglobin. Biochemistry 35, 11300-11309.

Hunter, C.L., Mauk, A.G., Douglas, D.J., 1997. Dissociation of heme from myoglobin and cytochrome *b*(5): Comparison of behavior in solution and the gas phase. Biochemistry 36, 1018-1025.

Hussain, H.A., Ward, J.M., 2003. Enhanced heterologous expression of two *Streptomyces griseolus* cytochrome P450s and *Streptomyces coelicolor* ferredoxin reductase as potentially efficient hydroxylation catalysts. Appl. Environ. Microbiol. 69, 373-382.

Jansson, I., Stoilov, I., Sarfarazi, M., Schenkman, J.B., 2000. Enhanced expression of CYP1B1 in *Escherichia coli*. Toxicology 144, 211-219.

Jepkorir, G., Rodriguez, J.C., Rui, H., Im, W., Lovell, S., Battaile, K.P., Alontaga, A.Y., Yukl, E.T., Moenne-Loccoz, P., Rivera, M., 2010. Structural, NMR spectroscopic, and computational investigation of hemin loading in the hemophore HasAp from *Pseudomonas aeruginosa*. J. Am. Chem. Soc. 132, 9857-9872.

Jones, D.K., Patel, N., Cheesman, M.R., Thomson, A.J., Raven, E.L., 2002. Leghaemoglobin: A model for the investigation of haem protein axial ligation. Inorg. Chim. Acta 331, 303-309.

Kery, V., Elleder, D., Kraus, J.P., 1995. δ-Aminolevulinate increases heme saturation and yield of human cystathionine β-synthase expressed in *Escherichia coli*. Arch. Biochem. Biophys. 316, 24-29.

Kimoto, H., Matsuyama, H., Yumoto, I., Yoshimune, K., 2008. Heme content of recombinant catalase from *Psychrobacter* sp T-3 altered by host *Escherichia coli* cell growth conditions. Protein Expr. Purif. 59, 357-359.

Kumar, R., Bhuyan, A.K., 2009. Entropic stabilization of myoglobin by subdenaturing concentrations of guanidine hydrochloride. J. Biol. Inorg. Chem. 14, 11-21.

León, R.G., Munier-Lehmann, H., Barzu, O., Baudin-Creuza, V., Pietri, R., Lopez-Garriga, J., Cadilla, C.L., 2004. High-level production of recombinant sulfide-reactive hemoglobin I from *Lucina pectinata* in *Escherichia coli*. High yields of fully functional holoprotein synthesis in the BLi5 *E. coli* strain. Protein Expr. Purif. 38, 184-195.

Londer, Y.Y., Pokkuluri, P.R., Orshonsky, V., Orshonsky, L., Schiffer, M., 2006. Heterologous expression of dodecaheme "nanowire" cytochromes *c* from *Geobacter sulfurreducens*. Protein Expr. Purif. 47, 241-248.

Mason, J.M., Bendall, D.S., Howe, C.J., Worrall, J.A.R., 2012. The role of a disulfide bridge in the stability and folding kinetics of *Arabidopsis thaliana* cytochrome c(6A). Biochim. Biophys. Acta 1824, 311-318.

Mulrooney, S.B., Waskell, L., 2000. High-level expression in *Escherichia coli* and purification of the membrane-bound form of cytochrome *b*(5). Protein Expr. Purif. 19, 173-178.

Pace, C.N., Scholtz, J.M., 1997. Measuring the conformational stability of a protein, in: Creighton, T. (Ed.), Protein Structure: A Practical Approach, 2nd ed. Oxford University Press, Oxford, pp. 299-321.

Pfeil, W., 1993. Thermodynamics of apocytochrome *b(5)* unfolding. Protein Sci. 2, 1497-1501.

Rivera, M., Walker, F.A., 1995. Biosynthetic preparation of isotopically labeled heme. Anal. Biochem. 230, 295-302.

Robinson, C.R., Liu, Y.F., Thomson, J.A., Sturtevant, J.M., Sligar, S.G., 1997. Energetics of heme binding to native and denatured states of cytochrome *b*(562). Biochemistry 36, 16141-16146.

Rodgers, K.R., Lukat-Rodgers, G.S., 2014. Biophysical perspectives on the acquisition, transport, and trafficking of heme in bacteria, in: Ferreira, G.C., Kadish, K.M., Smith, K.M., Guilard, R. (Eds.), Handbook of Porphyrin Science with Applications to Chemistry, Physics, Materials Science, Engineering, Biology and Medicine, Vol. 30: Heme Proteins, Part II. World Scientific, Hackensack, N.J, pp. 251-309.

Roy, A., Kucukural, A., Zhang, Y., 2010. I-TASSER: A unified platform for automated protein structure and function prediction. Nat. Protoc. 5, 725-738.

Saini, K., Ahluwalia, U., Deep, S., 2010. Determination of heat capacity of unfolding for marginally stable proteins from a single temperature induced protein unfolding profile. Thermochim. Acta 506, 28-33.

Sievers, F., Higgins, D.G., 2014. Clustal Omega, accurate alignment of very large numbers of sequences. Methods Mol Biol 1079, 105-116.

Sudhamsu, J., Kabir, M., Airola, M.V., Patel, B.A., Yeh, S.R., Rousseau, D.L., Crane, B.R., 2010. Co-expression of ferrochelatase allows for complete heme incorporation into recombinant proteins produced in *E. coli*. Protein Expr. Purif. 73, 78-82.

Swint, L., Robertson, A.D., 1993. Thermodynamics of unfolding for turkey ovomucoid third domain: Thermal and chemical denaturation. Protein Sci. 2, 2037-2049.

Teale, F.W., 1959. Cleavage of the heme protein by acid methyl ethyl ketone. Biochim. Biophys. Acta 35, 543.

Tiedemann, M.T., Stillman, M.J., 2011. Application of magnetic circular dichroism spectroscopy to porphyrins, phthalocyanines and hemes. J. Porph. Phthalo. 15, 1134-1149.

Travaglini-Allocatelli, C., Cutruzzolà, F., Bigotti, M.G., Staniforth, R.A., Brunori, M., 1999. Folding mechanism of *Pseudomonas aeruginosa* cytochrome *c*(551): Role of electrostatic interactions on the hydrophobic collapse and transition state properties. J. Mol. Biol. 289, 1459-1467.

Travaglini-Allocatelli, C., Gianni, S., Dubey, V.K., Borgia, A., Di Matteo, A., Bonivento, D., Cutruzzolà, F., Bren, K.L., Brunori, M., 2005. An obligatory intermediate in the folding pathway of cytochrome *c*(552) from *Hydrogenobacter thermophilus*. J. Biol. Chem. 280, 25729-25734.

Travaglini-Allocatelli, C., Gianni, S., Morea, V., Tramontano, A., Soulimane, T., Brunori, M., 2003. Exploring the cytochrome c folding mechanism - Cytochrome *c*(552) from *Thermus thermophilus* folds through an on-pathway intermediate. J. Biol. Chem. 278, 41136-41140.

Uluisik, R.C., Akbas, N., Lukat-Rodgers, G.S., Adrian, S.A., Allen, C.E., Schmitt, M.P., Rodgers, K.R., Dixon, D.W., 2017. Characterization of the second conserved domain in the heme uptake protein HtaA from *Corynebacterium diphtheriae*. J. Inorg. Biochem. 167, 124-133.

Warren, M.J., Smith, A.G., 2009. Tetrapyrroles: Birth, Life, and Death. Landes Bioscience, Austin, Tex.

Watanabe, M., Tanaka, Y., Suenaga, A., Kuroda, M., Yao, M., Watanabe, N., Arisaka, F., Ohta, T., Tanaka, I., Tsumoto, K., 2008. Structural basis for multimeric heme complexation through a specific protein-heme interaction - The case of the third NEAT domain of IsdH from *Staphylococcus aureus*. J. Biol. Chem. 283, 28649-28659.

Wen, X., Patel, K.M., Russell, B.S., Bren, K.L., 2007. Effects of heme pocket structure and mobility on cytochrome *c* stability. Biochemistry 46, 2537-2544.

Zhang, L., Liu, X.Q., Wang, C.T., Liu, X.Q., Cheng, G., Wu, Y.H., 2010. Expression, purification and direct eletrochemistry of cytochrome P450 6A1 from the house fly, *Musca domestica*. Protein Expr. Purif. 71, 74-78.

Zheng, Z., Gunner, A.R., 2008. Analysis of the electrochemistry of hemes with E(m)s spanning 800 mV. Proteins-Structure Function and Bioinformatics 75, 719-734.

4 CHARACTERIZATION OF HOMOLOGOUS HEME UPTAKE PROTEINS HTAB AND CHTB FROM *CORYNEBACTERIUM DIPHTHERIAE*

This chapter is intended for publication verbatim in Rizvan C. Uluisik, Brandon L. Ferrell, Gudrun S. Lukat-Rodgers, Courtni E. Allen, Michael P. Schmitt, Kenton R. Rodgers, and Dabney W. Dixon. The expression, purification, and UV-visible spectroscopy of the WT and mutants were performed at Georgia State University.

4.1 Abstract

Many pathogenic bacteria need iron for growth and virulence; hemin serves as a common source of iron in infection. *Corynebacterium diphtheriae* can take up hemin via a series of conserved DxtR-regulated heme transport-associated (HtaA CR) domains. After initial binding of the heme source protein to HtaA, ChtA and/or ChtC, hemin is thought to be transferred to HtaB or ChtB, which seem to be functionally equivalent in this organism. Herein, we compare and contrast HtaB or ChtB with one another and with the previously-studied second conserved domain of HtaA (HtaACR2). UV-visible and resonance Raman spectroscopy are consistent with an axial tyrosine ligand for HtaB or ChtB (HtaA-CR2 has alos a tyrosine). Sequence alignment and mutagenesis studies point to a histidine as the hydrogen-bonding partner of the axial tyrosine. HtaB and ChtB are less stable than HtaACR2 to unfolding via guanidinium hydrochloride or temperature. For HtaB, mutation of the axial tyrosine and its hydrogen-bonding partner significantly reduce the thermal stability in solution. A much smaller effect is seen in the gas phase.

4.2 Introduction

Corynebacterium diphtheriae is a Gram-positive bacterium that causes communicable infections of the upper respiratory tract and skin in humans. Strains that secrete the iron- and DtxR-

regulated diphtheria toxin are association with severe symptoms (Trost et al., 2012; Schmitt, 2014). Early work showed that strain C7 was able to use both heme and hemoglobin as iron sources in a low-iron medium (Schmitt, 1997b). A screen for heme- and hemoglobin-uptake-deficient mutants discovered a six-gene locus with a heme-binding protein (HmuT), and a putative permease (HmuU) and ATPase (HmuV), the latter two comprising an ABC transporter (Drazek et al., 2000). Three additional loci were discovered, the heme transport-associated proteins HtaA, HtaB and HtaC, with HtaB and HtaC transcribed from DtxR promoters independent of the gene cluster for the rest of the proteins (Kunkle and Schmitt, 2003; Allen and Schmitt, 2009).

HtaA, a surface-exposed 61-kDa membrane-anchored protein, has two conserved regions (CR1 and CR2) of approximately 150 amino acids (Allen and Schmitt, 2011). It can bind hemin, hemoglobin, myoglobin, heme-human serum albumin, and hemoglobin-haptoglobin (Allen and Schmitt, 2015). Sequence alignment and site-directed mutagenesis revealed two conserved tyrosines and a conserved histidine that were significant in binding of hemin and Hb. The N-terminal tyrosine of CR2 was critical for hemin utilization of this domain (Allen and Schmitt, 2011). Recent work has shown that HtaA has a tyrosine as the axial ligand to the heme and that unfolding of this protein is very slow (Uluisik et al., 2017)

HtaB is also a hemin-binding protein (36 kDa) with a single CR domain; the protein is mainly associated with the cell-membrane and exposed to the cell surface (Allen et al., 2013). The single CR domain of HtaB shares 27% identity and 38% similarity with HtaA-CR2 and somewhat less identity and similarity with HtaA-CR1. Like HtaA, HtaB has two conserved tyrosines and a conserved histidine. HtaB can receive heme from both HtaA-CR1 and HtaA-CR2; the K_D for hemin binding is 4.9 μM (Allen and Schmitt, 2009; Allen and Schmitt, 2011;

Allen et al., 2013). Unexpectedly, deletion of the *htaB* gene had no effect on growth when hemoglobin was the only iron source (Allen and Schmitt, 2009). This led to a search for additional heme-uptake pathways.

A re-investigation of two previously reported DtxR-regulated operons, *chtAB and cirA chtC* (Kunkle and Schmitt, 2003), gave insight into the roles of ChtA/C and ChtB, homologs of HtaA and HtaB, respectively (CirA does not bind hemin) (Allen et al., 2013; Allen and Schmitt, 2015). ChtA (83.9 kDa) and ChtC (74.3 kDa) each have a single N-terminal CR domain with significantly sequence similarity to the HtaA domains; all of these proteins can bind both hemin and hemoglobin. ChtB shows high sequence similarity to HtaB (44% identity and 63% similarity). Hemoglobin utilization assay studies showed that deletion or either *chtB* or *htaB* alone did not result in significant growth inhibition. However, a *chtB-htaB* double gene deletion showed a significant reduction of bacterial growth when compared to the wild-type strain. These observations led to the suggestion that HtaB and ChtB are surface-exposed hemin binding domains that play an interchangeable role in hemin uptake (Allen et al., 2013).

In view of the apparent interchangeability of HtaB and ChtB, as well as their overall similarity to the HtaA-CR domains, it is of interest to compare and contrast the biophysical aspects of these proteins. Resonance Raman (rR) spectroscopy was used to investigate the structural and electronic features of the heme micro-environment in the binding pocket. The stability of the protein folding was investigated via chemical and thermal denaturation techniques and collision-induced heme dissociation in the gas phase. These experimental results lead to a picture of three related proteins that are similar in many aspects, but nonetheless have noticeable differences, presumably significant in controlling the process of heme transfer. This work adds to the increasing knowledge of heme uptake in Gram-positive pathogenic bacteria across a

variety of species as outlined in recent reviews (Contreras et al., 2014; Rodgers and Lukat-Rodgers, 2014; Wilks and O'Neill, 2014; Sheldon and Heinrichs, 2015; Choby and Skaar, 2016; Sheldon et al., 2016).

4.3 Materials and Methods

4.3.1 HtaB-WT Strep-tag labeled constructs

An N-terminal Strep-tag labeled construct of HtaB-WT was synthesized and inserted into pET24a(+) plasmid at NdeI and HindIII restriction sites (GenScript, NJ). The construct included the HtaB peptide sequence between Ala25 and Asn292 (NCBI sequence reference number WP_004566989.1). A TEV cleavage sequence was inserted between the Strep-tag and HtaB-WT. A linker sequence of SGGGGG was used to separate the Strep-tag and the TEV cleavage sequence. The ChtB construct has been previously described (Allen et al., 2013).

4.3.2 HtaB-WT site-directed mutagenesis

Recombinant HtaB-WT mutants were prepared by site-directed mutagenesis using a QIAprep Spin Miniprep Kit according to the manufacturer's instructions. The primers were from Sigma Aldrich for Y56A and H121A substitutions (Table 4.2). Primers (500 ng) were mixed with 100 ng of pET24a(+) template plasmid in the reaction mixture. DpnI restriction endonuclease was used to eliminate the methylated template. The mutated plasmids were transformed into the competent *E. coli* strain BL21(DE3) using heat shock method. Sequence analysis was used to confirm the mutations.

4.3.3 Expression and purification

Strep-tag labeled HtaB-WT, ChtB-WT, and HtaB mutants were expressed and purified using the same protocol. Luria-Bertani (LB) medium was used for culturing the *E. coli* cells. The medium

contained 50 μg/ml kanamycin. For the HtaB constructs, 0.3% glucose was added. A small scale culture (10 ml) was incubated at 37 ºC at 220 rpm for 16 h, added to 500 ml of media and the resulting solution incubated at 37 ºC at 220 rpm until the OD_{600} reached 0.8. The cultures were induced by adding 50 μM isopropyl-β-D-thiogalactopyranoside (IPTG) and allowed to grow for 16 h at 28 ºC. The cells were harvested by centrifuging at 4 ºC at 3100 rpm for 30 min. The pellets were collected and stored in -80 ºC freezer overnight.

The cell pellet was re-suspended in buffer A (100 mM Tris-HCl, 150 mM NaCl, pH 8.0). The cells were lysed in a solution containing buffer A, 10 mM $MgCl_2$, 0.1 mM phenylmethanesulfonyl fluoride (PMSF), 0.2 mg/mL lysozyme, 5 μg/mL DNase I (from bovine pancreas, Roche) and 5 μg/mL RNase A (from bovine pancreas, Roche) and incubated on ice for 30 min. The cells were disrupted with a sonicator, and the cell debris was removed by centrifugation at 4 ºC at 6500 rpm for 30 min.

A GE Healthcare ÄKTA fast protein liquid chromatography instrument (FPLC) was used for purification at 4˚C. The protein solutions were loaded onto a Strep-Tactin Superflow column (5 mL, IBA BioTAGnology) which had been equilibrated with Buffer A. The unbound material was washed with Buffer A [5 column volumes (CV)]. The Strep-Tactin bound protein was eluted with 10 CV of Buffer B (100 mM Tris-HCl, 150 mM NaCl, 2.5 mM *d*-desthiobiotin, pH 8.0). A linear gradient of buffer A and B was used. The purity of the fractions was tested by sodium dodecyl sulfate polyacrylamide gel electrophoresis (SDS-PAGE). Approximately 0.8 mg/L of protein were isolated. Hemin loadings were approximately 30% for the HtaB-WT, 60% for ChtB, and 4% for each mutant.

4.3.4 Hemin transfer from metHb to HtaB-WT and HtaB-Y56A

Strep-tag purified HtaB-WT (7.2×10^{-9} moles of holoprotein with A_{Soret}:A_{280} ratio of 0.6) in buffer A was loaded onto a 5 mL Strep-Tactin column. A concentrated Hb solution (equine, Sigma-Aldrich) was prepared in buffer A (2.9×10^{-7} moles, 40 times excess) and allowed to flow through the column (1 ml/min). The column was washed with 20 CV of buffer A to remove Hb. Fractions were checked by UV-visible absorption spectroscopy to make sure the eluent was free of absorbing species. The column-bound HtaB-WT was eluted as described for the initial isolation. The hemin-bound fractions of HtaB-WT were concentrated using an Amicon Ultra-15 centrifugal filter at 6000 rpm and 4 ºC. The isolated holoprotein was 1.7×10^{-8} moles with A_{Soret}:A_{280} ratio of 1.6; thus, the hemin content of the total protein increased around 2.4 times. Similar results were observed for the Y56A mutant. The column-bound protein (8.3×10^{-10} moles of holoprotein with A_{Soret}:A_{280} ratio of 0.1) incubated with excess metHb resulted in approximately 4-fold increase in the hemin concentration (3.3×10^{-9} moles of holoprotein with A_{Soret}:A_{280} ratio of 1.4).

4.3.5 Addition of hemin to apoHtaB-WT and apoHtaB mutants

These experiments involved addition of hemin to the as-isolated HtaB-WT, HtaB-Y56A and HtaB-H121A (~ 30, 4, and 4% heme loaded, respectively). The protein solutions were prepared in 100 mM Tris-HCl, 150 mM NaCl pH 8.0. A solution of hemin in DMSO was added in increments to a final ratio of hemin to each apoprotein of ~ 0.9. The protein solutions were equilibrated 30 min after each addition of hemin.

4.3.6 UV-visible absorption spectroscopy

The electronic absorption of the proteins was measured with a Cary 50 Bio UV-visible spectrophotometer. The pyridine hemochrome assay was used to determine the extinction

coefficients (Berry and Trumpower, 1987). An average of three experiments gave an extinction coefficient of 1.26 x 10^5 M^{-1} cm^{-1} for HtaB-WT and 1.1 x 10^5 M^{-1} cm^{-1} for ChtB.

4.3.7 Time-scale of unfolding of HtaB-WT during chemical denaturation

Samples of HtaB-WT in 100 mM Tris-HCl with 150 mM NaCl at pH 8.0 were prepared. A stock solution of GdnHCl was prepared in the same buffer and the concentration was determined by the refractive index method (Pace and Scholtz, 1997). The GdnHCl stock solution was added to the protein solutions to give varying concentrations of GdnHCl (3.4, 3.6, 3.8, 4.0, 4.2, and 4.4). For each sample, the spectrum was followed at 25 ^oC after the addition of denaturant. The absorbance at 409 nm was fit to a single-term exponential function: (equation 1)

$$A = A_0 \exp(-k_U t) + c$$

where A is the absorbance at any point along the fitted unfolding curve, A_0 is the initial absorbance, k_U is the unfolding rate constant and t is time.

4.3.8 **Thermal denaturation in the presence of 1.0 M GdnHCl**

Thermal unfolding was carried out with the UV-visible spectrophotometer equipped with temperature control (TC 125, Quantum Northwest). A screw top quartz cuvette with 1 cm path length was used. Each protein solution was prepared in 50 mM NaH_2PO_4, pH 7.0, including 1.0 M GdnHCl. The solutions were heated and the spectrum recorded every 1 ^oC after a 1 min incubation.

Kaleidagraph (version 4.01, Synergy Software) was used to fit the data using a two-state protein unfolding model equation (Swint and Robertson, 1993): equation (2)

$$A = \frac{(A_F + m_F T) + (A_U + m_U T) exp\left[\frac{\Delta H_m}{R(T_m^{-1} - T^{-1})}\right]}{1 + exp\left[\frac{\Delta H_m}{R(T_m^{-1} - T^{-1})}\right]}$$

where A is the absorbance at any point along the unfolding curve, A_F is the absorbance of the folded state, A_U is the absorbance of the unfolded state, m_F is the slope of the folded state, m_U is the slope of the unfolded state, T_m is the temperature at which the protein is half unfolded, ΔH_m is the enthalpy of unfolding, R is the gas constant, and T is the temperature (Kelvin).

4.3.9 Electrospray ionization (ESI) mass spectrometry

ESI spectra were obtained using a Waters Micromass Q-TOF spectrometer in the positive mode. The fully holoprotein was prepared by adding of hemin to the as-isolated protein (approximately 30% heme loaded) as previously described. The protein solution (10 μM) was dialyzed against 20 mM ammonium acetate, pH 6.8. Spectra were recorded (flow rate 10 μl/min) at the following collision energy voltages: 5, 10, 15, 20, 25, 30, and 40 V. All other parameters were held constant (capillary voltage 3000 V, cone voltage 18 V, extraction voltage 1.5 V, desolvation gas temperature 100 ºC and source temperature 80 ºC). Deconvolution of the charged state was performed using the MaxEnt program with the MassLynx™ software. Peaks were rounded to the nearest Dalton; peak heights were used to calculate holoprotein percentages.

4.3.10 Resonance Raman (rR) spectroscopy

Resonance Raman (rR) spectra were recorded from ferric samples using the 413.1-nm emission line from a Kr^+ laser and from ferrous samples with 441.6-nm excitation from a HeCd laser. The Raman shifts for toluene, dimethyl sulfoxide, and methylene bromide were used as external standards for spectral calibration. Spectra were recorded at ambient temperature using the 135°

backscattering geometry with the laser beam focused to a line on a spinning 5 mm NMR tube. UV−visible spectra were recorded before and after rR experiments to verify that the samples were not altered by their exposure to the laser beam. The final protein concentration was 30 μM for the HtaB-WT. The buffers used were 100 mM glycine (9.6), Tris-HCl (pH 8.8 or 8.0), and sodium phosphate buffer (pH 5.8). Ferrous samples were prepared under anaerobic conditions by adding buffered dithionite in a 300-fold molar excess over heme. The Fe(II)-CO samples were prepared with a 300-fold molar excess of dithionite under an atmosphere of natural abundance CO or ^{13}CO at pH 8.8.

4.4 Results and Discussion

4.4.1 UV-visible absorbance spectroscopy of HtaB and ChtB

For HtaB-WT, the UV-visible spectrum shows a Soret maximum at 409 nm and four α/β bands at 505, 540, 517, and 626 nm (Fig. 4.1). The charge-transfer (CT) peak at ~ 620 nm is indicative of a high spin heme-iron interaction with an oxygen species, often seen in tyrosine-coordinated heme proteins (Tiedemann and Stillman, 2011; Rodgers and Lukat-Rodgers, 2014). A pH titration showed no significant spectral changes over the pH 6.9 – 11.2 range (data not shown).

Two conserved residues that may serve as heme axial ligands, Y56 and H121, were each mutated to alanine. The WT protein as approximately 30% heme loaded as purified. In contrast, purification of Y56A and H121A gave significantly reduced heme loading (both ~ 4% holoprotein). The low heme loading of the mutants is consistent with these residues being important for heme binding. The UV-visible absorption spectra for ferric HtaB-WT and the H121A mutant are similar (Fig. 4.1), with the peaks for H121A at 406, 496 and 617 nm. In contrast, the as-isolated Y56A mutant has a very different spectrum; the Soret maximum is at

412 and the α/β bands are at 546 and 567 nm. The loss of the 617 nm band is consistent with Y56 as a coordinating the heme in the binding pocket of HtaB-WT.

The UV-visible absorption spectrum of ChtB is similar to that of HtaB as well as the CR2 domain from HtaA (Uluisik et al., 2017) (Fig. 4.9). In each case, the Soret maximum is at approximately 409 nm and three α/β bands are seen, including one at approximately 626 nm, which is appropriate for an oxygen-ligated high-spin hemin center.

4.4.2 Heme addition

Attempts were made to increase the heme content of as-isolated HtaB-WT (A_{Soret}:A_{280} ratio of 0.6), as well as the Y56A and H121A mutants (A_{Soret}:A_{280} ratio of 0.1 for each), by titrating exogenous hemin up to 1 eq total hemin. The final A_{Soret}:A_{280} ratio was approximetly1.8 for all three proteins. No significant spectral changes were between the as isolated and heme titrated HtaB-WT (Fig. 4.10). The data suggest that the added heme was in the same environment as that found in the as-isolated protein. The spectrum of the heme titrated Y56A mutant was significantly different from that of the as-isolated protein (Fig. 4.11). The Soret band blue shifted only slightly, but the 546 and 567 nm peaks disappeared and new bands appeared at 497 and 613 nm. This spectrum is similar to that of the HtaB-WT protein. As described above, the band at approximately 626 nm is consistent with a 6-coordinate, high-spin complex in which an axial ligand is coordinated through an oxygen atom. As the presumed axial Y56 is no longer present, this spectrum may indicate a conformational change to provide another oxygen-coordinated axial ligand, presumably a tyrosine or water. Finally, the spectrum of heme titrated H121A was essentially identical to that of the as-isolated protein (Fig. 4.12), which in turn had a spectrum very similar to the WT protein.

The heme loading of as-isolated HtaB-WT and the Y56A mutant were also increased by transferring the hemin from metHb as previously described (Uluisik et al., 2017). The spectra of the resulting species were very similar to those observed following hemin addition (Fig. 4.11 and Fig. 4.13).

4.4.3 Resonance Raman of ferric HtaB-WT and ChtB

The rR spectrum of ferric HtaB is pH independent, as evidenced by the unchanging high-frequency spectrum over the pH range from 5.8 to 9.6 (Fig. 4.2). The ν_3, ν_{38}, and ν_2 core stretching frequencies of 1483, 1520 and 1561 cm^{-1}, respectively, reveal the heme to be in a 6-coordinate high spin (6cHS) state (Hu et al., 1996b). Another protein in a heme uptake pathway, *Yersinia pseudotuberculosis* (*Yp*) HasA, has been shown to exist as an equilibrium mixture of 6cHS and 5-coordinate high-spin (5cHS) states (Ozaki et al., 2014), the former presumably having with a water molecule as the sixth ligand (Table 4.1). *Yp*HasA also does not show a pH dependence over the pH range from 5 to 10. *Serratia marcescens* (*Sm*) HasA (Lukat-Rodgers et al., 2008) and *Cd*HmuT are mixtures of 6cHS and 6 coordinate low-spin (6cLS) states (Draganova et al., 2015). Even though the CR domain of HtaB shares approximately 27% sequence identity and 38% similarity with the CR2 domain of HtaA, the hemin binding motifs are distinct because *Cd*HtaA is 5cHS in the ferric form (Uluisik et al., 2017). HtaA exhibits a rR spectrum typical of 5cHS hemin that is bound to the protein through a proximal tyrosine ligand. The ν_3 (1490 cm^{-1}) and ν_2 (1568 cm^{-1}) rival the intensity of the ν_4 which is unusual for other hemin proteins but has been observed in bovine liver catalase (Chuang et al., 1988) and *Shigella dysenteriae* ShuT (Eakanunkul et al., 2005), both of which share the proximal Tyr binding motif as seen in Table 4.1.

Like its HtaB homolog, *Cd*ChtB forms a 6cHS hemin complex with spectral characteristics consistent with a proximal Tyr binding motif (Fig. 4.3). The ν_3, ν_{38}, and ν_2 core stretching frequencies of 1486, 1522 and 1560 cm^{-1}, respectively, indicate 6cHS hemin (Hu et al., 1996b). Unlike ferric HtaB, peripheral substituent modes in ChtB exhibit slight pH dependences, as seen in the shifts of the in-plane vinyl stretch from 1613 to 1627 cm^{-1}, the in-plane $C_\beta C_\beta$ stretch from 1560 to 1558 cm^{-1}, the in-plane pyrrole breathing mode from 761 to 754 cm^{-1}, out-of-plane pyrrole fold from 739 to 735 cm^{-1} and an increase at 666 cm^{-1}, and out-of-plane wags from 329 to 327 cm^{-1} and from 311 to 308 cm^{-1} (Fig. 4.3 and S4.5). None of these vibrations are particularly sensitive to the coordination number or spin state of the heme, as evidenced by the constancy in the ν_4 and ν_3 frequencies among these proteins. This indicates that the structural determinants for coordination number and spin state in the hemin binding pockets of HtaB and ChtB are similar, with the environments that impact conformations of the peripheral substituents being slightly variable.

4.4.4 Resonance Raman of ferrous HtaB-WT

Upon reduction with dithionite, HtaB was converted to a mixture of 5cHS and 6cLS ferrous states. This mixture was revealed by a ν_3 band at 1468 cm^{-1} and a small band at 1494 cm^{-1}, respectively (Fig. 4.14). The ν_{11}, ν_2, and ν_{10} core stretching frequencies of 1558 cm^{-1}, 1583 cm^{-1} and 1624 cm^{-1} respectively, are consistent with the speciation being dominated by the 5cHS heme state (Brogioni et al., 2006); the UV-visible Soret maximum of 428 nm is also consistent with this assignment. This result differs from both *Yp*HasA, which is solely 5cHS (ν_3, 1470 cm^{-1}), and *Cd*HmuT and *Sm*HasA, which do not form ferrous complexes under similar conditions (Lukat-Rodgers et al., 2008; Ozaki et al., 2014; Draganova et al., 2015). The rR spectra are also consistent with the UV-visible Soret maximum of 428 nm, suggesting a

predominately 5cHS speciation similar to what was reported for *Yp*HasA (Ozaki et al., 2014) (Fig. 4.14 inset).

When excited with the 441.6 nm laser light, the low frequency spectrum of HtaB contains a small band at 217 cm^{-1}, which is a typical Fe^{II}-His stretching frequency in 5cHS ferrous heme proteins (Fig. 4.4). Because of its red-shifted Soret band, blue (441.6-nm) Raman excitation selectively enhances Raman scattering by the modes of 5cHS having a proximal His ligand. Thus, it is possible to detect the presence of axial His ligation in 5cHS ferrous hemes, even if it is not the majority species (Kitagawa et al., 1979). It is possible that a His ligand is replacing the axial tyrosine in a fraction of the ferrous form. This type of displacement has been observed for the ferrous form of *S. pyogenes* NEAT-A (IsdA), in which the axial Tyr ligand in the ferric form is replaced by His in the ferrous form of the protein (Pluym et al., 2008). The small relative intensity of the 217 cm^{-1} band, in comparison to that of ν_{Fe-His} modes from other proteins, is likely due to a small amount of the protein being 5cHS with the remainder having Tyr coordinated in the axial position. These spectra suggest the ferrous HtaB is a mixture of complexes, comprising predominately a 5cHS Tyr complex with small contributions from a 5cHS His-bound and 6cLS Tyr/X-bound hemes.

Ferrous ChtB was solely 5cHS as evidenced by its ν_3 at 1468 cm^{-1} and Soret maximum of 425 nm (Fig. 4.15). The ν_{11}, ν_2, and ν_{10} core stretching frequencies of 1556 cm^{-1}, 1584 cm^{-1} and 1623 cm^{-1}, respectively, indicate a 5cHS heme environment, similar to the 5cHS contribution to the ferrous HtaB spectrum. The absence of bands attributable to a 6cLS form indicates that reduction destabilizes its 6cLS heme to an even greater extent than in HtaB.

4.4.5 Resonance Raman of ferrous carbonyl WT HtaB and ChtB

Through the sensitivity of Raman-active Fe-CO group frequencies to π backbonding and donor strength of the *trans* (proximal) ligand, resonance Raman spectra of heme protein carbonyls are useful probes of both the bonding and non-bonding properties of the heme pocket. The extent of π-backbonding is evidenced by the ν_{Fe-C}, ν_{C-O} frequencies which, when placed on a plot of ν_{Fe-CO} versus ν_{C-O} frequencies, yield insight into the electrostatic and steric properties of the distal heme pocket and the nature of the *trans* axial ligand (Vogel et al., 2000; Spiro and Wasbotten, 2005; Streit et al., 2010; Spiro et al., 2013). The Fe−^{13}CO isotopologs of HtaB and ChtB were used to verify the identity of rR bands corresponding to the Fe−C stretching (ν_{Fe-CO}), Fe-CO bending (δ_{Fe-CO}) and C−O stretching (ν_{C-O}) modes, as shown in Figures S4.8 and S4.9.

Under an atmosphere of carbon monoxide, the UV-visible spectra of ferrous HtaB and ChtB exhibit shifts of their Soret band maxima to 417 and 415 nm, respectively, along with sharpening and shifting of the Q bands (insets, Fig. 4.16 and 4.17). These absorbance changes are consistent with the formation of the HtaB and ChtB carbonyls.

The Soret-excited rR spectrum of HtaB−CO reveals two ν_{Fe-CO} bands at 503 and 532 cm^{-1}, which shift to 501 and 527 cm^{-1}, respectively, upon ^{13}CO substitution. Despite having two ν_{Fe-CO} stretches, the spectrum reveals only one ν_{C-O} band and a single δ_{Fe-CO} band at 1949 and 562 cm^{-1}, respectively, which shift to 1902 and 554 cm^{-1} in the ^{13}CO isotopolog (Fig. 4.16). ChtB−CO also exhibits two ν_{Fe-CO} bands [503(−3) and 531(−5) cm^{-1}], one δ_{FeCO} band at 563(−13) cm^{-1} and one ν_{C-O} band at 1953(−47) cm^{-1}, similar to what was observed for HtaB−CO (Fig. 4.17). Placement of these pairs of ν_{C-O} and ν_{Fe-CO} frequencies on the π-backbonding correlation plot is consistent with two heme carbonyls having different proximal ligands (Fig. 4.5). One form falls near the line correlating ν_{C-O} and ν_{Fe-CO} of carbonyls having

neutral imidazole ligands. The other falls on the correlation line neutral proximal ligands coordinated through an O atom. This position is consistent with a proximal Tyr ligand whose coordinated O atom interacts with a single hydrogen bond donor (*vide infra*).

The CO ligand in the *trans* ImH form is in a weak hydrogen bond interaction with the distal pocket as evidenced by its low position along the neutral imidazole line (Smulevich et al., 1988b)This interaction w likely involves the native, conserved Tyr56 axial ligand interacting with the exogenous CO ligand in a manner similar to that reported for *Cd*HmuT mutants R237A and M292A (Draganova et al., 2016). The position of the form having an O-bound proximal ligand, which is likely the conserved Tyr56, is indicative of stabilization of the oxygen by a single neutral hydrogen-bonding partner. The position is close to both *Yp*HasA (Ozaki et al., 2014) and *Sm*HasA (Caillet-Saguy et al., 2008) which have been shown to have a *trans* neutral histidine that is hydrogen bonded to the axial Tyr (Arnoux et al., 1999; Ozaki et al., 2014). The *trans* ligand environments of HtaB and ChtB differ from that of *Cd*HmuT, which has been shown to have a pair of hydrogen bonds from the guanidinium side chain of a nearby Arg residue (Draganova et al., 2015; Draganova et al., 2016). The positioning of the Arg hydrogen-bonding partner of the Tyr ligand in crystal structure of *Cg*HmuT has been shown (Muraki and Aono, 2015). A possible neutral hydrogen-bonding partner could be Tyr53 which could stabilize the Tyr56 heme ligand in HtaB, similar to what is seen with IsdB (Gaudin et al., 2011).

4.4.6 Time-scale of unfolding of HtaB-WT during chemical denaturation

Denaturant-induced unfolding of heme proteins is used to understand the factors that control heme binding at the active site (Pace and Scholtz, 1997). In previous work, we showed that *Cd*HtaA-CR2, a domain with significant sequence similarity to HtaB, was very stable in the presence of GdnHCl; e.g., a half-life of 330 min was observed even in the presence of 6.6 M

GdnHCl at 37 ^{o}C (Uluisik et al., 2017). HtaB was significantly less stable toward unfolding, e.g., a single first-order process with a half-life of 39 min was observed in the presence of 4.0 M GdnHCl at 25 ^{o}C (Table 4.3). As HtaB unfolded, the Soret band decreased and a shoulder peak at around 350 nm increased (data not shown). To assess the reversibility of the unfolding reaction, the GdnHCl (at 4.0 M) was removed via dialysis. Only 50% of the Soret absorbance was recovered (data not shown). Considering the loss of some protein due to precipitation in dialysis, these data suggest that the unfolding of HtaB-WT at 4.0 M GdnHCl was at least 50% reversible. The unfolding behavior of ChtB at 4.0 M GdnHCl was similar to that of HtaB (Fig 4.6).

4.4.7 Thermal stability of HtaB and ChtB

Thermal unfolding of as-isolated HtaB-WT, as well as the H121A and Y56A mutants, was used to probe the contribution of the axial ligands to the stability of the holoprotein. Heating of HtaB-WT to 70 ^{o}C did not show any significant spectral change; the protein began to precipitate above this temperature. Thermal unfolding experiments were therefore performed in the presence of 1.0 M GdnHCl. Figure S4.10 shows a representative unfolding spectrum (H121A mutant). The Soret absorbance gradually decreased. An isosbestic point at around 375 nm was visible up to the $T_{m,}$ (46 ^{o}C). The unfolding spectral changes were similar for the WT and mutants. Approximately 90% of the Soret absorbance was recovered for the WT and H121A mutant when the protein solutions were cooled to the initial temperature; no recovery was observed for the Y56A mutant. The apparent T_m values were 61, 46 and 27 ^{o}C (1 M GdnHCl) for HtaB-WT, and the H121A and Y56A mutants, respectively (Fig. 4.7). Thus, both H121 and Y56 are playing a role in heme binding. Y56 has a highly significant role, with a T_m more than 30 ^{o}C lower than WT, and no

recovery after cooling to room temperature. The importance of Y56 is in line with the rR backbonding correlation results showing that HtaB is likely a Tyr heme-coordinated protein.

The thermal unfolding of ChtB in 1 M GdnHCl was almost identical to that of HtaB, with apparent T_m value of 61 ^oC (data not shown). Allen and Schmitt showed that a single deletion of either *htaB* or *chtB* genes does not affect cell growth in *C. diphtheriae* (Allen and Schmitt, 2009; Allen et al., 2013). A double mutation of *htaB-chtB* genes, however, significantly affects the growth. The very similar data for HtaB and ChtB in terms of thermal stability, as well as the kinetics of GdnHCl-induced unfolding, are consistent with similar structures and heme binding sites; it is thus reasonable that these two proteins play a similar role in the heme uptake.

The significant differences in ease of unfolding of these three proteins presumably arise from local hydrophobic, electrostatic and hydrogen-bonding interactions in the heme pocket. Schmitt and co-workers have shown that HtaA can bind hemoglobin while HtaB does not. HtaA can transfer heme to HtaB (Allen and Schmitt, 2011). Growth studies show that either HtaB or ChtB can serve in terms of the growth of the cell with heme as an iron source (Allen and Schmitt, 2009; Allen et al., 2013). Thus, the presumed pathway for heme uptake involves heme transfer from HtaA to HtaB/ChtB. It is interesting to note that HtaA-CR2 binds hemin more tightly (60 nM, Strep-tag) than HtaB (4.9 µM, no tag) in solution (Allen and Schmitt, 2009, 2015). Thus, the role of protein/protein interactions is presumably important in determining the pathway of heme transfer (Draganova et al., 2015; Uluisik et al., 2017).

4.4.8 Heme dissociation in ESI mass spectrometry

The stability of as-isolated HtaB-WT and its mutants was also evaluated by monitoring the mass spectra as a function of collision energy (5 – 40 V). Each as-isolated protein was initially titrated with hemin (~ 0.9 of hemin:apoprotein ratio) to obtain holoprotein concentrations suitable for the

mass spectra experiments. Figure 4.8 shows that the percentage of holoprotein decreased approximately from 94% to 30% for WT and the H121A mutant. Y56A, which started with only 67% heme loading, showed a similar loss of hemin with increase in collision energy.

As observed previously for the studies on myoglobin and cytochrome b_5 (Hunter et al., 1997) as well as the HmuT heme transfer protein (Draganova et al., 2016), gas phase and solution phase data do not necessarily show a direct correlation. In the solution phase, the proteins are in the stability order WT > H121A > Y56A whereas in the gas phase, all three show comparable heme loss with increasing collision energy.

4.4.9 Relationship to other heme uptake pathways.

The heme uptake pathway studied herein, based on variations of the HtaACR domain, can be compared with the well-studied heme uptake strategy that involves NEAT domains (Honsa et al., 2014). Gram positive bacteria are largely divided into Firmicutes (low-G+C species) and Actinobacteria (high G+C species). Examples of clinically relevant Firmacutes include *Bacilllus*, *Clostridia*, *Listeria*, *Staphylococcus*, and *Streptococcus*, all of which use the NEAT domain, as has been studied experimentally for members of each of these classes (Sheldon and Heinrichs, 2015). A BLAST search performed in our laboratory indicates that none of these have HtaA conserved domains. In contrast, Actinobacteria seem to have adopted an HtaACR strategy. A bioinformatics search shows that *Corynebacteria* have HtaA but not NEAT domains, as do the clinically relevant *Actinomyces*, *Propionobacteria*, and *Rothia* classes.

An analysis of the sequences of 13 *C. diphtheriae* genomes showed that the hemin binding protein (*HtaABC*), hemin transport (*HmuTUV*), and heme oxygenase (*hmuO*) genes were highly conserved (Trost et al., 2012). Only about half of the strains had the *chtA* and *chtB*

genes. Lack of *chtA* appears to correlate with lack of *chtC* (Allen et al., 2013). Almost all of the strains lacking *chtA* and *chtC* had copies of *htaA* with point mutations that may compromise the functionality of this protein. For example, the C7 strain had a frameshift mutation in *htaA* which was predicted to give premature termination of the protein.

Perusal of the known HtaA and NEAT-based heme uptake strategies shows that many of the first proteins involved in these pathways have two of the conserved domains. This design may serve in more than one context. For the three NEAT domains in IsdH, evidence shows that IsdHN2 binds hemoglobin and transfers the heme to IsdN3 (Sjodt et al., 2016). For the two NEAT domains in Shr, the kinetics of heme uptake have been interpreted in terms of heme transfer to ShrN1, with ShrN2 serving as a heme storage domain, which can transfer heme back to ShrN1 for movement along the pathway when the exogenous heme level drops (Ouattara et al., 2013). *C. diphtheriae* HtaA can use heme from hemoglobin and myoglobin. However, heme in the hemoglobin-haptoglobin complex can be extracted only when both HtaA and ChtA or ChtC (all containing HtaACR domains) are available (Allen and Schmitt, 2015). This is a variation of the two-domain motif, and indicates that HtaA and ChtA/C are probably located near one another in three-dimensional space.

A number of uptake studies have looked at the details of how the heme in one protein is transferred to a specific partner. For example, Shr transfers heme to Shp, with the possibility of an intermediate with axial ligands from both proteins (Liu and Lei, 2005; Nygaard et al., 2006). Kinetic analysis of transfer from IdsA to IsdC to IsdE in *St. aureus* has been interpreted in terms of a "cog-wheel" mechanism, in which heme must be moved to IsdE before IsdC can be reloaded (Tiedemann et al., 2012); related work on this system includes studies from (Muryoi et al., 2008; Villareal et al., 2011; Abe et al., 2012). In *B. anthracis*, heme is transferred from IsdX1 to IsdC

and IsdX2 (Fabian et al., 2009) and BslKN to IsdC (Tarlovsky et al., 2010); in *L. monocytogenes* heme is transferred from Hbp1 to Hbp2 (Malmirchegini et al., 2014). For the HtaA pathway in *C. diphtheriae*, HtaB and ChtB can substitute for one another and ChtA and ChtC can substitute for one another (Allen et al., 2013; Allen and Schmitt, 2015). This HtaA "pathway" is therefore perhaps better envisioned as a series of alternative crossing paths for heme entry, with the usage of the various options being determined by not only the heme source and specific protein-protein interactions, but also the numbers of various protein species in the membrane as well as their approximation to one another in space.

4.5 Conclusions

Herein, we have investigated HtaB and ChtB from the HtaA heme uptake pathway in *C. diphtheriae*. For both of these domains, sequence alignment, UV-visible spectroscopy of WT and mutants, and the Raman spectra of the WT protein indicate that tyrosine is the heme axial ligand. A conserved histidine is also in the heme pocket, as indicated by the observation of two species for the Fe(II)CO species, one with a *trans* axial histidine and the second with *trans* oxygen-bound ligand. HtaACR domains are significantly stable to unfolding in solution (induced by either denaturants or temperature), consistent with the hypothesis that protein-protein interactions are needed to transfer the heme. The gas phase and solution stabilities are not necessarily related, as observed in other heme protein stability studies. Bioinformatics analyses of currently available species indicate that many species of *Actinobacteria*, in addition to *Corynebacteria*, use HtaA domains. The conserved (CR) domains of HtaA-type proteins are increasingly understood as a fundamental heme transfer motif. The apparently interchangeability of HtaB and ChtB in transferring heme from HtaA/ChtA/ChtC to HmuT may indicate that heme uptake does not follow a simple linear pathway, but rather proceeds along a network of

pathways, taking advantage of multiple protein-protein interactions, as well as protein organization in space, to maximize internalization of this important iron source.

4.6 Abbreviations

ABC transporter, ATP-binding cassette transporter; CO, carbon monoxide; CR, conserved region; CT, charge-transfer; CV, column volume; DMSO, dimethyl sulfoxide; ELISA, enzyme-linked immunosorbent assay; ESI, electrospray ionization; FPLC, fast protein liquid chromatography; GdnHCl, guanidinium hydrochloride; Hb, hemoglobin; HS, high spin; HSA, human serum albumin; IPTG, isopropyl β-D-1-thiogalactopyranoside; LB, Luria Bertani; LS, low-spin; NEAT, near-iron transporter; PMSF, phenylmethanesulfonyl fluoride; Q-TOF, quadrupole time-of-flight; rR, resonance Raman spectroscopy; SDS-PAGE, sodium dodecyl sulfate polyacrylamide gel electrophoresis; TEV, tobacco etch virus; WT, wild-type; 5cHS, pentacoordinate, high-spin; 6cHS, hexacoordinate, high-spin.

4.7 Acknowledgments

This work was supported by National Institutes of Health Grants AI072719 (to K.R.R.), GM094039 (to G.L.R.), the Research Corporation (to D.W.D.) and the Molecular Basis of Disease Program at Georgia State University (R.C.U.). We thank Kierra Brown and Brandford Adobaw for preliminary experiments and Dr. Siming Wang for help with mass spectrometry experiments.

Table 4.1 Comparison of rR core-size marker bands (cm^{-1}) of select ferric hemin proteins

Protein	Ligand(s)	ν_4	ν_3 6cHS	ν_3 5cHS	ν_3 6cLS	ν_{38}	ν_2 6cHS	ν_2 5cHS	ν_2 6cLS	Reference
Mb	His	1370	1483			1511	1563			(Hu et al., 1996b)
*Cd*HtaB	Tyr/His	1370	1483			1520	1561			This paper
*Cd*ChtB	Tyr/His	1370	1486			1522	1560			This paper
Catalase	Tyr	1373		1487		1522		1570		(Chuang et al., 1988)
*Sd*ShuT	Tyr	1371		1484		1520		1565		(Eakanunkul et al., 2005)
*Cd*HtaA	Tyr	1372		1490		1530		1568		(Uluisik et al., 2017)
*Cd*HmuT	Tyr/His	1371	1475		1504	1515	1556		1579	(Draganova et al., 2015)
*Sm*HasA	Tyr/His	1371	1476		1501	1517	1561		1580	(Caillet-Saguy et al., 2008)
*Yp*HasA	Tyr	1369	1480	1487		1522		1567		(Ozaki et al., 2014)

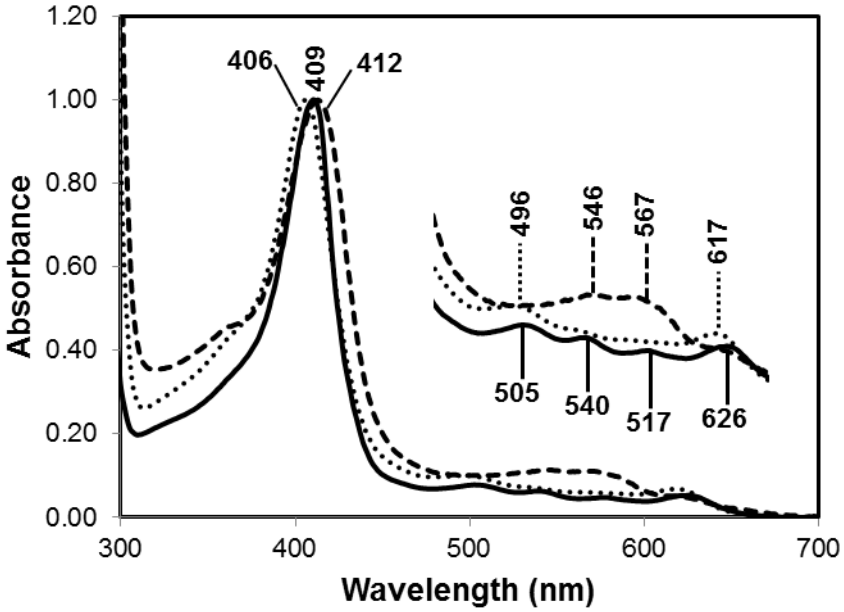

Figure 4.1 The UV-visible absorption of as-isolated ferric HtaB-WT (solid line), Y59A (dashed line), and H121A (dotted line). The protein solutions were prepared in 100 mM Tris-HCl, 150 mM NaCl pH 8.0.

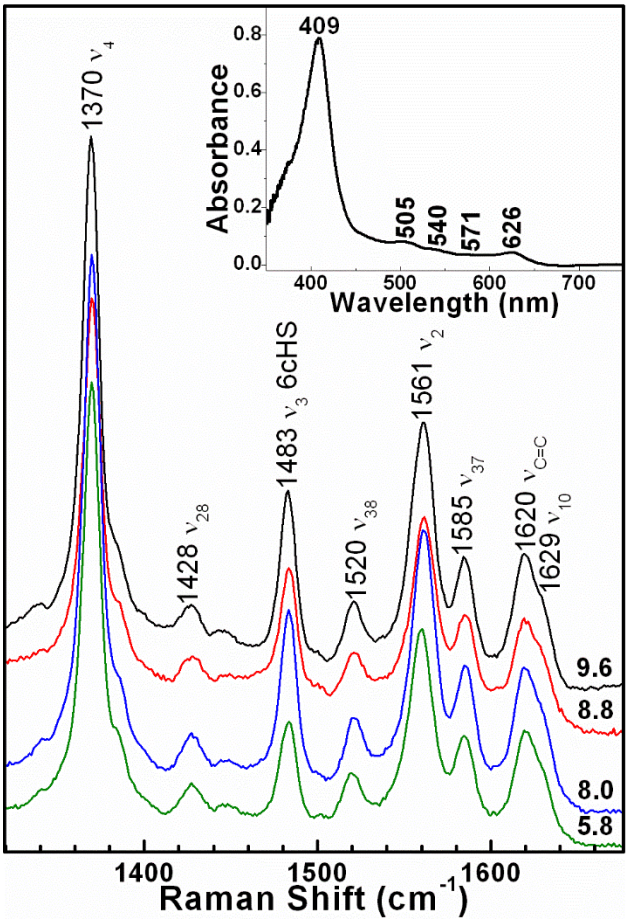

Figure 4.2 Ferric high frequency rR of HtaB as a function of pH. Glycine (pH 9.6, black), Tris-HCl (pH 8.8, red and 8.0, blue), and phosphate (pH 5.8, green) buffers at 100 mM were used.

Resonance Raman scattering was excited with 413.1-nm emission from a Kr^+ laser using 10 mW of power. The assignments are made by analogy with other heme proteins and on the basis of depolarization ratios evident from Figure S12.

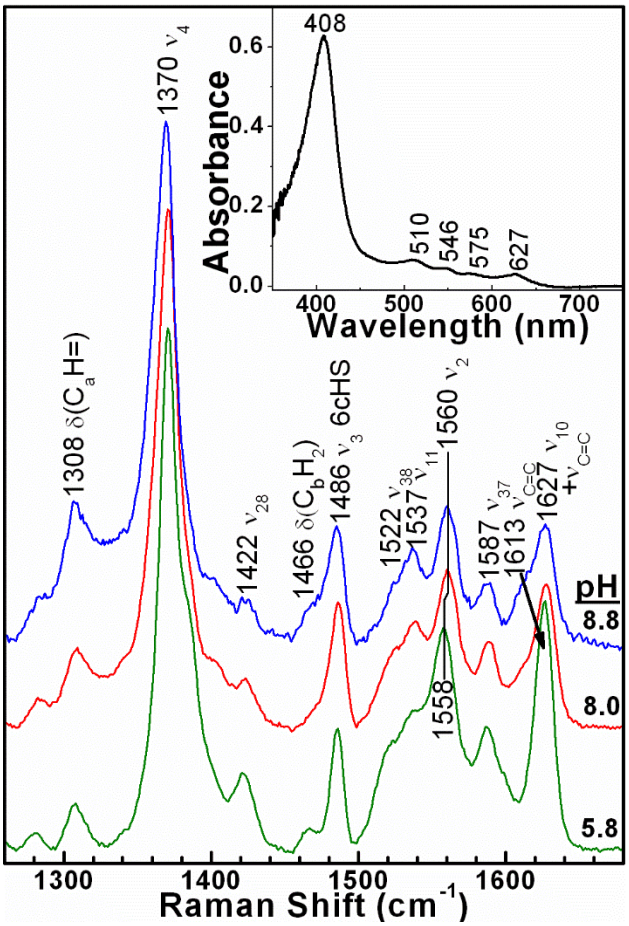

Figure 4.3 Ferric high frequency rR of ChtB as a function of pH.

Tris-HCl (pH 8.8, blue and 8.0, red) and phosphate (pH 5.8, green) buffers at 100 mM were used. The excitation wavelength from 413.1 nm from Kr ion laser with 11.4 mW of power. The assignments were made based on polarization data in figure S13 and by analogy with other heme proteins. The $\nu_{C=C}$ band shifts under the ν_{10} band as the pH is decreased indicating a change in the interactions between the vinyl groups and the heme pocket.

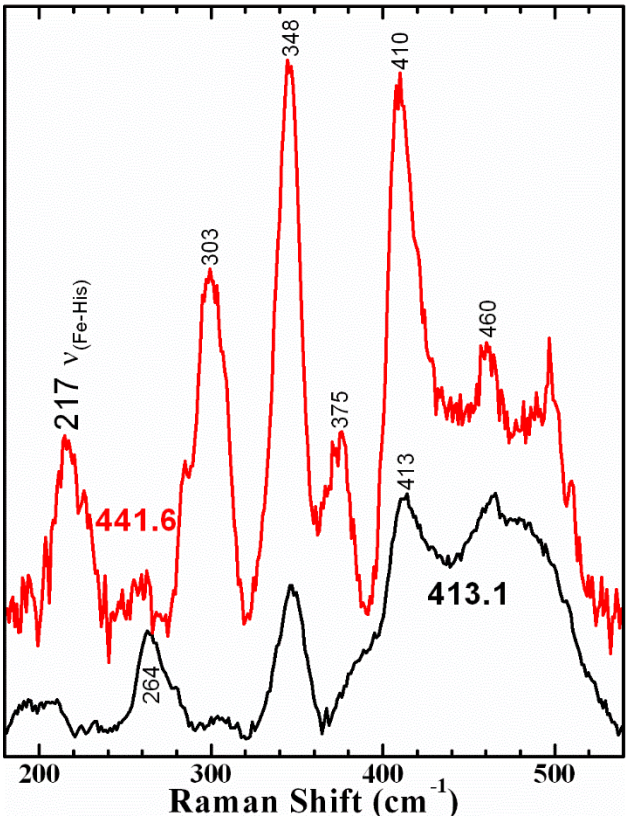

Figure 4.4 Low-frequency spectra of ferrous HtaB excited with 413.1 nm (10 mW, black, bottom, Kr^+) and 441.6 nm (1.6 mW, red, top, HeCd).

Both spectra have been normalized to the ν_7 band which lies outside the shown window. The resonance enhancement pattern with 441.6-nm excitation supports assignment of the 217-cm^{-1} band to the ν_{Fe-His} mode, leading to the conclusion that part of the heme is bound to the protein through a Fe−His bond (Kitagawa et al., 1979).

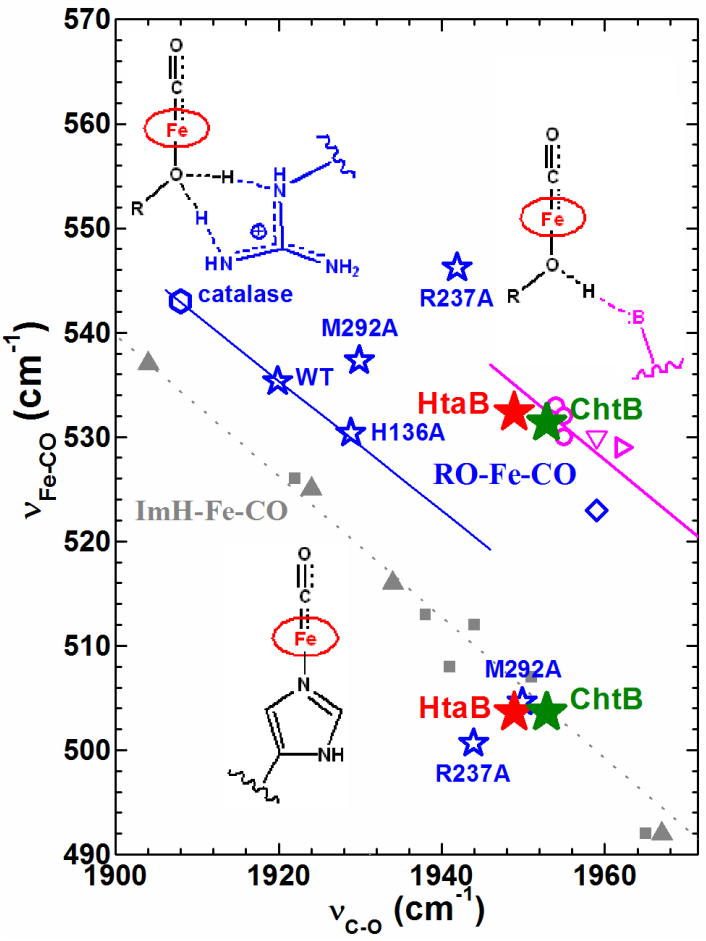

Figure 4.5 Backbonding correlation plot, relating ν_{Fe-CO} and ν_{C-O} frequencies for groups of proteins having the same *trans* (proximal) ligand.

The two forms of HtaB−CO are shown as filled red stars, while the two forms of ChtB−CO are filled green stars. HmuT and its mutants, unfilled blue stars (Draganova et al., 2015; Draganova et al., 2016); catalase, blue hexagon (Hu and Kincaid, 1992); and *Sm*HasA(WT), *Sm*HasA(H83A), *Sm*HasA(H32A), magenta ○ (Lukat-Rodgers et al., 2008). The data for HRP, ▲ and globins, ■ have been compiled previously (Lukat-Rodgers et al., 2008). The dotted line is the least squares fit for six-coordinate heme carbonyls in which the proximal ligand is neutral imidazole from a His residue (Smulevich et al., 1988a; Lukat-Rodgers et al., 2008; Streit et al., 2010) (and references therein). The solid blue line represents a compilation of heme proteins in which the ligand *trans* to CO is coordinated through an O atom that is hydrogen bonded to an Arg (two hydrogen bonds) (Hu and Kincaid, 1992; Draganova et al., 2015). The solid magenta line is the least squares fit for six-coordinate Fe−CO adducts which are coordinated through an O atom having a single hydrogen bond to His or Tyr (Lukat-Rodgers et al., 2008).

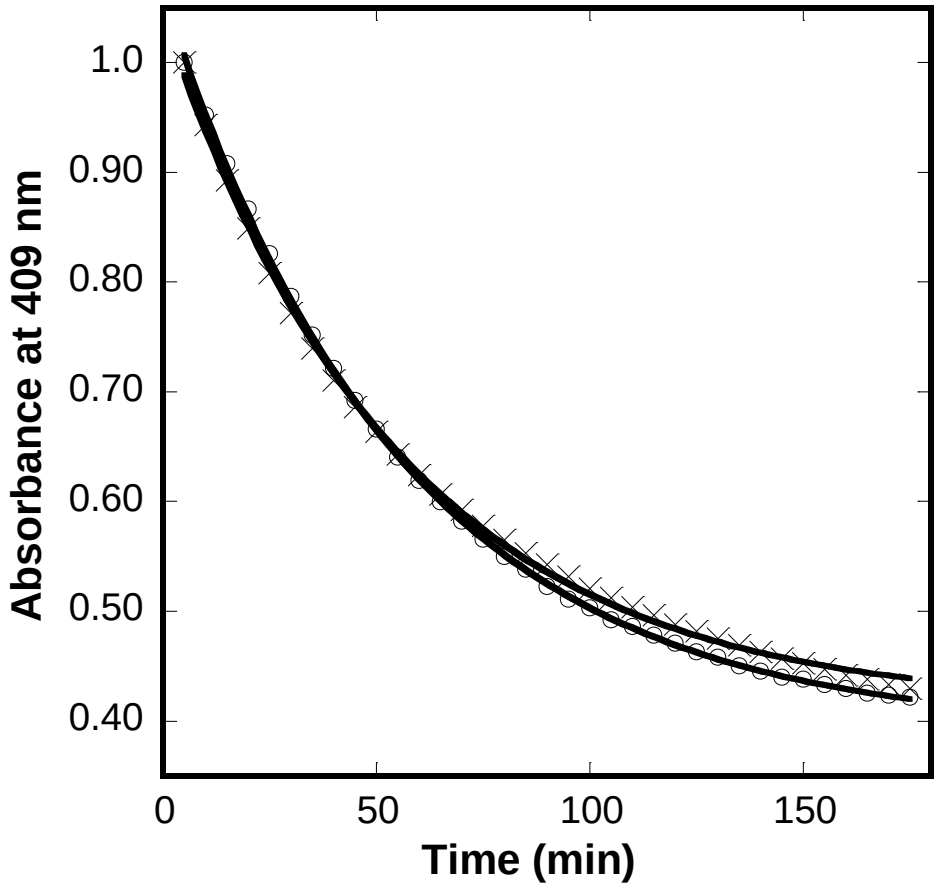

Figure 4.6 UV-visible absorbance as a function of time for HtaB-WT (○) and ChtB (×).

The unfolding reaction was carried out in 100 mM Tris-HCl, 150 mM NaCl pH 8.0 with 4 M GdnHCl. The data were fit using the single-term exponential decay function shown in Eq. 1.

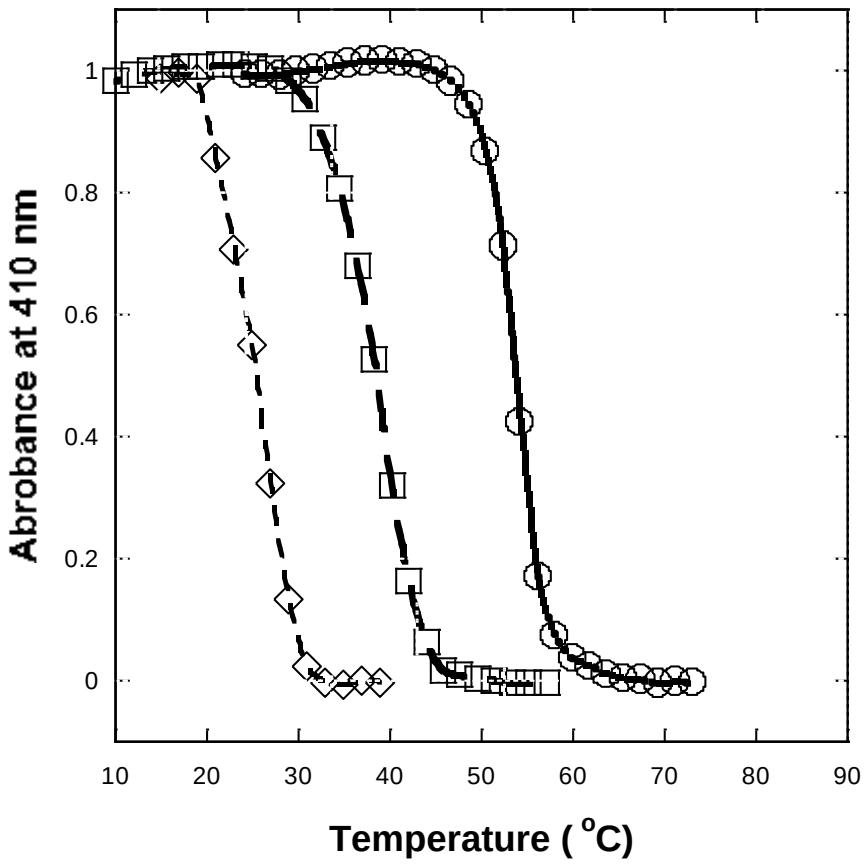

Figure 4.7 UV-visible absorbance as a function of temperature for HtaB-WT (circle), H121A (square), and Y56A (diamond) mutants. The buffer was 50 mM NaH_2PO_4, pH 7.0 with 1.0 M GdnHCl.

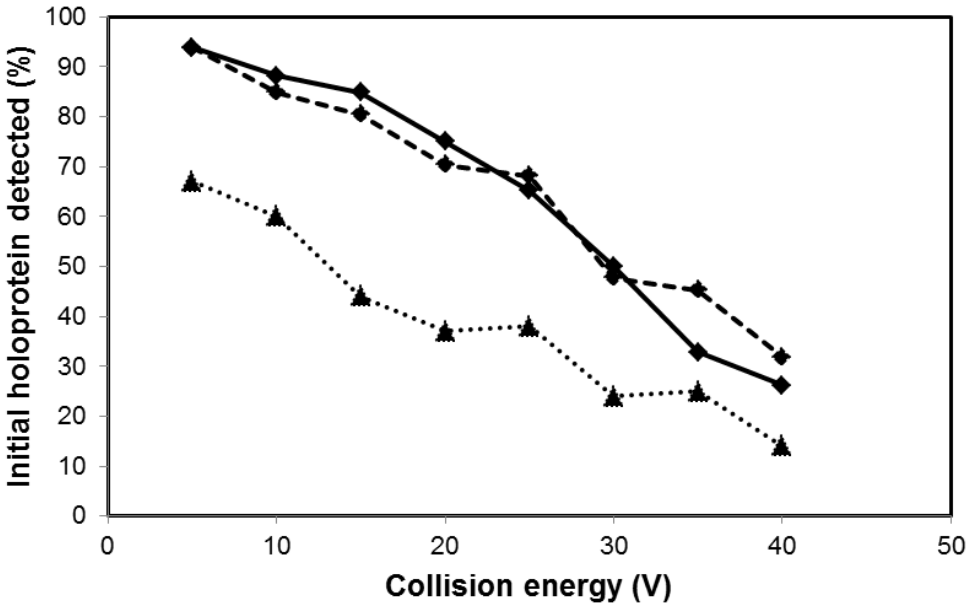

Figure 4.8 Electrospray ionization mass spectrometry detection of heme-bound holoHtaB-WT (solid line), HtaB-H121A (dashed line), and HtaB-Y56A (dotted line) as a function of collision energy voltage. The protein solutions were prepared in 20 mM ammonium acetate, pH 6.8.

4.8 References

Abe, R., Caaveiro, J.M.M., Kozuka-Hata, H., Oyama, M., Tsumoto, K., 2012. Mapping ultra-weak protein-protein interactions between heme transporters of *Staphylococcus aureus*. J. Biol. Chem. 287, 16477-16487.

Allen, C.E., Burgos, J.M., Schmitt, M.P., 2013. Analysis of novel iron-regulated, surface-anchored hemin-binding proteins in *Corynebacterium diphtheriae*. J. Bacteriol. 195, 2852-2863.

Allen, C.E., Schmitt, M.P., 2009. HtaA is an iron-regulated hemin binding protein involved in the utilization of heme iron in *Corynebacterium diphtheriae*. J. Bacteriol. 191, 2638-2648.

Allen, C.E., Schmitt, M.P., 2011. Novel hemin binding domains in the *Corynebacterium diphtheriae* HtaA protein interact with hemoglobin and are critical for heme iron utilization by HtaA. J. Bacteriol. 193, 5374-5385.

Allen, C.E., Schmitt, M.P., 2015. Utilization of host iron sources by *Corynebacterium diphtheriae*: Multiple hemoglobin-binding proteins are essential for the use of iron from the hemoglobin-haptoglobin complex. J. Bacteriol. 197, 553-562.

Arnoux, P., Haser, R., Izadi, N., Lecroisey, A., Delepierre, M., Wandersman, C., Czjzek, M., 1999. The crystal structure of HasA, a hemophore secreted by *Serratia marcescens*. Nat. Struct. Biol. 6, 516-520.

Berry, E.A., Trumpower, B.L., 1987. Simultaneous determination of hemes *a*, *b*, and *c* from pyridine hemochrome spectra. Anal. Biochem. 161, 1-15.

Brogioni, S., Feis, A., Marzocchi, M.P., Zederbauer, M., Furtmuller, P.G., Obinger, C., Smulevich, G., 2006. Resonance Raman assignment of myeloperoxidase and the selected mutants Asp94Val and Met243Thr. Effect of the heme distortion. J. Raman Spectrosc. 37, 263-276.

Caillet-Saguy, C., Turano, P., Piccioli, M., Lukat-Rodgers, G.S., Czjzek, M., Guigliarelli, B., Izadi-Pruneyre, N., Rodgers, K.R., Delepierre, M., Lecroisey, A., 2008. Deciphering the structural role of histidine 83 for heme binding in hemophore HasA. J. Biol. Chem. 283, 5960-5970.

Choby, J.E., Skaar, E.P., 2016. Heme synthesis and acquisition in bacterial pathogens. J. Mol. Biol. 428, 3408-3428.

Chuang, W.J., Johnson, S., Van Wart, H.E., 1988. Resonance Raman spectra of bovine liver catalase: Enhancement of proximal tyrosinate vibrations. J. Inorg. Biochem. 34, 201-219.

Contreras, H., Chim, N., Credali, A., Goulding, C.W., 2014. Heme uptake in bacterial pathogens. Curr. Opin. Chem. Biol. 19, 34-41.

Draganova, E.B., Adrian, S.A., Lukat-Rodgers, G.S., Keutcha, C.S., Schmitt, M.P., Rodgers, K.R., Dixon, D.W., 2016. *Corynebacterium diphtheriae* HmuT: Dissecting the roles of conserved residues in heme pocket stabilization. J. Biol. Inorg. Chem. 21, 875-886.

Draganova, E.B., Akbas, N., Adrian, S.A., Lukat-Rodgers, G.S., Collins, D.P., Dawson, J.H., Schmitt, M.P., Rodgers, K.R., Dixon, D.W., 2015. Heme binding by *Corynebacterium diphtheriae* HmuT: Function and heme environment. Biochemistry 54, 6598-6609.

Drazek, E.S., Hammack, C.A., Schmitt, M.P., 2000. *Corynebacterium diphtheriae* genes required for acquisition of iron from haemin and haemoglobin are homologous to ABC haemin transporters. Mol. Microbiol. 36, 68-84.

Eakanunkul, S., Lukat-Rodgers, G.S., Sumithran, S., Ghosh, A., Rodgers, K.R., Dawson, J.H., Wilks, A., 2005. Characterization of the periplasmic heme-binding protein ShuT from the heme uptake system of *Shigella dysenteriae*. Biochemistry 44, 13179-13191.

Fabian, M., Solomaha, E., Olson, J.S., Maresso, A.W., 2009. Heme transfer to the bacterial cell envelope occurs via a secreted hemophore in the Gram-positive pathogen *Bacillus anthracis*. J. Biol. Chem. 284, 32138-32146.

Gaudin, C.F.M., Grigg, J.C., Arrieta, A.L., Murphy, M.E.P., 2011. Unique heme-iron coordination by the hemoglobin receptor IsdB of *Staphylococcus aureus*. Biochemistry 50, 5443-5452.

Honsa, E.S., Maresso, A.W., Highlander, S.K., 2014. Molecular and evolutionary analysis of NEAr-iron Transporter (NEAT) domains. PLoS One 9.

Hu, S.H., Kincaid, J.R., 1992. Resonance Raman studies of the carbonmonoxy form of catalase - Evidence for and effects of phenolate ligation. FEBS Lett. 314, 293-296.

Hu, S.Z., Smith, K.M., Spiro, T.G., 1996. Assignment of protoheme resonance Raman spectrum by heme labeling in myoglobin. J. Am. Chem. Soc. 118, 12638-12646.

Hunter, C.L., Mauk, A.G., Douglas, D.J., 1997. Dissociation of heme from myoglobin and cytochrome *b*(5): Comparison of behavior in solution and the gas phase. Biochemistry 36, 1018-1025.

Kitagawa, T., Nagai, K., Tsubaki, M., 1979. Assignment of the Fe-nitrogen (His F8) stretching band in the resonance Raman spectra of deoxymyoglobin. FEBS Lett. 104, 376-378.

Kunkle, C.A., Schmitt, M.P., 2003. Analysis of the *Corynebacterium diphtheriae* DtxR regulon: Identification of a putative siderophore synthesis and transport system that is similar to the *Yersinia* high-pathogenicity island-encoded yersiniabactin synthesis and uptake system. J. Bacteriol. 185, 6826-6840.

Liu, M.Y., Lei, B.F., 2005. Heme transfer from streptococcal cell surface protein Shp to HtsA of transporter HtsABC. Infect. Immun. 73, 5086-5092.

Lukat-Rodgers, G.S., Rodgers, K.R., Caillet-Saguy, C., Izadi-Pruneyre, N., Lecroisey, A., 2008. Novel heme ligand displacement by CO in the soluble hemophore HasA and its proximal ligand mutants: Implications for heme uptake and release. Biochemistry 47, 2087-2098.

Malmirchegini, G.R., Sjodt, M., Shnitkind, S., Sawaya, M.R., Rosinski, J., Newton, S.M., Klebba, P.E., Clubb, R.T., 2014. Novel mechanism of hemin capture by Hbp2, the hemoglobin-binding hemophore from *Listeria monocytogenes*. J. Biol. Chem. 289, 34886-34899.

Muraki, N., Aono, S., 2015. Structural basis for heme recognition by HmuT responsible for heme transport to the heme transporter in *Corynebacterium glutamicum*. Chem. Lett. 45, 24-26.

Muryoi, N., Tiedemann, M.T., Pluym, M., Cheung, J., Heinrichs, D.E., Stillman, M.J., 2008. Demonstration of the iron-regulated surface determinant (Isd) heme transfer pathway in *Staphylococcus aureus*. J. Biol. Chem. 283, 28125-28136.

Nygaard, T.K., Blouin, G.C., Liu, M.Y., Fukumura, M., Olson, J.S., Fabian, M., Dooley, D.M., Lei, B.F., 2006. The mechanism of direct heme transfer from the streptococcal cell surface protein Shp to HtsA of the HtsABC transporter. J. Biol. Chem. 281, 20761-20771.

Ouattara, M., Pennati, A., Devlin, D.J., Huang, Y.S., Gadda, G., Eichenbaum, Z., 2013. Kinetics of heme transfer by the Shr NEAT domains of Group A Streptococcus. Arch. Biochem. Biophys. 538, 71-79.

Ozaki, S., Sato, T., Sekine, Y., Migita, C.T., Uchida, T., Ishimori, K., 2014. Spectroscopic studies on HasA from *Yersinia pseudotuberculosis*. J. Inorg. Biochem. 138, 31-38.

Pace, C.N., Scholtz, J.M., 1997. Measuring the conformational stability of a protein, in: Creighton, T. (Ed.), Protein Structure: A Practical Approach, 2nd ed. Oxford University Press, Oxford, pp. 299-321.

Pluym, M., Muryoi, N., Heinrichs, D.E., Stillman, M.J., 2008. Heme binding in the NEAT domains of IsdA and IsdC of *Staphylococcus aureus*. J. Inorg. Biochem. 102, 480-488.

Rodgers, K.R., Lukat-Rodgers, G.S., 2014. Biophysical perspectives on the acquisition, transport, and trafficking of heme in bacteria, in: Ferreira, G.C., Kadish, K.M., Smith, K.M., Guilard, R. (Eds.), Handbook of Porphyrin Science with Applications to Chemistry, Physics, Materials Science, Engineering, Biology and Medicine, Vol. 30: Heme Proteins, Part II. World Scientific, Hackensack, N.J, pp. 251-309.

Schmitt, M.P., 1997. Utilization of host iron sources by *Corynebacterium diphtheriae*: Identification of a gene whose product is homologous for eukaryotic heme oxygenases and is required for acquisition of iron from heme and hemoglobin. J. Bacteriol. 179, 838-845.

Schmitt, M.P., 2014. Iron acquisition and iron-dependent gene expression in *Corynebacterium diphtheriae*, in: Burkovski, A. (Ed.), *Corynebacterium diphtheriae* and Related Toxigenic Species: Genomics, Pathogenicity and Applications. Springer, pp. 95-121.

Sheldon, J.R., Heinrichs, D.E., 2015. Recent developments in understanding the iron acquisition strategies of gram positive pathogens. FEMS Microbiol. Rev. 39, 592-630.

Sheldon, J.R., Laakso, H.A., Heinrichs, D.E., 2016. Iron Acquisition Strategies of Bacterial Pathogens. Microbiology Spectrum 4.

Sjodt, M., Macdonald, R., Spirig, T., Chan, A.H., Dickson, C.F., Fabian, M., Olson, J.S., Gell, D.A., Clubb, R.T., 2016. The PRE-derived NMR model of the 38.8-kDa tri-domain IsdH protein from Staphylococcus aureus suggests that it adaptively recognizes human hemoglobin. J. Mol. Biol. 428, 1107-1129.

Smulevich, G., Mauro, J.M., Fishel, L.A., English, A.M., Kraut, J., Spiro, T.G., 1988a. Cytochrome c peroxidase mutant active site structures probed by resonance Raman and infrared signatures of the CO adducts. Biochemistry 27, 5486-5492.

Smulevich, G., Mauro, J.M., Fishel, L.A., English, A.M., Kraut, J., Spiro, T.G., 1988b. Cytochrome *c* peroxidase mutant active site structures probed by resonance Raman and infrared signatures of the CO adducts. Biochemistry 27, 5486-5492.

Spiro, T.G., Soldatova, A.V., Balakrishnan, G., 2013. CO, NO and O_2 as vibrational probes of heme protein interactions. Coord. Chem. Rev. 257, 511-527.

Spiro, T.G., Wasbotten, I.H., 2005. CO as a vibrational probe of heme protein active sites. J. Inorg. Biochem. 99, 34-44.

Streit, B.R., Blanc, B., Lukat-Rodgers, G.S., Rodgers, K.R., DuBois, J.L., 2010. How active-site protonation state influences the reactivity and ligation of the heme in chlorite dismutase. J. Am. Chem. Soc. 132, 5711-5724.

Swint, L., Robertson, A.D., 1993. Thermodynamics of unfolding for turkey ovomucoid third domain: Thermal and chemical denaturation. Protein Sci. 2, 2037-2049.

Tarlovsky, Y., Fabian, M., Solomaha, E., Honsa, E., Olson, J.S., Maresso, A.W., 2010. A *Bacillus anthracis* S-Layer homology protein that binds heme and mediates heme delivery to IsdC. J. Bacteriol. 192, 3503-3511.

Tiedemann, M.T., Heinrichs, D.E., Stillman, M.J., 2012. Multiprotein heme shuttle pathway in *Staphylococcus aureus*: Iron-regulated surface determinant cog-wheel kinetics. J. Am. Chem. Soc. 134, 16578-16585.

Tiedemann, M.T., Stillman, M.J., 2011. Application of magnetic circular dichroism spectroscopy to porphyrins, phthalocyanines and hemes. J. Porph. Phthalo. 15, 1134-1149.

Trost, E., Blom, J., Soares, S.D., Huang, I.H., Al-Dilaimi, A., Schroder, J., Jaenicke, S., Dorella, F.A., Rocha, F.S., Miyoshi, A., Azevedo, V., Schneider, M.P., Silva, A., Camello, T.C., Sabbadini, P.S., Santos, C.S., Santos, L.S., Hirata, R., Mattos-Guaraldi, A.L., Efstratiou, A., Schmitt, M.P., Hung, T.T., Tauch, A., 2012. Pangenomic study of *Corynebacterium diphtheriae* that provides insights into the genomic diversity of pathogenic isolates from cases of classical diphtheria, endocarditis, and pneumonia. J. Bacteriol. 194, 3199-3215.

Uluisik, R.C., Akbas, N., Lukat-Rodgers, G.S., Adrian, S.A., Allen, C.E., Schmitt, M.P., Rodgers, K.R., Dixon, D.W., 2017. Characterization of the second conserved domain in the heme uptake protein HtaA from *Corynebacterium diphtheriae*. J. Inorg. Biochem. 167, 124-133.

Villareal, V.A., Spirig, T., Robson, S.A., Liu, M., Lei, B., Clubb, R.T., 2011. Transient weak protein-protein complexes transfer heme across the cell wall of *Staphylococcus aureus*. J. Am. Chem. Soc. 133, 14176-14179.

Vogel, K.M., Kozlowski, P.M., Zgierski, M.Z., Spiro, T.G., 2000. Role of the axial ligand in heme-CO backbonding; DFT analysis of vibrational data. Inorg. Chim. Acta 297, 11-17.

Wilks, A., O'Neill, M.J., 2014. Extracellular heme uptake and metabolism in bacterial pathogenesis, in: Ferreira, G.C., Kadish, K.M., Smith, K.M., Guilard, R. (Eds.), Handbook of Porphyrin Science with Applications to Chemistry, Physics, Materials Science, Engineering, Biology and Medicine, Vol 26: Heme Biochemistry. World Scientific, Hackensack, NJ, pp. 267-315.

4.9 Supplementary Information

Table 4.2 HtaB site-directed mutagenesis primers. The mutation sites are shown bold

Primer Name	Primer sequence (5'-3')
H121A-Forward	CGTTTTAGTGGTG**CGC**ACGGCATCTTG
H121A-Reverse	CAAGATGCCGTG**CGC**ACCACTAAAACG
Y56A-Forward	CGCTGGCTTC**GCG**GAAGCTGGCTCTG
Y56A-Reverse	CAGAGCCAGCTTCC**GCG**AAGCCAGCG

Table 4.3 Dependence of unfolding rate kinetic rate constants of as-isolated HtaB-WT on GdnHCl concentration at room temperature

[GdnHCl], M	k min^{-1}	[a]$t_{1/2}$ min
3.4	0.00426 ± 0.00003	163
3.6	0.00865 ± 0.00004	80
3.8	0.00922 ± 0.00009	75
4.0	0.01790 ± 0.00012	39
4.2	0.04740 ± 0.00050	15
4.4	0.05100 ± 0.00050	14

[a]Half-life values were calculated for the first order protein unfolding processes using the equation of $t_{1/2} = 0.693 / k$.

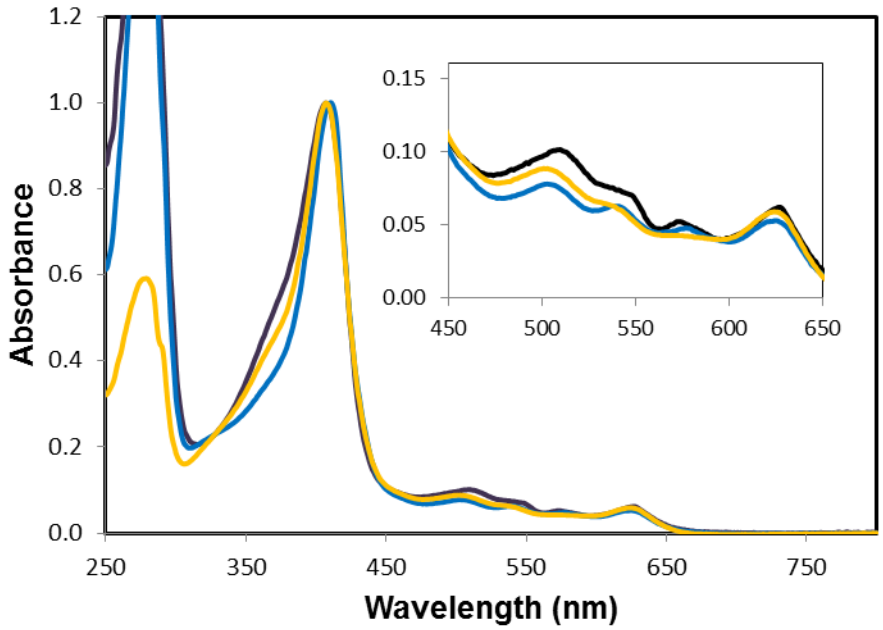

Figure 4.9 UV-visible spectra of as-isolated HtaB (blue), as-isolated ChtB (orange), and as-isolated HtaA-CR2 (black). The proteins were prepared in 100 mM Tris-HCl, 150 mM NaCl pH 8.0. Spectra are normalized to 1.0 at the Soret.

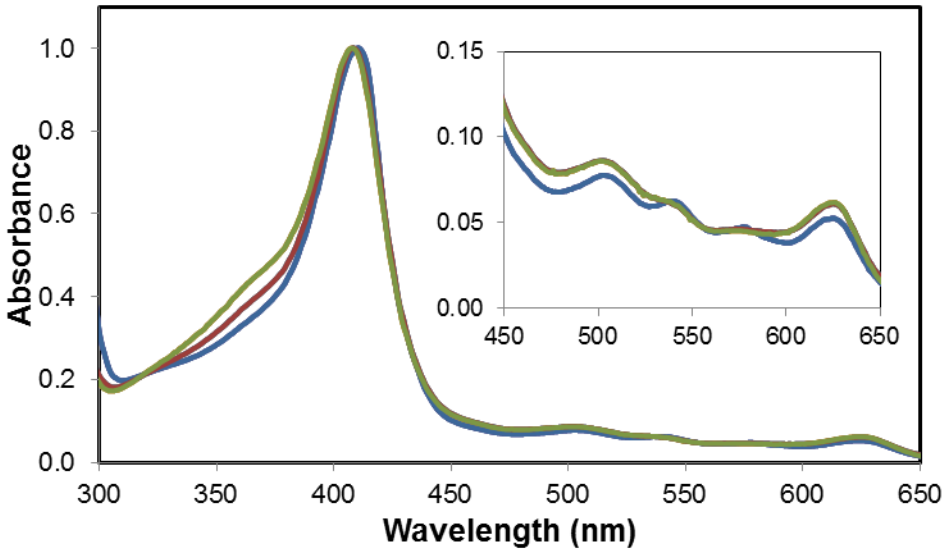

Figure 4.10 UV-visible spectra of as-isolated HtaB-WT (blue), titrated with hemin (green), and reconstituted on a Strep-tag column with hemin from metHb (red). Inset shows the α/β region. The proteins were prepared in 100 mM Tris-HCl, 150 mM NaCl pH 8.0. Spectra are normalized to 1.0 at the Soret.

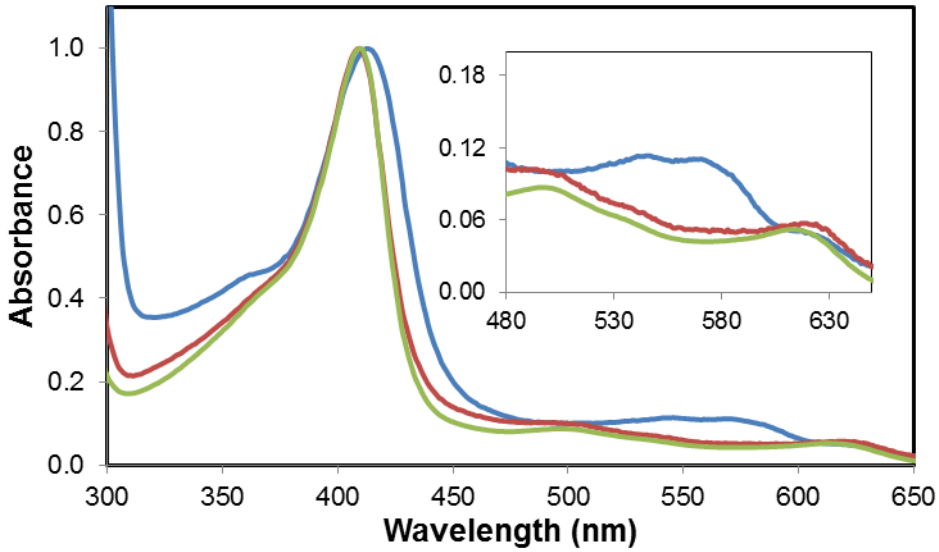

Figure 4.11 UV-visible spectra of as-isolated HtaB-Y56A (blue), titrated with hemin (green), and reconstituted on a Strep-tag column with hemin from metHb (red). Inset shows the α/β region. The proteins were prepared in 100 mM Tris-HCl, 150 mM NaCl pH 8.0. Spectra are normalized to 1.0 at the Soret.

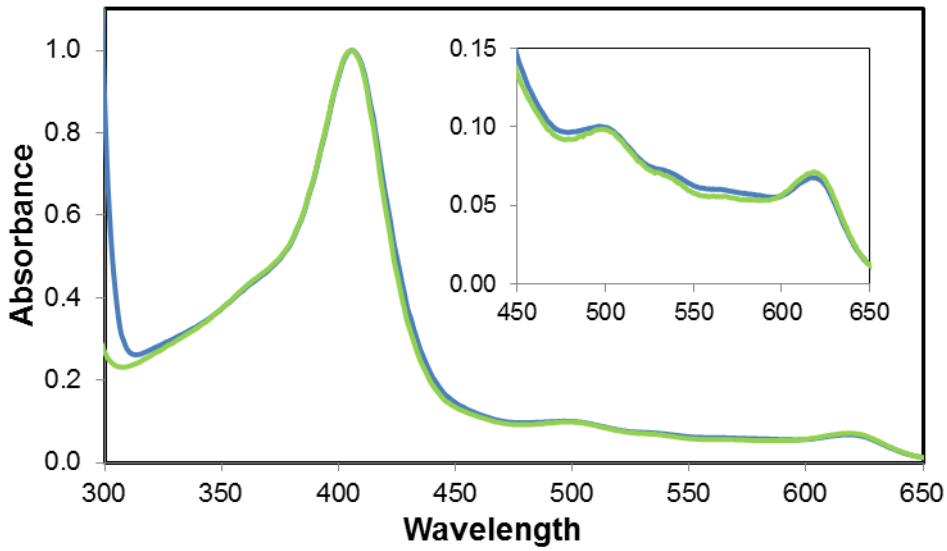

Figure 4.12 UV-visible spectra of as-isolated HtaB-H121A (blue) and titrated with hemin (green). Inset shows the α/β region. The proteins were prepared in 100 mM Tris-HCl, 150 mM NaCl pH 8.0. Spectra are normalized to 1.0 at the Soret.

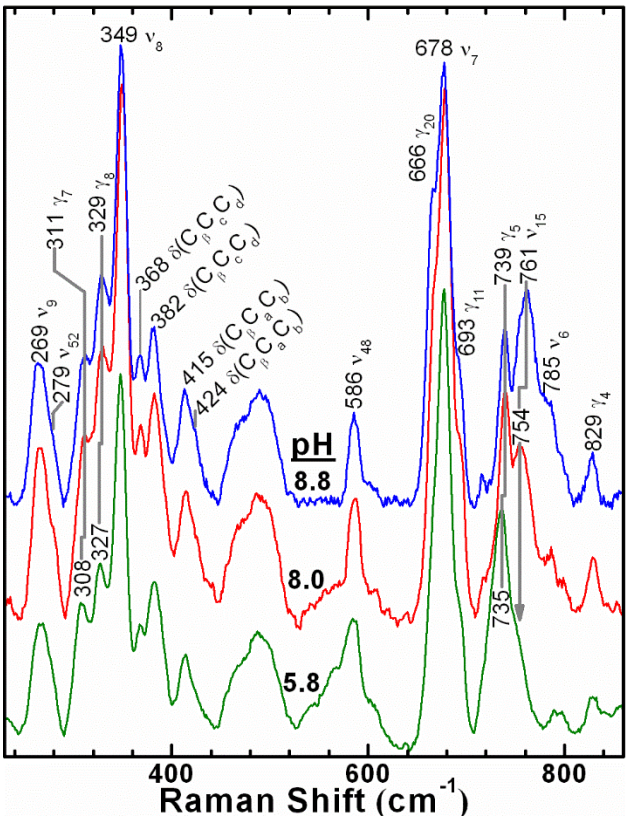

Figure 4.13 Low-frequency rR spectra of WT ChtB as a function of pH.

Tris-HCl (pH 8.8, blue and 8.0, red) and phosphate (pH 5.8, green) buffers were used at 100 mM. Raman scattering was excited with 413.1-nm emission from a Kr^+ laser, 11.4 mW. The band assignments were made based on depolarization ratios (data not shown) and by analogy to other heme proteins. Changes in relative intensities of bands attributable to propionate and vinyl bending suggest that the heme-protein interactions near the heme edge are sensitive to pH. Changes in relative intensities and frequencies of bands near 740 and 760 cm^{-1} are suggestive of a pH-dependent change in deviation of the porphine core from planarity.

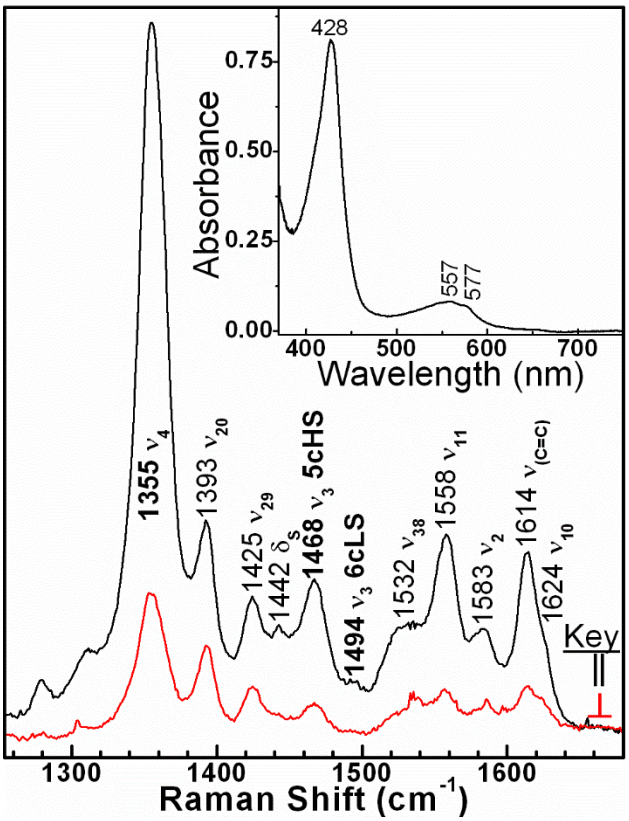

Figure 4.14 Ferrous high frequency rR spectra of pH 8.8 HtaB as excited with 413.1 nm Kr^+ laser with 4.8 mW power.

Parallel polarized (black) and perpendicular polarized (red) spectra allow for the identification of totally symmetric and non-totally symmetric core size marker bands. Inset shows the UV-visible spectrum of ferrous HtaB.

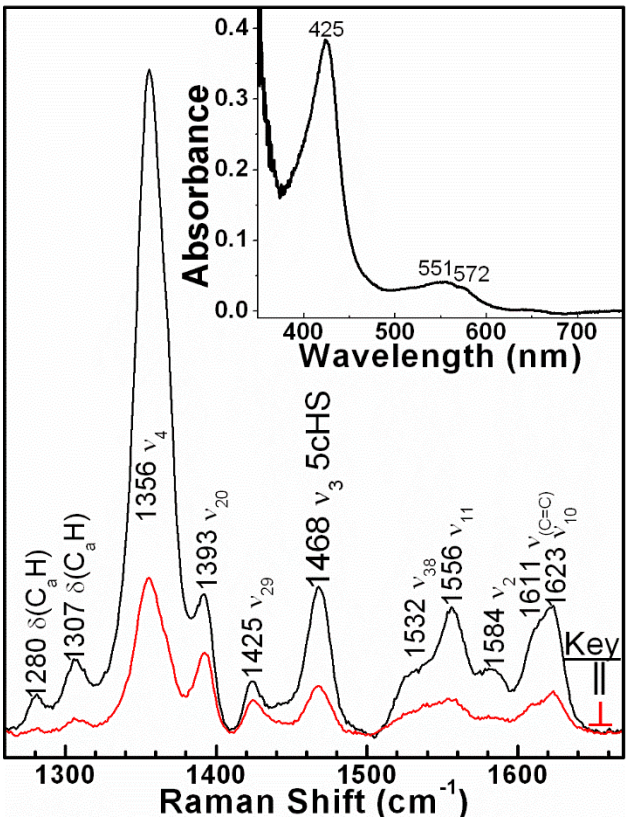

Figure 4.15 High-frequency rR spectra of ferrous ChtB at pH 8.8, excited with 413.1-nm emission from a Kr^+ laser with power of 10.2 mW.

Parallel polarized (black) and perpendicular polarized (red) spectra allow for the identification of the totally symmetric and non-totally symmetric core size marker bands. Inset shows the UV-visible spectrum of ferrous ChtB.

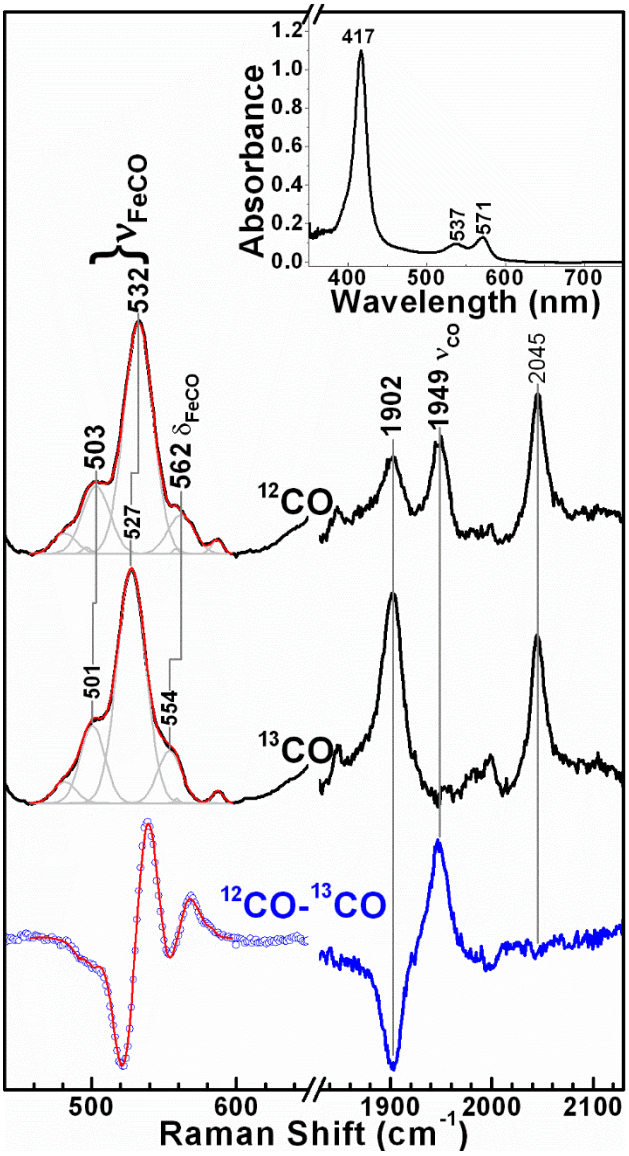

Figure 4.16 Resonance Raman spectra of the heme carbonyls of WT HtaB. Raman scattering was excited using 413.1-nm emission from a Kr^+ laser; 5.7 mW.

Natural-abundance HtaB−CO (top), HtaB−^{13}CO (middle) and ^{12}CO−^{13}CO difference (blue, bottom) spectra are shown in the ν_{Fe-CO}, δ_{FeCO} and ν_{C-O} regions. Bands in the low-frequency region were fit using Gaussian peak functions (gray). These bands were used to calculate the red difference spectrum superimposed on the blue points in the bottom left spectrum. The bands sensitive to ^{13}CO substitution are labeled with their respective mode designations. Spectra were recorded at pH 8.8. Inset: UV-visible absorbance spectrum of HtaB−CO.

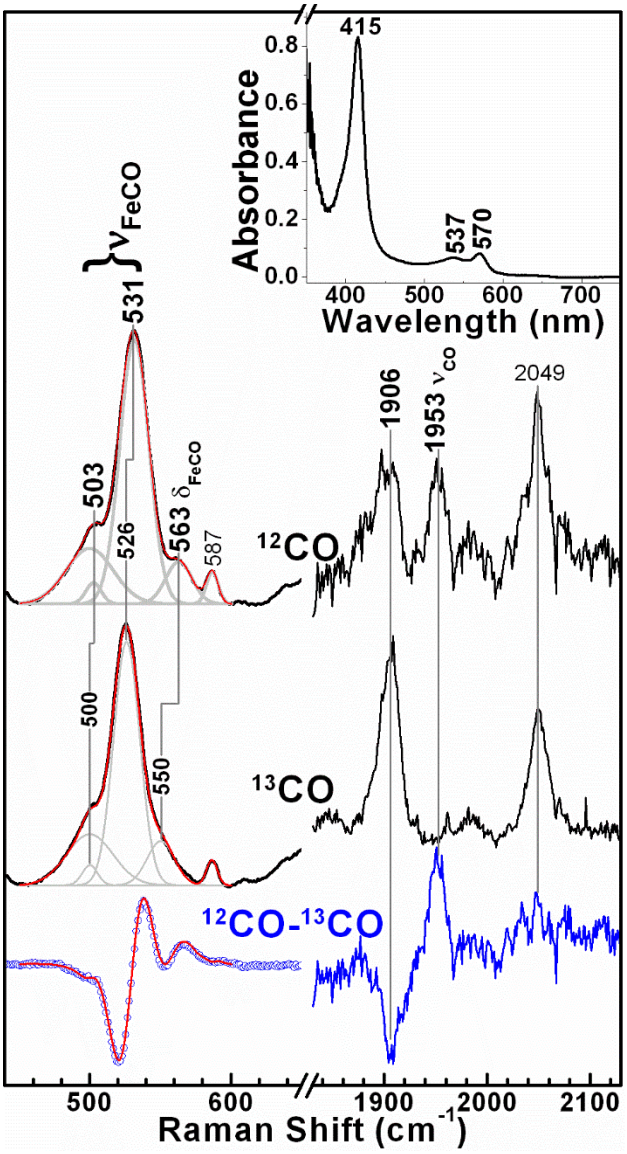

Figure 4.17 Resonance Raman spectra of the ferrous carbonyls of WT ChtB with conditions and interpretation as described in the legend of Fig. 4.16.

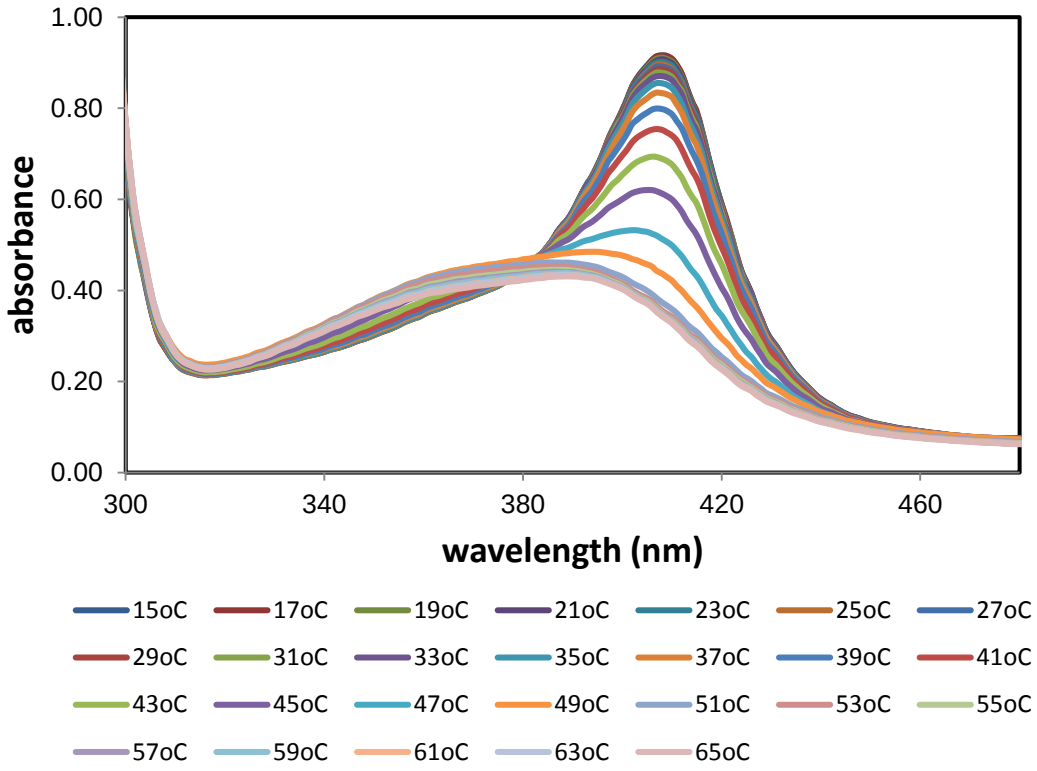

Figure 4.18 Thermal unfolding spectra of HtaB-H121A from 65ºC to 15 ºC. The protein was in 50 mM NaH_2PO_4 pH 7.0 buffer including 1.0 M GdnHCl.

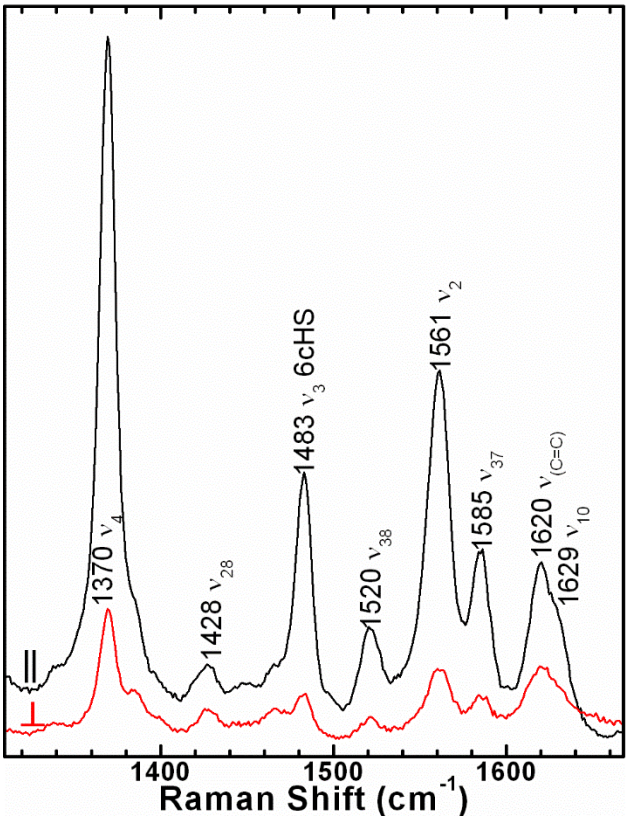

Figure 4.19 High frequency rR spectrum of ferric HtaB in 100 mM Tris pH 8.0 with 413.1-nm excitation from Kr^+ laser with 10 mW of power.

Parallel (black) and perpendicular (red) polarized Raman scattering are shown to identify the totally symmetric and non-totally symmetric core size marker bands.(Hu et al., 1996a)

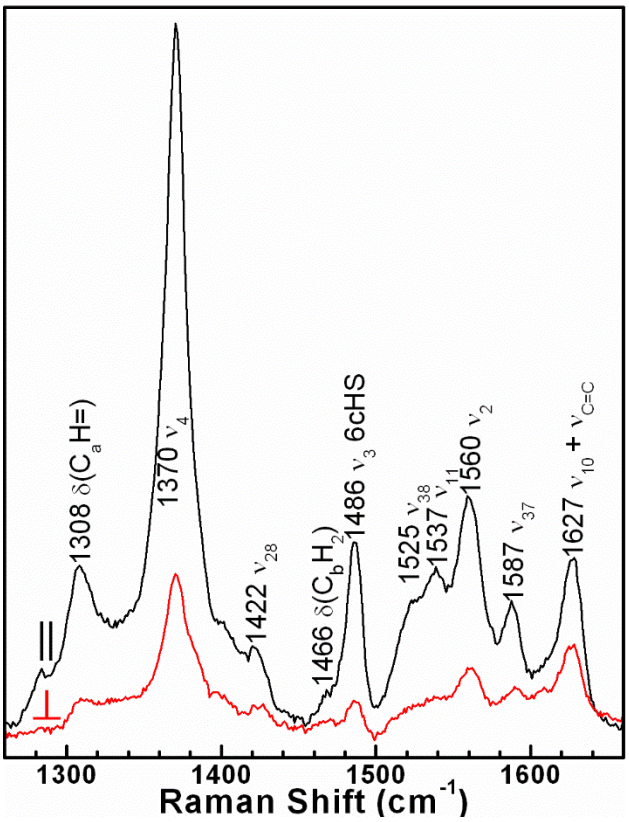

Figure 4.20 Polarized high-frequency rR spectra of WT ferric ChtB. Conditions as described for figure S11, except the laser power was 11.4 mW.

4.10 References

Abe, R., Caaveiro, J.M.M., Kozuka-Hata, H., Oyama, M., Tsumoto, K., 2012. Mapping ultra-weak protein-protein interactions between heme transporters of *Staphylococcus aureus*. J. Biol. Chem. 287, 16477-16487.

Abu Tarboush, N., Jensen, L.M., Feng, M., Tachikawa, H., Wilmot, C.M., Davidson, V.L., 2010. Functional importance of tyrosine 294 and the catalytic selectivity for the bis-Fe(IV) state of MauG revealed by replacement of this axial heme ligand with histidine. Biochemistry 49, 9783-9791.

Abu Tarboush, N., Shin, S., Geng, J.F., Liu, A.M., Davidson, V.L., 2012. Effects of the loss of the axial tyrosine ligand of the low-spin heme of MauG on its physical properties and reactivity. FEBS Lett. 586, 4339-4343.

Akbas, N., Draganova, E.B., Block, D.R., Sook, B.R., Chan, Y.F., Zhuo, J., Eichenbaum, Z., Rodgers, K.R., Dixon, D.W., 2016. Heme-bound SiaA from *Streptococcus pyogenes*: Effects of mutations and oxidation state on protein stability. J. Inorg. Biochem. 158, 99-109.

Allen, C.E., Burgos, J.M., Schmitt, M.P., 2013. Analysis of novel iron-regulated, surface-anchored hemin-binding proteins in *Corynebacterium diphtheriae*. J. Bacteriol. 195, 2852-2863.

Allen, C.E., Schmitt, M.P., 2009. HtaA is an iron-regulated hemin binding protein involved in the utilization of heme iron in *Corynebacterium diphtheriae*. J. Bacteriol. 191, 2638-2648.

Allen, C.E., Schmitt, M.P., 2011. Novel hemin binding domains in the *Corynebacterium diphtheriae* HtaA protein interact with hemoglobin and are critical for heme iron utilization by HtaA. J. Bacteriol. 193, 5374-5385.

Allen, C.E., Schmitt, M.P., 2015. Utilization of host iron sources by *Corynebacterium diphtheriae*: Multiple hemoglobin-binding proteins are essential for the use of iron from the hemoglobin-haptoglobin complex. J. Bacteriol. 197, 553-562.

Alontaga, A.Y., Rodriguez, J.C., Schoenbrunn, E., Becker, A., Funke, T., Yukl, E.T., Hayashi, T., Stobaugh, J., Moenne-Loccoz, P., Rivera, M., 2009. Structural characterization of the hemophore HasAp from *Pseudomonas aeruginosa*: NMR spectroscopy reveals protein-protein interactions between holo-HasAp and hemoglobin. Biochemistry 48, 96-109.

Amisha Kamal, J.K., Behere, D.V., 2002. Thermal and conformational stability of seed coat soybean peroxidase. Biochemistry 41, 9034-9042.

Amisha Kamal, J.K.A., Behere, D.V., 2008. Kinetic stabilities of soybean and horseradish peroxidases. Biochem. Eng. J. 38, 110-114.

Andersen, N.H., Nørgaard, A., Jensen, T.J., Ulstrup, J., 2002. Sequential unfolding of the two-domain protein *Pseudomonas stutzeri* cytochrome *c*(4). J. Inorg. Biochem. 88, 316-327.

Andrade, M.A., Ciccarelli, F.D., Perez-Iratxeta, C., Bork, P., 2002. NEAT: A domain duplicated in genes near the components of a putative Fe(3+) siderophore transporter from Gram-positive pathogenic bacteria. Genome Biol. 3, RESEARCH0047.

Aranda, R., Worley, C.E., Liu, M., Bitto, E., Cates, M.S., Olson, J.S., Lei, B.F., Phillips, G.N., 2007. Bis-methionyl coordination in the crystal structure of the heme-binding domain of the streptococcal cell surface protein Shp. J. Mol. Biol. 374, 374-383.

Arnesano, F., Banci, L., Bertini, I., Koulougliotis, D., 1998. Solution structure of oxidized rat microsomal cytochrome *b*(5) in the presence of 2 M guanidinium chloride: Monitoring the early steps in protein unfolding. Biochemistry 37, 17082-17092.

Arnoux, P., Haser, R., Izadi, N., Lecroisey, A., Delepierre, M., Wandersman, C., Czjzek, M., 1999. The crystal structure of HasA, a hemophore secreted by *Serratia marcescens*. Nat. Struct. Biol. 6, 516-520.

Asher, C., de Villiers, K.A., Egan, T.J., 2009. Speciation of ferriprotoporphyrin IX in aqueous and mixed aqueous solution is controlled by solvent identity, pH, and salt concentration. Inorg. Chem. 48, 7994-8003.

Austin, C.J.D., Mizdrak, J., Matin, A., Sirijovski, N., Kosim-Satyaputra, P., Willows, R.D., Roberts, T.H., Truscott, R.J.W., Polekhina, G., Parker, M.W., Jamie, J.F., 2004. Optimised expression and purification of recombinant human indoleamine 2,3-dioxygenase. Protein Expression and Purification. 37, 392-398.

Balderas, M.A., Nobles, C.L., Honsa, E.S., Alicki, E.R., Maresso, A.W., 2012. Hal is a *Bacillus anthracis* heme acquisition protein. J. Bacteriol. 194, 5513-5521.

Benson, D.R., Rivera, M., 2013. Heme uptake and metabolism in bacteria. Met. Ions Life Sci. 12, 279-332.

Bernardes, A., Textor, L.C., Santos, J.C., Cuadrado, N.H., Kostetsky, E.Y., Roig, M.G., Bavro, V.N., Muniz, J.R.C., Shnyrov, V.L., Polikarpov, I., 2015. Crystal structure analysis of peroxidase from the palm tree *Chamaerops excelsa*. Biochimie 111, 58-69.

Berry, E.A., Trumpower, B.L., 1987. Simultaneous determination of hemes *a*, *b*, and *c* from pyridine hemochrome spectra. Anal. Biochem. 161, 1-15.

Bowler, B.E., 2007. Thermodynamics of protein denatured states. Mol. Biosyst. 3, 88-99.

Braun, V., Hantke, K., 2011. Recent insights into iron import by bacteria. Curr. Opin. Chem. Biol. 15, 328-334.

Brogioni, S., Feis, A., Marzocchi, M.P., Zederbauer, M., Furtmuller, P.G., Obinger, C., Smulevich, G., 2006. Resonance Raman assignment of myeloperoxidase and the selected mutants Asp94Val and Met243Thr. Effect of the heme distortion. J. Raman Spectrosc. 37, 263-276.

Burkhard, K.A., Wilks, A., 2007. Characterization of the outer membrane receptor ShuA from the heme uptake system of *Shigella dysenteriae* - Substrate specificity and identification of the heme protein ligands. J. Biol. Chem. 282, 15126-15136.

Caillet-Saguy, C., Turano, P., Piccioli, M., Lukat-Rodgers, G.S., Czjzek, M., Guigliarelli, B., Izadi-Pruneyre, N., Rodgers, K.R., Delepierre, M., Lecroisey, A., 2008. Deciphering the structural role of histidine 83 for heme binding in hemophore HasA. J. Biol. Chem. 283, 5960-5970.

Chan, A.C.K., Lelj-Garolla, B., Rosell, F.I., Pedersen, K.A., Mauk, A.G., Murphy, M.E.P., 2006. Cofacial heme binding is linked to dimerization by a bacterial heme transport protein. J. Mol. Biol. 362, 1108-1119.

Chipperfield, J.R., Ratledge, C., 2000. Salicylic acid is not a bacterial siderophore: A theoretical study. Biometals 13, 165-168.

Choby, J.E., Skaar, E.P., 2016. Heme synthesis and acquisition in bacterial pathogens. J. Mol. Biol. 428, 3408-3428.

Chuang, W.J., Johnson, S., Van Wart, H.E., 1988. Resonance Raman spectra of bovine liver catalase: Enhancement of proximal tyrosinate vibrations. J. Inorg. Biochem. 34, 201-219.

Collier, G.S., Pratt, J.M., De Wet, C.R., Tshabalala, C.F., 1979. Studies on haemin in dimethyl sulphoxide/water mixtures. Biochem. J. 179, 281-289.

Collier, R.J., 2001. Understanding the mode of action of diphtheria toxin: A perspective on progress during the 20th century. Toxicon 39, 1793-1803.

Contreras, H., Chim, N., Credali, A., Goulding, C.W., 2014. Heme uptake in bacterial pathogens. Curr. Opin. Chem. Biol. 19, 34-41.

Culbertson, D.S., Olson, J.S., 2010. Role of heme in the unfolding and assembly of myoglobin. Biochemistry 49, 6052-6063.

Daou, N., Buisson, C., Gohar, M., Vidic, J., Bierne, H., Kallassy, M., Lereclus, D., Nielsen-LeRoux, C., 2009. IlsA, a unique surface protein of *Bacillus cereus* required for iron acquisition from heme, hemoglobin and ferritin. PLoS Pathog. 5.

DeLano, W., L., 2015. The PyMOL Molecular Graphics System, Version 1.7.4 Schrödinger, LLC. http://www. pymol. org.

Deniau, C., Gilli, R., Izadi-Pruneyre, N., Létoffé, S., Delepierre, M., Wandersman, C., Briand, C., Lecroisey, A., 2003. Thermodynamics of heme binding to the HasA(SM) hemophore: Effect of mutations at three key residues for heme uptake. Biochemistry 42, 10627-10633.

Draganova, E.B., Adrian, S.A., Lukat-Rodgers, G.S., Keutcha, C.S., Schmitt, M.P., Rodgers, K.R., Dixon, D.W., 2016. *Corynebacterium diphtheriae* HmuT: Dissecting the roles of conserved residues in heme pocket stabilization. J. Biol. Inorg. Chem. 21, 875-886.

Draganova, E.B., Akbas, N., Adrian, S.A., Lukat-Rodgers, G.S., Collins, D.P., Dawson, J.H., Schmitt, M.P., Rodgers, K.R., Dixon, D.W., 2015. Heme binding by *Corynebacterium diphtheriae* HmuT: Function and heme environment. Biochemistry 54, 6598-6609.

Drazek, E.S., Hammack, C.A., Schmitt, M.P., 2000. *Corynebacterium diphtheriae* genes required for acquisition of iron from haemin and haemoglobin are homologous to ABC haemin transporters. Mol. Microbiol. 36, 68-84.

Du, J., Sono, M., Dawson, J.H., 2011. The H93G myoglobin cavity mutant as a versatile scaffold for modeling heme iron coordination structures in protein active sites and their characterization with magnetic circular dichroism spectroscopy. Coord. Chem. Rev. 255, 700-716.

Eakanunkul, S., Lukat-Rodgers, G.S., Sumithran, S., Ghosh, A., Rodgers, K.R., Dawson, J.H., Wilks, A., 2005. Characterization of the periplasmic heme-binding protein ShuT from the heme uptake system of *Shigella dysenteriae*. Biochemistry 44, 13179-13191.

Edelstein, S.J., Rehmar, M.J., Olson, J.S., Gibson, Q.H., 1970. Functional aspects of the subunit association-dissociation equilibria of hemoglobin. J. Biol. Chem. 245, 4372-4381.

Egeberg, K.D., Springer, B.A., Martinis, S.A., Sligar, S.G., Morikis, D., Champion, P.M., 1990. Alteration of sperm whale myoglobin heme axial ligation by site-directed mutagenesis. Biochemistry 29, 9783-9791.

Ekworomadu, M.T., Poor, C.B., Owens, C.P., Balderas, M.A., Fabian, M., Olson, J.S., Murphy, F., Balkabasi, E., Honsa, E.S., He, C., Goulding, C.W., Maresso, A.W., 2012. Differential function of Lip residues in the mechanism and biology of an anthrax hemophore. PLoS Pathog. 8.

Fabian, M., Solomaha, E., Olson, J.S., Maresso, A.W., 2009. Heme transfer to the bacterial cell envelope occurs via a secreted hemophore in the Gram-positive pathogen *Bacillus anthracis*. J. Biol. Chem. 284, 32138-32146.

Farrand, A.J., Skaar, E.P., 2014. Heme and infectious diseases, in: Ferreira, G.C., Kadish, K.M., Smith, K.M., Guilard, R. (Eds.), Handbook of Porphyrin Science with Applications to Chemistry, Physics, Materials Science, Engineering, Biology and Medicine, Vol 26: Heme Biochemistry. World Scientific, Hackensack, NJ, pp. 317-377.

Feng, Y.Q., Sligar, S.G., 1991. Effect of heme binding on the structure and stability of *Escherichia coli* apocytochrome b_{562}. Biochemistry 30, 10150-10155.

Gasteiger, E., Hoogland, C., Gattiker, A., Duvaud, S., Wilkins, M.R., Appel, R.D., Bairoch, A., 2005. Protein identification and analysis tools on the ExPASy server, in: Walker, J.M. (Ed.), The Proteomics Protocols Handbook. Humana Press, Totowa, N.J, pp. 571-607.

Gaudin, C.F.M., Grigg, J.C., Arrieta, A.L., Murphy, M.E.P., 2011. Unique heme-iron coordination by the hemoglobin receptor IsdB of *Staphylococcus aureus*. Biochemistry 50, 5443-5452.

Geng, J.F., Dornevil, K., Davidson, V.L., Liu, A.M., 2013. Tryptophan-mediated charge-resonance stabilization in the bis-Fe(IV) redox state of MauG. Proc. Natl. Acad. Sci. U. S. A. 110, 9639-9644.

Graves, A.B., Morse, R.P., Chao, A., Iniguez, A., Goulding, C.W., Liptak, M.D., 2014. Crystallographic and Spectroscopic Insights into Heme Degradation by *Mycobacterium tuberculosis* MhuD. Inorg. Chem. 53, 5931-5940.

Grigg, J.C., Cooper, J.D., Cheung, J., Heinrichs, D.E., Murphy, M.E.P., 2010a. The *Staphylococcus aureus* siderophore receptor HtsA undergoes localized conformational changes to enclose staphyloferrin A in an arginine-rich binding pocket. J. Biol. Chem. 285, 11162-11171.

Grigg, J.C., Mao, C.X., Murphy, M.E., 2011. Iron-coordinating tyrosine is a key determinant of NEAT domain heme transfer. J. Mol. Biol. 413, 684-698.

Grigg, J.C., Ukpabi, G., Gaudin, C.F., Murphy, M.E., 2010b. Structural biology of heme binding in the *Staphylococcus aureus* Isd system. J. Inorg. Biochem. 104, 341-348.

Hadfield, T.L., McEvoy, P., Polotsky, Y., Tzinserling, V.A., Yakovlev, A.A., 2000. The pathology of diphtheria. J. Infect. Dis. 181, S116-S120.

Hao, D.C., Zhu, P.H., Yang, S.L., Yang, L., 2007. Enhanced production of human cytochrome P4502C9 by *Escherichia coli* BL21(DE3)pLysS through the novel use of grey relational analysis and Plackett-Burman design. World J. Microbiol. Biotechnol. 23, 71-78.

Hargrove, M.S., Krzywda, S., Wilkinson, A.J., Dou, Y., Ikeda-Saito, M., Olson, J.S., 1994. Stability of myoglobin: A model for the folding of heme proteins. Biochemistry 33, 11767-11775.

Hargrove, M.S., Olson, J.S., 1996. The stability of holomyoglobin is determined by heme affinity. Biochemistry 35, 11310-11318.

Hargrove, M.S., Whitaker, T., Olson, J.S., Vali, R.J., Mathews, A.J., 1997. Quaternary structure regulates hemin dissociation from human hemoglobin. J. Biol. Chem. 272, 17385-17389.

Hargrove, M.S., Wilkinson, A.J., Olson, J.S., 1996. Structural factors governing hemin dissociation from metmyoglobin. Biochemistry 35, 11300-11309.

Ho, W.W., Li, H.Y., Eakanunkul, S., Tong, Y., Wilks, A., Guo, M.L., Poulos, T.L., 2007. Holo- and apo-bound structures of bacterial periplasmic heme-binding proteins. J. Biol. Chem. 282, 35796-35802.

Honsa, E.S., Fabian, M., Cardenas, A.M., Olson, J.S., Maresso, A.W., 2011. The five near-iron transporter (NEAT) domain anthrax hemophore, IsdX2, scavenges heme from hemoglobin and transfers heme to the surface protein IsdC. J. Biol. Chem. 286, 33652-33660.

Honsa, E.S., Maresso, A.W., 2011. Mechanisms of iron import in anthrax. Biometals 24, 533-545.

Honsa, E.S., Maresso, A.W., Highlander, S.K., 2014. Molecular and evolutionary analysis of NEAr-iron Transporter (NEAT) domains. PLoS One 9.

Honsa, E.S., Owens, C.P., Goulding, C.W., Maresso, A.W., 2013. The near-iron transporter (NEAT) domains of the anthrax hemophore IsdX2 require a critical glutamine to extract heme from methemoglobin. J. Biol. Chem. 288, 8479-8490.

Hu, S., Smith, K.M., Spiro, T.G., 1996a. Assignment of protoheme resonance Raman spectrum by heme labeling in myoglobin. Journal of the American Chemical Society 118, 12638-12646.

Hu, S.H., Kincaid, J.R., 1992. Resonance Raman studies of the carbonmonoxy form of catalase - Evidence for and effects of phenolate ligation. FEBS Lett. 314, 293-296.

Hu, S.Z., Smith, K.M., Spiro, T.G., 1996b. Assignment of protoheme resonance Raman spectrum by heme labeling in myoglobin. J. Am. Chem. Soc. 118, 12638-12646.

Huang, X., Wang, C.X., Celeste, L.R., Lovelace, L.L., Sun, S.F., Dawson, J.H., Lebioda, L., 2012. Complex of myoglobin with phenol bound in a proximal cavity. Acta Crystallogr. Sect. F-Struct. Biol. Cryst. Commun. 68, 1465-1471.

Hunter, C.L., Mauk, A.G., Douglas, D.J., 1997. Dissociation of heme from myoglobin and cytochrome *b*(5): Comparison of behavior in solution and the gas phase. Biochemistry 36, 1018-1025.

Hussain, H.A., Ward, J.M., 2003. Enhanced heterologous expression of two *Streptomyces griseolus* cytochrome P450s and *Streptomyces coelicolor* ferredoxin reductase as potentially efficient hydroxylation catalysts. Appl. Environ. Microbiol. 69, 373-382.

Jansson, I., Stoilov, I., Sarfarazi, M., Schenkman, J.B., 2000. Enhanced expression of CYP1B1 in *Escherichia coli*. Toxicology 144, 211-219.

Jepkorir, G., Rodriguez, J.C., Rui, H., Im, W., Lovell, S., Battaile, K.P., Alontaga, A.Y., Yukl, E.T., Moenne-Loccoz, P., Rivera, M., 2010. Structural, NMR spectroscopic, and computational investigation of hemin loading in the hemophore HasAp from *Pseudomonas aeruginosa*. J. Am. Chem. Soc. 132, 9857-9872.

Jin, Y.Y., Nagai, M., Nagai, Y., Nagatomo, S., Kitagawa, T., 2004. Heme structures of five variants of hemoglobin M probed by resonance Raman spectroscopy. Biochemistry 43, 8517-8527.

Jones, D.K., Patel, N., Cheesman, M.R., Thomson, A.J., Raven, E.L., 2002. Leghaemoglobin: A model for the investigation of haem protein axial ligation. Inorg. Chim. Acta 331, 303-309.

Jonsson, I.M., Mazmanian, S.K., Schneewind, O., Bremell, T., Tarkowski, A., 2003. The role of *Staphylococcus aureus* sortase A and sortase B in murine arthritis. Microbes Infect. 5, 775-780.

Kery, V., Elleder, D., Kraus, J.P., 1995. δ-Aminolevulinate increases heme saturation and yield of human cystathionine β-synthase expressed in *Escherichia coli*. Arch. Biochem. Biophys. 316, 24-29.

Kimoto, H., Matsuyama, H., Yumoto, I., Yoshimune, K., 2008. Heme content of recombinant catalase from *Psychrobacter* sp T-3 altered by host *Escherichia coli* cell growth conditions. Protein Expr. Purif. 59, 357-359.

Kitagawa, T., Nagai, K., Tsubaki, M., 1979. Assignment of the Fe-nitrogen (His F8) stretching band in the resonance Raman spectra of deoxymyoglobin. FEBS Lett. 104, 376-378.

Krewulak, K.D., Vogel, H.J., 2008. Structural biology of bacterial iron uptake. Biochim. Biophys. Acta 1778, 1781-1804.

Kumar, R., Bhuyan, A.K., 2009. Entropic stabilization of myoglobin by subdenaturing concentrations of guanidine hydrochloride. J. Biol. Inorg. Chem. 14, 11-21.

Kumar, R., Lovell, S., Matsumura, H., Battaile, K.P., Moenne-Loccoz, P., Rivera, M., 2013. The hemophore HasA from *Yersinia pestis* ($HasA_{yp}$) coordinates hemin with a single residue, Tyr75, and with minimal conformational change. Biochemistry 52, 2705-2707.

Kumar, R., Matsumura, H., Lovell, S., Yao, H.L., Rodriguez, J.C., Battaile, K.P., Moenne-Loccoz, P., Rivera, M., 2014. Replacing the axial ligand tyrosine 75 or its hydrogen bond partner histidine 83 minimally affects hemin acquisition by the hemophore HasAp from *Pseudomonas aeruginosa*. Biochemistry 53, 2112-2125.

Kunkle, C.A., Schmitt, M.P., 2003. Analysis of the *Corynebacterium diphtheriae* DtxR regulon: Identification of a putative siderophore synthesis and transport system that is similar to the *Yersinia* high-pathogenicity island-encoded yersiniabactin synthesis and uptake system. J. Bacteriol. 185, 6826-6840.

Kuter, D., Venter, G.A., Naidoo, K.J., Egan, T.J., 2012. Experimental and time-dependent density functional theory characterization of the UV-visible spectra of monomeric and μ-oxo dimeric ferriprotoporphyrin IX. Inorg. Chem. 51, 10233-10250.

Lee, A.J., Clark, R.W., Youn, H., Ponter, S., Burstyn, J.N., 2009. Guanidine hydrochloride-induced unfolding of the three heme coordination states of the CO-sensing transcription factor, CooA. Biochemistry 48, 6585-6597.

Lei, B.F., Smoot, L.M., Menning, H.M., Voyich, J.M., Kala, S.V., Deleo, F.R., Reid, S.D., Musser, J.M., 2002. Identification and characterization of a novel heme-associated cell surface protein made by *Streptococcus pyogenes*. Infect. Immun. 70, 4494-4500.

León, R.G., Munier-Lehmann, H., Barzu, O., Baudin-Creuza, V., Pietri, R., Lopez-Garriga, J., Cadilla, C.L., 2004. High-level production of recombinant sulfide-reactive hemoglobin I from *Lucina pectinata* in *Escherichia coli*. High yields of fully functional holoprotein synthesis in the BLi5 *E. coli* strain. Protein Expr. Purif. 38, 184-195.

Linder, D.P., Silvernail, N.J., Barabanschikov, A., Zhao, J.Y., Alp, E.E., Sturhahn, W., Sage, J.T., Scheidt, W.R., Rodgers, K.R., 2014. The diagnostic vibrational signature of pentacoordination in heme carbonyls. J. Am. Chem. Soc. 136, 9818-9821.

Liu, M.Y., Lei, B.F., 2005. Heme transfer from streptococcal cell surface protein Shp to HtsA of transporter HtsABC. Infect. Immun. 73, 5086-5092.

Londer, Y.Y., Pokkuluri, P.R., Orshonsky, V., Orshonsky, L., Schiffer, M., 2006. Heterologous expression of dodecaheme "nanowire" cytochromes *c* from *Geobacter sulfurreducens*. Protein Expr. Purif. 47, 241-248.

Lukat-Rodgers, G.S., Rodgers, K.R., Caillet-Saguy, C., Izadi-Pruneyre, N., Lecroisey, A., 2008. Novel heme ligand displacement by CO in the soluble hemophore HasA and its proximal ligand mutants: Implications for heme uptake and release. Biochemistry 47, 2087-2098.

Malmirchegini, G.R., Sjodt, M., Shnitkind, S., Sawaya, M.R., Rosinski, J., Newton, S.M., Klebba, P.E., Clubb, R.T., 2014. Novel mechanism of hemin capture by Hbp2, the hemoglobin-binding hemophore from *Listeria monocytogenes*. J. Biol. Chem. 289, 34886-34899.

Maresso, A.W., Garufi, G., Schneewind, O., 2008. *Bacillus anthracis* secretes proteins that mediate heme acquisition from hemoglobin. PLoS Pathog. 4.

Mason, J.M., Bendall, D.S., Howe, C.J., Worrall, J.A.R., 2012. The role of a disulfide bridge in the stability and folding kinetics of *Arabidopsis thaliana* cytochrome c(6A). Biochim. Biophys. Acta 1824, 311-318.

Mattle, D., Zeltina, A., Woo, J.S., Goetz, B.A., Locher, K.P., 2010. Two stacked heme molecules in the binding pocket of the periplasmic heme-binding protein HmuT from *Yersinia pestis*. J. Mol. Biol. 404, 220-231.

Mattos-Guaraldi, A., Moreira, L., Damasco, P., Hirata Junior, R., 2003. Diphtheria remains a threat to health in the developing world: An overview. Mem. Inst. Oswaldo Cruz 98, 987-993.

Mazmanian, S.K., Skaar, E.P., Gaspar, A.H., Humayun, M., Gornicki, P., Jelenska, J., Joachmiak, A., Missiakas, D.M., Schneewind, O., 2003. Passage of heme-iron across the envelope of *Staphylococcus aureus*. Science 299, 906-909.

Mokry, D.Z., Nadia-Albete, A., Johnson, M.K., Lukat-Rodgers, G.S., Rodgers, K.R., Lanzilotta, W.N., 2014. Spectroscopic evidence for a 5-coordinate oxygenic ligated high spin ferric heme moiety in the *Neisseria meningitidis* hemoglobin binding receptor. Biochim. Biophys. Acta 1840, 3058-3066.

Moriwaki, Y., Terada, T., Tsumoto, K., Shimizu, K., 2015. Rapid heme transfer reactions between NEAr transporter domains of *Staphylococcus aureus*: A theoretical study using QM/MM and MD simulations. PLoS One 10.

Mulrooney, S.B., Waskell, L., 2000. High-level expression in *Escherichia coli* and purification of the membrane-bound form of cytochrome *b*(5). Protein Expr. Purif. 19, 173-178.

Muraki, N., Aono, S., 2015. Structural basis for heme recognition by HmuT responsible for heme transport to the heme transporter in *Corynebacterium glutamicum*. Chem. Lett. 45, 24-26.

Muryoi, N., Tiedemann, M.T., Pluym, M., Cheung, J., Heinrichs, D.E., Stillman, M.J., 2008. Demonstration of the iron-regulated surface determinant (Isd) heme transfer pathway in *Staphylococcus aureus*. J. Biol. Chem. 283, 28125-28136.

Nagai, M., Yoneyama, Y., Kitagawa, T., 1989. Characteristics in tyrosine coordinations of four hemoglobins M probed by resonance Raman spectroscopy. Biochemistry 28, 2418-2422.

Nagai, M., Yoneyama, Y., Kitagawa, T., 1991. Unusual carbon monoxide bonding geometry in abnormal subunits of hemoglobin M Boston and hemoglobin M Saskatoon. Biochemistry 30, 6495-6503.

Nobles, C.L., Maresso, A.W., 2011. The theft of host heme by Gram-positive pathogenic bacteria. Metallomics 3, 788-796.

Nygaard, T.K., Blouin, G.C., Liu, M.Y., Fukumura, M., Olson, J.S., Fabian, M., Dooley, D.M., Lei, B.F., 2006. The mechanism of direct heme transfer from the streptococcal cell surface protein Shp to HtsA of the HtsABC transporter. J. Biol. Chem. 281, 20761-20771.

Ouattara, M., Cunha, E.B., Li, X., Huang, Y.S., Dixon, D.W., Eichenbaum, Z., 2010. Shr of Group A streptococcus is a new type of composite NEAT protein involved in sequestering haem from methaemoglobin. Mol. Microbiol. 78, 739-756.

Ouattara, M., Pennati, A., Devlin, D.J., Huang, Y.S., Gadda, G., Eichenbaum, Z., 2013. Kinetics of heme transfer by the Shr NEAT domains of Group A Streptococcus. Arch. Biochem. Biophys. 538, 71-79.

Ozaki, S., Sato, T., Sekine, Y., Migita, C.T., Uchida, T., Ishimori, K., 2014. Spectroscopic studies on HasA from *Yersinia pseudotuberculosis*. J. Inorg. Biochem. 138, 31-38.

Pace, C.N., 1986. Determination and analysis of urea and guanidine hydrochloride denaturation curves. Methods Enzymol. 131, 266-280.

Pace, C.N., Scholtz, J.M., 1997. Measuring the conformational stability of a protein, in: Creighton, T. (Ed.), Protein Structure: A Practical Approach, 2nd ed. Oxford University Press, Oxford, pp. 299-321.

Patel, N., Seward, H.E., Svensson, A., Gurman, S.J., Thomson, A.J., Raven, E.L., 2003. Exploiting the conformational flexibility of leghemoglobin: A framework for examination of heme protein axial ligation. Arch. Biochem. Biophys. 418, 197-204.

Pfeil, W., 1993. Thermodynamics of apocytochrome *b(5)* unfolding. Protein Sci. 2, 1497-1501.

Pin, S., Alpert, B., Cortès, R., Ascone, I., Chiu, M.L., Sligar, S.G., 1994. The heme iron coordination complex in His64(E7)Tyr recombinant sperm whale myoglobin. Biochemistry 33, 11618-11623.

Pishchany, G., Sheldon, J.R., Dickson, C.F., Alam, M.T., Read, T.D., Gell, D.A., Heinrichs, D.E., Skaar, E.P., 2014. IsdB-dependent hemoglobin binding is required for acquisition of heme by *Staphylococcus aureus*. J. Infect. Dis. 209, 1764-1772.

Pluym, M., Muryoi, N., Heinrichs, D.E., Stillman, M.J., 2008. Heme binding in the NEAT domains of IsdA and IsdC of *Staphylococcus aureus*. J. Inorg. Biochem. 102, 480-488.

Pluym, M., Vermeiren, C.L., Mack, J., Heinrichs, D.E., Stillman, M.J., 2007. Protoporphyrin IX and heme binding properties of *Staphylococcus aureus* IsdC. J. Porph. Phthalo. 11, 165-171.

Ran, Y.C., Malmirchegini, G.R., Clubb, R.T., Lei, B.F., 2013. Axial ligand replacement mechanism in heme transfer from streptococcal heme-binding protein Shp to HtsA of the HtsABC transporter. Biochemistry 52, 6537-6547.

Ran, Y.C., Zhu, H., Liu, M.Y., Fabian, M., Olson, J.S., Aranda, R.I., Phillips, G.N., Dooley, D.M., Lei, B., 2007. Bis-methionine ligation to heme iron in the streptococcal cell surface protein Shp facilitates rapid hemin transfer to HtsA of the HtsABC transporter. J. Biol. Chem. 282, 31380-31388.

Ricchelli, F., Jori, G., Gobbo, S., Tronchin, M., 1991. Liposomes as models to study the distribution of porphyrins in cell membranes. Biochim. Biophys. Acta 1065, 42-48.

Rivera, M., Walker, F.A., 1995. Biosynthetic preparation of isotopically labeled heme. Anal. Biochem. 230, 295-302.

Robinson, C.R., Liu, Y.F., Thomson, J.A., Sturtevant, J.M., Sligar, S.G., 1997. Energetics of heme binding to native and denatured states of cytochrome *b*(562). Biochemistry 36, 16141-16146.

Rodgers, K.R., Lukat-Rodgers, G.S., 2014. Biophysical perspectives on the acquisition, transport, and trafficking of heme in bacteria, in: Ferreira, G.C., Kadish, K.M., Smith, K.M., Guilard, R. (Eds.), Handbook of Porphyrin Science with Applications to Chemistry, Physics, Materials Science, Engineering, Biology and Medicine, Vol. 30: Heme Proteins, Part II. World Scientific, Hackensack, N.J, pp. 251-309.

Roncone, R., Monzani, E., Labo, S., Sanangelantoni, A.M., Casella, L., 2005. Catalytic activity, stability, unfolding, and degradation pathways of engineered and reconstituted myoglobins. J. Biol. Inorg. Chem. 10, 11-24.

Roy, A., Kucukural, A., Zhang, Y., 2010. I-TASSER: A unified platform for automated protein structure and function prediction. Nat. Protoc. 5, 725-738.

Saini, K., Ahluwalia, U., Deep, S., 2010. Determination of heat capacity of unfolding for marginally stable proteins from a single temperature induced protein unfolding profile. Thermochim. Acta 506, 28-33.

Sanchez-Ruiz, J.M., 2010. Protein kinetic stability. Biophys. Chem. 148, 1-15.

Schmitt, M.P., 1997a. Transcription of the *Corynebacterium diphtheriae hmuO* gene is regulated by iron and heme. Infect. Immun. 65, 4634-4641.

Schmitt, M.P., 1997b. Utilization of host iron sources by *Corynebacterium diphtheriae*: Identification of a gene whose product is homologous for eukaryotic heme oxygenases and is required for acquisition of iron from heme and hemoglobin. J. Bacteriol. 179, 838-845.

Schmitt, M.P., 2014. Iron acquisition and iron-dependent gene expression in *Corynebacterium diphtheriae*, in: Burkovski, A. (Ed.), *Corynebacterium diphtheriae* and Related Toxigenic Species: Genomics, Pathogenicity and Applications. Springer, pp. 95-121.

Schmitt, M.P., Drazek, E.S., 2001. Construction and consequences of directed mutations affecting the hemin receptor in pathogenic *Corynebacterium species*. J. Bacteriol. 183, 1476-1481.

Schmitt, M.P., Holmes, R.K., 1991. Iron-dependent regulation of diphtheria toxin and siderophore expression by the cloned *Corynebacterium diphtheriae* repressor gene Dtxr in *C. diphtheriae* C7 strains. Infect. Immun. 59, 1899-1904.

Scott, E.E., Paster, E.V., Olson, J.S., 2000. The stabilities of mammalian apomyoglobins vary over a 600-fold range and can be enhanced by comparative mutagenesis. J. Biol. Chem. 275, 27129-27136.

Segond, D., Khalil, E.A., Buisson, C., Daou, N., Kallassy, M., Lereclus, D., Arosio, P., Bou-Abdallah, F., Le Roux, C.N., 2014. Iron acquisition in *Bacillus cereus*: The roles of IlsA and bacillibactin in exogenous ferritin iron mobilization. PLoS Pathog. 10.

Sharma, K.D., Andersson, L.A., Loehr, T.M., Terner, J., Goff, H.M., 1989. Comparative spectral analysis of mammalian, fungal, and bacterial catalases. Resonance Raman evidence for iron-tyrosinate coordination. J. Biol. Chem. 264, 12772-12779.

Sharp, K.H., Schneider, S., Cockayne, A., Paoli, M., 2007. Crystal structure of the heme-IsdC complex, the central conduit of the Isd iron/heme uptake system in *Staphylococcus aureus*. J. Biol. Chem. 282, 10625-10631.

Sheldon, J.R., Heinrichs, D.E., 2015. Recent developments in understanding the iron acquisition strategies of gram positive pathogens. FEMS Microbiol. Rev. 39, 592-630.

Sheldon, J.R., Laakso, H.A., Heinrichs, D.E., 2016. Iron acquisition strategies of bacterial pathogens. Microbiology Spectrum 4.

Sievers, F., Higgins, D.G., 2014. Clustal Omega, accurate alignment of very large numbers of sequences. Methods Mol Biol 1079, 105-116.

Sievers, G., Gadsby, P.M., Peterson, J., Thomson, A.J., 1983. Magnetic circular dichroism spectra of soybean leghaemoglobin *a* at room temperature and 4.2 K. Biochim. Biophys. Acta 742, 637-647.

Sjodt, M., Macdonald, R., Spirig, T., Chan, A.H., Dickson, C.F., Fabian, M., Olson, J.S., Gell, D.A., Clubb, R.T., 2016. The PRE-derived NMR model of the 38.8-kDa tri-domain IsdH protein from Staphylococcus aureus suggests that it adaptively recognizes human hemoglobin. J. Mol. Biol. 428, 1107-1129.

Smith, A.D., Wilks, A., 2012. Extracellular heme uptake and the challenges of bacterial cell membranes. Curr. Top. Membr. 69, 359-392.

Smulevich, G., Mauro, J.M., Fishel, L.A., English, A.M., Kraut, J., Spiro, T.G., 1988a. Cytochrome *c* peroxidase mutant active site structures probed by resonance Raman and infrared signatures of the CO adducts. Biochemistry 27, 5486-5492.

Smulevich, G., Mauro, J.M., Fishel, L.A., English, A.M., Kraut, J., Spiro, T.G., 1988b. Cytochrome c peroxidase mutant active site structures probed by resonance Raman and infrared signatures of the CO adducts. Biochemistry 27, 5486-5492.

Sook, B.R., Block, D.R., Sumithran, S., Montañez, G.E., Rodgers, K.R., Dawson, J.H., Eichenbaum, Z., Dixon, D.W., 2008. Characterization of SiaA, a streptococcal heme-binding protein associated with a heme ABC transport system. Biochemistry 47, 2678-2688.

Spiro, T.G., Soldatova, A.V., Balakrishnan, G., 2013. CO, NO and O_2 as vibrational probes of heme protein interactions. Coord. Chem. Rev. 257, 511-527.

Spiro, T.G., Wasbotten, I.H., 2005. CO as a vibrational probe of heme protein active sites. J. Inorg. Biochem. 99, 34-44.

Stojiljkovic, I., Perkins-Balding, D., 2002. Processing of heme and heme-containing proteins by bacteria. DNA Cell Biol. 21, 281-295.

Streit, B.R., Blanc, B., Lukat-Rodgers, G.S., Rodgers, K.R., DuBois, J.L., 2010. How active-site protonation state influences the reactivity and ligation of the heme in chlorite dismutase. J. Am. Chem. Soc. 132, 5711-5724.

Sudhamsu, J., Kabir, M., Airola, M.V., Patel, B.A., Yeh, S.R., Rousseau, D.L., Crane, B.R., 2010. Co-expression of ferrochelatase allows for complete heme incorporation into recombinant proteins produced in *E. coli*. Protein Expr. Purif. 73, 78-82.

Swint, L., Robertson, A.D., 1993. Thermodynamics of unfolding for turkey ovomucoid third domain: Thermal and chemical denaturation. Protein Sci. 2, 2037-2049.

Tarlovsky, Y., Fabian, M., Solomaha, E., Honsa, E., Olson, J.S., Maresso, A.W., 2010. A *Bacillus anthracis* S-Layer homology protein that binds heme and mediates heme delivery to IsdC. J. Bacteriol. 192, 3503-3511.

Teale, F.W., 1959. Cleavage of the heme protein by acid methyl ethyl ketone. Biochim. Biophys. Acta 35, 543.

Tiedemann, M.T., Heinrichs, D.E., Stillman, M.J., 2012. Multiprotein heme shuttle pathway in *Staphylococcus aureus*: Iron-regulated surface determinant cog-wheel kinetics. J. Am. Chem. Soc. 134, 16578-16585.

Tiedemann, M.T., Muryoi, N., Heinrichs, D.E., Stillman, M.J., 2009. Characterization of IsdH (NEAT domain 3) and IsdB (NEAT domain 2) in *Staphylococcus aureus* by magnetic circular dichroism spectroscopy and electrospray ionization mass spectrometry. J. Porph. Phthalo. 13, 1006-1016.

Tiedemann, M.T., Stillman, M.J., 2011. Application of magnetic circular dichroism spectroscopy to porphyrins, phthalocyanines and hemes. J. Porph. Phthalo. 15, 1134-1149.

Ton-That, H., Marraffini, L.A., Schneewind, O., 2004. Protein sorting to the cell wall envelope of Gram-positive bacteria. Biochim. Biophys. Acta 1694, 269-278.

Tong, Y., Guo, M., 2007. Cloning and characterization of a novel periplasmic heme-transport protein from the human pathogen *Pseudomonas aeruginosa*. J. Biol. Inorg. Chem. 12, 735-750.

Tong, Y., Guo, M., 2009. Bacterial heme-transport proteins and their heme-coordination modes. Arch. Biochem. Biophys. 481, 1-15.

Travaglini-Allocatelli, C., Cutruzzolà, F., Bigotti, M.G., Staniforth, R.A., Brunori, M., 1999. Folding mechanism of *Pseudomonas aeruginosa* cytochrome *c*(551): Role of electrostatic interactions on the hydrophobic collapse and transition state properties. J. Mol. Biol. 289, 1459-1467.

Travaglini-Allocatelli, C., Gianni, S., Dubey, V.K., Borgia, A., Di Matteo, A., Bonivento, D., Cutruzzolà, F., Bren, K.L., Brunori, M., 2005. An obligatory intermediate in the folding pathway of cytochrome *c*(552) from *Hydrogenobacter thermophilus*. J. Biol. Chem. 280, 25729-25734.

Travaglini-Allocatelli, C., Gianni, S., Morea, V., Tramontano, A., Soulimane, T., Brunori, M., 2003. Exploring the cytochrome c folding mechanism - Cytochrome *c*(552) from *Thermus thermophilus* folds through an on-pathway intermediate. J. Biol. Chem. 278, 41136-41140.

Trost, E., Blom, J., Soares, S.D., Huang, I.H., Al-Dilaimi, A., Schroder, J., Jaenicke, S., Dorella, F.A., Rocha, F.S., Miyoshi, A., Azevedo, V., Schneider, M.P., Silva, A., Camello, T.C., Sabbadini, P.S., Santos, C.S., Santos, L.S., Hirata, R., Mattos-Guaraldi, A.L., Efstratiou, A., Schmitt, M.P., Hung, T.T., Tauch, A., 2012. Pangenomic study of *Corynebacterium diphtheriae* that provides insights into the genomic diversity of pathogenic isolates from cases of classical diphtheria, endocarditis, and pneumonia. J. Bacteriol. 194, 3199-3215.

Uluisik, R.C., Akbas, N., Lukat-Rodgers, G.S., Adrian, S.A., Allen, C.E., Schmitt, M.P., Rodgers, K.R., Dixon, D.W., 2017. Characterization of the second conserved domain in the heme uptake protein HtaA from *Corynebacterium diphtheriae*. J. Inorg. Biochem. 167, 124-133.

Vieille, C., Zeikus, G.J., 2001. Hyperthermophilic enzymes: Sources, uses, and molecular mechanisms for thermostability. Microbiol. Mol. Biol. Rev. 65, 1-43.

Villareal, V.A., Spirig, T., Robson, S.A., Liu, M., Lei, B., Clubb, R.T., 2011. Transient weak protein-protein complexes transfer heme across the cell wall of *Staphylococcus aureus*. J. Am. Chem. Soc. 133, 14176-14179.

Vogel, K.M., Kozlowski, P.M., Zgierski, M.Z., Spiro, T.G., 2000. Role of the axial ligand in heme-CO backbonding; DFT analysis of vibrational data. Inorg. Chim. Acta 297, 11-17.

Wagner, K.S., White, J.M., Lucenko, I., Mercer, D., Crowcroft, N.S., Neal, S., Efstratiou, A., 2012. Diphtheria in the postepidemic period, Europe, 2000-2009. Emerg. Infect. Dis. 18, 217-225.

Wandersman, C., Delepelaire, P., 2004. Bacterial iron sources: From siderophores to hemophores. Annu. Rev. Microbiol. 58, 611-647.

Wandersman, C., Delepelaire, P., 2012. Haemophore functions revisited. Mol. Microbiol. 85, 618-631.

Wandersman, C., Delepelaire, P., 2014. Heme-delivering proteins in bacteria, in: Ferreira, G.C., Kadish, K.M., Smith, K.M., Guilard, R. (Eds.), Handbook of Porphyrin Science with Applications to Chemistry, Physics, Materials Science, Engineering, Biology and Medicine, Vol 26: Heme Biochemistry, pp. 191-222.

Warren, M.J., Smith, A.G., 2009. Tetrapyrroles: Birth, Life, and Death. Landes Bioscience, Austin, Tex.

Watanabe, M., Tanaka, Y., Suenaga, A., Kuroda, M., Yao, M., Watanabe, N., Arisaka, F., Ohta, T., Tanaka, I., Tsumoto, K., 2008. Structural basis for multimeric heme complexation through a specific protein-heme interaction - The case of the third NEAT domain of IsdH from *Staphylococcus aureus*. J. Biol. Chem. 283, 28649-28659.

Wen, X., Patel, K.M., Russell, B.S., Bren, K.L., 2007. Effects of heme pocket structure and mobility on cytochrome *c* stability. Biochemistry 46, 2537-2544.

Wijma, H.J., Floor, R.J., Janssen, D.B., 2013. Structure- and sequence-analysis inspired engineering of proteins for enhanced thermostability. Curr. Opin. Struct. Biol. 23, 588-594.

Wilks, A., O'Neill, M.J., 2014. Extracellular heme uptake and metabolism in bacterial pathogenesis, in: Ferreira, G.C., Kadish, K.M., Smith, K.M., Guilard, R. (Eds.), Handbook of Porphyrin Science with Applications to Chemistry, Physics, Materials Science, Engineering, Biology and Medicine, Vol 26: Heme Biochemistry. World Scientific, Hackensack, NJ, pp. 267-315.

Wittung-Stafshede, P., 1999. Effect of redox state on unfolding energetics of heme proteins. Biochim. Biophys. Acta 1432, 401-405.

Woo, J.S., Zeltina, A., Goetz, B.A., Locher, K.P., 2012. X-ray structure of the *Yersinia pestis* heme transporter HmuUV. Nat. Struct. Mol. Biol. 19, 1310-1315.

Xiao, Q., Jiang, X., Moore, K.J., Shao, Y., Pi, H., Dubail, I., Charbit, A., Newton, S.M., Klebba, P.E., 2011. Sortase independent and dependent systems for acquisition of haem and haemoglobin in *Listeria monocytogenes*. Mol. Microbiol. 80, 1581-1597.

Zapotoczna, M., Heilbronner, S., Speziale, P., Foster, T.J., 2012. Iron-Regulated Surface Determinant (Isd) Proteins of *Staphylococcus lugdunensis*. J. Bacteriol. 194, 6453-6467.

Zhang, L., Liu, X.Q., Wang, C.T., Liu, X.Q., Cheng, G., Wu, Y.H., 2010. Expression, purification and direct eletrochemistry of cytochrome P450 6A1 from the house fly, *Musca domestica*. Protein Expr. Purif. 71, 74-78.

Zheng, Z., Gunner, A.R., 2008. Analysis of the electrochemistry of hemes with E(m)s spanning 800 mV. Proteins-Structure Function and Bioinformatics 75, 719-734.

Zhu, H., Li, D.F., Liu, M.Y., Copie, V., Lei, B.F., 2014. Non-heme-binding domains and segments of the *Staphylococcus aureus* IsdB protein critically contribute to the kinetics and equilibrium of heme acquisition from methemoglobin. PLoS One 9.

5 GENERAL CONCLUSIONS

This dissertation focuses on the biochemical and biophysical characterization of heme-binding proteins in the heme uptake pathway of the gram-positive bacterium *Corynebacterium diphtheriae.* Because iron is an essential nutrient for most bacteria, and because heme is the major source of iron in humans, understanding of the heme uptake mechanism of pathogenic bacteria may allow development alternative antibiotic therapeutics. A variety of techniques has been used to investigate the characteristics of these proteins including site-directed mutagenesis, UV-visible absorption, circular dichroism (CD), fluorescence, resonance Raman (rR), and MCD spectroscopies, and mass spectrometry (MS), as well as chemical and thermal unfolding studies.

The second conserved domain of HtaA (HtaA-CR2) from *C. diphtheriae* likely utilizes a conserved tyrosine and/or a histidine residue in heme binding, as hypothesized from sequence alignment of this protein with many other homologs. Bioinformatics analysis indicates a structure with a significant number of β-sheets. Homology modeling of HtaA-CR2 indicated that the protein does not have significant homology with the structurally known proteins in the protein data bank (PDB), thus indicating that HtaA-CR2 has a novel structure.

The UV-visible absorbance spectra, as well as rR spectra in ferric, ferrous and ferrous-CO forms, are consistent with the a tyrosine axial ligand for the heme. These results are also in line with the mutation studies on Y361A and H412A proteins; both of these mutants show significantly lower heme binding in comparison with the WT protein. However, there is no evidence showing direct interaction between the heme and a histidine, suggesting that H412 plays a significant role in heme binding other than the heme iron ligation. Reconstitution via

unfolding and refolding gave a different form of the protein. On-column hemin loading studies using excess metHb as a heme donor or direct exogenous hemin titration studies were successful in giving increased heme content without significantly changing the UV-visible spectrum. HtaA-CR2 is a highly stable protein; chemical denaturation studies with GdnHCl or GdnSCN (both up to 4 M) at room temperature did not unfold the protein. A single unfolding process was observed at higher concentrations of GdnHCl (6.6 – 7.4 M) at 37 ^{o}C. Thermal unfolding experiments had to be performed in the presence of GdnHCl (1.5 – 3.0 M). In contrast, the WT apoprotein and the mutant proteins unfolded readily with a midpoint unfolding denaturant concentration of ~ 1.3 M. These data suggest that the heme binding significantly contributes to the stability of the protein. The high stability might prevent heme loss during heme capture and heme transfer to the partner protein.

The heme uptake proteins HtaB and ChtB were also studied. Sequence alignment, UV-visible spectroscopy of WT and mutants as well as rR studies on both the ferric and ferrous forms of the WT proteins indicate that tyrosine is the heme axial ligand in both proteins. The rR spectra of the ferrous-CO HtaB and ChtB species each had two forms of heme ligation, one with a *trans* axial histidine and the second with *trans* oxygen-bound ligand. These data suggest that the tyrosine and the histidine are both in a close proximity to the heme iron. The oxygen-bound species in each instance falls on the line including a single hydrogen-bonding partner. These results are in line with tyrosine as the axial ligand in ferric and ferrous form of the proteins, with histidine likely as the hydrogen-binding partner to the tyrosine. HtaB is less stable than HtaA-CR2. A half-life of 39 min was observed in the presence of 4.0 M GdnHCl at 25 ^{o}C compared with 330 min in the presence of 6.6 M GdnHCl at 37 ^{o}C for HtaA-CR2. The unfolding of ChtB was similar to that of HtaB. Along with the similar unfolding behavior and same heme axial

ligands, these proteins also show high amino acid sequence similarity and identity; the biophysical data as well as literature studies of deletion mutants that suggest HtaB and ChtB might be playing a interchangeable role in heme transfer of *C. diphtheriae*.

Bioinformatics analyses of currently available species indicate that along with *Corynebacteria*, many species of *Actinobacteria* use HtaA domains. The conserved (CR) domains of HtaA-type proteins stands as a novel heme transfer protein motif. The interchangeability of HtaB and ChtB in transferring heme from HtaA/ChtA/ChtC to HmuT may indicate that networks of pathways are preferred in heme transfer of *C. diphtheriae* rather than a simple linear heme transfer. Such systems would take advantage of multiple protein-protein interactions and protein distribution in space in order to maximize the efficiency of heme transport.

Antibiotic resistance is an increasing concern in the treatment of diseases caused by pathogenic bacteria. Targeting the iron uptake pathways of human bacterial pathogens might allow development of alternative therapeutic agents. Because majority of the iron in human body is found in heme, characterization of bacterial heme uptake pathways is vital if new agents are to be developed based on the strategy of blocking heme entry. *C. diphtheriae* continue to be an international health issue, especially in less developed areas in the world. Our studies provide the biophysical characterization of three proteins in the heme uptake pathways of this organism. This study reveals two characteristics of heme uptake pathways that may have broad importance. First, HtaA-CR2 is very stable, perhaps necessitated by the need to retain bound heme (free heme is toxic in the cell) and perhaps fostering heme transfer to specific partners in a complex. Second, HtaB and ChtB appear interchangeable, both in structural and biophysical terms from our work and growth studies described in the literature. These findings may indicate that

networks of pathways are involved in taking heme into the cell. These observations in *C. diphtheriae* provide new paradigms for heme uptake in pathogenic bacteria in general.